Long QT syndrome: The identification and verification of putative KCNE2-interacting proteins

by Annika Neethling

Thesis presented in partial fulfilment of the requirements for the degree of Master of Science (Human Genetics) in the Faculty of Medicine and Health Sciences at Stellenbosch University

Supervisor: Dr. Craig Kinnear
Faculty of Medicine and Health Sciences
Department of Biomedical Sciences

December 2013

DECLARATION

By submitting this thesis electronically, I declare that the entirety of the work contained therein is my own, original work, that I am the sole author thereof (save to the extent explicitly otherwise stated), that reproduction and publication thereof by Stellenbosch University will not infringe any third party rights and that I have not previously in its entirety or in part submitted it for obtaining any qualification.

Date: ……17/09/2013……

Abstract

Long QT syndrome (LQTS) is a cardiac repolarization disorder affecting every 1:2000-1:3000 individuals. This disease is characterized by a prolonged QT interval on the surface electrocardiogram (ECG) of patients. Symptoms of LQTS range from dizziness and syncope to more severe symptoms such as seizures and sudden cardiac death (SCD). Clinical features of LQTS are a result of the precipitations of Torsades de Pointes, which is a polymorphic form of ventricular tachycardia. A number of genetic forms of LQTS have been identified with more than 700 mutations in 12 different genes leading to disease pathogenesis. However it has been estimated that approximately 25% of patients with compelling LQTS have no mutations within the known LQT genes. This proves to be problematic since treatment regimens depend on the genetic diagnosis of affected individuals. Of the known mutated genes, *KCNE2* is associated with LQT6. *KCNE2* encodes the beta-subunit of potassium ion channel proteins. These proteins contain cytoplasmic C-terminal domains in which many mutations have been identified.

We hypothesize that genes encoding KCNE2-interacting proteins might be identified as disease-causing or modifying genes. The present study aimed to use yeast two-hybrid (Y2H) methodology to screen a pre-transformed cardiac cDNA library in order to identify putative interactors of the C-terminal of KCNE2. Through specific selection methods the number of KCNE2 ligands was reduced from 296 to 83. These interactors were sequenced and 14 were identified as putative interacting proteins. False positive ligands were excluded based on their function and subcellular location. Ultimately three strong candidate ligands were selected for further analysis: Alpha-B crystallin (CRYAB), Filamin C (FLNC) and voltage-dependent anion-selective channel protein 1 (VDAC1). Three-dimensional (3D) co-localization and co-immunoprecipitation were used to verify these proposed interactions and succeeded in doing so.

The genes encoding verified interactors will be screened in our SA panel of LQT patients, to potentially identify novel LQT causative or modifying genes. Furthermore, the interactions verified in the present study may shed some light on the mechanism of pathogenesis of LQT causative mutations in *KCNE2*.

Opsomming

Lang QT-sindroom (LQTS) is 'n hart her-polariserende siekte wat elke 1:2000-1:3000 individue affekteer. Hierdie siekte word gekenmerk deur 'n lang QT-interval op die oppervlak elektrokardiogram (EKG) van pasiënte. Simptome van LQTS wissel van duiseligheid en floutes tot meer ernstige simptome soos stuiptrekkings of aanvalle en skielike kardiale dood (SKD). Kliniese kenmerke van LQTS is 'n gevolg van die neerslag van Torsades de Pointes; 'n polimorfiese vorm van ventrikulêre tagikardie. Verskeie genetiese vorms van LQTS is geïdentifiseer met meer as 700 mutasies in 12 verskillende gene wat lei tot siekte patogenese. Dit is ergter beraam dat ongeveer 25% van pasiënte met dwingende LQTS geen mutasies in die bekend LQT gene besit nie. Dit is problematies aangesien siekte behandeling af hang van die genetiese diagnose van geaffekteerde individue. Een van die bekende gemuteerde gene is *KCNE2* wat verband hou met LQT6. *KCNE2* kodeer die beta-subeenheid van kalium ioonkanaal proteïene. Hierdie proteïene bevat sitoplasmiese C-terminale waarin baie mutasies alreeds geïdentifiseer is.

Ons veronderstel dat gene wat proteïene kodeer wat met KCNE2 interaksie toon, geïdentifiseer kan word as siekte veroorsaakende of wysigings gene. Die huidige studie het die gis twee-hibried metode gebruik om 'n vooraf-getransformeerde hart cDNS biblioteek te sif om vermeende protein interaksies van die C-terminaal van KCNE2 te identifiseer. Deur middel van seleksie metodes is die aantal KCNE2 ligande verminder van 296 tot 83. Die identiteit van die proteïene is bekend gemaak deur volgorderbepaling waarna 14 geïdentifiseer is as proteïene wat moontlik interaksie kan toon met KCNE2. Vals positiewe ligande is uitgesluit op grond van hul funksie en subsellulêre lokasering. Drie kandidaat ligande is gekies vir verdere analise: Alfa-B crystallin (CRYAB), Filamin C (FLNC) en spanning-afhanklike anioon-selektiewe kanaal proteïen 1 (VDAC1). Drie-dimensionele (3D) mede-lokalisering en mede-immunopresipitasie tegnieke is gebruik om hierdie voorgestelde interaksies te verifieer en het geslaag om dit te doen.

Die gene wat geverifieerde proteïene kodeer, sal gekeur word in ons Suid-Afrikaanse paneel van LQT pasiënte om sodoende potensieel nuwe LQT veroorsakende of wysigings gene te identifiseer. Verder kan die geverifieer interaksies in die huidige studie lig werp op die meganisme van die ontstaan van LQT veroorsakende mutasies in *KCNE2*.

Index

	Page
Acknowledgements	**vi**
List of abbreviations	**vii**
List of figures	**xiii**
List of tables	**xv**
Chapter 1: Introduction	**1**
Chapter 2: Materials and methods	**39**
Chapter 3: Results	**73**
Chapter 4: Discussion	**90**
References	**116**
Appendix I: Reagents	**133**
Appendix II: Vectors	**141**
Appendix III: Calculations	**143**
Appendix IV: Aligned sequence of *KCNE2*	**144**
Appendix V: Tables of primary and secondary clones	**145**
Appendix VI: Prokaryotic and eukaryotic phenotypes	**174**
Appendix VII: List of suppliers	**175**

Acknowledgements

It is with great pleasure that I acknowledge the following individuals who have actively contributed to this thesis.

I would like to thank my supervisor, Dr Craig Kinnear for all his support and guidance throughout the course of my thesis. You were a dedicated, inspiring project leader, but also a kind and thoughtful friend who could make (and take) a joke to lighten my sometimes anxious mood. Thank you for all the effort and intellectual input you contributed towards my thesis. You encouraged me to persist and I could not have asked for a better supervisor.

I would like to express my gratitude towards Mrs Jomien Mouton. You supported me from my first day in the laboratory up to the last word of this thesis. Even though you had your own project to worry about you always made time for me. You taught me the majority of the techniques I know today and without your assistance, attention and knowledgeable input this thesis would not be possible. Over the years you became not only an amazing mentor but a very dear friend who made the difficult days a little easier.

I also owe thanks to Mrs Carin de Villiers for performing the initial yeast two-hybrid screen and for all the helpful intellectual input toward this project. I would also like to thank Mrs Susan Cooper for her assistance with the confocal microscope.

This study would not have been possible without the financial support from the Harry Crossley Foundation, SU/CSIR and the Stella and Paul Loewenstein Charitable and Educational Trust.

To my fellow students (especially Juanelle du Plessis and Brigitte Glanzmann); I would like to thank you for your kind support. You were always there to listen and give advice on a professional, but more importantly, a personal level. Without you the past few years would certainly have been much more challenging.

To my loving parents (Junita and Kobus), sisters (Heloïse and Amor) and boyfriend (Briaan Cooper); you are precious and irreplaceable people in my life and I thank you for your devoted and caring support over the past few years.

Finally, I would like to thank God for blessing me with amazing family and friends and for giving me the opportunity and strength to persevere.

List of abbreviations

#	Number
3-AT	3-Amino-1, 2, 4-triazole
3D	Three-dimensional
µg	Microgram
µl	Microlitre
A	Alanine
aa	amino acid
AD	Activation domain
Ade	Adenine
ABP	Actin binding protein
ACTC1	Actin, cardiac isoform 1
ADE2	Phosphoribosylaminoimidazole carboxylase gene
Amp	Ampicillin
ANK2	ankyrin 2, neuronal
AKAP9	A kinase (PRKA) anchor protein (yotiao) 9
ATCC	American type culture collection
AV	Atrioventricular
BCL2L1	BCL2-like 1
BCKDK	Branched-chain alpha-ketoacid dehydrogenase kinase
BD	Binding domain
BLAST	Basic local alignment search tool
BLASTN	Basic local alignment search tool (nucleotide)
BLASTP	Basic local alignment search tool (protein)
bp	Base pair
BSA	Bovine serum albumin
C	Cytosine
ºC	Degree Celsius
Ca^{2+}	Calcium

CACNA1c	calcium channel, voltage-dependent, L type, alpha 1C subunit
CAV3	Caveolin 3
cDNA	Complementary DNA
cfu	Colony forming units
CIAP	*Calf intestinal alkaline phosphatase*
cm^2	Square centimeter
Co.	Company
CO_2	carbon dioxide
Co-IP	Co-immunoprecipitation
COL1A1	Collagen, type 1, alpha 1
Corp.	Corporation
CRYAA	Alpha-A crystallin
CRYAB	Alpha-B crystallin
CRYBB2	Beta-B2 crystallin
C-terminal	Carboxyl terminal
cTnC	Troponin C, cardiac isoform
cTnI	Troponin I, cardiac isoform
cTNT	Troponin T, cardiac isoform
Da	Daltons
dATP	Deoxy-adenosine triphosphate
DCM	Dilated cardiomyopathy
dCTP	Deoxy-cytosine triphosphate
ddH_2O	Distilled deionised water
dGTP	Deoxy-guanosine triphosphate
DMEM	Dulbecco's modified eagle media
DMSO	Dimethyl sulphoxide
DNA	Deoxyribonucleic acid
DRM	Desmin-related myopathy
dNTP	Deoxy-nucleotide triphosphate
dTTP	Deoxy-thymine triphosphate

E.coli	*Escherichia coli*
ECG	Electrocardiogram
EDTA	Ethylene-diamine-tetra-acetic acid
ER	Endoplasmic reticulum
FLNA	Filamin A, alpha
FLNB	Filamin B, beta
FLNC	Filamin C, gamma
G	Guanine
g	grams
GAPDH	Glyceraldehyde-3-phosphate dehydrogenase
GER	Germany
GSN	Gelsolin
HA	Haemagglutinin
HCN1	hyperpolarization activated cyclic nucleotide-gated potassium channel 1
HCN2	hyperpolarization activated cyclic nucleotide-gated potassium channel 2
HERG	Human Eag-related gene
His	Histidine
HIS3	Histidine 3 gene
HK	Hong Kong
HRP	Horseradish peroxidase
HSP	Heat shock protein
HSPB1	Heat shock protein, beta 1
HSPB2	Heat shock protein, beta 2
HSPB8	Heat shock 22kDa protein 8
I-band	Isotropic band
ICD	Implantable cardioverter defibrillator
Inc.	Incorporated
Ig	Immunoglobulin
I_{kr}	Rapid component of delayed rectifier potassium current
I_{Ks}	Slow component of delayed rectifier potassium current

JP	Japan
K^+	Potassium
kb	Kilo bases
KCND2	Voltage-gated potassium channel, subfamily D, member 2
KCNE1	Voltage-gated potassium channel, subfamily E, member 1
KCNE2	Voltage-gated potassium channel, subfamily E, member 2
KCNE3	Voltage-gated potassium channel, subfamily E, member 3
KCNH2	Voltage-gated potassium channel, subfamily H (eag-related), member 2
KCNJ2	Potassium inwardly-rectifying channel, subfamily J, member 2
KCNQ1	Voltage-gated potassium channel, KQT-like subfamily, member 1
kDa	Kilo Dalton
L	Litre
LB	Luria-Bertani broth
LCSD	Left cardiac sympathetic denervation
Leu	Leucine
LiAC	Lithium acetate
Log	Logarithm
LQTS	Long QT syndrome
Ltd.	Limited
LV	Left ventricular
Lys	Lysine
M	Molar
MCS	Multiple cloning site
MEL1	Alpha galactosidase gene
MFM	Myofibrillar myopathy
mg	Milligram
$MgCl_2$	Magnesium chloride
MiRP1	MinK-related peptide 1
mink	Minimal potassium subunit
ml	Millilitre

mM	Millimolar
mRNA	Messenger ribonucleic acid
mV	Millivolt
MYOM1	Myomesin 1
Na^+	Sodium
NCBI	National Centre for Biotechnological Information
NIT2	Nitrilase family member 2
NL	The Netherlands
nm	nanometer
N-terminal	Amino terminal
O_2	Oxygen
OD	Optical density
OMM	Outer mitochondrial membrane
ORF	Open reading frame
PBS	Phosphate buffered saline
PCI	Phenol/chloroform/isoamyl alcohol
PCR	Polymerase chain reaction
PEG	olyethylene glycol
PIPES	Piper-N, N-bis (2-ethanesulfonic acid,) 1.5 Sodium
PKC	Protein kinase C
PMSF	Phenylmethylsulphonyl fluoride
POMP	Proteasome maturation protein
PTPRK	Protein tyrosine phosphatase, receptor type Kappa
QDO	Quadruple dropout
QTc	Corrected QT
RCM	Restrictive cardiomyopathy
RNA	Ribonucleic acid
RSA	South Africa
rpm	Revolutions per minute
SA	Sinoatrial

SB	Sodium borate
SCD	Sudden cardiac death
S.cerevisiae	*Saccharomyces cerevisiae*
SCN5A	Voltage-gated sodium channel alpha subunit, type 5
SD	Single dropout
SDS	Sodium dodecyl sulphate
SDS-PAGE	Sodium dodecyl sulphate polyacrylamide gel electrophoresis
sHSP	Small heat shock protein
SIDS	Sudden infant death syndrome
SNP	Single nucleotide polymorphism
STON1	Stonin protein 1
T	Thymine
Ta	Annealing temperature
TBST	Tris-buffered saline Tween-20
TDO	Triple dropout
TPM3	Tropomyosin 3
tRNA	Transfer ribonucleic acid
Trp	Tryptophan
TTN	Titin protein
TW	Taiwan
USA	United States of America
Ura	Uracil
UK	United Kingdom
UV	Ultraviolet
VDAC1	Voltage-dependent anion-selective channel protein 1
www	World wide web
Y2H	Yeast two-hybrid
YPDA	Yeast peptone dextrose adenine

List of figures

Figure 1.1: Ion flow in action potential.

Figure 1.2: Contraction of cardiac muscles through cross-bridge formation.

Figure 1.3: The electrical conduction system of the heart.

Figure 1.4: Schematic diagram of normal sinus rhythm for a human heart as seen on an ECG.

Figure 1.5: Illustration of the prolonged QT interval on an electrocardiogram (ECG).

Figure 1.6: Ion channels in cardiac cells associated with LQTS.

Figure 1.7: The structure of a typical voltage-gated cardiac ion channel.

Figure 1.8: Inheritance lines of the *KCNQ1*-A341V mutation from the common founder couple.

Figure 1.9: A figure representing the KCNE2 transmembrane protein and three known N-teminal domain mutations.

Figure 1.10: KCNE2 genomic and protein sequence

Figure 1.11: Schematic representation of proposed trafficking and association of KCNE1, KCNE2 and HERG.

Figure 1.12: *KCNE2* mutations mapped onto a representation of the transmembrane protein.

Figure 2.1: Summery of methodology followed in the present study.

Figure 2.2: An illustration of a Yeast two-hybrid system.

Figure 2.3: Representation of a Haemocytometric counting chamber

Figure 3.1: Linear growth curve of the yeast strain AH109 transformed with either pGBKT7-*KCNE2* bait construct or a non-recombinant pGBKT7 plasmid.

Figure 3.2: Interaction specificity testing through heterologous mating of baits and prey plasmids.

Figure 3.3: Fluorescent imaging and co-localization analysis of KCNE2 and CRYAB in differentiated H9C2 cardiomyocytes.

Figure 3.4: Fluorescent imaging and co-localization analysis of KCNE2 and FLNC in differentiated H9C2 cardiomyocytes.

Figure 3.5: Fluorescent imaging and co-localization analysis of KCNE2 and VDAC1 in differentiated H9C2 cardiomyocytes.

Figure 3.6: Co-immunoprecipitation of KCNE2 with prey proteins CRYAB, FLNC and VDAC1.

Figure 4.1: Structural domains of human HSP27, HSP22 and αB crystallin proteins.

Figure 4.2: Predicted association between KCNE2 and CRYAB proteins.

Figure 4.3: Structure of the human Filamin C protein.

Figure 4.4: Predicted association between KCNE2 and FLNC proteins.

Figure 4.5: Secondary structure of VDAC1

Figure 4.6: Schematic representation of KCNE2 transmembrane protein

Figure 4.7: Schematic diagram of the Kv channel organization.

Figure 4.8: Predicted association between KCNE2 and VDAC1 proteins.

List of tables

Table 1.1: The suggested Bazzet-corrected QTc values (in ms) for prolonged QT diagnosis

Table 1.2: Long QT syndrome diagnostic criteria

Table 1.3: High-risk subsets for aborted cardiac arrest or sudden cardiac death by age

Table 1.4: Genes associated with specific subtypes of Long QT Syndrome

Table 1.5: Stressors associated with some of the more common types of LQTS

Table 2.1: Nucleotide sequences of primers used to amplify the C-terminal of *KCNE2*

Table 2.2: Primers used for sequencing inserts from Y2H cloning vectors

Table 2.3: DNA ligation reaction ratios

Table 2.4: Standard Trypsin volumes for detachment of cells from growth surface

Table 2.5: Different nutritional selection plates for the yeast strains AH109 and Y187

Table 2.6: List of primary and secondary antibodies and their optimized concentrations used in Co-immunoprecipitation as well as Western blot assays

Table 2.7: List of primary and secondary antibodies and their optimized concentrations used in co-localization assays

Table 3.1: Effect of the pGBKT7-*KCNE2* bait construct on AH109 mating efficiency

Table 3.2: Library mating efficiency as established by progeny colonies on growth selection media

Table 3.3: Grouping of primary and secondary clones based on the x-α-galactosidase colour production and intensity

Table 3.4: Identification of primary putative interactor clones from Y2H screen

Table 3.5: Identification of secondary putative interactor clones from Y2H screen

Table 3.6: Comparison of coefficients used to quantify co-localization analysis

Table 3.7: Quantification of co-localization for the interaction between KCNE2 and CRYAB proteins

Table 3.8: Quantification of co-localization for the interaction between KCNE2 and FLNC proteins

Table 3.9: Quantification of co-localization for the interaction between KCNE2 and VDAC1 proteins

Chapter 1

Introduction

	Page
1.1 THE HEART	**2**
1.1.1 Mechanism of cardiac muscle contraction	**2**
1.1.2 Electrocardiography (ECG)	**5**
1.2 LONG QT SYNDROME	**7**
1.2.1 Long QT Syndrome (LQTS) – a cardiac ion channel disorder	**7**
1.2.2 Classification and diagnosis of Long QT syndrome	**9**
1.2.3 Risk assessment	**12**
1.2.4 Therapeutic approaches	**13**
1.2.5 Genetics of LQTS	**14**
1.3 SOUTH AFRICAN FOUNDER FAMILY	**21**
1.4 GENETIC MODIFIERS	**23**
1.4.1 Genetic modifiers of LQTS	**23**
1.5 KCNE2 POTASSIUM ION CHANNEL	**29**
1.5.1 KCNE2 genomic structure	**29**
1.5.2 KCNE2 protein structure	**30**
1.5.3 KCNE2 trafficking and interacting proteins	**33**
1.5.4 KCNE2 channel dysfunction and LQTS	**35**
1.6 PRESENT STUDY	**37**

1.1 THE HEART

1.1.1 Mechanism of cardiac muscle contraction

The heart is the primary organ responsible for the supply of blood and oxygen to all the parts of the body. This organ is composed of involuntary striated muscles known as the myocardium which contain cardiac ion channels enabling the heart to contract. This allows the synchronization of every heart beat (Glaaser et al. 2003).

At rest, all myocardial cells have a negative membrane potential at approximately -70mV that will change with stimulation by electrical signals. This causes opening of the voltage-gated ion channels and subsequent influx of positively charged calcium and sodium ions (Ca^{2+} and Na^{+}) into the cardiac muscle cells. The cell membrane undergoes rapid depolarization due to the membrane potential becoming either more positive or less negative (Figure 1.1) (Glaaser et al. 2003).

At diastolic levels of intracellular Ca^{2+}, the troponin I in the troponin complex, which is composed of cardiac troponin T (cTnT), cardiac troponin I (cTnI) and cardiac troponin C (cTnC), inhibits the interaction between myosin and actin. The binding of Ca^{2+} to cTnC during systole induces conformation changes that relieve the inhibitory effects of cTnI; thereby promoting the formation of actomyosin cross bridges (Figure 1.2) (Parmacek and Solaro 2004). This ultimately leads to the power stroke when actin filaments slide past the myosin filaments resulting in cardiac muscle cell contraction (Figure 1.2) (Parmacek and Solaro 2004; Pinnell et al. 2007).

Repolarization follows directly afterwards, changing the membrane potential back to a more negative value which causes the cell to return to its resting state. This occurs as a result of the opening of fast acting potassium (K) channels and efflux of K ions (K^{+}) out of the cell (Figure 1.1). Following this, the slow K channels are opened, thus releasing excess K^{+} from the cell (Glaaser et al. 2003). At the same time the Ca^{2+} channels will close.

In order for the muscle cells to be able to contract again, it is necessary for the concentrations of K^{+} and Na^{+} to be restored to their original resting potential state by means of K^{+}/Na^{+} pumps in the sarcolemma (Xu 2013). The duration of this event, which is more commonly known as the refractory period, is much longer for cardiac muscle than for skeletal muscle and plays a role in

preventing prolonged cardiac muscle contraction. The refractory period is important to ensure sufficient time between each contraction, allowing the heart chambers to be filled with blood before the next contraction (Pinnell et al. 2007).

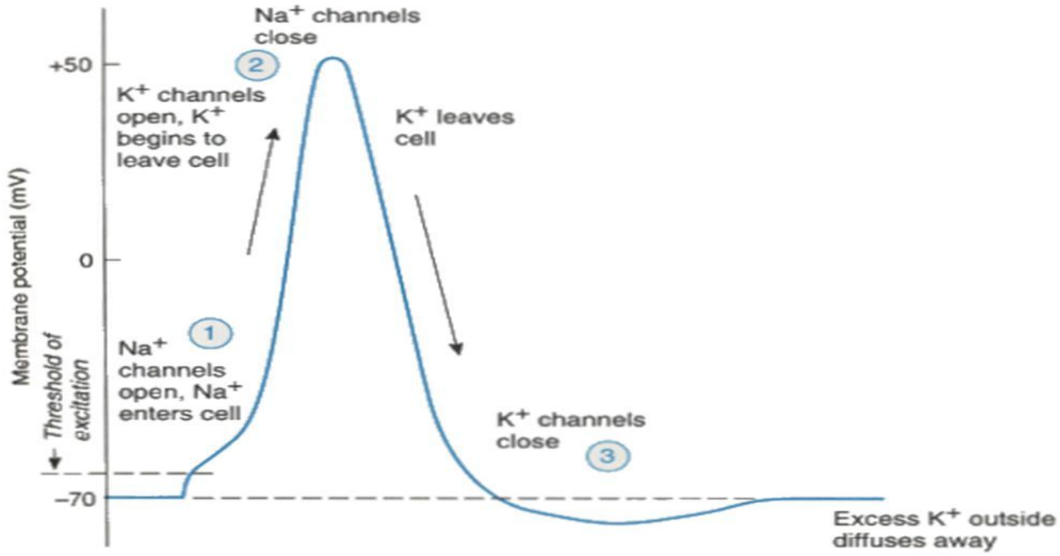

Figure 1.1: Ion flow in action potential. 1) Depolarization where Na^+ channels opens releasing Na^+ into the cell. 2) Repolarization where Na^+ channels are closed and K^+ channels are opened, causing K^+ ions to leave the cell. 3) K^+ channels close. Figure taken from: http://www.mindcreators.com/neuronbasics.htm

The contraction of the myocardium occurs spontaneously and is controlled by the sinoatrial (SA) node (Figure. 1.3) which is the impulse-generating tissue located in the right atrium of the heart (Rastogi 1997; Starr et al. 2010). Once the impulse reaches the atrioventricular (AV) node (Figure 1.3), the contraction spreads towards the ventricles and enters the ventricular septum where the action potential is conducted through the bundle of His (Figure 1.3) (Rastogi 1997; Starr et al. 2010).

This bundle then separates into two branches that connect with Purkinje fibres and the endocardium. Ultimately, the action potential reaches the ventricular myocardium (Rastogi 1997; Starr et al. 2010). It is this excitation wave spreading over the heart that causes cardiac myocyte membrane depolarization (Clancy 2005; Pinnell et al. 2007).

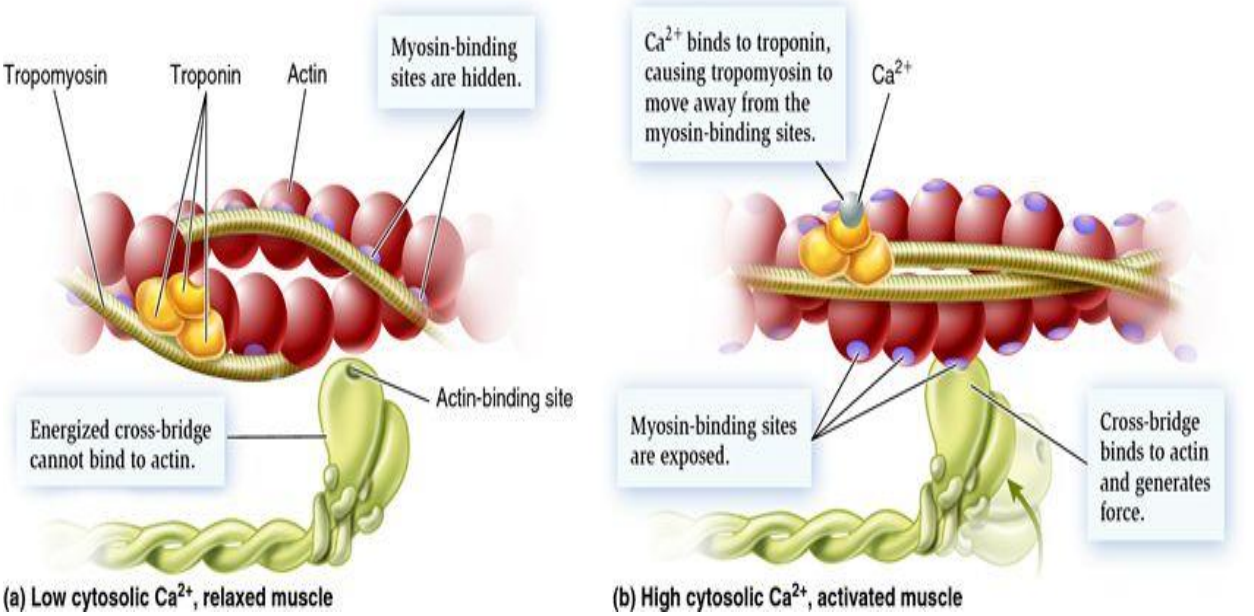

Figure 1.2: Contraction of cardiac muscles through cross-bridge formation. a) When Ca^{2+} levels are low, the myosin binding sites are blocked by tropomyosin. b) With increase in cytosolic Ca^{2+} levels, Ca^{2+} binds to troponin which will release the myosin-binding sites on actin, allowing cross-bridge formation of actin and myosin. Figure taken from: http://biology-forums.com/gallery/.jpeg

The heart has previously been described as a functional syncytium that allows electrical impulses to be passed between cells in close proximity through gap junctions; causing the myocardium to function as a single contractile unit (Spach and Starmer 1995; Stein 2008). Gap junctions are intercellular connections between cells, connecting the cytoplasm of adjacent cells allowing free movement of ions and molecules (<1000Da) from one cell to the other (Kelsell et al. 2001). This makes it possible for the myocardium to depolarize quickly and efficiently thus aiding in contraction of the heart.

The contractility may however be compromised, resulting in damaging effects to the heart should there be aberrant electric signals and incorrect signalling between the gap junctions (Spach and Starmer 1995; Stein 2008). For example: if the gap junctions close incorrectly after an episode of myocardial infarction it will lead to tissue damage which ultimately hinders the tissue from participating in the synchronous contraction of the myocardium - thus causing an irregular heart rhythm (Spach and Starmer 1995; Glaaser et al. 2003).

Defects in cardiac ion channels would lead to defects in ion currents that will result in the variation in duration and degree of excitation as well as plateau phases during depolarization and repolarization (Glaaser et al. 2003). This irregular beating of the heart results in arrhythmia or arrhythmic disorders leading to syncope, seizures and sudden cardiac death (SCD) (Lehnart et al. 2007; Schwartz et al. 2008).

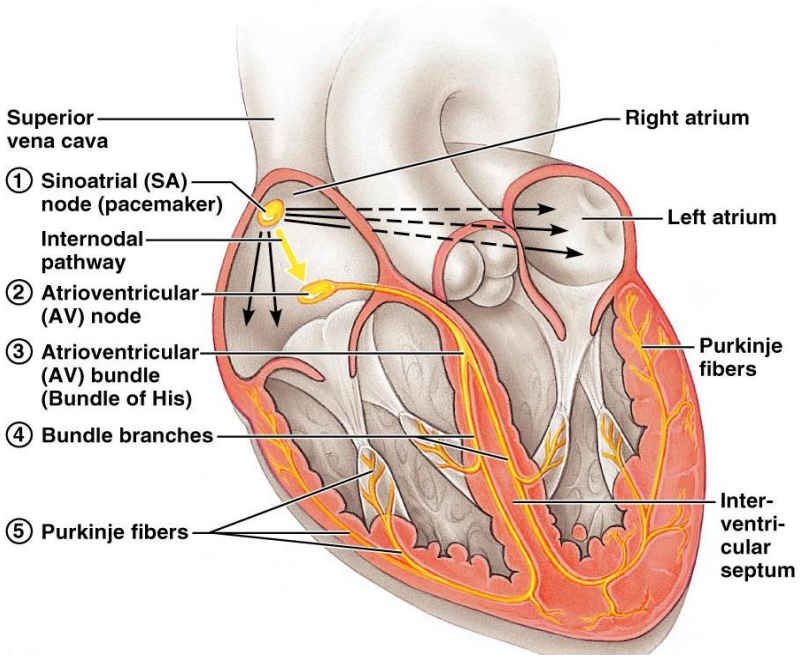

Figure 1.3: The electrical conduction system of the heart. Electrical impulses start at the SA node and run through the atria into the AV node. The signal causes the atria to contract after which the action potential is spread through the Bundle of His branching left and right. Ultimately the ventricles also contract. Figure taken from: http://kakistudy.blogspot.com/2011/03/heartbeat-mechanism.html

1.1.2 Electrocardiography (ECG)

Electrocardiography (ECG) is a transthoracic, non-invasive diagnostic tool used to interpret the electrical activity of the heart over a period of time. The basic principle of an electrocardiogram (ECG) involves the recording of electrical impulses during each phase of the cardiac cycle. These impulses are detected by electrodes attached to the surface of the skin (Glaaser et al. 2003; Becker 2006).

A typical EGC tracing of a cardiac cycle consists of a P wave that represents arterial depolarization (Figure 1.4), a QRS complex that reflects ventricular depolarization (Figure 1.4)

as well as a T wave which is an indicator of ventricular repolarization (Figure 1.4) (Becker 2006).

Under normal physiological circumstances, in healthy individuals, the heart beats between 60-100 times per minute (bpm). This is referred to as the normal sinus rhythm (Pinnell et al. 2007).

When looking at the representation of an ECG (Figure 1.4), one can see the QRS complex, the P wave peaking before each QRS complex, the P-R interval as well as the T wave, all in normal range and duration. These parameters are used as indicators to determine whether the electrical signal was correctly generated by the SA node and is moving at a normal rate through the heart (Glaaser et al. 2003; Becker 2006).

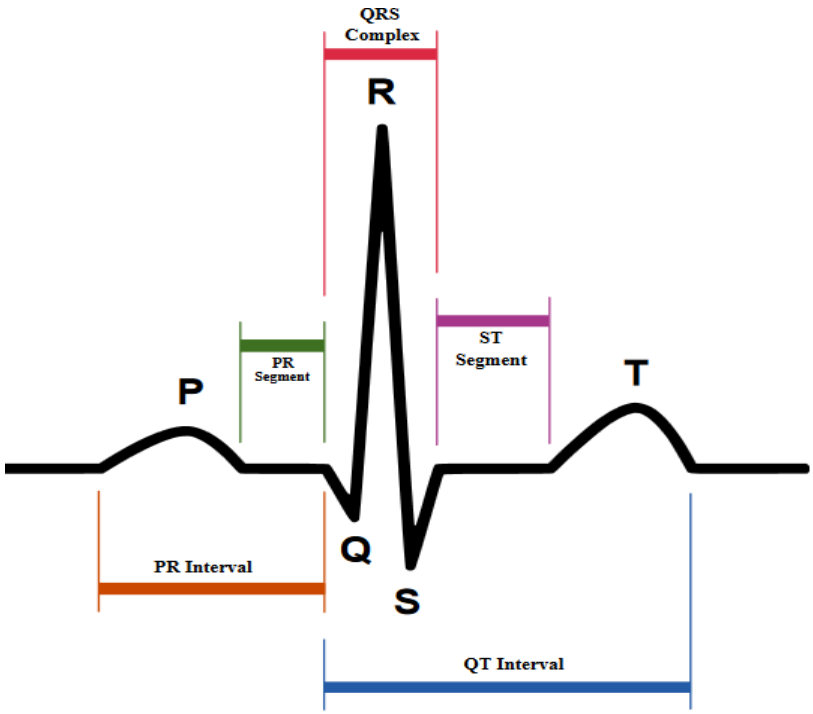

Figure 1.4: Schematic diagram of normal sinus rhythm of a human heart as seen on an ECG. The P-wave is a result of atrial depolarization. The QRS complex is the average of depolarization waves of the inner and outer cardiomyocytes. The T-wave resembles the repolarization of ventricles. Figure created by Agateller (Anthony Atkielski). Figure taken from: https://en.wikipedia.org/wiki/QRS_complex

Changes in the duration and magnitude of the action potential may be due to a number of factors, some of which include changes in cell-to-cell interaction, inherited ion channel defects and

therapeutic interference. These changes will be recorded and interpreted as inconsistencies on an ECG (Shimizu and Antzelevitch 1997; Gima and Rudy 2002; Clancy 2005).

Previous studies indicated that alterations in the QRS complex cause conduction defects, with expansion of this complex resulting in reduction of conduction velocity. This is thought to be a result of defective ion channels (Tan et al. 2001; Clancy 2005).

Additional abnormalities can be detected by ECGs such as the prolongation of QT intervals (Figure 1.5). This phenomenon occurs as a result of prolonged action potential generated in the heart, causing repolarization to be delayed. The longer QT intervals may ultimately change the morphology of the T wave. Thus, individuals with abnormal ECG findings are at higher risk for developing life threatening arrhythmias which are closely associated with sudden cardiac death (SCD) (Priori et al. 1997; Shimizu and Antzelevitch 1999; Schwartz et al. 2001).

Moreover, many of these fatal arrhythmic episodes have been found to be dependent on heart rate. Therefore, abrupt deviations in the normal heart rate due to exercise or auditory stimulation at rest, for example, may result in such arrhythmic events (Schwartz et al. 2001; Glaaser et al. 2003).

To date a number of diseases have been associated with such life threatening cardiac arrhythmic episodes such as cardiomyopathy (Elliott et al. 2008), myocarditis (Feldman and McNamara 2000) and Long QT syndrome (Schwartz et al. 2008) to name a few. However, in the present study we will be focussing on the last mentioned disease (Long QT syndrome).

1.2 LONG QT SYNDROME

1.2.1 LQTS – a cardiac ion channel disorder

Long QT syndrome (LQTS) has an estimated prevalence of 1:2000 – 1:3000 (Schwartz 2009; Schulze Bahr 2012) and can either be inherited or acquired, with the latter believed to be induced by therapeutic intervention for treating ventricular arrhythmias but also other disorders not related to cardiac arrhythmic diseases (Sanguinetti et al. 1995; Moric-Janiszewska 2012). However, this acquired form of LQTS may also manifest as a result of electrical or structural abnormalities caused by other cardiac disorders such as cardiomyopathies and cardiac ischemia (Glaaser et al. 2003; Clancy 2005).

Long QT syndrome has been described as an arrhythmogenic ion channel disorder, characterized by abnormal ventricular repolarization, ultimately resulting in QT interval prolongation in otherwise healthy young individuals (Figure 1.5) (Vincent 1998; Ackerman and Clapham 1997; Gordon et al. 2007; Schwartz 2009). This may result in episodes of malignant ventricular tachycardia or arrhythmia, known as Torsades de Pointes (TdP), as well as SCD (Sanguinetti et al. 1995; Schwartz et al. 2008).

The first report of LQTS was published in 1957 by Anton Jervell and Fred Lange-Nielsen, who described LQTS in combination with congenital neuronal deafness and episodes of syncope (Jervell and Lange-Nielsen 1957). A number of years later, in 1964, Romano and Ward described a similar cardiac condition with symptoms such as recurring syncope, prolongation of the QT interval as well as a family history of sudden death, but without the feature of congenital neuronal deafness (Romano et al. 1963; Ward 1964).

Later it became evident, through research and genetic analyses, that this genetic disorder described by Jervell and Lange-Nielsen with symptoms including congenital neuronal deafness, was a result of homozygous mutations. This resulted in severe phenotypes and high risk for SCD (Medeiros-Domingo et al. 2007a).

The syndrome described by Romano and Ward (Romano-Ward syndrome) on the contrary, was due to the presence of heterozygous mutations which did not result in deafness, but displayed variable disease severity. This meant that patients with one or more disease-causing mutation in more than one gene, had a more severe phenotype than patients with a single gene mutation, placing the aforementioned affected individuals at higher risk for SCD (Brink et al. 2005).

The clinical features of LQTS are also extremely variable. Patients can be asymptomatic, develop reoccurring seizures and syncope, or in the worst case, present with SCD (Medeiros-Domingo et al. 2007a).

It is thought that the clinical variability of LQTS is due to incomplete penetrance of underlying mutations, functional status of interacting genes, age, gender, environmental factors (such as food and poison) as well as therapeutic interventions (Abbott 1999; Lehnart et al. 2007).

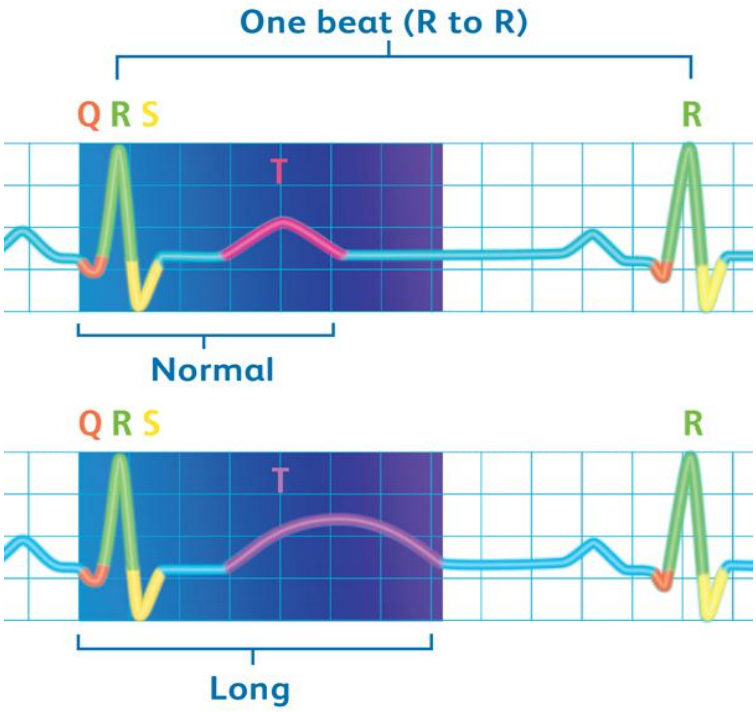

Figure 1.5: Illustration of the prolonged QT interval on an electrocardiogram (ECG). The QRS complex is the average of the depolarization waves from all the cardiac cells. The distance between the consecutive R-peaks in the QRS complex represents one heartbeat. The QT interval of individuals with Long QT syndrome will be longer (bottom figure) as compared to the QT intervals of unaffected individuals (top figure). Adapted from: http://www.genedx.com/wp-content/uploads/2010/12/LQT.jpg

As mentioned previously, some of the subtypes of LQTS are known to have a more severe phenotype and it has been reported that in 10-15% of lethal cases, SCD was the first and final symptom of the patients (Vincent 1998; Goldenberg et al. 2006).

1.2.2 Classification and diagnosis of Long QT syndrome

The diagnosis of LQTS is based on the clinical and family history of individuals as well as the ECG results. The ECG measurement of the QT interval in patients is absolutely essential for the accurate diagnosis of LQTS. The interval should be measured and calculated as a mean value of at least three cardiac cycles from the QRS complex to the end of the T wave (Goldenberg et al. 2008) (Figure 1.2). A formula known as the Bazett formula ($QT = QT/\sqrt{RR}$; [RR being the interval from the onset of one QRS complex to the onset of the next QRS complex, measured in seconds]) is used to correct the QT interval (QTc) for heart rate which differs between males and females (Table 1.1).

It is standard practice to use the longest QT interval when evaluating the patient for LQTS. When it is found that the QT interval is notably prolonged (Figure 1.5) the diagnosis is undeniable, particularly when it is accompanied by a positive clinical and family history (Goldenberg et al. 2006).

Table 1.1: The suggested Bazzet-corrected QTc values (in ms) for prolonged QT diagnosis

Long QT rating	1-15 yrs	Adult male	Adult female
Normal	< 400	< 430	< 450
Borderline	440 – 460	430 – 450	450 – 470
Prolonged	> 460	> 450	> 470

Abbreviations: <, less than; >, more than; ms, milliseconds; yrs, years. Table adapted from: Goldenberg et al. 2006.

Family history of symptoms such as syncope and a prolonged QT interval both play a vital role in the diagnosis of LQTS as this disease is known to segregate within families (Schwartz 2009). In order to simplify the diagnosis, Schwartz and colleagues developed a scoring system (Table 1.2) which is based on personal and available family history as well as symptoms and ECG findings (Schwartz 1993; Schwartz 2012).

Misdiagnosis of LQTS in Africa is not uncommon and exists as result of a number of reasons. These range from a lack of communication which include language and cultural obstructions or the high incidence of infectious diseases (such as Tuberculosis and HIV), and poverty causing famine and early death which masks rare diseases such as LQTS (Brink and Corfield 2009).

Another possible reason for the misdiagnosis and/or mismanagement of disease such as LQTS and other similar diseases is the relatively poor medical infrastructure in rural areas of South Africa and Africa in previous years.

However, the South African Medical Research Council (MRC) has published an annual report 2011/2012 which includes the mandate of the Centre for Molecular and Cellular Biology (CMCB) to improve research on multifactorial disorders (for example cancer) as well as infectious diseases such as Tuberculosis (http://www.mrc.ac.za/annualreport/annualreport1112.pdf).

Table 1.2: Long QT syndrome diagnostic criteria

			Points
	Electrocardiographic findings[#]		
A	QTc *	≥ 480ms	3
		460-479ms	2
		450-459(male)ms	1
B	QTc * 4th minute of recovery from exercise stress test ≥480ms		1
C	Torsades de Pointes (TdP) **		2
D	T wave alternans		1
E	Notched T wave in 3 leads		1
F	Low heart rate for age[†]		0.5
	Clinical History		
A	Syncope **	With stress	2
		Without stress	1
B	Congenital deafness		0.5
	Family History		
A	Family members with definite LQTS[‡]		1
B	Unexplained sudden cardiac death below age 30 among immediate family members[‡]		0.5

[#] In the absence of medications or disorders known to affect these ECG features
[*] QTc calculated by Bazzet's formula where QTc = QT/√RR
[**] Mutually exclusive
[†] Resting heart rate below the second percentile for age
[‡] The same family member cannot be counted in **A** and **B**

Score	
≤ 1 point	Low probability of LQTS
1.5 – 3 points	Intermediate probability of LQTS
≥ 5 points	High probability of LQTS

Abbreviations: <, less than; ≤, less than or equal to; LQTS, Long QT Syndrome; >, more than; ≥, more than or equal to; ms, milliseconds; QTc, corrected QT interval. Table adapted from: Schwartz 1993; Schwartz 2012.

1.2.3 Risk assessment

In 2008, Goldenberg and co-workers identified a set of risk factors for symptoms such as SCD, in individuals with LQTS. However, these risk factors only serve as a baseline reference and the most useful predictor of lethal cardiac events in LQTS still remains the family history as well as the patients' history of syncope, other cardiac events such as aborted cardiac arrest (ACA) and a QTc of >500ms (Table 1.3) (Goldenberg et al. 2008).

Table 1.3: High-risk subsets for aborted cardiac arrest or sudden cardiac death by age

Age	High risk subsets
Childhood (1-12 years)	Males with prior syncope and/or QTc > 500ms Females with prior syncope
Adolescence (13-20 years)	Males and females with either 1, 2 or more of the following: QTc ≥ 530ms ≥ 1 episode of syncope in the past year ≥ 2 episodes of syncope in the past 2-10 years
Adulthood (21-40 years)	Possess 1 or more of the following: Female gender Interim syncope after age 18 years QTc ≥ 500ms
41-60 years	Possess 1 or more of the following: Female gender Syncope in the past 10 years QTc ≥ 500ms LQTS3 genotype
61-75 years	Syncope in the past 10 years

Abbreviations: LQTS, Long QT Syndrome; ≥, more than or equal to; ms, milliseconds; QTc, corrected QT interval. Table adapted from: Goldenberg et al. 2008.

In 2006 Goldenberg and colleagues presented evidence that most affected individuals in their study cohort who experienced at least one cardiac event during early childhood had elevated risk for experiencing SCD (Goldenberg et al. 2006). This emphasized the importance of a patients' history of cardiac events. It was also reported that of the 44 patients included in this investigation, half died at least one or two decades after experiencing their first cardiac event, implying a continuous risk for LQTS patients. These tragedies come to pass despite 88% of patients receiving beta-blocker therapy (Goldenberg et al. 2006).

1.2.4 Therapeutic approaches

There are a number of therapeutic approaches and management strategies available for individuals affected by LQTS; some of which include pharmacological therapy, implanted cardioverter defibrillators (ICD), surgical approaches, and lifestyle changes. Moreover, in inherited forms of the disease, the treatment strategy is dependent on the causal gene mutation (Goldenberg and Moss 2008).

Pharmacotherapy for the treatment of LQTS generally consists of the administration of beta-blockers, a heterogeneous group of antihypertensive agents with an antagonistic action on beta-adrenergic receptors in the heart (Gorre and Vandekerckhove 2010). The main function of these drugs is therefore to depress myocardial function by reversing the beta-adrenergic signal transduction abnormalities as well as slowing down the remodelling process and ultimately regulate the heart rhythm (Satwani et al. 2004).

These beta-blockers are divided into three classes based on their anti-adrenergic profile. The first class contains the drugs propranolol and timolol which are non-selective compounds; blocking β_1 and β_2-receptors with equal affinity and do not have any other significant pharmacological properties. The second class includes metoprolol and bisprolol for example, which are cardio selective compounds, blocking β_1-receptors to a much greater extent than β_2-receptors. And finally, the third class contains compounds such as carvedilol and bucindolol which blocks β_1 and β_2-receptors with an equal affinity and in addition exhibit antioxidant and vasodilator properties respectively (Moss et al. 2000; Satwani et al. 2004).

This first-line prophylactic therapy is typically administered to all intermediate and high risk patients as these drugs interfere with the normal binding to receptors of epinephrine and other

stress hormones; weakening the effect of the stress response and ultimately disrupt cardiac arrhythmias (Schwartz et al. 2006).

This medication has been used successfully to reduce the risk of lethal and life threatening cardiac events (Schwartz et al. 2001). However, there are a number of affected individuals who do not respond to beta-blocker treatment and experience recurrent cardiac events (Schwartz et al. 2001). This may be due to the response to different genetic loci (Napolitano 2005). Additional therapeutic procedures were therefore developed to manage these symptomatic patients (Goldenberg et al. 2008) and these procedures are described in detail below.

Surgical approaches such as the implantation of ICDs and left cardiothoracic sympathetic denervation (LCSD) have also been used to successfully treat LQTS. Studies have shown that ICD in combination with beta-blocker medication is effective treatment for patients who do not respond to treatment when only beta-blocker medication is administered (Crotti et al. 2008).

Left cardiothoracic sympathetic denervation involves the removal of the left stellate ganglion to provide adequate cardiac denervation. This procedure is only considered in patients who remain symptomatic and experience recurrent syncope despite beta-blocker medication and ICD implantation (Goldenberg et al. 2008).

Ultimately, changes in lifestyle should be considered to improve quality of life and increase life expectancy by avoiding stressors including stringent exercise and competitive sports (Schwartz et al. 2006). Also, as far as possible, patients are urged to avoid, loud, starling noises and situations that could aggravate or excite them (Goldenberg et al. 2008).

1.2.5 Genetics of LQTS

Inherited forms of LQTS will usually manifest as an autosomal dominant disorder. Autosomal recessive forms of this disease are less common and usually associate with a more severe phenotype. These inherited forms of LQTS are also known to be caused by mutations in genes that encode mainly ion channel proteins, accessory subunits as well as proteins involved in regulating the action potential within the heart (Glaaser et al. 2003).

Yang and colleges also suggested that common polymorphisms, be it inherited or occur as *de novo* polymorphisms, may increase the patients susceptibility to longer QT intervals and arrhythmic events (Yang et al. 2002).

Previous studies have indicated that many inherited forms of arrhythmia syndromes exist without the presence of any other structural heart diseases (Goldenberg et al. 2006; Lehnart et al. 2007; Schulze Bahr 2012). Of these, LQTS can be utilized as a model disease due to the relatively high prevalence of the disease as well as the fact that LQTS is found across all ethnic groups (Lehnart et al. 2007; Schulze Bahr 2012).

To date, and over 700 mutations in at least 12 genes have been shown to cause inherited forms of LQTS. These mutations are randomly dispersed throughout the coding regions of the 12 genes and have been implicated in the development of different sub forms of the disease (Table 1.4).

Some of these different forms of LQTS are more common than others and manifest with arrhythmias alone whereas rare forms of LQTS, such as LQT8, are usually associated with additional structural cardiac abnormalities (Schulze Bahr 2012).

Long QT syndrome has a large genetic component that is evident in at least 75 % of patients diagnosed with this condition (Goldenberg et al. 2008). Mutations identified in the 12 genes listed in table 1.4 either lead to decreased repolarising potassium channel currents or to inadequate entering of sodium and/or calcium into, and potassium ions out of the cardiomyocytes due to defective ion channels (Figure 1.6) (Goldenberg et al. 2008).

There are three ion currents that are largely involved in the lengthening of cardiac action potential and prolongation of QT intervals namely: $I_{Ks,}$ I_{Kr} and I_{Na} channels. I_{Ks} channels are responsible for the slowly activating delayed rectifier potassium currents (Splawski et al. 2000).

I_{Kr} channels, on the other hand are responsible for the rapidly activating, delayed rectifier potassium current which allows potassium ions to move more easily into rather than out of the cell (Splawski et al. 2000; Hibino et al. 2010).

Table 1.4: Genes associated with specific subtypes of Long QT Syndrome

Gene Symbol	Subtype	Gene Name	Chromosome
AKAP9	LQT11	A-kinase anchor protein 9	7q21-q22
ANK2	LQT4	Ankyrin-B	4q25-q27
CACNA1*c*	LQT8	Calcium channel, L type, alpha 1 polypeptide isoform	12p13.3
CAV3	LQT9	Caveolin-3	3p25
KCNE1	LQT5	Voltage-gated potassium channel , Isk-related subfamily, member 1	21p22
KCNE2	LQT6	Voltage-gated potassium channel , Isk-related subfamily, member 2	21p22
KCNH2	LQT2	Potassium channel, voltage gated, H2	7q35-q36
KCNJ2	LQT7	Inwardly rectifying potassium channel	17q23.1-24.2
KCNQ1	LQT1	KQT-like voltage-gated potassium channel-1	11p15.5
SCN4B	LQT10	Sodium channel, voltage gated, type IV beta subunit	11q23.3
SCN5A	LQT3	Alpha polypeptide of voltage-gated sodium channel type V	3p21-p23
SNTA1	LQT12	Syntrophin, alpha 1	20q11.2

Abbreviations: Isk, slow activating delayed rectifier potassium currents ; LQT, Long QT; p, chromosomal short arm; q, chromosomal long arm. Table adapted from: Ackerman et al. 2011

I_{Na} channels are responsible for sodium current in the heart (Splawski et al. 2000). When I_{Ks} and I_{Kr} are reduced or I_{Na} is increased in the heart, the cardiac action potential will be prolonged, the QT interval will lengthen and the risk for arrhythmia will be increase (Splawski et al. 2000).

The ion channels that are associated with the development of LQTS are generally transmembrane proteins that transport specific ions such as potassium (K^+), sodium (Na^+) and calcium (Ca^{2+}) through the cell membrane (Figure 1.6). These channels are voltage-dependent; they are therefore only activated when the intracellular voltage reaches the required value. The specific voltage necessary for activation differs between channels and is dependent on the channel subunit, either the alpha (α) or beta (β) subtype (Figure 1.7) (Medeiros-Domingo et al. 2007a).

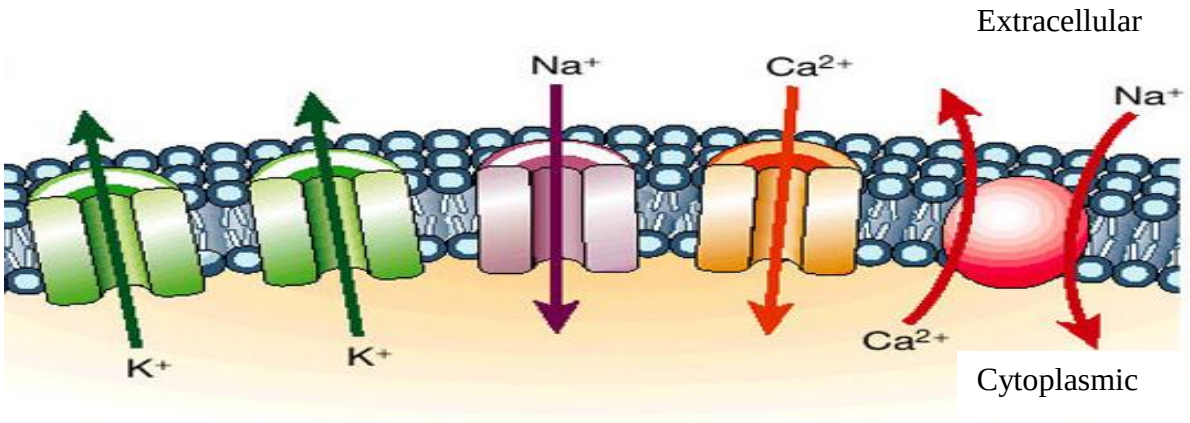

Figure 1.6: Ion channels in cardiac cells associated with LQTS. Potassium ion (K^+) channels facilitate the efflux of K^+ from the cell. Sodium ion (Na^+) channels and calcium ion (Ca^{2+}) channels mediate influx of their respective ions. The Na^+/Ca^{2+} ion exchanger channel carries three Na^+ ions to the cytoplasm for each Ca^{2+} transported to the extracellular matrix across the membrane. Adapted from: Marbán 2002.

These channels form molecular complexes which are essential for the regulation of cardiomyocyte, and ultimately cardiac muscle contraction. These complexes are made up of a protein unit that forms the membrane pore (pore-forming or α-subunit) as well as one or more secondary regulatory proteins which are usually auxiliary subunits (for example β-subunits) (Figure 1.7).

Interestingly, the location of the mutations is believed to influence the severity of the disease. In a previous study, Moss and colleagues provided evidence that mutations in the pore region of the *KCNH2* gene was associated with a more severe clinical phenotype (Moss et al. 2002).

Similarly Brink and co-workers reported that the A341V mutation in the pore region of the KCNQ1 protein was related to an unusually severe clinical phenotype in the South African population (Brink et al. 2005).

On the contrary, Shimizu and colleagues suggested that LQTS1 patients with mutations in the transmembrane region of the KCNQ1 proteins were at higher risk for cardiac events (Shimizu et al. 2004).

Thus, it appears that the specific genes involved as well as the location of mutations within those genes are responsible for the degree of channel impairment. Accordingly, Vincent suggested that a variable degree of impairment in the HERG potassium channel will be present in LQTS2 patients carrying the different mutations in different locations (Vincent 1998).

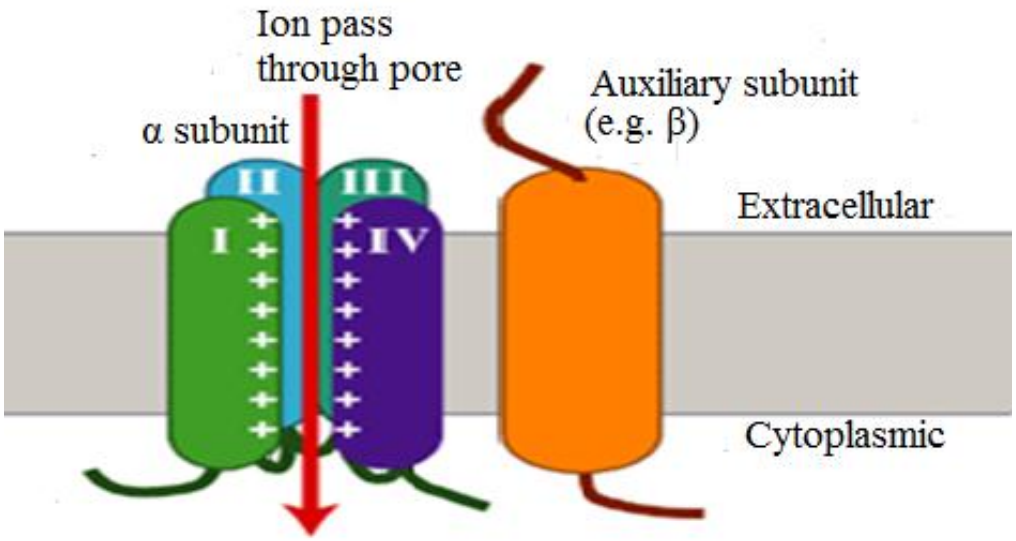

Figure 1.7: The structure of a typical voltage-gated cardiac ion channel. The figure shows the assembled alpha (α) and auxiliary (β) subunits of a typical voltage-gated ion channel to form a complete channel for ion transport. Adapted from: http://journals.cambridge.org/fulltext_content/ERM/ERM1_19/S1462399499001349sup022.gif

Previously, genetic testing for LQTS was mainly performed for research purposes at universities and other institutes. However, more recently it became commercially available for diagnostic purposes (Goldenberg et al. 2008). Since mutations in different genes are responsible for each of the known LQTS subtypes (Table 1.4), genetic testing has become an invaluable and necessary tool for the accurate diagnosis of the disease.

The various LQTS subtypes are associated with certain harmful stressors (Table 1.5), that can be avoided if the LQTS subtype is properly diagnosed. Moreover, the correlation between genotype and phenotype in specific subtypes of LQTS has improved our understanding of the mechanisms of arrhythmias as well as the life-threatening cardiac events suffered by individuals with LQTS (Schwartz et al. 2001).

Table 1.5: Stressors associated with some of the more common types of LQTS

Genotype	Stressor for cardiac events
LQT1	Stringent exercise (swimming)
LQT2	Startling event (alarm clock)
LQT3	Resting state

Abbreviations: LQTS, Long QT Syndrome. Table adapted from: (Goldenberg et al. 2008; Schwartz 2012)

An advantage of genetic testing is that closely related, at-risk family members can be identified before they exhibit any symptoms. Furthermore, genetic screening has been shown to be beneficial for prenatal and pre-implantation genetic diagnosis of LQTS (Goldenberg et al. 2008).

Genetic testing should be considered for individuals experiencing symptoms associated with LQTS such as syncope and abnormal ECG results as well as individuals with a positive family history or familial LQTS. It is equally important that one month old infants with a QTc > 470ms be screened for LQTS mutations. In a 2009 study, Schwartz and colleagues found that 43% of newborns with a QTc > 470ms were identified as carriers of LQTS causing mutations and that 90% of infants with a QTc > 460ms in the first month of life - who maintained this QTc value for at least one year after birth - were carriers of LQTS causing mutations (Schwartz 2009; Schwartz 2012). This provided evidence that genetic testing allows for the identification of presumably healthy infants who in fact are at high risk for SCD (Schwartz 2012).

It was also suggested that the diagnostic criteria (Table 1.2) should be used to select patients with a score > 3 point regardless of presence or absence of cardiac events for genetic screening. Additionally, the results should be used to identify the “silent” mutation carriers through cascade screening (Schwartz 2012).

Cascade screening is thought to be one of the most important features of genetic testing since it allows for the identification of mutation carriers that are generally overlooked. This form of predictive DNA testing consists of screening the entire family for the disease-causing mutation identified in the patient/proband. This is essential since first-degree relatives have a 50% risk of carrying the same mutation (Hofman et al. 2010). This guarantees adequate patient treatment and protection from lethal arrhythmic events due to the high success rate of inherited disease treatment (Schwartz 2009; Hofman et al. 2010). This method also allows asymptomatic, yet genetically affected individuals to be identified early on and started on the proper medications (Schwartz 2012).

When a patient is selected for genetic screening and mutations are identified, the results can have one of the following outcomes: the patient may be positive for any of the known mutations, negative for any of the known mutations or a variant of unknown clinical significance may be identified. This distinguishes the carriers from non-carriers (Hofman et al. 2010).

When a known disease-causing mutation has been identified in an individual a convincing LQTS diagnosis can be made (Hofman et al. 2010). All first-degree family members (parents, siblings and children) of these patients will subsequently be given the choice to be screened for the same disease-causing mutation. The identification of mutations allows physicians to advise patients on which stressors to avoid (Table 1.5) in order to minimise the chances of experiencing life-threatening cardiac events (Hofman et al. 2010). In cases where family members are mutation-positive it is important to monitor the newly diagnosed individual since variable phenotypic expression is observed in individuals of the same family with the same disease-causing mutation (Brink et al. 2005).

In some cases a variant is identified of which the clinical significance is unknown. The potential pathogenic role of the variant can therefore not be confirmed. In order to prove that the variant is pathogenic, closely related family members should be tested. If it is found that an affected relative has the same variant, chances are greater that the variant is indeed pathogenic (disease-causing) and the variant will then be reconsidered as a family-specific mutation. (Tester et al. 2006). To prove that this is true a panel of unrelated control individuals who do not have ECGs indicative of LQTS should be screened for the newly identified variant. If the mutation is absent in the control panel and present in affected individuals only, it could be considered pathogenic.

For further verification of pathogenesis, functional studies have to be conducted to determine the mechanism of pathogenesis.

Ultimately, the identification of mutations, different types of mutations as well as their different functions are vital in determining the disease outcome. It is clear that LQTS is more complex than initially thought, and that mutation-specific risk stratification will be integrated into clinical diagnosis (Schwartz 2012).

1.3 SOUTH AFRICAN FOUNDER FAMILY

In South Africa, a number of LQTS cases have been reported including individuals from Asian, Coloured and mostly White ethnicities (Heradien et al. 2007). In 2005 a study by Brink and co-workers described a cohort of 22 South African families who shared the same *KCNQ1* mutation (A341V) (Brink et al. 2005). Ancestry of this LQTS cohort, which included 345 family members, was traced back to a common Afrikaner founder couple (of mixed Dutch and Huguenot origin) that married in the year 1730 and gave rise to this South African LQTS founder effect (Figure 1.8) (Brink et al. 2005). A founder effect can be defined as the loss of genetic variation that occurs when a new population is established by a small group of individuals from a larger population.

In order to determine if these findings could, without a doubt, be ascribed to a founder effect and to ensure that the mutation identified in this cohort did not occur independently on one or more occasions, Brink and co-workers used genealogical studies as well as haplotype data to confirm the lines of descent of the *KCNQ1*-A341V mutation (Figure 1.8) (Brink et al. 2005).

Among the 345 family members, 166 members were mutation carriers which consisted of 54% females and 46% males. The majority (79%) of the mutation carriers were symptomatic and had experienced their first cardiac events before the age of 10 years. Surprisingly, 14% of affected individuals experienced SCD before the age of 40 years. With this evidence, researchers speculated that the *KCNQ1*-A341V mutation was associated with a more prominent risk of life threatening cardiac events when compared to other mutations segregating with the LQTS1 subtype (Brink et al. 2005).

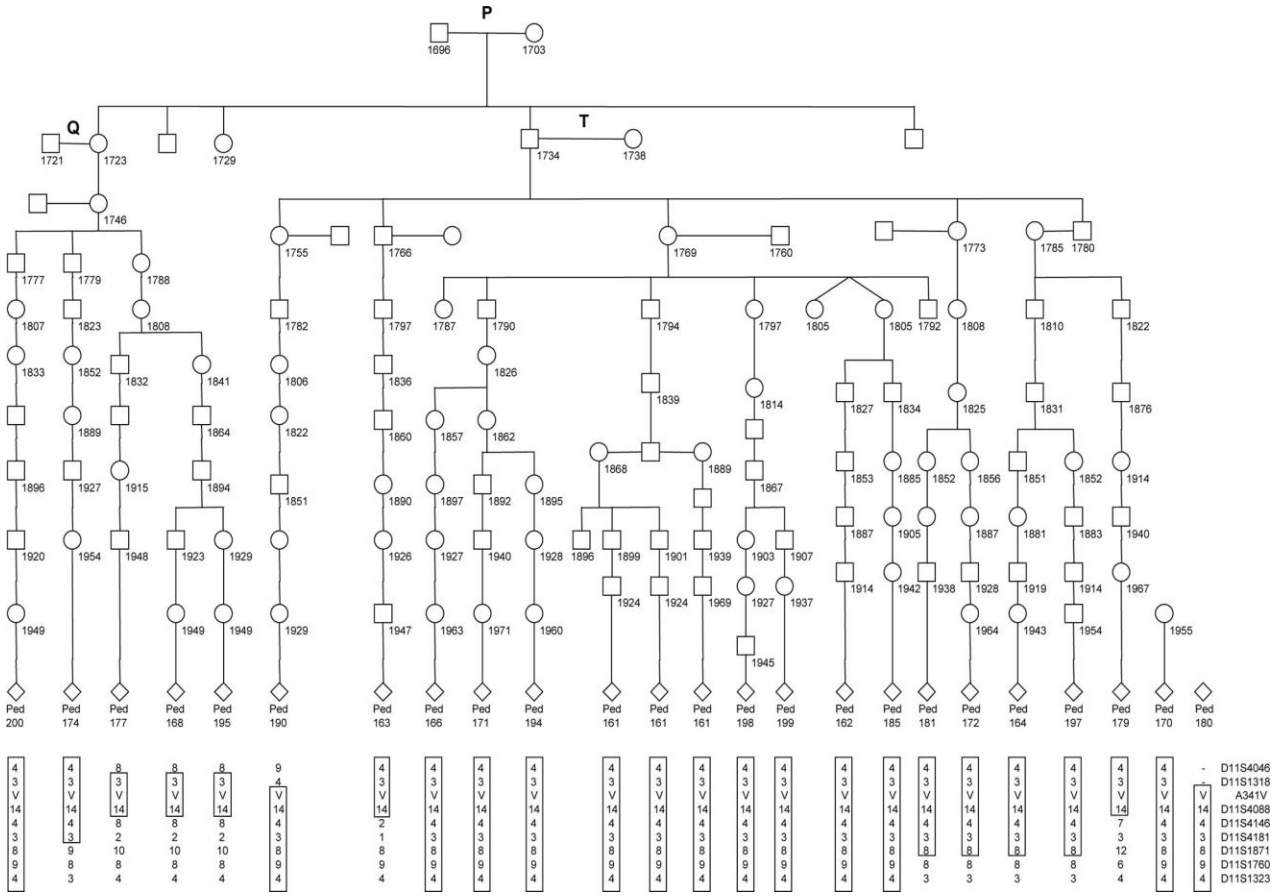

Figure 1.8: Inheritance lines of the *KCNQ1*-A341V mutation from the common founder couple (P). A similar haplotype with minimal recombination segregates along with the mutation over 10 generations. No genealogical information could be found for pedigree 170 and 180. The common haplotypes are indicated with borders, and the index cases are indicated as diamonds. The squares signify males and the circles females. Ped is an abbreviation for pedigree and the letters P, Q and T are indicators for the couples in the first two generations from which the mutation was inherited. Figure taken from: Brink et al. 2005.

In a subsequent South African study where a total number of 51 cases of *KCNQ1*-A341V mutations were reported, only 29% were correctly diagnosed with the disease while 40% of cases were misdiagnosed as epilepsy and 31% remained undiagnosed (Brink and Corfield 2009).

LQT1 patients carrying the A341V mutation exhibited more severe symptoms as well as more LQTS related deaths than other LQTS1 patients. This holds true for South African patients as well as other individuals that have been examined worldwide. Symptoms also seemed to appear at a younger age for A341V-carriers. When compared to non-A341V carriers, Brink and Corfield provided evidence showing that A341V-carriers have life threatening cardiac events and

longer QTc values earlier in life than other LQTS patients; even when treated with beta-blocker medication (Brink et al. 2005; Brink and Corfield 2009).

1.4 GENETIC MODIFIERS

Over the years genetic modifiers have been shown play an important role in the phenotypic variability in complex disease and that Mendelian as well as non-Mendelian genetic disorders display extreme inter- and intra-familial phenotypic variability (Houlston and Tomlinson 1998).

1.4.1 Genetic modifiers of LQTS

As mentioned previously LQTS is one of many diseases that will present with severe phenotypic variability, thought to be caused by incomplete penetrance (Crotti et al. 2005). Furthermore, it is believed that single ion defects might not be the sole cause of arrhythmic events and that the arrhythmias might be caused by a combination of ion defects and genetic modifiers (Keating and Sanguinetti 2001; Crotti et al. 2009). Through a myriad of studies over the years, numerous single nucleotide polymorphisms (SNPs) in known LQTS genes have been identified and confirmed to contribute to the QTc interval durations.

Mutations in *KCNQ1* have been shown to be the cause of LQT1 (Table 1.4) and is by far the most common form of inherited LQTS. LQT1 is believed to be responsible for approximately 45 % of reported cases (Splawski et al. 2000). This gene encodes the pore-forming subunit of the ion channel that mediates I_{Ks}. Mutations identified in *KCNQ1* lead to the loss of channel function which results in the reduction in repolarising potassium currents and ultimately a delay in repolarization of the cardiac action potential.

In an interesting study by Yu and colleagues the effect of QT-related and diabetes-related variants in *KCNQ1* on the QT interval were investigated. The cohort consisted of 2415 Type 2 diabetes patients and 1163 control individuals from a Chinese population. Four SNPs in *KCNQ1* were selected (rs12296050, rs12576239, rs2237892 and rs2237895) and genotyped. Interestingly, none showed association with QT interval in patients with Type 2 diabetes. On the contrary one of the SNPs (rs12296050) was found to be associated with a prolonged QT interval

in the control group. This indicated that *KCNQ1* is linked to QT interval duration in a Chinese population with normal glucose regulation (Yu et al. 2013).

In our South African founder population, Schwartz indicated that the *KCNQ1*-A341V mutation has a far more severe clinical manifestation than other LQT1-causitve mutations (Schwartz 2012). This high degree of severity was previously ascribed to the fact that the A341V mutation contains a mildly dominant-negative effect and does not result in a total loss of function effect. It should be noted, however that the complete mechanism is not known as arrhythmic risk continues to be higher when compared with *KCNQ1* mutations that contain a strong dominant negative effect (Brink and Corfield 2009).

In the same South African population it has been found that the occurrence of frequent polymorphisms in the *NOS1AP* gene will increase the risk of sudden death by 2 fold in patients with the *KCNQ1*-A341V mutation (Schwartz 2012). The *NOS1AP* gene, which encodes a nitric oxide synthase adaptor protein, has subsequently been implicated as a contributor to QT interval duration as well as an increased risk factor for SCD in the general population (Crotti et al. 2009).

Crotti and his co-workers investigated the theory that common variants in *NOS1AP* could modify the risk of clinical expression as well as the degree of QT-interval prolongation in a South African LQTS cohort (Crotti et al. 2009). Two variants of *NOS1AP* (rs4657139 and rs16847548) were significantly associated with the occurrence of symptoms with clinical severity as well as the probability of experiencing cardiac arrest and SCD. Additionally, these two variants were also associated with a greater chance of having QT intervals that fell in the top 40% of values among all mutation carriers in the study. These results showed that the variants of the *NOS1AP* gene not only influence the QTc interval, but also affect the risk for life-threatening cardiac arrhythmias and SCD in LQTS patients - ultimately labeling *NOS1AP* as a genetic modifier of LQTS (Crotti et al. 2009).

Nonetheless, with genetic tests identifying pathogenic mutations, it is possible to change management options and to use a more direct line of attack in order to protect the patients (Schwartz 2012).

Mutations identified in *KCNH2* (better known as *HERG*) are thought to be responsible for up to 40% of LQTS cases (LQT2, Table 1.4). HERG mediates the I_{Kr} current which is an important

regulator of repolarization of the cardiac action potential. Most mutations identified in *HERG* leads to a reduced potassium current and ultimately loss of function or reduced function of I_{Kr} channels. Previous studies have provided evidence that HERG channel dysfunctions will not only lead to inherited LQTS, but also acquired forms of LQTS (Sanguinetti et al. 1995).

Another group of investigators screened the *KCNH2* gene for novel mutations. The *KCNH2*-K897T (rs1805123) polymorphism was identified and researchers suggested examining a cohort of 170 LQT1 patients to elucidate the association between this SNP and QTc interval duration as well as its effect on modifying the phenotype of LQTS (Laitinen et al. 2000). A subsequent study demonstrated that the *KCNH2*-K897T SNP modified the clinical expression of the latent A1116V LQT2 mutation and that this common variant (K897T) would most likely not cause disease on its own (Crotti et al. 2005).

In 2007 an American study was conducted which included 1730 unrelated patients from the Framingham Heart study (Newton-Cheh et al. 2007). Seventeen SNPs as well as the previously associated SNP - rs1805123 (K897T) – in *KCNH2* were selected for genotyping. The study showed that only one of the 17 SNPs (rs3807375) along with the rs1805123 SNP was associated with the QT interval duration in both men and women (Newton-Cheh et al. 2007).

A previous study showed that a subset of patients carrying mutations in ion channels displaying incomplete penetrance, were prone to drug-induced forms of LQTS that are commonly associated with malignant arrhythmias (Napolitano et al. 2000). When a mutation screen of LQTS-related genes was performed, the Y315C point mutation was identified in *KCNQ1*. It was established that this mutation caused a severe loss of I_{Ks} function within cells causing a delay in repolarization of the cardiac action potential, despite the analysis of numerous ECG results that ruled out the presence of prolonged QT intervals (Napolitano et al. 2000).

Kubota and co-workers identified another *KCNQ1* mutation in a patient with prolonged QT interval as well as TdP induced by hypokalaemia (referring to the condition in which the potassium concentration is very low). This missense mutation, R259C, is believed to be the molecular source for the dysfunction of I_{Ks} currents underlying sporadic cases of hypokalaemia-induced LQTS. Researchers subsequently suggested that cases of patients with acquired LQTS, carrying genes with such mild mutations, might be more common than expected and accentuated

the significance of performing mutation screening to detect these "silent" forms of LQTS (Kubota et al. 2000).

In the same year a study was completed that included mutation screening of five of the known LQTS-related genes (*KCNQ1*, *HERG*, *SCN5A*, *KCNE1*, and *KCNE2*). Of the 262 study subjects, 68 had mutations in *HERG* of which 52 of the mutations were novel. A similar number of mutations were identified in *KCNQ1* (75 mutations). Additionally, 8%, 3% and 2% of mutations were found in *SCN5A*, *KCNE1* and *KCNE2* respectively (Splawski et al. 2000).

The *SCN5A* gene, which is associated with the LQT3 subtype, is believed to be responsible for 7% of cases of inherited LQTS. This gene encodes the alpha subunit of a sodium channel that is in charge of cardiac depolarisation. Mutations in this gene leads to a gain-of-function that will influence the normal upholding of the depolarising current and ultimately leads to the prolongation of the action potentials (Wang et al. 1995).

To date, not a single case of LQTS have been diagnosed and documented in the black South African population, whereas 88% of LQTS index cases were identified in the White population (Heradien et al. 2007). On the contrary in other countries such as the United States of America (USA), a large number of cases have been documented in black populations. One such study included the *SCN5A* variant - rs7626962 (S1103Y or S1102Y) - that is believed to be a common variant in black populations but a rare variant in other ethnic groups. Previous studies have linked this SNP to the risks of SCD, drug-induced arrhythmias as well as sudden infant death syndrome (SIDS) in black populations (Jeff et al. 2011).

Subsequently Jeff and co-workers selected 72 variants of the *SCN5A* gene to be genotyped in 3054 unrelated individuals and found that 14 had significant associations with the QT interval duration. One of the 14 variants, rs7627552, was found to be the SNP best associated with P-wave and PR durations on the ECG (Jeff et al. 2011).

Mutations in *minK*, better known as the *KCNE1* gene, are responsible for approximately 5% of inherited LQTS cases (Splawski et al. 1997). This gene encodes the beta subunit of a potassium channel that mediates the I_{Ks} current and co-assembles with KCNQ1 in order to form the functional channel. In a previous study, it was found that *KCNE1* mutations, similar to *KCNQ1*

mutations, change the repolarization of action potentials in the myocardium (Splawski et al. 1997).

In a study by Friedlander and co-workers, a linkage and association analysis was conducted to investigate whether variants in *KCNE1* had any effect on the QTc intervals of an Israeli population. It was found through a family-based association analysis that the G38S SNP showed significant association with QTc intervals and that this SNP is modified by gender (male) (Friedlander et al. 2005).

Over the years, four Finnish founder mutations have been identified; two in *KCNQ1* (G589D and IVS7-2A>G) and two in *KCNH2* (L552S and R176W) (Lahtinen et al. 2011). In a recent study the common D85N variant in *KCNE1* was investigated for its effect on age, sex, and QTc interval duration in LQTS patients carrying these Finnish founder mutations. This association study was conducted due to the fact that D85N has been linked to prolongation of QT intervals through inhibiting I_{Ks} (*KCNQ1*) and I_{Kr} (*KCNH2*) currents, thus making *KCNE1* a suitable candidate for a modifier gene in LQTS (Lahtinen et al. 2011). The association between D85N and clinical variables resembling disease severity was also investigated. The results obtained from this study indicated an association between D85N and QT prolongation in males with the *KCNQ1* G589D variant, but not in females with the same variant. Additionally, within the G589D mutation group, *KCNE1* D85N carriers were mostly identified as probands. This led to the suggestion that *KCNE1* D85N is a gender specific modifier of QT interval in LQT1 and could possibly be linked to an increase in disease severity (Lahtinen et al. 2011).

The LQT6 subtype can be caused by a number of mutations identified in *KCNE2*, also known as the mink-related peptide (MiRP1). This gene encodes the accessory β-subunit of the voltage-gated potassium ion channel. The β-subunit regulates the I_{Kr} current in the heart and co-assembles with HERG to form the complete and functional potassium channel (Abbott 1999). The mutations associated with this gene are thought to be loss-of-function mutations and cause prolongation of action potentials by inhibiting the I_{Kr} current in the heart (Abbott 1999). In a study conducted by Abbott and colleagues, three missense *KCNE2* mutations (Q9E, M54T and I57T) that are believed to be more commonly found in patients with drug-induced TdP, were identified. It is therefore recognized that missense mutations in the *KCNE2* gene are related to

inherited and acquired forms of arrhythmias as well as alterations in the ion channel functions (Abbott 1999; McCrossan et al. 2009).

Subsequent investigations of *KCNE2* led to the identification of a missense mutation (C29T) which encodes the T10M variant. This variant forms part of a cluster of variants previously identified as acquired LQTS SNPs (T8A and Q9E) (Figure 1.9). However, in this study, the T10M variant was inherited from the father of the proband and present in other asymptomatic family members but not in 578 ethnically matched controls (Gordon et al. 2007). Gordon and co-workers set out to find the functional significance of this disease causing variant in *KCNE2* ion channels. Results showed that the variant reduces the current density and slows down the inactivation and recovery of KCNE2/HERG but does not affect the KCNE2/KCNQ1 currents. It was proposed that the T10M mutation may likely be intensified when accompanied by environmental and/or other genetic factors and that *KCNE2* does indeed regulate HERG in the human heart (Gordon et al. 2007).

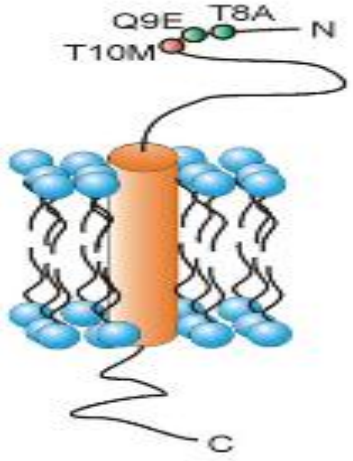

Figure 1.9: A figure representing the KCNE2 transmembrane protein and three known N-terminal domain mutations. Three of the known *KCNE2* mutations (T8A, T10M and Q9E) are indicated in this figure of which the *KCNE2* C29T mutation encodes a T10M substitution in *KCNE2*, close to the LQTS variants, T8A and Q9E. Adapted from: Gordon et al. 2007.

McCrossan and co-workers investigated *KCNE1* and *KCNE2* mutations that have previously been associated with LQTS. Two *KCNE1* variants (D76N and S74L) were shown to reduce the current density and delayed deactivation of an α-subunit – Kv2.1 (McCrossan et al. 2009). Variants in *KCNE2* (M45T and I57T) reduced KCNE2/HERG currents and was previously shown to be associated with inherited and acquired (drug-induced) LQTS (Abbott 1999; Gordon et al. 2007; McCrossan et al. 2009). The R27C variant present in *KCNE2* has been linked to atrial fibrillation and an increase in KCNE2/KCNQ1 currents without affecting other KCNE2 channel functions. Furthermore, it has also been demonstrated that KCNE1 and KCNE2 were

modifiers of Kv2.1 function and that inherited mutations in either of these subunits may contribute to cardiac arrhythmias through a number of mechanisms (McCrossan et al. 2009)

Following this discussion on genetic modifiers, one can speculate that mutations found in these ion channel genes directly influence the current changes that regulate action potential. The ECG findings associated with these mutations include prolonged QT intervals as well as ventricular tachycardia. Evidence also suggests that the mutations identified in such a varied subset of genetic modifiers can lead to the susceptibility of severe cardiac arrhythmias (Cheng et al. 2003)

To date, several studies have been conducted in order to discover novel disease-causing mutations in genes associated with LQTS or in genes known to modify disease phenotype. However, as mentioned earlier, 25% of patients clinically diagnosed with LQTS have no apparent genetic cause for their disease (Napolitano 2005; Medeiros-Domingo et al. 2007b; Newton-Cheh et al. 2009). Consequently, *KCNE2* was chosen to be investigated for novel interacting modifier genes. Mutations in *KCNE2* have been linked to congenital as well as drug-induced LQTS and therefore proved to be an interesting candidate for this study (Abbott 1999).

1.5 KCNE2 POTASSIUM ION CHANNEL

1.5.1 KCNE2 genomic structure

Abbott and co-workers cloned and characterized the potassium voltage-gated channel, I_{Ks}-related family, member 2 (*KCNE2*) gene that encodes the MiRP1 protein (Abbott 1999). This protein forms part of a largely diverse class of membrane proteins with a variety of functions made possible by α- and regulatory β-subunits from which these channels are assembled. These subunits are encoded by the KCNE family that comprises five known human genes (*KCNE1*-5) (McCrossan and Abbott 2004).

KCNE2 was found to be located on the long (q) arm of chromosome 21 at position 21.12 on the forward strand. This gene encodes a small transmembrane protein of 123 amino acids (aa), has a transcript length of 803 base pairs (bp) and contains two coding exons (Figure 1.10) (Abbott 1999; www.ensembl.org). However, investigators indicated that the *KCNE1* gene, encoding MinK, was previously mapped to this same locus and found that these two genes are arrayed in opposite orientation of each other and are only separated by 79kb.

Abbott and colleagues subsequently suggested that *KCNE2* and *KCNE1* are related by means of gene duplication and divergent evolution and that *KCNE2* shares a 27% identity and a 45% homology to *KCNE1* (Abbott 1999).

Following the identification and classification of *KCNE2* several studies have shown high levels of expression of *KCNE2* in cardiac and skeletal muscle (Abbott 1999) as well as the brain (Ying et al. 2012), pancreas, kidney, placenta and colon. Lower levels of expression are found in liver, ovary, testis and small intestines with near to undetectable levels of expression present in the lung (Tinel et al. 2000). When compared to expression of other *KCNE* proteins, it was found that *KCNE2* is less expressed in the heart, especially in the ventricles (Bendahhou et al. 2005). Nevertheless, *KCNE2* is present in the heart and the highest expression levels of *KCNE2* is localized to the SA node and up to 40% in atrial tissue (Yu et al. 2001).

1.5.2 KCNE2 protein structure

KCNE2 contains one extracellular N-terminal that includes two predicted N-glycosylation sites (N6 and N29) (Figure 1.10 and Figure 1.12) (Zhang et al. 2012), one transmembrane domain and one intracellular C-terminal domain that includes protein kinase C-mediated (PKC) consensus phosphorylation sites (T71 and S74; Figure 1.10) (Abbott 1999; McCrossan and Abbott 2004).

This small integral membrane subunit has been shown to co-assemble with HERG - the *KCNH2* gene product - in order to form a functional unit of the I_{Kr} channel (Abbott 1999). However, in a subsequent study by Jiang and colleagues it was found that a very small amount of KCNE2 showed association with HERG in co-immunoprecipitation analysis (Jiang et al. 2009).

This gave rise to the suggestion that this specific protein has other possible interacting partners (Jiang et al. 2004). Other investigators suggested that KCNE2 might interact/associate with KCNQ1 and KCNQ3 and draw out a voltage-dependent current. Or it may also associate with Hyperpolarization Activated Cyclic Nucleotide-Gated Potassium Channel 1 and 2 (HCN1and HCN2) to increase the potassium current (Yu et al. 2001).

The association of KCNE proteins with the appropriate α-subunits have been found to take place in the endoplasmic reticulum (ER) (Chandrasekhar et al. 2006) as well as at the plasma membrane (Jiang et al. 2009) with more than one protein co-assembling with the channel

complex. Evidence suggests that one of the KCNE proteins could take the place of another family member to influence the current properties (Eldstrom and Fedida 2011).

In a 2008 study, Abbott and colleagues determined the secondary structure of KCNE2 as largely α-helical and concluded that the predicted transmembrane and intracellular domains require an extensive hydrophobic interaction in order for the molecule to take on an ordered, non-aggregated structure (Abbott et al. 2008).

The N-terminal domain was found to be the only water-soluble domain in this study which indicated the consistency with the predicted extracellular location of this section. Abbott and co-workers mention that the function of the N-terminal of KCNE2 has not yet been elucidated but the removal of residues four-nine from the N-terminal of KCNE1 results in the loss of channel function. This might be extrapolated to KCNE2 due to the homology shared between these two subunits (Abbott et al. 2008).

Additionally two inherited mutations (Q9E and T8A) located in the N-terminal of KCNE2 (Figure 1.12) have been associated with acquired (drug-induced) forms of arrhythmias (Abbott 1999). One of these mutations - Q9E - was found to increase the sensitivity of I_{Kr} channel blockage for drugs such as clarithromycin. This complicates the repolarization action of mutant I_{Kr} complexes and is believed to contribute to the prolongation of the QTc interval of the cardiac action potential; regardless of the presence of drugs (Abbott 1999).

The transmembrane domain structure of KCNE1 has proven to be more difficult to determine than anticipated; with several studies suggesting controversial conformations for this domain. Some investigators proposed a β-conformation, while others concluded an α-helical structure for this section of the protein (Abbott et al. 2008).

Similarly, the transmembrane domain of KCNE2 presented with some difficulty but was ultimately identified through infrared spectroscopy as predominantly α-helical with a minor intra-molecular β-strand conformation (Abbott et al. 2008).

The intracellular C-terminal domain of KCNE2 was shown to be insoluble in water, indicating that a hydrophobic interaction is essential for solubility as well as an ordered secondary structure of this domain (Abbott et al. 2008).

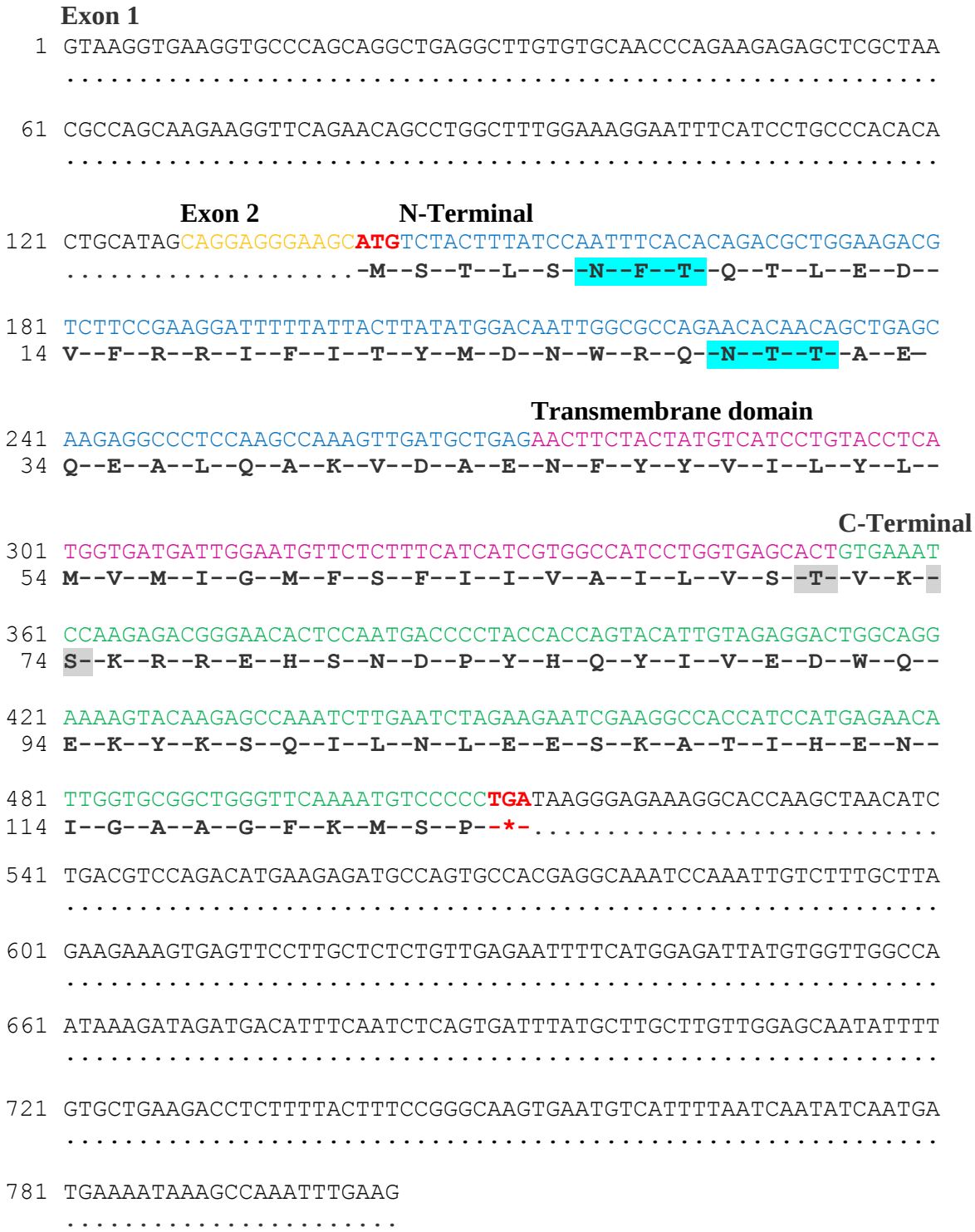

Figure 1.10: KCNE2 genomic and protein sequence. The sequence in orange marks the beginning of the second exon. The red codons, ATG and TGA, resembles the start and stop codons respectively. The sequences in blue, purple and green indicate the N-terminus, the transmembrane domain and the C-terminus respectively. The section highlighted in light-blue in the protein sequence indicates the two glycosylation sites whereas the grey shaded area resembles the two PKC sites. Adapted from Eldtorm 2011and www.ensembl.org.

Finally Abbott and co-workers concluded that, although their findings were consistent with previous studies, it should be noted that KCNE2 is glycosylated at two sites in the N-terminal domain (Figure 1.10 and Figure 1.12) as well at the PKC sites in the C-terminal domain (Figure 1.10) and that this, in conjunction with KCNE2 interaction with α-subunits, might alter the structure of the KCNE2 protein (Abbott et al. 2008).

1.5.3 KCNE2 trafficking and interacting proteins

Previous studies have shown the association between KCNE2 and HERG as well as between KCNE1 and HERG (McDonald et al. 1997) however, studies elucidating the functional effects of KCNE2 on HERG were contradicting. Abbott showed that the co-assembly between KCNE2 and HERG lead to altered voltage-dependent activation of the channels, requiring a more positive potential when compared to channels formed only with HERG subunits (Abbott 1999). On the other hand, Lu and co-workers indicated that there was a significant decrease in current in the early phases of action potential for KCNE2/HERG channels (Lu et al. 2003). Another study concluded that KCNE2 accelerated HERG deactivation and shifted HERG activation voltage dependence in the hyperpolarizing direction when co-expressed (Weerapura et al. 2002).

Um and co-workers decided to investigate these discrepancies between KCNE1 and KCNE2 through studying the biological differences in protein processing and physical interactions with HERG. They found that during biogenesis of channels, HERG had a greater prevalence for assembling with KCNE1 rather than KCNE2. This was ascribed to differences in trafficking rates of the KCNE1 and KCNE2 and not due to different affinities for these proteins (Um and McDonald 2007).

It is important that translated proteins are translocated to their specific cellular location in an ordered and structural manner through the Golgi apparatus. Proteins are passed through the ER and sent to the Golgi apparatus to be modified by specific enzymes and packaged into vesicles from where they are then transported to their final destination. In the case of KCNE2 the proteins are transported to the cell membrane (Peer 2011).

In a study by Abbott, co-immunoprecipitation experiments of KCNE2 and KCNE1 showed the association of the KCNE β-subunits with their respective α-subunits before reaching the cell membrane (Abbott 1999).

Um and McDonald used an ER retention signal to study the effects of KCNE trafficking and their association with HERG (Figure 1.11). The results indicated that the retention signal of KCNE2 yielded an increased amount of higher molecular weight bands which is consistent with a protein that can translocate to the Golgi apparatus but is retained within the ER where prolonged exposure to glycosylation enzyme is allowed (Um and McDonald 2007).

Furthermore, with fluorescent staining of both KCNE and HERG protein, it was clear that HERG and KCNE2 was predominantly confined to the cell surface. An enhanced association was found between KCNE2/HERG. Additionally, Um and McDonald suggested that the co-assembly of KCNE2 and HERG would be expected more to occur if KCNE2 was retained within the ER for longer periods (Um and McDonald 2007).

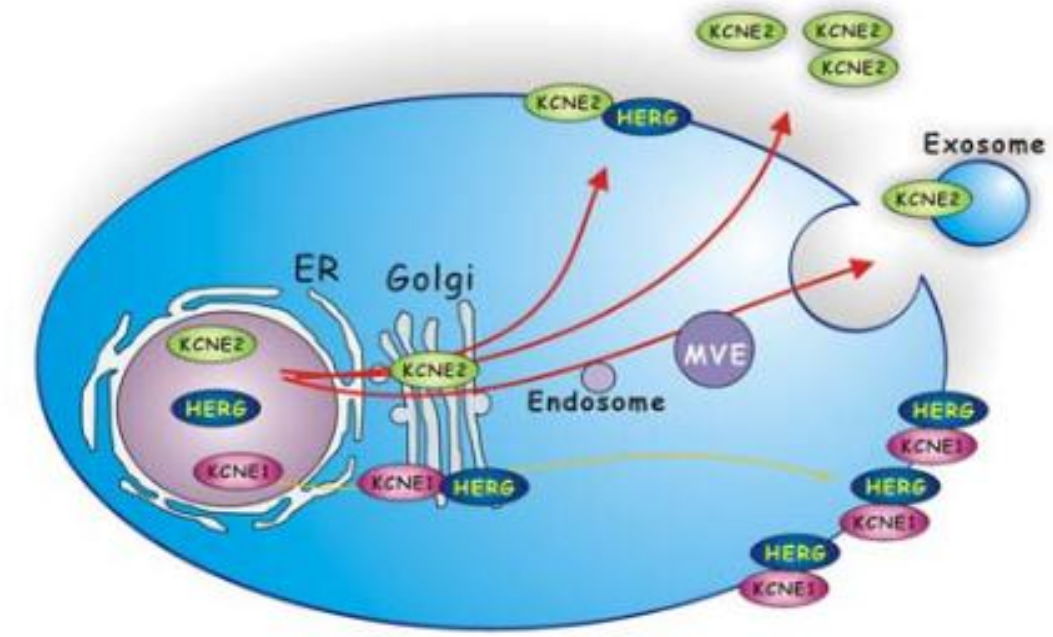

Figure 1.11: Schematic representation of proposed trafficking and association of KCNE1, KCNE2 and HERG. The red arrows indicate the more rapid trafficking of KCNE2 whereas the yellow arrow shows the slower trafficking of KCNE1and HERG to the cell membrane. KCNE2 trafficking is facilitated by endosomes as well as multivesicular endosomes (MVE). The export of KCNE2 from the cell surface is enabled through exosomes where extracellular proteins may exist as monomers of oligomers. Adapted from: Um and McDonald 2007.

The association of KCNE1 and KCNE2 with HERG has significant implications for cardiac conduction, inherited forms of arrhythmia and pro-arrhythmic drug sensitivity (Abbott and

Goldstein 2001). Thus, it is important to study and characterize their specific functions particularly since there is significant controversy surrounding this subject.

Um and McDonald studied the physical interaction between these proteins and their respective trafficking pathways and found that HERG associates more readily with KCNE1 than with KCNE2. However if forward trafficking of KCNE2 is chemically or molecularly interrupted or slowed down, co-assembly of HERG and KCNE2 is increased. Investigators speculate that the prevention of forward trafficking changed the subcellular delivery of KCNE2 and that the interruption caused a significant increase in KCNE2 accumulation in the cell (Figure 1.11). This was not observed for KCNE1 or HERG. A large amount of KCNE2 was also reported to be exported from the cell (Figure 1.11). Subsequently it was concluded that KCNE2 is likely to be processed and trafficked to the cell surface more rapidly than KCNE1 and HERG (Um and McDonald 2007) (Figure 1.11).

Over the years, several studies have provided evidence that KCNE2 interacts with a variety of potassium channels. Some of these channels include the I_{Ks} complex (Jiang et al. 2009), Kv1.4, Kv2.1 (McCrossan et al. 2009), Kv3.1 and KV3.2 (Lewis et al. 2004), Kv4.2 (*KCND2*) and Kv4.3 as well as HCN1 and HCN2 as mentioned earlier (Yu et al. 2001).

1.5.4 KCNE2 channel dysfunction and LQTS

How are changes in the *KCNE2* gene related to pathological conditions? Firstly defects in *KCNE2* are the cause of long QT syndrome type 6 (LQT6) (Abbott 1999) as well as familial atrial fibrillation type 4 (ATFB4) which is a common cardiac arrhythmic disorder characterized by the disorganized electrical activity and ineffective contraction of the atria (McMichael 1982; Yang et al. 2004). This causes blood stasis in the atria and ultimately reduces filling of the ventricle. Similarly to LQTS, ATFB4 can result in heart palpitations, syncope and heart failure (Yang et al. 2004).

It has been estimated that more than 10 mutations in *KCNE2* have been linked to the most common form of LQTS i.e. Romano-Ward syndrome (Eldstrom and Fedida 2011) (Figure 1.12). These mutations changes the ability of the protein to regulate cardiac muscle potassium channels, causing the potassium channels to open at a slower rate and close more rapidly than usual,

reducing the flow of positively charged potassium ions out of these cardiac muscle cells (Towbin and Vatta 2001). This channel dysfunction leads to the symptoms experienced by LQTS patients; i.e. cardiac arrhythmia, syncope and SCD (Ward 1964).

Familial atrial fibrillation is a relatively rare condition found in a small subset of patients and is caused by a single mutation in *KCNE2*. This mutation changes the arginine amino acid at position 27 to a cysteine in the KCNE2 protein - R27C. Contrasting the mutations found in *KCNE2* responsible for LQTS, it has been found that the R27C mutation increases the flow of potassium ions through channels regulated by KCNE2 in cardiac muscle cells. This may lead to changes in the normal rhythm of the heart and give rise to atrial fibrillation (Yang et al. 2004).

Many of the mutations identified in *KCNE2* have functionally been characterized and are located across the entire protein (Figure 1.12). For example, the I57T and A116V mutations have been shown to decrease channel conductance at the cell surface (Abbott and Goldstein 2001). The Q9E mutation causes a positive shift in activation voltage whereas the T8A mutation leads to a negative shift in activation.

Additionally, the *KCNE2*-M54T mutation was shown to cause a faster deactivation and no shift in the voltage-dependent activation (Abbott 1999). The V56M mutation was found to accelerate the inactivation of co-assembled channels (Isbrandt et al. 2002) whereas the T10M mutation caused an almost 30% reduction in current amplitude as well as a slower recovery from inactivation (Gordon et al. 2007).

Drug-induced LQTS or acquired LQTS can also be considered another disorder caused by mutations in the *KCNE2* gene and other LQT genes (Abbott 1999). These drugs include medications used to treat infections, seizures as well as arrhythmias and psychotic disorders such as quinidine (used for malaria infection) and thioridazine (used for psychotic disorders). The mechanism by which mutations cause drug-induced LQTS has been shown to mostly involve blockage of the rapid component of the delayed rectifier potassium current (I_{Kr}) (HERG) and, to a lesser extent, other potassium and sodium channels.

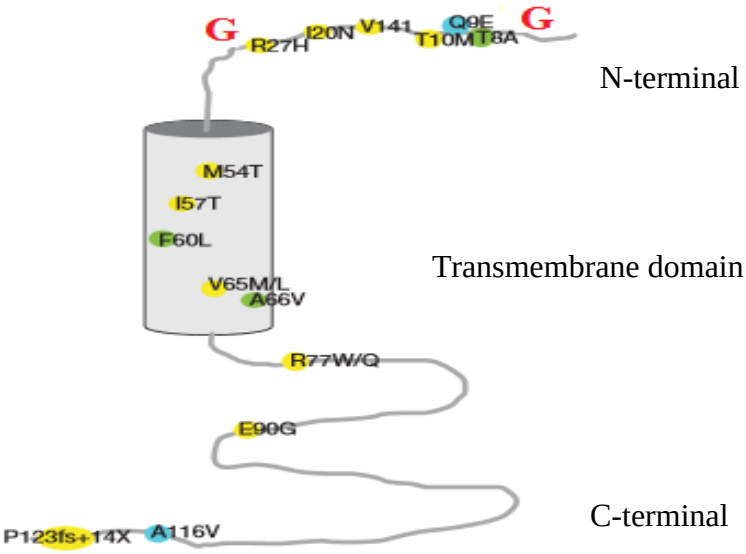

Figure 1.12: *KCNE2* mutations mapped onto a representation of the transmembrane protein. The extracellular N-terminus and known mutations and two glycosylation sites (red capital letter G) in that domain, the transmembrane domain and known mutations as well as the intracellular C-terminal domain with previously identified mutations are indicated and mapped to their positions in this figure. Adapted from: Eldstrom and Fedida 2011.

The structure of ion channels provides high-affinity binding for a wide range of molecule. Thus, by introducing mutation into these channels it would reduce the binding affinity for a variety of drugs and ultimately cause disruption of the channel and drug-induced LQTS (Moss et al. 2000; Kannankeril et al. 2010).

1.6 PRESENT STUDY

As mentioned, congenital LQTS can be inherited in either an autosomal dominant or autosomal recessive manner with an estimated prevalence of approximately one in 2500 individuals (Schwartz 2009; Schulze Bahr 2012). A number of investigations have shown that it is an important cause of cardiac arrest in young, otherwise healthy individuals (Vincent 1998). Over 700 mutations in 12 genes have been linked to the pathogenesis of the disorder, however, for approximately 25% of patients with compelling LQTS clinical diagnoses, no causative mutations have been found (Napolitano 2005; Medeiros-Domingo et al. 2007b; Newton-Cheh et al. 2009). It is therefore important to identify new candidate genes to screen for LQTS causative mutations.

The present study aims to approach this problem by performing yeast two-hybrid analysis (Y2H) to identify potential novel candidate genes for LQTS. It has been well established that LQTS is involved in the dysfunction of cardiac ion channels and that eight of the 12 genes that have been mutated in congenital LQTS encode ion channels and their accessory proteins.

Hypothesis:

We therefore hypothesize that genes encoding proteins that interact with ion channels could also be mutated in LQTS. Furthermore, in addition to environmental factors, other disease-modifying genes exist that influences the expression of the LQTS phenotype. Consequently, we believe that the genes encoding KCNE2-interacting proteins may also be considered as candidate disease-modifying genes that can be screened in a cohort of LQTS patients.

Objectives

In the present study, we used the C-terminal domain of KCNE2, whose encoding gene is frequently mutated in LQT6 (Figure 1.13), as bait to screen a pre-transformed cardiac cDNA library using Yeast two-hybrid (Y2H) analysis.

We chose to focus on the C-terminal domain since many of the LQTS causative mutations have been found in this part of the *KCNE2* gene. We foresee that this study will help us gain a better understanding into the role of *KCNE2* in LQTS as well as provide us with novel candidate genes to screen for LQTS-causative mutations.

The objectives of the study are to perform an Y2H screen and to verify the newly identified interactions using independent biochemical analysis, which include 3D co-localization and co-immunoprecipitation.

Chapter 2

Materials and methods

Page

2.1 DNA EXTRACTION **43**

2.1.1 Bacterial plasmid purification using the Zyppy™ Plasmid Miniprep Kit **43**

2.1.2 Bacterial plasmid purification using GTpure™ Plasmid Miniprep Kit **43**

2.1.3 Yeast plasmid purification **44**

2.1.4 DNA purification using the Wizard® SV Gel and PCR Clean-up System **45**

2.1.5 Gel purification of products from agarose gels using the Wizard® SV Gel and PCR Clean-up System **45**

2.2 POLYMERASE CHAIN REACTION (PCR) **45**

2.2.1 Oligonucleotide primer design and synthesis **45**

2.2.1.1 Primers for generation of insert for Y2H cloning 45

2.2.1.2 Primers for Y2H insert sequencing 46

2.2.2 PCR-amplification for generation of *KCNE2* C-terminus fragment **47**

2.2.3 Bacterial colony PCR **47**

2.3 GEL ELECTROPORESIS **48**

2.3.1 Agarose gel electrophoresis **48**

2.3.2 Sodium dodecyl sulphate polyacrylamide gel electrophoresis (SDS-PAGE) **48**

2.4 AUTOMATED DNA SEQUENCING **49**

2.5 SEQUENCE ANALYSIS **49**

2.5.1 DNA sequence analysis **49**

2.5.2 Protein sequence analysis **50**

2.6 RESTRICTION ENZYME DIGEST **50**

2.6.1 Restriction enzyme digest for cloning inserts **50**

2.6.2 Restriction mapping for yeast two-hybrid (Y2H) prey clones **51**

2.7 GENERATION OF CONSTRUCTS 52
2.7.1 Generation of Y2H construct 52
2.7.2 Alkaline phosphatase treatment of vector 52
2.7.3 DNA ligation 52

2.8 BACTERIAL STRAINS, YEAST STRAINS AND CELL LINES 53
2.8.1 Bacterial strains 53
2.8.2 Yeast strains 53

2.9 GENERATION OF *E.coli* DH5α COMPETENT CELLS 54

2.10 CULTURING OF THE H9C2 CELL LINE 54
2.10.1 Culture of H9C2 cells from frozen stocks 54
2.10.1.1 Thawing the cells 54
2.10.1.2 Removing DMSO from stocks and culturing cells 55
2.10.2 Splitting cell cultures 55
2.10.3 Differentiation of H9C2 cells 56

2.11 TRANSFORMATION OF PLASMIDS INTO PROKARYOTIC CELLS 56
2.11.1 Bacterial transformations 56
2.11.2 Yeast transformations 57

2.12 ASSESSMENT OF Y2H CONSTRUCTS 58
2.12.1 Phenotypic assessment of yeast strains 58
2.12.2 Toxicity test of transformed cells 58
2.12.3 Mating efficiency testing 59

2.13 Y2H ANALYSIS 60
2.13.1 Cardiac cDNA library 61
2.13.2 Establishment of bait culture 61
2.13.3 Haemocytometric cell count 62
2.13.4 Library mating 63
2.13.5 Library titre and Library mating efficiency 64
2.13.6 Activation detection of nutritional reporter genes 64
2.13.6.1 Selection of transformant yeast colonies 64

2.13.6.2 Selection of diploid yeast colonies containing putative interactor peptides 65
2.13.7 Activation detection of colourimetric reporter genes **65**
2.13.7.1 X-α-galactosidase assay 65
2.13.8 Rescuing prey plasmids from diploid colonies **66**
2.13.9 Interaction specificity test **66**
2.14 CO-IMMUNOPRECIPITATION (Co-IP) PREPARATION **67**
2.14.1 Hypoxia treatment of differentiated H9C2 cardiomyocytes **67**
2.14.2 Cell lysis **67**
2.14.3 Bradford protein concentration determination **68**
2.15 CO-IMMUNOPRECIPITATION (Co-IP) **68**
2.16 WESTERN BLOTTING **69**
2.16.1 Membrane blocking **69**
2.16.2 Addition of primary antibody **69**
2.16.3 Addition of secondary antibody **70**
2.16.4 Chemiluminescent visualization of membrane proteins **70**
2.17 THREE-DIMENSIONAL CO-LOCALIZATION **71**
2.17.1. Three-dimensional co-localization assay **71**

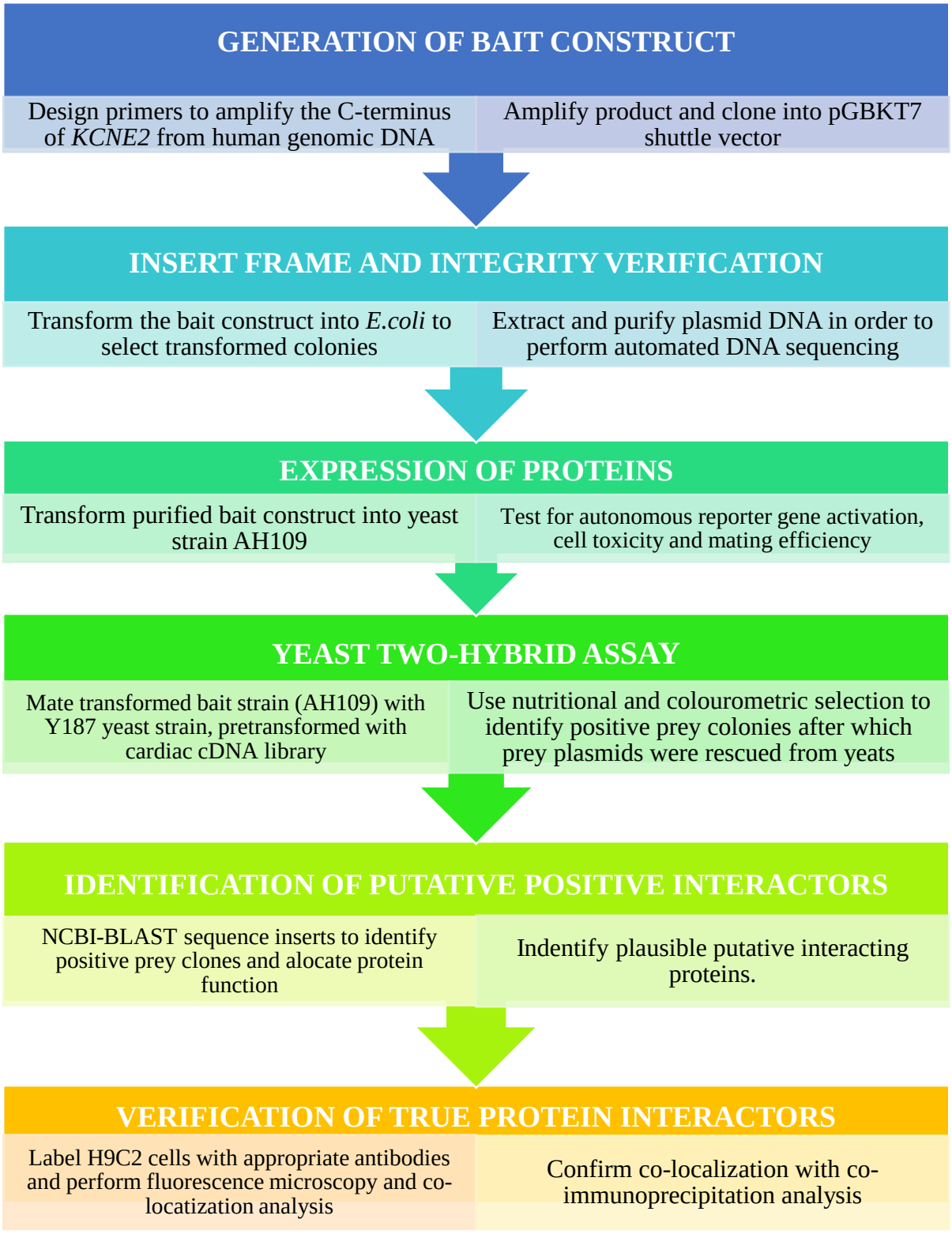

Figure 2.1: Summary of methodology followed in the present study.

2.1 DNA EXTRACTION

2.1.1 Bacterial plasmid purification using the Zyppy™ Plasmid Miniprep Kit

In order to isolate the specific plasmids from successfully transformed *Escherichia coli* (*E.coli*) cultures, single colonies were picked from the antibiotic selection plates and inoculated in 50ml polypropylene tubes. These tubes contained 10ml Luria-Bertani Broth (LB) media (Appendix I) as well as the appropriate antibiotic (Ampicillin or Kanamycin). The bacterial cultures were then incubated at 37ºC overnight in a shaking YIH DER model LM-530 (Scilab Instrument Co., Ltd., TW) incubator.

After the incubation period the cultures were centrifuged in a Beckman model TJ-6 centrifuge (Beckman Coulter, Scotland, UK) for 10min at 2400rpm. The supernatant was discarded and the pellet resuspended in 600µl dH_2O. The Zyppy™ Plasmid Miniprep Kit (Zymo Research Corp., USA) was then used as per manufacturer's instructions and the plasmid purified and eluted with 30µl of dH_2O.

After purification, a volume of 2µl of plasmid preparation was used to assess quality and the concentration of the plasmid determned using a Nanodrop Spectrophotometer (Thermo Scientific, USA). The remainder of the purified product was used as template for yeast transformation reactions (Section 2.11.2). This kit was also used to assist in yeast plasmid purification (Section 2.1.3) and was found to yield higher concentrations than the GTpure™ Plasmid Miniprep Kit (Section 2.1.2) initially used for bacterial plasmid purification.

2.1.2 Bacterial plasmid purification using the GTpure™ Plasmid Miniprep Kit

The specific *E.coli* colonies containing the plasmids of interest were picked from the antibiotic selection plates or 100µl of the bacterial glycerol stock was inoculated in 50ml polypropylene tubes containing 10ml of LB media (Appendix I) as well as the appropriate antibiotic. The cultures were incubated at 37ºC shaking in a YIH DER model LM-530 (Scilab Instrument Co., Ltd., TW) incubator at 250rpm overnight.

The following day the cultures were centrifuged for 10 minutes at 2600rpm in a Beckman model TJ-6 centrifuge (Beckman Coulter, UK) and the supernatant discarded. The plasmid DNA were

then extracted from the pellets using the GTpure™ Plasmid Miniprep kit (Gene Tech Co., Ltd., HK) as indicated by the manufacturer's instructions.

After purification, 2µl of the plasmid preparation was used to determine the purity and concentration of the sample by using a Nonodrop Spectrophotometer (Thermo Scientific, USA) and the remainder of the product used for sequencing reactions following recommendation by the manufacturer.

2.1.3 Yeast plasmid purification

Plasmids of interest were isolated from yeast (*Saccharomyces cerevisiae*) cultures by inoculating 100µl of the yeast glycerol stocks in 1ml of single dropout (SD) media (Appendix I) containing the correct dropout supplement (BD Biosciences, Clontech, USA) in 15ml polypropylene tubes. The cultures were placed in a shaking incubator (Scilab Instrument Co., Ltd., TW) at 30ºC overnight, shaking at 250rpm. The following day, 4ml of YPDA media (Appendix I) was added to the overnight cultures. The cultures were incubated in a shaking incubator at 30ºC for an additional four to five hours. Subsequently the cultures were centrifuged at 3000rpm for five minutes in a Beckman model TJ-6 centrifuge (Beckman Coulter, UK) and the supernatant discarded by pouring off the liquid.

The pellets were then resuspended in the residual supernatant and transferred to a clean 2ml Eppendorf tube and subsequently centrifuged at 15000rpm for 30 seconds in a bench top centrifuge (Labnet International Inc., USA). The supernatant was discarded and to the pellet 200µl yeast lysis buffer (Appendix I), 200µl Phenol Chloroform Isoamyl alcohol (PCI) and 0.3g sterile 450-600µm glass beads (Sigma-Aldrich (Pty) Ltd., RSA) was added. The cells were then vortexed for at least two minutes followed by centrifugation at 15000rpm for 10 minutes at room temperature in a bench top centrifuge (Labnet International Inc., USA) for phase separation.

The top aqueous layer was then transferred to sterile 1.5ml Eppendorf tubes. An additional lysis step was included by adding 100µl lysis buffer (Zyppy Plasmid Miniprep Kit, Zymo Research Corp., USA) to the aqueous layer as well as 350µl neutralization buffer (Zyppy Plasmid Miniprep Kit, Zymo Research Corp., USA) and 200µl membrane binding solution (Wizard® Purefection Mini Plasmid DNA purification kit, Promega Corp., USA). The mixtures were then

centrifuged for 10 minutes at 15000rpm in a bench top centrifuge (Labnet International Inc., USA). The aqueous layers were then transferred to the spin columns of the Wizard® Purefection Mini Plasmid DNA purification kit and purified as per manufacturers' instructions (section 2.1.4). Following purification, DNA was eluted with 35µl of sterile water.

2.1.4 DNA purification using the Wizard® SV Gel and PCR Clean-up System

Purification of the yeast plasmid preparations (Section 2.1.3), PCR-amplified products (Section 2.2) as well as restriction enzyme digest clean-up experiments (Section 2.6) were performed using the Wizard® SV Gel and PCR Clean-up System (Promega Corp., USA) according to the manufacturers' instructions. The products were used for bacterial transformation reactions (Section 2.12.1) and cloning reactions (Section 2.6) respectively.

2.1.5 DNA purification from agarose gels using the Wizard® SV Gel and PCR Clean-up System

When performing restriction enzyme digestions, the final digested product was electrophoresed in a 1% agarose gel (Section 2.3.1) and viewed under short wave ultraviolet (UV) light. If the band was indeed the correct size, a sterile blade was used to remove the segment of the gel that contained the DNA fragment of interest. The agarose gel slice was transferred to an autoclaved eppendorf tube after which the DNA was purified using the Wizard® SV Gel and PCR Clean-up System following the manufacturer's protocol and instructions.

2.2 POLYMERASE CHAIN REACTION (PCR)

2.2.1 Oligonucleotide primer design and synthesis

2.2.1.1 Primers for generation of insert for Y2H cloning

Primers used to PCR-amplify the C-terminus of *KCNE2* were designed using Oligo Analyzer Integrated DNA Technologies software (http://eu.idtdna.com/analyzer/applications/oligoanalyzer/) and synthesized at the University of Cape Town DNA synthesis Laboratory (University of Cape Town, RSA).

The GenBank database (http://www.ncbi.nlm.nih.gov/Entrez) mRNA sequence for *KCNE2* (NM_172201.1) (Appendix I) was used as a reference sequence for designing the forward and

reverse primers. Each primer set was analysed for self-complementarities, primer-primer complementarities and hairpin structures. The GC content and melting temperature compatibility could also be determined using this software.

The primer sequences were finally submitted to the Basic Local Alignment Search Tool (BLAST) (http://www.ncbi.nlm.nih.gov/BLAST) in order to determine whether they were able to anneal to other genomic DNA sequences.

To facilitate the cloning of the PCR-amplified *KCNE2* amplicon into the pGBKT7 shuttle vector (BD Bioscience, Clontech, USA) restriction enzyme sites were incorporated into the primers. The forward primer was designed to contain the *NdeI* restriction site in the 5 prime (5') end, while the reverse primer contained the *EcoR1* restriction enzyme site as well as the stop codon (TGA).

The sequence of the primers used for cloning the KCNE2 C-terminal encoding amplicon into pGBKT7 is shown in table 2.1.

Table 2.1: Nucleotide sequences of primers used to amplify the C-terminal of *KCNE2*

Primer	Sequence	Ta (ºC)
KCNE2-F^{Nde1}	**5' - ACTGCAGAACATATG CTCAAATCCAAGAGACGG - 3'**	50
KCNE2-R^{EcoR1}	**5' - ACTGCAGAAGAATTCCTATCAGGGGAACATTTTGAAC - 3'**	51

Abbreviations: Ta = Annealing temperature, ˚C = Degrees Celsius. The **blue** text represents a tag which facilitates restriction enzyme digestion, while the **green** and **purple** sequences correspond to the *Nde1* and *EcoR1* restrictions sites respectively. The short **pink** sequence symbolizes the stop codon and the **black** text represents the sequence of the primer which will anneal to the DNA in the PCR amplification reaction.

2.2.1.2 Primers for Y2H insert sequencing

Vector-specific primers were designed to flank the multiple cloning sites (MCS) of pGBKT7 and pACT2 shuttle vectors (BD Bioscience, Clontech, USA) (Appendix II). This was necessary in order to sequence the inserts cloned into these Y2H vectors. The sequences used to generate the primers were acquired from the Clontech™ Matchmaker™ vector guide (www.clontech.com) and are shown in table 2.2.

Table 2.2: Primers used for sequencing inserts from Y2H cloning vectors

Primers	Sequence	Ta(˚C)
pGBKT7-F	5'- GTAATACGACTCACTATAGGGC -3'	64
pGBKT7-R	5'-AAACCCCTCAAGACCCGTTT-3'	60
pACT2-F	5'-CTATTCGATGATGAAGATACCCCACCAAACCC-3'	68
pACT2-R	5'-GTGAACTTGCGGGGTTTTTCAGTATCTACGA-3'	68

Abbreviations: Ta = Annealing temperature, ˚C = Degrees Celsius

2.2.2 PCR-amplification for generation of *KCNE2* C-terminus fragment

Since the C-terminus of KCNE2 is encoded by a single exon (exon 2) of the *KCNE2* gene, the fragment of interest was amplified from human DNA (Section 2.13.1) by means of PCR. The product of this amplification was subsequently cloned into the Y2H bait vector, pGBKT7 (Section 2.7) (Appendix II).

For the amplification reaction, 20ng of genomic DNA was used in a final reaction volume of 50µl. The reaction included 150ng of each primer, forward and reverse (Table 2.1), 5x Buffer, 10mM dNTP's (dATP, dCTP, dTTP and dGTP) (Kapa Biosystems (Pty) Ltd., RSA) 25mM $MgCl_2$, 5u/µl long range Taq™ DNA polymerase (Kapa Biosystems (Pty) Ltd., RSA) as well as sterile distilled water to a final volume of 50µl. The reaction was performed in a Mastercycler® ep PCR system (Eppendorf, GER). The cycle parameters consisted of a denaturing step at 95ºC for four minutes, followed by 30 cycles of 95ºC for 30 seconds, 68°C for 30 seconds and 72ºC for 30 seconds after which an extension step followed for 10 minutes at 72ºC. The products of the PCR reaction was then visualized on a 1% agarose gel under UV light to verify amplification of the correct fragment (Section 2.3.1).

2.2.3 Bacterial colony PCR

The vectors used in Y2H do not support blue-white selection. Therefore, in order to identify bacterial colonies harbouring the recombinant plasmid constructs, bacterial colony PCRs were performed. Small amounts from the individual bacterial colonies were used as DNA templates which were selected from the appropriate agar plates. Vector-specific primers were used to amplify the desired fragments (Table 2.2).

The reaction was carried out in a Mastercycler® ep PCR system with a final reaction volume of 50µl. The reaction consisted of 150ng/µl of vector-specific forward and reverse primers (Table2.2), 25µl Readymix (Kapa Biosystems (Pty) Ltd., RSA) and distilled water was used to make up the final volume. The thermal cycling parameters were as follows: a denaturing step at 95ºC for eight minutes, followed by 30 cycles of 94ºC for 30 seconds, Ta (Table 2.2.) for 30 seconds and 72ºC for one minute, followed by an elongation step at 72ºC for five minutes.

In each of the PCR reactions described in the paragraphs above, a negative control was included (i.e. no DNA was included in one specific sample for each PCR reaction) to detect any contamination during the process.

The final PCR products were then visualized by gel electrophoresis on a 1% agarose gel for verification (Section 2.3.1).

2.3 GEL ELECTROPORESIS

2.3.1 Agarose gel electrophoresis

In the present study, agarose gel electrophoresis was used either to visualize fragments that have been amplified by PCR (Section 2.2), plasmid preparation integrity (Section 2.1.1), for excision of DNA fragments for purification after restriction digest (Section 2.1.5) or for visualization of identical prey-inserts identified by restriction mapping (Section 2.6.2).

2.3.2 Sodium dodecyl sulphate polyacrylamide gel electrophoresis (SDS-PAGE)

Proteins from co-immunoprecipitation (Co-IP) reactions (Section 2.15) as well as western blot analyses (Section 2.16) were electrophoresed in Mini-PROTEAN® TGX™ precast polyacrylamide gels (Bio-Rad Laboratories (Pty) Ltd., RSA) containing 1% Sodium dodecyl sulphate **(**SDS) ranging from 4% to 15% depending on the size of the proteins (Appendix I). Typically 10µl - 35µl loading dye (Appendix I) was mixed with 150µg of Co-IP reaction product or 50µg whole cell lysate (Section 2.10.4) for western blot analysis and incubated at 95°C for five minutes. Ten microlitres of molecular weight marker (Spectra™ Multicolor Broad Range Protein Ladder, Thermo Scientific, USA) was co-electrophoresed with the protein products. The samples were loaded onto the vertical gel along with two negative controls (HA-probe and

protein agarose G) and electrophoresed at 100V for approximately 1 hour in 1x SDS-PAGE running buffer (Appendix I).

2.4 AUTOMATED DNA SEQUENCING

The bacterial cultures were grown in 10ml Luria-Bertani (LB) media (Appendix I) along with 10µl or 20µl of the appropriate antibiotic (either 50mg/ml Ampicillin or 100mg/ml Kanamycin respectively) at 37ºC in a shaking incubator (Scilab Instrument Co., Ltd., TW). Following this, the plasmids were extracted and purified using the Zyppy™ Plasmid Miniprep Kit (Section 2.1.1). The samples were diluted to a final concentration of 200ng/µl and the gene fragment specific primers (Table 2.1) as well as the vector-specific primers (Table 2.2) were diluted to 1.1pmol each. The tubes were labeled accordingly and send for automated sequencing on an ABI Prism™ 377 or ABI Prism™ 3100 sequencer (P.E. Biosystems, USA) at the Central DNA Sequencing Facility at Stellenbosch University (Central Analytical Facilities-DNA Sequencing Unit, Department of Genetics, University of Stellenbosch, RSA).

2.5 SEQUENCE ANALYSIS

All sequenced data was analysed using the BioEdit Sequence Alignment Editor Software system (Ibis Biosciences, USA) as well as the DNAman software (Lynnon Corp., USA) to verify the sequence integrity and identity of the fragments generated. The generated fragments were compared to their reference sequences obtained from GenBank database (www.ncbi.nlm.nih.gov/Entrez).

2.5.1 DNA sequence analysis

DNA sequence analysis was done to verify the sequence integrity of the *KCNE2* fragment generated by PCR amplification (Section 2.2.2) as well as to identify Y2H putative interactor prey clones selected during the Y2H library screening.

The C-terminus fragment of *KCNE2* generated in this study was compared to the *KCNE2* reference sequence from the GenBank database (www.ncbi.nlm.nih.gov/Entrez) to establish whether the sequence integrity and reading frame were maintained. The Y2H prey constructs

were identified by BLASTn comparison of the nucleotide sequences against the GenBank database (www.ncbi.nlm.nih.gov/Entrez) and the Ensembl database. (www.ensembl.org).

2.5.2 Protein sequence analysis

The DNA insert sequences identified in the Y2H screen were translated into protein in the frame dictated by the of the GAL4 activation domain reading frame (reading frame 1). The protein sequences were subsequently compared to human reference protein sequences in the Swissprot database using BLASTp in order to identify the protein.

Once proteins have successfully been identified, GeneCards (http://www.genecards.org/) and neXtProt (http://www.nextprot.org/) were used to analyse the proteins and determine their location, structure and function.

2.6 RESTRICTON ENZYME DIGESTION

2.6.1 Restriction enzyme digest for cloning inserts

In order to clone the PCR-generated (Section 2.2.2) fragment into the specific pGBKT7 bait vector (Appendix II) for Y2H analysis, the fragment as well as the plasmid were consecutively double-digested using appropriate restriction enzymes (*NdeI* and *EcoRI*). The restriction enzymes as well as their corresponding buffers were provided by New England Biolabs (New England Biolabs® Inc., RSA). Primers designed to amplify this insert and specific restriction enzyme sites which were included in the primer sequences can be seen in table 2.1.

The PCR fragment of *KCNE2* and the plasmid DNA of the shuttle vector was used as the DNA template for the restriction enzyme digest reactions which was prepared in a final volume of 50µl consisting of the following reagents: 30µl of the PCR-generated fragment or 20µl of vector DNA, 5µl restriction enzyme buffer, 2µl *Nde1* restriction enzyme and sterile water to make up the final volume of 50µl. The mixtures were incubated for two hours at 37ºC in a model 329 stationary CO_2 incubator (Former Scientific, USA). Following the incubation period, the enzymes were heat inactivated at 65ºC for 5 minutes after which the samples were purified using the Wizard® SV Gel and PCR Clean-up System (Promega Corp., USA) (Section 2.1.4) and eluted with 43µl sterile water.

The eluted mixtures were used as templates for the second digest reaction to which 5µl of enzyme buffer and 2µl *EcoR1* restriction enzyme was added. The samples were then incubated at 37ºC for another two hours. The samples were subsequently heat inactivated and finally purified using the Wizard® SV Gel and PCR Clean-up System (Promega Corp., USA) (Section 2.1.4) and eluted with 30µl sterile water.

To guarantee that the double-digested pGBKT7 vector do not anneal to itself, the vector was treated with *Calf Intestinal Alkaline Phosphatase (CIAP)* (Section 2.7.2) before being used in the DNA ligation (Section 2.7.3) reactions. The final digested fragments were loaded onto a 1% agarose gel, electrophoresed (Section 2.3.1) and subsequently purified using the Wizard™ SV Gel and PCR Clean-up system (Section 2.1.5).

2.6.2 Restriction mapping for yeast two-hybrid (Y2H) prey clones

Restriction mapping was performed on Y2H prey-inserts that interacted with the pGBKT7-*KCNE2* construct. This was carried out with the purpose of grouping identical prey plasmids identified by Y2H analysis. These inserts were transformed into *E.coli* (Section 2.11.1) and ultimately the plasmids purified using the Zyppy™ Miniprep kit (Section 2.1.1). The purified plasmids were digested with *HaeIII* restriction enzyme (New England Biolabs® Inc., RSA) in a final volume of 10µl digest mixture consisting of 5µl plasmid DNA, 1µl enzyme buffer, 0.2µl *HaeIII* enzyme and 3.8µl ddH_2O. The samples were then incubated at 37ºC for two hours and subsequently viewed on a 1.5% agarose gel (Section 2.3.1).

The restriction pattern for each sample was analysed and compared to each other. Samples that showed the same restriction digest patterns for the *HaeIII* digest were selected and digested with a second enzyme, *RsaI* (Promega Corp., USA), in a subsequent reaction with the same conditions as the previously described reaction. This was done to verify the similarities between inserts.

If it was found that the inserts had the same patterns for the *HaeIII* as well as the *RsaI* restriction enzyme digest, they were considered to be identical clones and one sample was chosen out of the group as a representative.

2.7 GENERATION OF CONSTRUCTS

2.7.1 Generation of Y2H construct

The pGBKT7 shuttle vector (Appendix II) was used as the bait vector into which the Y2H bait-insert was cloned (Section 2.2). Following automated sequence analysis (Section 2.5) to verify the integrity of the insert as well as the reading frame conservation of the sequence, the construct was transformed into the yeast strain AH109 (Section 2.11.2). This construct was subsequently used to screen a Clontech MATCHMAKER pre-transformed cardiac cDNA library (BD Biosciences, Clontech, USA) (Section 2.13.1). The library consisted of cardiac cDNAs which was cloned into pACT2 prey-vectors (Appendix II) and transformed into the yeast strain Y187.

2.7.2 Alkaline phosphatase treatment of vector

The ends of the linearised plasmids, which had been double digested with restriction enzymes *Nde1* and *EcoR1*, were *CIAP*-treated to remove the phosphate groups and thus prevent the plasmid to re-anneal to itself and reform a circularized vector.

Briefly, 30µl pGBKT7 vector DNA, 2µl *CIAP* (Promega Corp., USA), 10µl *CIAP* buffer (Promega Corp., USA) and 58µl of sterile water were transferred to a 1.5ml sterile Eppendorf tube. The reaction mixture was incubated at 37ºC for 15 minutes followed by 15 minute incubation at 56ºC to inactivate the *CIAP*. Following this, an extra 2µl of *CIAP* was added to the reaction after which the incubation and inactivation cycles were repeated.

The *CIAP*-treated pGBKT7 vector was subsequently purified using the Wizard™ SV Gel and PCR Clean-up System (Promega Corp., USA) (Section 2.1.4) and used in the ligation reactions (Section 2.7.3).

2.7.3 DNA ligation

In order to generate the construct for Y2H analysis, DNA ligation reactions were performed. The ligation reaction was done using three separate dilution ratios to ensure the optimum conditions for the constructs to be produced (Table 2.3).

Table 2.3: DNA ligation reaction ratios

Reagents	Ratios 1:1	1:3	1:5
Insert DNA	1µl	3µl	5µl
Vector DNA	1µl	1µl	1µl
T_4 DNA Ligase buffer (10x buffer)	1µl	1µl	1µl
T_4 DNA Ligase (5 Weiss units/µl)	1µl	1µl	1µl
ddH_2O	6µl	4µl	2µl
Total volume	**10µl**	**10µl**	**10µl**

The T_4 DNA ligase buffer as well as the 5 Unit T_4 DNA ligase reagent was supplied by Promega Corp., USA. The ratio of insert DNA to vector DNA was 1:1.

The ligation reactions were incubated at 4ºC for a period of 16 hours (overnight) to allow ligation of the insert and vector DNA to take place. Subsequently, 5µl of each reaction was transformed into *E.coli* (DH5α bacterial strain; Appendix VI) (Section 2.12.1) and plated onto LB agar plates (Appendix I) containing the appropriate antibiotic. The plates were incubated at 37˚C in a stationary incubator in a model 329 stationary CO_2 incubator (Former Scientific, USA) overnight. Successful transformed colonies were subsequently identified by colony PCR (Section 2.2.3).

2.8 BACRTERIAL STRAINS, YEAST STRAINS AND CELL LINES

2.8.1 Bacterial Strains

The transformation of ligation reactions (Section 2.7.3) into *E.coli* strain DH5α was carried out in order to select and purify Y2H constructs. The transformed colonies were selected according to their ability to grow on antibiotic selection LB agar plates (Appendix I) and the recombined plasmids identified by colony PCR (Section 2.2.3). For the selection of pGBKT7 recombinant plasmids, Kanamycin (100mg/ml stock) was used as the antibiotic and when selecting pACT2 recombinant plasmids, Ampicillin (50mg/ml stock) was used.

2.8.2 Yeast Strains

After identification of the recombined *KCNE2*-pGBKT7 construct, the purified product was cloned into the AH109 yeast strain (Section 2.11.2). The clones present in the pre-transformed

Clontech MATCHMAKER cDNA library (Section 2.13.1) which was used in the Y2H screen had been transformed into the yeast strain Y187.

2.9 GENERATION OF *E.coli* DH5α COMPETENT CELLS

An aliquot of 20µl of *E.coli* DH5α frozen (-80ºC) glycerol stock was used to inoculate 10ml of LB media (Appendix I) without any antibiotics in a 50ml polypropylene tube. The tube was incubated at 37ºC in a shaking incubator (YIH DER model LM-530, Scilab Instrument Co., Ltd., TW) for 16 hours at 200rpm after which 300µl of the culture was inoculated in 2L Erlenmeyer flask containing 200ml of LB media (Appendix I). These flasks were shaken on a Labcon orbital shaker (Labcon (Pty), Ltd., RSA) at room temperature for 16 hours at 70rpm until the culture reach the mid-log growth phase (OD_{600nm} = 0.6).

Once the culture has reached the acquired optical density, the 200ml liquid culture was transferred to 4 x 50ml polypropylene tubes and centrifuged for 15 minutes at 4ºC, 3000rpm in a Beckman model TJ-6 centrifuge (Beckman Coulter, Scotland, UK). The supernatant was discarded and the pellet resuspended in 8ml of ice-cold CAP buffer (Appendix I).

The suspension was centrifuged again in a Beckman model TJ-6 centrifuge (Beckman Coulter, Scotland, UK) at 4ºC, 3000rpm to re-pellet the cells. The supernatant was removed for the second time and the pellet resuspended in 4ml of ice-cold CAP buffer (Appendix I). The cells were transferred in volumes of 200µl into 2ml eppendorf tubes and stored at -80ºC until it was needed for bacterial transformation reactions (Section 2.12.1).

2.10 CULTURING OF THE H9C2 CELL LINE

2.10.1 Culture of H9C2 cells from frozen stocks

2.10.1.1 Thawing the cells

Frozen *Rattus norvegicus* (rat) H9C2 cardiac myocytes were purchased from the American Type Culture Collection (ATCC, USA). The frozen stock was thawed rapidly by immersing the tube in a 37ºC water bath for 10 minutes. After adequate thawing of the cells, the vile was immediately sterilized by spraying the outside with 70% ethanol.

2.10.1.2 Removing DMSO from stocks and culturing cells

Dimethyl sulphoxide (DMSO) is used as a cryoprotectant and added to cell media to reduce ice forming, thereby preventing cell death during the freezing process. It is used in a slow-freeze method after which cells can be stored in liquid nitrogen. In order to remove this toxic substance from the frozen stocks and to ensure viability of the cells the following method was used: The thawed stock culture was added to 1ml of pre-warmed growth media (Appendix I) in a 12ml Greiner tube (Greiner Bio-one, GER) and mixed by moderate pipetting. Another 5ml of growth media was added to the tube and the cells pelleted by centrifugation at 1000rpm for one minute using a Sorval® GLC-4 General Laboratory centrifuge (Separations Scientific, RSA). The supernatant was removed and the pellet resuspended in an additional 5ml of growth media and the cells pelleted again using a Sorval® GLC-4 General Laboratory centrifuge (Separations Scientific, RSA). The cell pellet was subsequently resuspended in 10ml of growth media and transferred into a T25 culture flask. The flask was lightly swirled to make sure the cells were distributed evenly throughout the flask. The flask was then incubated in a Farma-therosteri-cycle 5% carbon dioxide ($CO_{2)}$ humidified incubator (Farma International, USA) at 37ºC.

2.10.2 Splitting cell cultures

When cells were needed for various experiments, they were cultured at 37ºC in a Farma-therosteri-cycle 5% CO_2 humidified incubator (Farma International, USA) and split every two to four days depending on when they reached approximately 80-90% confluency. Before splitting the cells, the growth media was removed with a sterile pipette and the cells washed with trypsin to remove dead cells and/or cell debris. After this wash step, the trypsin was removed and an additional volume of trypsin (Table 2.4) was added to facilitate detachment of the cells from the growth surface. The flask was then incubated at room temperature for approximately 10-15 minutes after which a volume of growth media was added (Table 2.4) in which the detached cells were resuspended.

The suspension was transferred to a 12ml Greiner tube (Greiner Bio-one, GER) and centrifuged at 1000rpm for 30 seconds using a Sorval® GLC-4 General Laboratory centrifuge (Separations Scientific, RSA) to create a pellet. The pellet was resuspended in 4ml of growth media. Depending on the confluency of the cells before the splitting process began, the size of the flask

as wells as the number of flasks into which the cells will be split, an estimated volume of resuspended cells were placed into flasks containing fresh sterile growth media.

Table 2.4: Standard Trypsin volumes for detachment of cells from growth surface

Flask size	Volume of Trypsin	Volume of media
Small (25cm^2)	1ml	4ml
Medium (75cm^2)	3ml	4ml
Large (150cm^2)	5ml	4ml

Abbreviations: cm^2, square centimetre; ml, millilitre

2.10.3 Differentiation of H9C2 cells

In order to facilitate differentiation of cardiomyocytes into myotubes, the growth medium was removed from the flasks or 6-well plates after 24 hours of incubation at 37ºC in a Farma-therosteri-cycle 5% CO_2 humidified incubator (Farma International, USA). The cells were washed with a small volume of differentiation medium (Appendix I) after which the appropriate volume of differentiation medium was added to each container (3ml to each well of the 6-well plates or 23ml to a large 150cm^2 culture flasks). The cells were then incubated for 10-14 days at 37ºC in a Farma-therosteri-cycle 5% CO_2 humidified incubator (Farma International, USA). On the fifth day, the cells were washed again and new differentiation media was added and on day 10-14, the cells were viewed on an Olympus IX 81 motorised inverted microscope (Olympus, GER) to confirm differentiation of the cells. The cells were later used in 3D co-localization assays (Section 2.17).

2.11 TRANSFORMATION OF PLASMIDS INTO PROKARYOTIC CELLS

2.11.1 Bacterial transformations

Prior to transforming plasmids of interest into the bacteria, tubes containing 200µl aliquots of *E.coli* DH5α cells (Section 2.9) were removed from the -80ºC freezer and thawed on ice for 20 minutes. Once the cells had thawed, 5µl of plasmid preparation (Section 2.1.1) or 5µl of ligation reaction (Section 2.7.3) was added to the tube and the mixture was incubated on ice for an

additional 20 minutes. Following this incubation step, the samples were heat-shocked for exactly 45 seconds at 42ºC in a heating block (Dry Block Heater HB2) (Hägar designs, RSA).

The samples were removed and incubated at room temperature for two minutes. Following this, 1ml of LB media (Appendix I) was added to each sample and incubated at 37ºC for one to two hours shaking at 200rpm in a YIH DER model LM-530 (Scilab Instrument Co., Ltd., TW) shaking incubator.

The samples were subsequently centrifuged for four minutes in a bench top centrifuge (Labnet International Inc., USA). Next, 200µl of the supernatant was drawn off with a pipette and the rest discarded. The 200µl was used to resuspend the pellet and plate the sample on LB agar plates (Appendix I) containing the appropriate antibiotic. The plates were inverted and incubated for 16 hours at 37ºC in a model 329 stationary CO_2 incubator (Former Scientific, USA).

2.11.2 Yeast transformations

In order to perform yeast transformations, 200µl aliquots of the yeast strain to be transformed (AH109 or Y187) were plated onto YPDA agar plates (Appendix I). These were inverted and incubated at 30ºC for three to four days in a Sanyo MIR262 stationary ventilated incubator (Sanyo Electronic Co., Ltd., JP). Once the yeast has grown enough, a volume representing 20-50µl of yeast cells were picked from the plate and resuspended in 1ml of sterile Millipore water in a 2ml Eppendorf tube. The cells were pelleted by centrifugation for 30 seconds at 2000g in an Eppendorf model 5417C centrifuge (Eppendorf International, GER). The supernatant was discarded and the pellet resuspended in 1ml of Lithium Acetate (Appendix I) and incubated at 30ºC for five minutes in a stationary ventilated incubator (Sanyo Electronic Co., Ltd., JP). Again the cells were pelleted by centrifugation at 2000g for 30 seconds in an Eppendorf model 5417C centrifuge (Eppendorf International, GER) and all the Lithium Acetate removed with a pipette. Following this, five reagents were rapidly added to the pellet in the following order: 240µl 50% Polyethylene glycol (PEG), 36µl 1M Lithium Acetate, 25µl of 2mg/ml heat-denatured and snap-cooled herring sperm DNA (Promega Corp., USA), 10-20µl *E.coli* plasmid preparation (Section 2.1.1) and 30-40µl sterile Millipore water. The sample was then generously mixed by vortexing for at least one minute, using a Snijders model 34524 press-to-mix vortex (Snijders Scientific, NL). The sample was incubated at 42ºC for 25 minutes in a dry heating block (Dry Block

Heater, HB2) (Hägar designs, RSA). After incubation, the cells were pelleted again by centrifuging the tubes for 30 seconds at 2000rpm in an Eppendorf model 5417C centrifuge (Eppendorf International, GER). The supernatant was completely removed with a pipette and the pellet resuspended in 200µl of sterile Millipore water. The suspension was plated onto the appropriate selection plates (Appendix I), inverted and incubated at 30ºC for two to five days in a Sanyo MIR262 stationary ventilated incubator (Sanyo Electronic Co., Ltd., JP).

2.12 ASSESMENT OF Y2H CONSTRUCTS

2.12.1 Phenotypic assessment of yeast strains

Both yeast strains used in the Y2H analysis (AH109 and Y187) were assessed based on their phenotype, prior to transformations being performed. The strains were both plated onto agar plates lacking individual essential amino acids (Appendix I), i.e., SD^{-Ade}, SD^{-Trp}, SD^{-His}, SD^{-Leu} and SD^{-Ura}. Yeast cells that have not yet been transformed and were able to grow on SD^{-Ura} and unable to grow on SD^{-Ade}, SD^{-Trp}, SD^{-His} and SD^{-Leu} plates were used for transformations and subsequently Y2H analysis.

The bait construct was transformed into AH109 (Section 2.11.2) and streaked out onto each of the respective plates SD^{-Ade}, SD^{-Trp}, SD^{-His}, SD^{-Leu} and SD^{-Ura}. The reason for this test was to ensure that the transformed AH109 strain was not able to activate transcription of reporter genes automatically. The yeast strain AH109 containing the successfully transformed bait construct should be able to grow only on SD^{-Trp} and SD^{-Ura} agar plates, while the Y187 yeast strain containing the prey construct should only be able to grow on SD^{-Leu} and SD^{-Ura} plates.

2.12.2 Toxicity test of transformed cells

In order to continue with the Y2H library mating (Section 2.13.4), it was essential to test whether the bait-construct had a toxic effect on the AH109 yeast host strain. This was done by generating a linearised growth curve of AH109 transformed with the *KCNE2*-pGBKT7 bait construct as well as the AH109 transformed with an intact, non-recombinant pGBKT7 vector. The cultures were set up simultaneously under identical experimental conditions which were as follows: each of the strains was grown in culture until it reached the stationary phase. This was done by placing the yeast in SD^{-Trp} media (Appendix I) in 50ml polypropylene tubes followed by

incubation at 30ºC in a YIH DER model LM-530 (Scilab Instrument Co., Ltd., TW) shaking incubator. A 1:10 dilution of each sample was made in SD^{-Trp} media and incubated for a further 24 hours in a 200ml Erlenmeyer flask at 30ºC in a YIH DER model LM-530 (Scilab Instrument Co., Ltd., TW) incubator shaking at 200rpm. During this incubation period, 1ml aliquots were taken every two hours over a period of eight hours and the optical density (OD) measured at 600nm. A reading at the 24 hour time point was also taken. Following these measurements, a linearised growth curve was set up using the log values of these OD measurements over the time periods set out. The slopes of the graphs were used to compare the difference in growth rate between these two transformed AH109 strains.

2.12.3 Mating efficiency testing

Preliminary yeast matings were performed in small scale in order to determine what affect the bait construct had on the mating efficiency of the AH109 yeast strain. In order to do this, AH109 transformed with the pGBKT7-*KCNE2* construct was mated with the prey host strain, Y187 transformed with a non-recombinant prey vector, pACT2 or the control vector pTD1.1 (BD Biosciences, Clontech, USA). Control matings was also performed which included AH109 transformed with non-recombinant pGBKT7 or the control vector pGBKT-53 (BD Biosciences, Clontech, USA) to be mated with the prey host strain, Y187 transformed with non-recombinant prey vector pACT2 or the control vector, pTD1.1.

Table 2.5: Different nutritional selection plates for the yeast strains AH109 and Y187

	Nutritional Selection plates	
Yeast strains	**SD^{-Trp}**	**SD^{-Leu}**
AH109 pGBKT7-*KCNE2*	✓	
AH109 pGBKT7	✓	
AH109 pGBKT-53	✓	
Y187 pACT2		✓
Y187 pTD1.1		✓

Abbreviations: SD, single dropout; -Trp, without Tryptophan; -Leu, without Leucine.

All the strains used in the mating efficiency testing were plated onto their appropriate selection plates (Table 2.5) and incubated at 30ºC for two to five days inverted in a Sanyo MIR262 stationary ventilated incubator (Sanyo Electronic Co., Ltd., JP).

After the two to five day incubation period, a single colony was picked from each plate and used in the mating efficiency experiment. The matings were performed in 1ml YPDA media (Appendix I) which was placed in a 2ml Eppendorf tube and subsequently incubated at 30ºC in a YIH DER model LM-530 (Scilab Instrument Co., Ltd., TW) incubator shaking at 200rpm.

Following a 16 hour incubation period, serial dilutions (1:10, 1:100, 1:1000 and 1:10 000) of the mating cultures were plated onto SD^{-Trp}, SD^{-Leu} and $SD^{-Trp-Leu}$ agar plates and were incubated at 30ºC for four to five days inverted in a Sanyo MIR262 stationary ventilated incubator (Sanyo Electronic Co., Ltd., JP). Following this, the colonies on each plate were counted and the mating efficiency calculated (Appendix III).

2.13 Y2H ANALYSIS

Briefly, the Y2H screening system is one of the most common molecular techniques used to identify protein-protein interactions (Berggård et al. 2007). The advantages of using Y2H are that the system is fairly easy to use, little optimization is needed and can be completed within a reasonable time frame and the system is reasonably priced. The Y2H analysis also allows the identification of low affinity interactions and provides simultaneous protein identification and gene cloning (Berggård et al. 2007).

The yeast transcription factor (*Gal4*) is comprised of two domains; the GAL4 DNA-binding domain (GAL4-BD) and the GAL4 activation domain (GAL4-AD) that facilitates transcriptional activation (Figure 1.13). The bait protein (in this study the C-terminal of KCNE2) is expressed as a fusion protein along with the GAL4-BD and the prey proteins are expressed as fusion proteins with GAL4-AD (Figure 2.2). If a positive interaction takes place between the bait and prey protein, the GAL4-BD and GAL4-AD are brought together and ultimately initiates transcriptional activation of the reporter genes (Chapter 2).

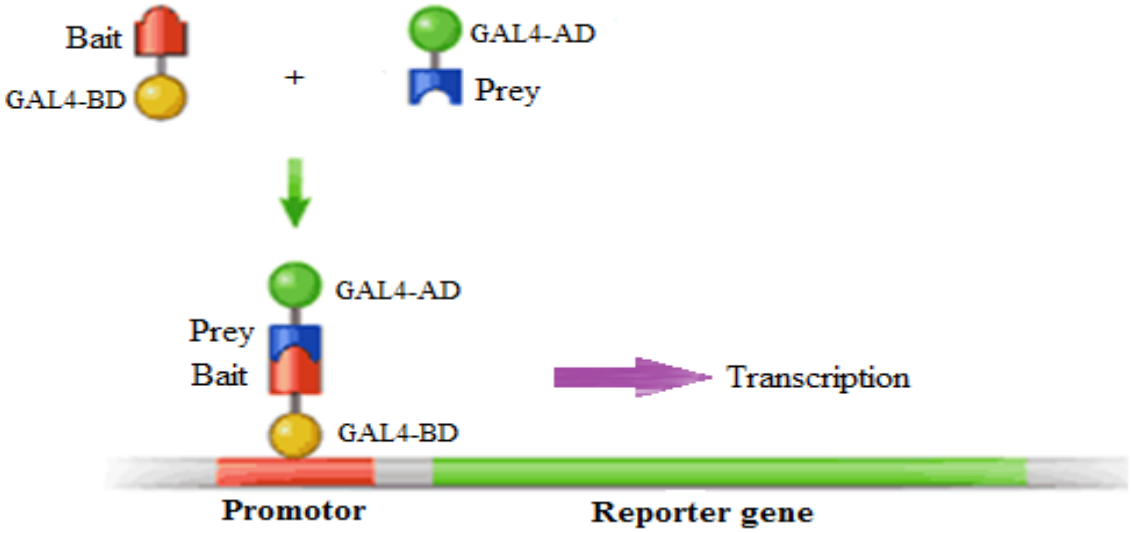

Figure 2.2: **An illustration of a Yeast two-hybrid system**. The yeast transcription factor (*Gal4*) is comprised of two domains; the GAL4 DNA-binding domain (GAL4-BD) and the GAL4 activation domain (GAL4-AD). In the Y2H system two plasmids are constructed; one encoding the bait protein fused to the GAL4-BD and the other encoding the prey protein fused with the GAL4-AD. With positive interaction between the bait and prey proteins, transcription is activated and the reporter gene/s are activated. Adapted from: http://www.scq.ubc.ca/the-yeast-two-hybrid-assay-an-exercise-in-experimental-eloquence/

2.13.1 Cardiac cDNA library

In order to carry out the Y2H library assay, a pre-transformed Clontech MATCHMAKER human cardiac cDNA library (BD Bioscience, Clontech, USA) was used. This consisted of the *S.cerevisiae* Y187 yeast strain transformed with a cardiac cDNA library in the pACT2 cloning vector.

This library was constructed from a pool of normal, whole hearts of 3 Caucasian males between the ages of 28 and 47 years. The library was *Xho*I-$(dT)_{15}$ primed and it was estimated to contain approximately $3.5x10^6$ independent clones which were inserted into the pACT2 vector at locations between the *Xho*I and *EcoR*I sites. The ranges of insert sizes were between 0.4 and 4.0kb with the average fragment for this library being approximately 2.0kb in size.

2.13.2 Establishment of bait culture

After the successful transformation of the bait vector (pGBKT7-*KCNE2*) into AH109, four single colonies were picked from the selection plate and inoculated into four separate 500ml

Erlenmeyer flasks, each containing 50ml of SD^{-Trp} liquid media (Appendix I). The flasks were incubated in a shaking YIH DER model LM-530 (Scilab Instrument Co., Ltd., TW) incubator shaking at 30ºC overnight. The reason for generating four bait cultures was to facilitate the pooling of the initial cultures which will allow the generation of a final bait culture of at least $1x10^{10}$, i.e. 100-fold excess of bait to prey, to ensure high mating efficiency. Following overnight incubation, the four initial bait cultures were transferred to four separate 50ml polypropylene tubes and the cells pelleted by centrifugation at 3000rpm for 10 minutes in a Beckman model TJ-6 centrifuge (Beckman Coulter, Scotland, UK).

The supernatants were discarded and the pellets resuspended together in 50ml SD^{-Trp} media. Subsequently the suspension was transferred to a single 500ml Erlenmeyer flask and the pooled culture was incubated for 16 hours at 30ºC shaking at 200rpm in a YIH DER model LM-530 (Scilab Instrument Co., Ltd., TW) incubator. After incubation, the titre of the bait culture was determined by measuring the OD of a 1ml aliquot of the bait culture at 600nm. The titre was confirmed by means of haemocytometer cell count (Section 214.3).

The pooled bait culture was centrifuged at room temperature at 30ºC for 10 minutes in a Beckman model TJ-6 centrifuge (Beckman Coulter, Scotland, UK) to pellet the cells, after which the supernatant was removed and the cells resuspended in the residual SD^{-Trp} media. This volume was used to make 10µl aliquots of culture to be used in subsequent control mating experiments.

2.13.3 Haemocytometric cell count

In order to verify the titre of the bait culture that will be used in the library mating experiment, a Neubauer Haemocytometer (Figure 2.3) (Superior, GER) was used to count the cells. This was done by placing the glass coverslip over the counting surface of the Haemocytometer and pipetting 10µl of the cell culture into the filling notch in counting chamber (Figure 2.3). The chamber filled by means of capillary action.

The chamber was placed on the platform of a microscope (Nikon TMS, Nikon Instruments Inc., USA) and the cells view under the lowest magnification. The cells that were in the correct areas of the Haemocytometer were counted and used in a formula to calculate the number of cells per microliter. The calculation specifications are shown in Appendix III.

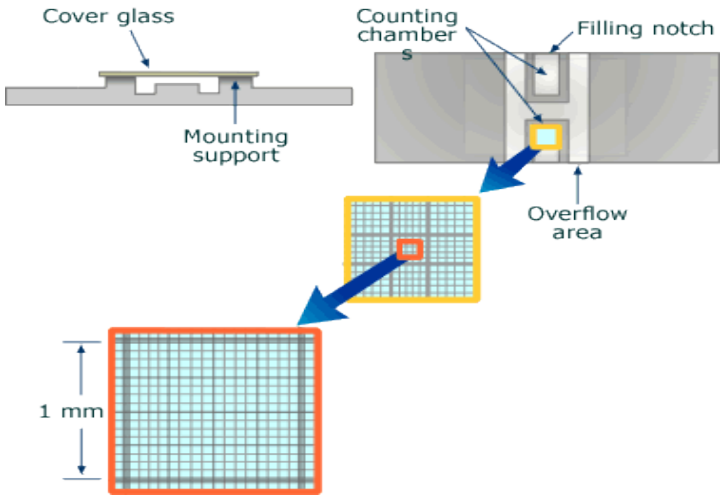

Figure 2.3: Representation of a Haemocytometric counting chamber. Neubauer Haemocytometer side view, top view and enlarged view of counting grid. The Haemocytometer consists of a thick glass slide with two counting chambers which are each divided into 9 1mm squares. The grid on the surface of the counting chamber is engraved. Figure taken from: http://www.swtafe.vic.edu.au/toolbox/lab_ops/laboratory/studynotes/SNHaemo.htm

2.13.4 Library mating

To perform library mating experiments, a 1ml aliquot of the pre-transformed cardiac cDNA library (BD Bioscience, Clontech, USA) was removed from the -80ºC freezer and thawed at room temperature. The library sample was vortexed using a Snijders model 34524 press-to-mix vortex (Snijders Scientific, NL). A 10µl aliquot was pipetted into a sterile 1.5ml sterile micro-centrifuge tube for library titering (Section 2.13.5).

The pellet containing the AH109 pGKKT7-*KCNE2* construct (Section 2.13.2) was resuspended in 45ml of 2x YPDA media (Appendix I) supplemented with 10µg/ml Kanamycin (Kan) in a 2L Erlenmeyer flasks. The remaining 990µl of the aliquoted library culture was added to the Flask This mating culture was incubated overnight at 30ºC, while shaking at 200rpm in a YIH DER model LM-530 shaking incubator (Scilab Instrument Co., Ltd., TW). After the incubation period, the mating culture was transferred into a single sterile 50ml polypropylene centrifuge tube and the cells pelleted by centrifugation at 3000rpm for five minutes in a Multex centrifuge (MSE Instruments, UK) after which the supernatant was discarded. The flask in which the library mating was performed was rinsed twice with 40ml of 2x YPDA media containing 10µg/ml Kan and used to resuspend the pellet. After resuspending the pellet, the cells were re-pelleted by centrifugation for 10 minutes at 3000rpm (Multex centrifuge, MSE Instruments,

UK). After the final centrifugation step, the supernatant was removed and the pellet resuspended in 15ml of 0.5x YPDA media containing 10µg/ml Kan (Appendix I).

In order to determine the bait:library mating efficiency (Section 2.13.5), a serial dilution (1:1, 1:100, 1:1000, 1:10 000) of this cell suspension was made and 100µl of each dilution subsequently plated onto SD^{-Leu} , SD^{-Trp} and SD $^{-Leu-Trp}$ agar plates. Two-hundred and fifty microlitres of the remaining mating culture was plated onto each of 60 140mm Triple Dropout (TDO) agar plates (agar plates lacking tryptophan, leucine and histidine) (Appendix I). The TDO plates were subsequently incubated inverted, in a Sanyo MIR262 stationary incubator at 30°C for three weeks.

2.13.5 Library titre and Library mating efficiency

The serial dilution of the mating cultures described in section 2.13.4 were plated onto SD^{-Leu} , SD^{-Trp} and $SD^{-Leu-Trp}$ 90mm agar plates (Appendix I) and incubated upside down at 30°C for four days in a Sanyo MIR262 stationary ventilated incubator (Sanyo Electronic Co., Ltd., JP). Subsequently the colonies were counted in order to perform the calculations necessary to establish the mating efficiency of the library and the number of library plasmids screened (Appendix II).

2.13.6 Activation detection of nutritional reporter genes

2.13.6.1 Selection of transformed yeast colonies

The yeast strain transformed with the bait construct pGBKT7-*KCNE2* (Section 2.11.2) was plated onto SD^{-Trp} agar plates and incubated for four days at 30°C in a Sanyo MIR262 stationary ventilated incubator (Sanyo Electronic Co., Ltd., JP). Following the incubation period, transformant colonies were picked and used in small and large scale bait cultures (Section 2.13.2) as well as interaction specificity tests (Section 2.13.9).

2.13.6.2 Selection of diploid yeast colonies containing putative interactor peptides

Diploid colonies, (the yeast colonies containing the bait- and prey-fusion peptides), were identified by plating the yeast colonies firstly onto TDO and then quadruple dropout (QDO)

plates (Appendix I). The yeast cells that were able to grow on the TDO plates signified the transcriptional activation of the *HIS3* nutritional reporter gene, while growth on the QDO plates suggested transcriptional activation of the *HIS3* as well as the *ADE2* nutritional reporter genes. For further verification of *HIS3* reporter gene activation, 3-Amino-1, 2, 4-triazole (3-AT) was added to QDO plates (Appendix I). This is a heterocyclic organic compound which acts as a competitive inhibitor of the product of the *HIS3* gene, which is an enzyme catalysing the sixth step of histidine production. Thus, by adding 3-AT to the QDO selection plates, cultures which are dependent on plasmids containing the *HIS3* gene to produce histidine, would have to produce higher levels of histidine in order for them to survive. The activation of these reporter genes are evidence of the bait and prey peptides interacting within the diploid colonies. Nutritional selection was performed as follows:

The library mating culture (Section 2.13.4) was plated onto 140mm TDO agar plates (Appendix I) and incubated at 30°C inverted for three weeks in a Sanyo MIR262 stationary ventilated incubator (Sanyo Electronic Co., Ltd., JP). The growth of the colonies were examined every seventh day and colonies with a growth diameter of 2mm and more were selected and plated onto QDO agar plates (Appendix I). These plates were then incubated in a Sanyo MIR262 stationary ventilated incubator (Sanyo Electronic Co., Ltd., JP) at 30°C for four days. Following the incubation period, the growing colonies were judged on their ability to activate the necessary nutritional reporter genes and streaked onto fresh QDO agar plates containing 3-AT (Appendix I) and incubated for a further four days at 30°C in a Sanyo MIR262 stationary ventilated incubator (Sanyo Electronic Co., Ltd., JP). These plates were then used for the x-α-galactosidase assay (Section 2.13.7) which assessed the activation of the *MEL1* reporter gene.

2.13.7 Activation detection of colourimetric reporter genes

2.13.7.1 X-α-galactosidase assay

The x-α-galactosidase assays were performed in order to test the activation of the *MEL1* reporter gene by the specific interactions between the bait and prey peptides (Section 2.13.6.2). This assay was performed as follows: Diploid yeast colonies (which could activate the *HIS3* and *ADE2* genes) identified through methods in section 2.13.6.3 were replicated onto Hybond N^+ nylon membranes and placed colony side up onto QDO plates containing 20mg/ml x-α-

galactosidase solution (BD Bioscience, Clontech, USA). The plates were placed in a Sanyo MIR262 stationary ventilated incubator (Sanyo Electronic Co., Ltd., JP) for two days at 30°C. Following the incubation period, the intensity of the blue colour produced by the colonies that activated the *MEL1* reporter gene was analysed.

2.13.8 Rescuing prey plasmids from diploid colonies

In order to identify putative proteins interactors detected through the Y2H screen, the prey plasmids needed to be isolated from the diploid yeast colonies. The plasmid DNA was extracted from the diploid yeast cells as described in section 2.1.3 after which it was transformed into *E.coli* DH5α bacterial cells as discussed in section (2.11.1). The transformed cells were plated onto LB agar plates containing 50mg/ml Ampicillin (Appendix I), only allowing growth of transformed cells containing the prey constructs. These prey constructs were subsequently isolated using the method described in section 2.1.1. The purified constructs were then transformed into the yeast strain Y187 (Section 2.11.2) in order to be used in the interaction specificity tests (Section 2.13.9).

2.13.9 Interaction specificity test

Interaction specificity tests along with nutritional (Section 2.13.6) and colourimetric (Section 2.13.7) reporter gene assays were necessary to establish whether or not the interactions between the pGBKT7-*KCNE2* construct and the putative prey interactors identified in the Y2H screen were specific. The Y187 colonies expressing the specific prey plasmids were individually mated with the yeast strain AH109 transformed with pGBKT7-*KCNE2* bait construct, AH109 transformed with non-recombinant pGBKT7, AH109 transformed with the pGBKT7-53 control bait-plasmid encoding murine p53 (BD Bioscience, Clontech, USA) and AH109 transformed with pGBKT7-*WFS1*.

The protein encoded by *WFS1* is a neuronal-specific transmembrane protein which shows highest expression in the brain and is localized to the endoplasmic reticulum, thus no interaction with *KCNE2* is expected.

The diploid colonies were selected and streaked onto TDO and QTO selection plates (Appendix I) to test their ability to activate the specific reporter genes (Section 2.13.6.2), thus establishing whether the prey-peptides were able to interact with the heterologous baits as well as with the AH109 pGBKT7-*KCNE2* bait construct. Prey peptides that only interacted with the AH109 pGBKT7-*KCNE2* bait construct were identified as specific putative interactors. Inserts of these colonies were selected for nucleotide sequencing (Section 2.4) and their sequences subsequently analysed (Section 2.5) in order to determine their identities.

2.14 CO-IMMUNOPRECIPITATION (Co-IP) PREPARATION

2.14.1 Hypoxia treatment of differentiated H9C2 cardiomyocytes

To create hypoxic conditions, medium tissue culture flasks with 70%–80% confluent differentiated H9C2 cells were used. The culture medium was removed from the flasks and replaced with 18ml Esuni buffer (Appendix I). The flasks were placed in the hypoxia chamber along with one Petri dish filled with sterile water to provide adequate humidification of the cultures. A hypoxic environment was created by removing all or most of the oxygen (O_2) from the system. This was achieved by flushing the system with a 1% O_2 gas mixture at a flow rate of 20L/minute for approximately four minutes. The chamber was then placed in a tissue culture incubator with 2% O_2 and 5% CO_2 at 37 °C for two hours. Following the incubation period, the cells were lysed as described in section 2.14.2.

2.14.2 Cell lysis

After the differentiation of H9C2 cardiomyocytes in large tissue culture flasks or medium tissue culture flasks for Hypoxia treatment (section 2.14.1) for approximately 14 days (Section 2.10.3), the cells needed to be lysed in order to be used for subsequent co-immunoprecipitation (Section 2.15) and western blot (Section 2.16) analysis. Lysis of cells was achieved as follows: The growth media was removed and 5ml of trypsin was added to the flask. The flask was incubated at 37ºC for 10-15 minutes to facilitate the detachment of the cells after which a cell scraper was used to scrape the remaining cells off from the growth surface. The detached cells were transferred to a 50ml polypropylene tube to which a volume of 30ml of growth media was added to deactivate the trypsin. The tubes were centrifuged at 4ºC for three minutes at 2500rpm in a

Beckman model TJ-6 centrifuge (Beckman Coulter, Scotland, UK). The supernatant was discarded and the pellet resuspended in 1ml of PBS (Appendix I) and the suspension transferred to 2ml eppendorf tubes. The cells were re-pelleted at 9000rpm for two minutes and the PBS removed with a pipette. Lysis buffer was prepared (Appendix I) and 300µl used to resuspend the pellet. The mixture was placed on ice for at least 15 minutes after which one scoop, approximately 0.5ml, of ZROB05 Ceria Zirconium Oxide beads (0.5mm diameter) (Next Advance Inc., USA) was added to the suspension and placed in a Bullet Blender® (Gentaur, UK) for one minute at speed four. The blending step was repeated three times with five minute waiting periods in between. Centrifugation at 9000rpm followed in a bench top centrifuge (Labnet International Inc., USA) for two minutes after which the supernatant was transferred to fresh 1.5ml eppendorf tubes and stored at -80ºC until required.

2.14.3 Bradford protein concentration determination

Before storage of samples prepared in section 2.14.2, 1µl of each lysed sample was aliquoted and used to perform a Bradford assay in order to assess the protein concentration. This was done as follows:

In order to calculate the standard curve, 10µl of serial diluted bovine serum albumin (BSA) ranging from 0-1000µg/µl was loaded into the wells of a luminometer plate together with1µl of the lysate samples in duplicate. Two hundred microlitres of Bradford reagent was added to all of the standard as well as the lysate samples. The plates were read on a Synergy HT luminometer (BioTek Instruments Inc., USA) and were used to determine the protein concentration of each well. The KC4™ v 3.4 program (BioTek Instruments Inc., USA) was used to calculate and set up the standard curve, as well as each sample's protein concentration at an absorbance of 595nm.

2.15 CO-IMMUNOPRECIPITATION (CO-IP)

Following sections 2.14, the lysates were thawed on ice and pre-cleared by adding 30µl Protein G agarose beads to each sample and incubating it at 4ºC on a rotating wheel for 30 minutes. Following incubation, the samples were centrifuged at 9000rpm for 30 seconds in a bench top centrifuge (Labnet International Inc., USA) and the supernatant transferred to fresh 1.5ml eppendorf tubes. One microgram of the appropriate primary antibody was added to each lysate

samples and the volume made up to 100µl by adding lysis buffer containing protease inhibitors and phenylmethylsulfonyl fluoride (PMSF) (Appendix I). This mixture was incubated overnight at 4ºC on a rotating wheel.

The following morning, 60µl of Protein G agarose was added to each sample after which an incubation period of one hour followed at 4ºC rotating. Afterwards, the beads were collected by centrifugation at 9000rpm for 30 seconds in a bench top centrifuge (Labnet International Inc., USA). The beads were washed four times with ice cold prepared lysis buffer (Appendix I) by mixing it and collecting it again by means of centrifugation at 9000rpm for 30 seconds in a bench top centrifuge (Labnet International Inc., USA).

After completion of all the wash steps, 35µl of SDS loading dye (Appendix I) was added to each sample and denatured at 95ºC for five minutes after which the beads were pelleted again and the supernatant loaded onto SDS-PAGE gel (Section 2.3.2). Co-immunoprecipitation (Co-IP) analysis was performed in order to verify the interactions of the putative positive prey interactors with the C-terminal of KCNE2 as identified by the Y2H experiments (Section 2.13).

2.16 WESTERN BLOTTING

2.16.1 Membrane blocking

Following SDS-PAGE (Section 2.3.2), the proteins were transferred to a membrane using the iBlot® Dry Blotting system (Invitrogen, RSA).

After complete transfer of the proteins onto the membrane, the membranes were removed from the transfer apparatus and washed in TBST for approximately two minutes. Afterwards, the membrane was placed in 5% fat free powder milk (Weigh-less) supplemented with 0.01% Tween-20 to ensure the blockage of all not specific binding sites. The membrane was incubated at room temperature for one hour shaking on a Stuart® orbital shaker SSL1(Barloworld Scientific Ltd., UK).

2.16.2 Addition of primary antibody

After blocking of the membranes (Section 2.15.1), the membranes were rinsed with TBST and the primary antibodies diluted in 5% fat free powder milk supplemented with 0.01% Tween-20

(Table 2.6). The membranes were then placed in a container along with the appropriate primary antibody and incubated overnight shaking at 4°C on an Orbit 300 shaker (Labnet International Inc., USA).

2.16.3 Addition of secondary antibody

Following section 2.16.2, the membranes were washed in TBST (Appendix I) for approximately 15 minutes after which the membranes were placed in 5% fat free powder milk supplemented with 0.01% Tween-20 containing the appropriate horseradish peroxidase (HRP) conjugated secondary antibodies (Santa Cruz Biotechnology Inc., USA) (Table 2.6). The membranes were placed on a shaker for one hour shaking at room temperature on a Stuart® orbital shaker SSL1(Barloworld Scientific Ltd., UK). Subsequently, the membranes were rinsed twice in TBST and then washed for at least 30 minutes in TBST (Appendix I).

Table 2.6: List of primary and secondary antibodies and their optimized concentrations used in Co-immunoprecipitation as well as Western blot assays

Antigen	Primary antibody	Optimum ratio	Secondary antibody	Optimum ratio
KCNE2	KCNE2*	1:200	Donkey anti-rabbit*	1:2000
CRYAB	CRYAB†	1:1000	Donkey anti-mouse*	1:2000
FLNC	Filamin 2*	1:1000	Donkey anti-goat*	1:2000
VDAC1	VDAC1†	1:200	Donkey anti-mouse*	1:2000

Manufacturer: †, Abcam, Biocom Biotech, RSA; *, Santa Cruz Biotechnology Inc., USA.

2.16.4 Chemiluminescent visualization of membrane proteins

Following sections 2.16.1-2.16.3, the membranes were taken to a dark room where the two substrate components of the SuperSignal® West Pico Chemiluminescent Substrate kit (Thermo Scientific, USA), SuperSignal West Pico Luminol/Enhancer solution and the SuperSignal West Pico Stable Peroxide solution, were mixed in a ratio of 1:1 and used to label the membranes for five minutes. After removing the excess chemiluminescent reagent, the membranes were placed in an autoradiography cassette and covered with a transparent plastic sheet after which they were

exposed to CL-Xposure™ autoradiography film (Thermo Scientific, USA). A glow-in-the-dark sticker was placed on the right hand corner next to the membranes for orientation purposes.
The exposure time varied between 10 seconds and three minutes, depending on the strength of the signal. Following adequate exposure, the film was developed in a Hyperprocessor™ automatic autoradiography film processor (Amersham Pharmacia Biotech UK Ltd., UK) and the protein bands visualized.

2.17 THREE-DIMENSIONAL CO-LOCALIZATION

The co-localization assay was used in order to assess the protein-protein interactions in a physical cellular environment. The bait protein (KCNE2) as well as the prey proteins of interest were expressed in H9C2 rat cardiomyocytes and labeled with appropriate primary and secondary antibodies (Section 2.16.2 and 2.16.3). Fluorescence microscopy followed using the Zeiss LSM 510 Meta confocal microscope housed at the Department of Anatomy imaging facility (University of Cape Town, RSA). The images acquired were processed for co-localization. The protein antibodies are indicated in Table 2.7.

2.17.1 Three-dimensional co-localization assay

Rat H9C2 cardiomyocytes were detached from the growth surface of flasks (Section 2.10.2 and Table 2.4) and counted by means of a Haemocytometric cell counting chamber (Section 2.13.3) to establish seeding of 10000 cells per well of a 6-well plate. Each of the 6-well chambers contained 3ml of growth media (Appendix I) and a glass cover slip (Lasec, RSA). After 24 hours, the growth media was removed and differentiation media (Appendix I) was added to all the wells (Section 2.10.3) and left to differentiate for approximately 14 days.

Subsequently the media was removed and the cells briefly rinsed with PBS (Appendix I). The cells were fixed for five minutes at room temperature in 4% Paraformaldehyde (Appendix I) and then washed in PBS three times for 10 minutes. The cells were then incubated in 1% BSA for one hour at room temperature. The 1% BSA solution acts as the blocking solution to ensure blockage of all non-specific binding sites. Following the incubation period, the cells were incubated with the appropriate pair of primary antibodies (Table 2.7) diluted in 1% BSA

(Blocking solution). The slides were then transferred to a sealed container and incubated at 4ºC overnight.

Table 2.7: List of primary and secondary antibodies and their optimized concentrations used in co-localization assays

Antigen	Primary antibody	Optimum ratio	Secondary antibody	Optimum ratio
KCNE2	KCNE2*	1:50	Donkey anti-rabbit Alexa 488 (Green)¥	1:500
CRYAB	CRYAB†	1:20	Donkey anti-mouse Cy3 red¥	1:500
FLNC	Filamin 2*	1:50	Donkey anti-goat Cy3 red¥	1:500
VDAC1	VDAC1†	1:50	Donkey anti-mouse Cy3 red¥	1:500

Manufacturer: †, Abcam, Biocom Biotech, RSA; *, Santa Cruz Biotechnology Inc., USA; ¥, Jackson ImmunoResearch Laboratories Inc., USA

The following day the cells were washed with PBS for 10 minutes, repeating the wash step three times. The cells were then labeled with the appropriate secondary antibodies (Table 2.7) which were diluted in PBS and incubated at room temperature for 90 minutes in the dark.

With every experiment, negative controls were included that consisted of H9C2 cardiomyocytes labeled with secondary antibodies only. This was necessary for constructing baseline values for each fluorochrome (secondary antibodies) before acquiring the single and z-stacks images. Subsequently, the cells were washed with PBS for 10 minutes, repeating the wash step three times. A 1:200 dilution of the nucleic acid stain Hoechst H-33342 (Sigma-Aldrich (Pty) Ltd., RSA) was made for staining the nuclear material blue and thus for orientation purposes during the acquisition of z-stack images as well as single images. The cells were incubated with Hoechst at room temperature for 10 minutes after which a 10 minute wash step with PBS followed. Mowiol, containing n-propylgallate as anti-fade (Appendix I), was used to mount the cells onto glass slides. The completed slides were stored at 4ºC in the dark until viewing. After viewing and acquisition of a minimum of three single images, three overlay images as well as three z-stacked images from the appropriately labeled H9C2 cardiomyocytes, the co-localization analysis was performed using the ZEN 2011 lite edition software package. Carl Zeiss (http://microscopy.zeiss.com/microscopy/en_de/downloads/zen.html).

Chapter 3

Results

Page

3.1 YEAST TWO-HYBRID ANALYSIS **74**

3.1.1 Generation of Y2H bait construct **74**

3.1.2 Assessment of the AH109 bait strain **74**

3.1.2.1 Phenotypic assessment 74

3.1.2.2 Toxicity test 74

3.1.2.3 Mating efficiency of AH109 transformed with bait construct 75

3.1.3 Y2H screen of the pre-transformed cardiac cDNA library **76**

3.1.3.1 Bait culture titre 76

3.1.3.2 Library titre and library mating efficiency 76

3.1.3.3 Y2H screen of pre-transformed cardiac cDNA library 77

3.1.3.4 Interaction specificity test 78

3.1.3.5 Sequence analysis of putative interactor peptides 78

3.2 LIGANDS CHOSEN FOR FURTHER ANALYSIS **80**

3.2.1 Alpha-B crystallin **81**

3.2.2 Filamin C **82**

3.2.3 Voltage-dependent anion-selective channel protein 1 **83**

3.3 THREE-DIMENSIONAL CO-LOCALIZATION **83**

3.4 CO-IMMUNOPRECIPITATION (CO-IP) OF KCNE2 AND PUTATIVE Y2H INTERACTORS **88**

The following section will describe the results of the processes used to identify plausible LQTS candidate genes.

3.1 YEAST TWO-HYBRID ANALYSIS

3.1.1 Generation of Y2H bait construct

Following successful generation of the pGBKT7-*KCNE2* bait construct, the construct was sequenced to establish whether the reading frame had been maintained and also to determine the integrity of the reading frame. Sequence analysis confirmed that the pGBKT7-*KCNE2* insert was in the correct reading frame. The insert sequence was preserved throughout the multiple rounds of PCR amplification that had been used to create the fragment (Section 2.2.2) (Appendix IV).

3.1.2 Assessment of the AH109 bait strain

3.1.2.1 Phenotypic assessment

The bait construct was successfully transformed into the AH109 *S.cerevisiae* yeast strain and was able to grow on SD^{-Trp} selection plates. Growth on SD^{-Leu} and SD^{-Ada} plates was however inhibited, thus confirming that the pGKBT7-*KCNE2* construct did not autonomously activate transcription of the host reporter genes (Section 2.13.1). Conversely, moderate growth was observed when colonies were streaked onto SD^{-His} plates. The transformed yeast cells showed growth on SD^{-Ura} plates, indicating that the phenotype of the *S.cerevisiae* AH109 strain was not altered. Additionally, this growth indicated that the phenotype of the yeast remained conserved following transformation with the pGBKT7-*KCNE2* bait construct.

3.1.2.2 Toxicity Test

In order to establish whether the pGBKT7-*KCNE2* bait construct was toxic to the yeast strain AH109, a growth curve was generated (Section 2.12.2) in which growth of AH109 transformed with the bait construct was compared to that of AH109 transformed with a non-recombinant pGBKT7 plasmid. When comparing the slopes of the linearized test curves of the AH109 strain transformed with the bait construct and the AH109 transformed with the non-recombinant plasmid, there was no significant difference (Figure 3.1). This indicates that these transformants were able to grow at similar rates. It was therefore determined that the pGBKT7-*KCNE2* construct was not toxic to the yeast.

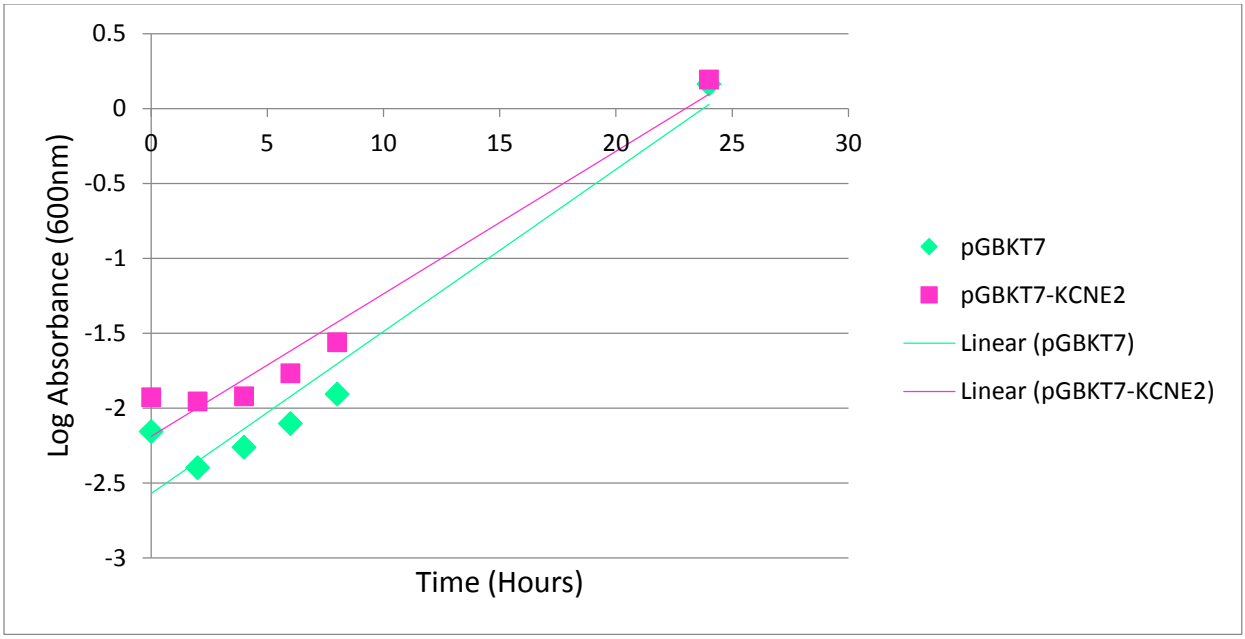

Figure 3.1: Linear growth curve of the yeast strain AH109 transformed with either pGBKT7-*KCNE2* bait construct (purple squares and purple line) or a non-recombinant pGBKT7 plasmid (green diamonds and green line). The growth rates of the two yeast transformants were compared to each other by measuring absorbance at 600nm every two hours in order to determine whether the bait construct had a toxic effect on the AH109 strain. This was determined by calculating the slope of each curve. It was concluded that the growth of the host strain was not affected by the bait construct as the slopes were similar and comparable.

3.1.2.3 Mating efficiency of AH109 transformed with bait construct

Small scale mating efficiency testing was performed (Section 2.12.3) in order to determine whether the transformation of pGBKT7-*KCNE2* had affected the ability of the AH109 to mate. The mating efficiency results ultimately showed that the bait construct did not affect the mating efficiency of the AH109 yeast strain. The observed mating efficiency was calculated at 10.2% (Appendix III), which is higher than the minimum 2% mating efficiency specified by the manufacturer of the MATCHMAKER Y2H system (BD Biosciences, clontech, USA) (Table 3.1).

Table 3.1: Effect of the pGBKT7-*KCNE2* bait construct on AH109 mating efficiency

Mating	Mating efficiency
pGBKT7-*KCNE2* (AH109) × pACT2 (Y187)	10.2%
pGBKT7-53 (AH109) × pACT2 (Y187)	2.15%

3.1.3 Y2H screen of pre-transformed cardiac cDNA library

3.1.3.1 Bait culture titre

The titre of the bait culture was established by counting the cells with a Haemocytometric counting chamber (Section 2.13.3). The average of the total amount of cells counted on both sides of the chamber was 603 and following calculations (Appendix III) the bait culture titre amounted to 6.03×10^9 colony forming units (cfu)/ml, with the commercial transformed bait titre estimated at 5×10^7.

3.1.3.2 Library titre and library mating efficiency

The library titre and mating efficiency was established as described in section 2.13.5 and after the four day incubation period, approximately 2984 cfu were counted on the 1:10000 dilution SD^{-Leu} plate. Following the necessary calculations (Appendix II) a library titre of 2.9×10^8 was established.

The number of offspring *S.cerevisiae* cells that were present on the SD^{-Trp}, SD^{-Leu} and $SD^{-Trp-Leu}$ media plates was counted (Table 3.2) and the library mating efficiency calculated to 2.1%, which is slightly higher than the manufacturer's recommended minimum value of 2% (Appendix III).

Table 3.2: Library mating efficiency as established by progeny colonies on growth selection media

	Library mating: pGBKT7-*KCNE2* × pACT2			
Mating culture dilution	**1:10**	**1:100**	**1:1000**	**1:10000**
SD^{-Trp}	*	*	*	*
SD^{-Leu}	*	*	725	87
$SD^{-Trp-Leu}$	220	45	15	0
Mating efficiency (%)	**2.1%**			

* Too many colonies to count. Abbreviations: SD, single dropout; -Trp, without Tryptophan; -Leu, without Leucine; -Trp-Leu, without Tryptophan and Leucine.

Further analysis included determining the number of pre-transformed cardiac cDNA clones screened, which was calculated to be 3.066×10^5 independent clones with a final resuspension volume of 14.6ml (Appendix III).

3.1.3.3 Y2H screen of pre-transformed cardiac cDNA library

The diploid yeast colonies identified through procedures explained in section 2.13.6, were exposed to a cascade of nutritional selection with increasing stringency in order to enhance the chances of identifying true interactors.

The screen ultimately yielded 721 clones that were able to grow on TDO plates containing 10mM 3-AT (Section 2.13.6.2) (Appendix I), thus indicating that they were capable of activating the *HIS*3 reporter gene. For the second stage, the 721 clones were transferred to QDO plates containing 10mM 3-AT (Section 2.13.6.2) and after four days, 427 clones were selected based on their ability to activate both the *HIS3* and *ADE*2 reporter genes as determined by the growth on the nutritional selection plates (Appendix I).

Subsequently, the ability of the 427 clones to activate the colourimetric reporter gene, *MEL1* (Section 2.13.7) was evaluated. After the two day incubation period, it was determined that 379 clones were able to activate the *MEL*1 reporter gene. This was established by plating the 427 clones onto QDO plates containing 10mM 3-AT as well as 20mg/ml x-α-galactosidase solution (Appendix I).

Table 3.3: Grouping of primary and secondary clones based on the x-α-galactosidase colour production and intensity

Group	x-α-galactosidase Colour intensity	Number of clones per group
Primary	+++ (High)	85
Secondary	++ (Medium)	294

The 379 selected clones were divided into two groups. This division was based on the x-α-galactosidase colour intensity of each individual clones (Appendix V). Clones with a higher or

brighter blue colour (labeled +++) were selected as Primary clones and clones with less blue colour intensities (labeled ++) were grouped as Secondary clones (Appendix V and Table 3.3).

To determine whether any of the 294 secondary clones were duplicates of one another, restriction enzyme digestion with two frequent cutting enzymes (*HaeIII* and *RsaI*) was performed on each of the clones and their restriction pattern subsequently compared to each other (Section 2.6.2).

The digests patterns indicated that 83 of the 294 secondary clones were duplicates, and this ultimately resulted in the elimination of those 83 samples. The remaining 211 secondary clones along with the 85 primary clones were selected for interaction specificity testing.

3.1.3.4 Interaction specificity test

The plasmids of the diploid colonies that were able to activate expression of all three reporter genes (*HIS*3, *ADE*2 and *MEL*1) were rescued from the selected clones (Section 2.13.8). This was done in order to facilitate heterologous mating experiments and to test the specificity of the bait and prey interactions. The experiments were performed as described in section 2.13.9 and the growth of the diploid colonies recorded (Appendix V).

3.1.3.5 Sequence analysis of putative interactor peptides

Upon completion of the interaction specific tests, 39 primary clones and 44 secondary clones were identified as candidate interactors. These prey constructs were able to grow on QDO selection plates when mated with the pGBKT7-*KCNE2* bait plasmid but not when mated with the pGBKT7, pGBKT7-53 and pGBKT7-*WFS1* plasmids (Figure 3.2).

This was followed by sequencing of the clones and the identification of the inserts in each of them. The identity of the clones was determined through the mining of publically available nucleotide (http://www.ncbi.nlm.nih.gov) and protein (http://www.ensemble.org) databases (Appendix V).

Of the 39 primary clones sequenced, 35 contained inserts that were not selected for further investigation as their open reading frames (ORF) fused to the GAL4-AD ORF did not match the ORFs predicted from the gene locus in either NCBI GenBank or Ensembl protein databases.

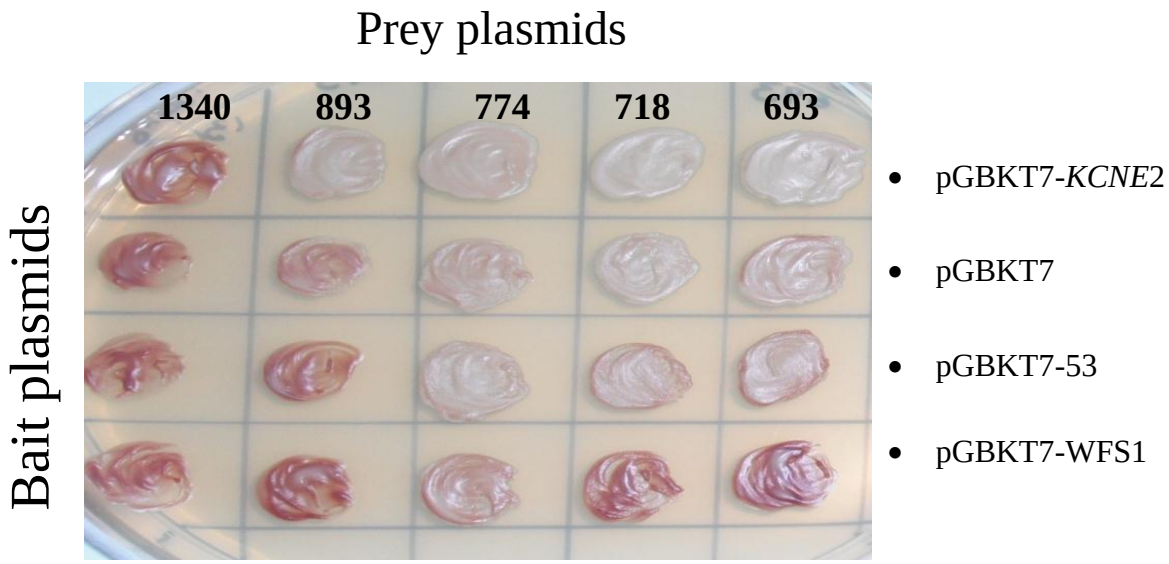

Figure 3.2: Interaction specificity testing through heterologous mating of baits and prey plasmids. An example of a QDO selection plate showing the growth of diploid colonies following heterologous mating of five individual prey colonies (# 693, 718, 774, 893, 1340 in columns) with bait constructs (pGBKT7-*KCNE2*, pGBKT7, pGBKT7-53 and pGBKT7-*WFS1* in rows). Colony #893 is a good example of a specific interactor, as it only showed binding specificity for the pGBKT7-*KCNE2* bait protein. No growth was seen when mated with the pGBKT7, pGBKT7-53 and pGBKT7-*WFS1*bait plasmids as indicated by the red colour of colonies. Colony #1340 was identified as a non-interactor as it did not show growth when mated with any of the bait plasmids and colony #774 was identified as a non-specific interactor as it showed growth with mating of all bait plasmids.

This is not a completely unexpected finding, given that only one out of every six clones represented in Matchmaker™ pre-transformed cDNA libraries are in the correct reading frames (MATCHMAKER Two-Hybrid Assay Kit User Manual). Table 3.4 provides the identities of the four remaining clones selected for further assessment.

Thirty-four of the 44 secondary clones were discarded for the same reasons as mentioned above and the identities of the remaining 10 secondary prey constructs are shown table 3.5.

Through the use of NCBI and Ensembl, false positive ligands were identified and eliminated as possible interactors. These online databases also allowed a total of three ligands that were to be excluded based on the fact that their cellular location would make it impossible to interact with the cytoplasmic C-terminal of a plasma membrane-bound protein such as KCNE2 (#122, #398 and #1880) (Table 3.4 and Table 3.5). Additionally, four ligands were excluded because their known functions make them unlikely to interact with KCNE2 (#18, #64, #293 and #668) (Table 3.4 and Table 3.5).

Table 3.4: **Identification of primary putative interactor clones from Y2H screen**

Clone #	BLASTn Acc # (e-value)	Identity	BLASTp Acc # (e-value)	Identity	Cellular location
122	NM_000088.3 (0.0)	*Homo sapiens* collagen, type I, alpha 1, mRNA	EAW94630.1 (7E-157)	COL1A1	Extracellular matrix
398	NC_012920.1 (0.0)	*Homo sapiens* mitochondrion, complete genome	ADB44568.1 (6E-17)	NADH dehydrogenase subunit 1	Mitochondrial inner membrane
501	**NM_001127487.1 (0.0)**	***Homo sapiens* filamin C, gamma, mRNA**	**1V05_A (2E-57)**	**FLNC**	**Cytoplasm, Cell membrane, Sarcomere**
668	NM_002844.3 (0.0)	*Homo sapiens* protein tyrosine phosphatase, receptor type, K, mRNA	EAW48088.1 (1E-106)	PTPRK	Cell membrane

Clones in bold were selected for further verification. Abbreviations: Acc, Accession; #, number; e-value, expectation value.

The seven remaining clones where subsequently prioritised based on their function and subcellular location. Ultimately three clones where chosen for further analysis as part of the present study. These ligands include Alpha-B crystallin (CRYAB), Filamin C (FLNC) as well as Voltage-dependent anion-selective channel protein 1 (VDAC1) (Table 3.4 and Table 3.5).

3.2 LIGANDS CHOSEN FOR FURTHER ANALYSIS

The three above mentioned clones were selected for further analysis as they resembled good candidates for true *KCNE*2 interactors. In order to verify the interactions between *KCNE*2 and the three candidate interactors, co-immunoprecipitation and 3D co-localization analyses were performed.

A brief summary of each of the three candidate interactors, their functions as well as their subcellular locations are given, along with the rationale for selecting these proteins for further analysis and verification as possible *KCNE*2 ligands.

Table 3.5: Identification of secondary putative interactor clones from Y2H screen

Clone #	BLASTn Acc # (e-value)	Identity	BLASTp Acc # (e-value)	Identity	Cellular location
15	**NR_036625.1 (0.0)**	**Voltage-dependent anion-selective channel protein 1**	**NP_003365.1 (0.0)**	**VDAC1**	**Mitochondrial outer membrane, Cell membrane**
18	NM_002046.3 (0.0)	glyceraldehyde-3-phosphate dehydrogenase	NP_001243728.1 6E-153	GAPDH	Cytoplasm, Nucleus
22	NM_133379.3 (0.0)	Titin	CAD12458.1 2E-76	TTN	Cytoplasm, Nucleus
64	NM_006873.3 (0.0)	Stonin 1 protein	AFE71436.1 1E-46	STON1	Cytoplasm, Cell membrane
93	NM_019856.1 (0.0)	Myomesin 1	NP_062830.1 2E-56	MYOM1	Sarcomere, M-band
95	**NM_001885.1 (0.0)**	**Alpha-B crystalline**	**EAW67166.1 6E-55**	**CRYAB**	**Cytoplasm, Nucleus**
250	NM_005159.4 (0.0)	Cardiac alpha Actin	EAW92317.1 1E-117	ACTC1	Cytoplasm, Cytoskeleton
293	NM_020202.4 (0.0)	Nitrilase family member 2	BAG57372.1 8E-106	NIT2	Cytoplasm
436	NM_015932.5 (0.0)	Proteasome maturation protein	NP_057016.1 6E-96	POMP	Cytoplasm, Nucleus, Microsome membrane
1880	NM_001122957.1 (1.00E-104)	Branched-chain alpha-ketoacid dehydrogenase kinase	AAB82714.1 2E-32	BCKDK	Mitochondrial matrix

Clones in bold were selected for further verification. Abbreviations: Acc, Accession; #, number; e-value, expectation value.

3.2.1 Alpha-B crystallin

Alpha crystallins are composed of two subunits, αA and αB, and from part of the small heat shock protein (sHSP) family (Boelens et al. 2001). These small proteins accumulate under stress

conditions after which they have been shown to translocate from the cytoplasm to the nucleus (Kato et al. 1992). These sHSP act as molecular chaperones - but they cannot be seen as so-called 'conventional chaperones' as they do not renature and release proteins as true chaperones would (Vicart et al. 1998). Alternatively, they hold the proteins in large soluble aggregates (Berry et al. 2001).

Alpha crystallins have been shown to have autokinase activity and play a role in the intracellular design of the cell (Clements et al. 2007). They are differentially expressed - with alpha-B crystallin being expressed in a wide range of cell types (Golenhofen et al. 2004), tissues and organs such as the heart. Alpha crystallins have been associated with myofibrillar myopathy and desmin-related cardiomyopathy (Vicart et al. 1998; Golenhofen et al. 2004; Ghosh et al. 2007).

Furthermore, in a parallel Y2H screen conducted in our laboratory, focusing on the identification of novel interactors of *KCNE1*, alpha-B crystallin was also identified as a putative interactor. For these reasons, we chose alpha-B crystallin for further analysis.

3.2.2 Filamin C

Filamin C, also known as acting binding protein, is involved in the cross linking of actin filaments into complex networks (Gariboldi et al. 1994). These networks are located in the cortical cytoplasm of the cell. The filamin protein plays an important role in anchoring membrane proteins for the actin cytoskeleton (Gariboldi et al. 1994) and has been linked to various signalling networks (Dalkilic et al. 2006).

This muscle-specific filamin (Gariboldi et al. 1994) may also exhibit structural functions at the Z-lines in muscle cells (Dalkilic et al. 2006) and has been shown to interact with *KCND2* (potassium voltage-gated channel subfamily D member 2) (Petrecca et al. 2000).

The *KCND2* gene, which is similar to *KCNE2*, encodes a protein that forms potassium ion channels that are responsible for: regulating heart rate, transporting epithelial electrolytes and contraction of smooth muscle. *KCND2*, like *KCNE2*, has also been associated with arrhythmia (Drago et al. 2008) and Long QT syndrome (Frank-Hansen et al. 2005). For these reasons, FLNC was identified as a plausible putative interactor of the C-terminal of KCNE2.

3.2.3 Voltage-dependent anion-selective channel protein 1

Voltage-dependent anion-selective channel protein 1 (VDAC1), also known as the mitochondrial porin, is a channel protein located on the outer membrane of the mitochondria. This protein plays a key role in the exchange of ions and other metabolites across the mitochondrial membrane, forming the main interface between mitochondrial and cellular metabolism. This allows the protein to regulate metabolic and energetic functions of the mitochondria (Shoshan-Barmatz and Golan 2012).

VDAC1 also forms channels in the plasma membrane that are thought to be involved in transmembrane electron transport, regulating cell volume as well as apoptosis (Kayser et al. 1989; Okada et al. 2004).

Expression of this protein is found across a number of different tissues including the heart and skeletal muscle with previous studies linking VDAC1 to myocardial ischemia and reperfusion (Kerner et al. 2012). It is therefore reasonable to suggest that VDAC1, which also encodes a voltage-dependant channel, may interact with the C-terminus of KCNE2.

3.3 THREE-DIMENSIONAL CO-LOCALIZATION

In order to evaluate the interactions between KCNE2 and each of its putative interacting proteins, 3D co-localization analysis was executed using confocal microscopy (Section 2.17.1).

The visual co-localization output indicates that each of the three putative interactors namely CRYAB (Figure 3.3), FLNC (Figure 3.4) and VDAC1 (Figure 3.5), occupied the same three-dimensional subcellular space as KCNE2.

The images were corrected for background noise by including negative control images with every experiment and image acquiring (Section 2.17.1).

In the figures resulting from the co-localization analysis, **F** represents a scatter diagram which considers all pixels that have the same position in both source images (**A** and **B**) to be a pair. For each pair of pixels from the two source images, the signal intensity of pixels from channel 1 (Ch3-T2, red) were interpreted as X-axis coordinates and the signal intensity of pixels from channel 2 (Ch2-T1, green) as Y-axis coordinates. Each pixel of the diagram represents a value

that illustrates how often a particular pixel pair has occurred. These scatterplots are important as they provide a qualitative indication of the degree of co-localization (Dunn et al. 2011). The crosshair in each diagram corresponds to the threshold values determined by the pixel intensity of the single images acquired for KCNE2 (Ch2-T1) and the three prey interactors; CRYAB (Ch3-T2), FLNC (Ch3-T2) and VDAC1 (Ch3-T2).

In order to quantify the co-localization results, three coefficients were calculated by means of specially designed algorithms (Zinchuk et al. 2007; Dunn et al. 2011) (Table 3.6.).

Considering the visual representation of co-localization (Figure 3.3 - Figure 3.5) as well as the quantification coefficients (Table 3.6), significant co-localization was observed between KCNE2 and all three of the candidate interactors (Table 3.7 - Table 3.9).

Table 3.6: Comparison of coefficients used to quantify co-localization analysis

Coefficients	Meaning	Values
Weighted Co-localization Coefficient	Illustrates the contribution of each of the two channels to the pixels of interest	**0 – 1.0** If Ch3-T1 is 1.0 and Ch2-T1 is 0.2 for red-green pair, it means that all (100%) red pixels co-localize with green, but only 20% of green pixels co-localize with red
Overlap Coefficient	Signifies the actual overlap of signals and represents the true degree of co-localization	**0 – 1.0** Where 0.5 suggests that 50% of both selected channels co-localize etc.
Pearson's correlation coefficient (Correlation R)	The correlation of intensity distribution between channels	**-1.0 – 1.0** **0** indicates no significant correlation, **-1** indicates negative correlation and **1** indicates positive correlation

Table 3.6 Adapted from (Zinchuk et al. 2007)

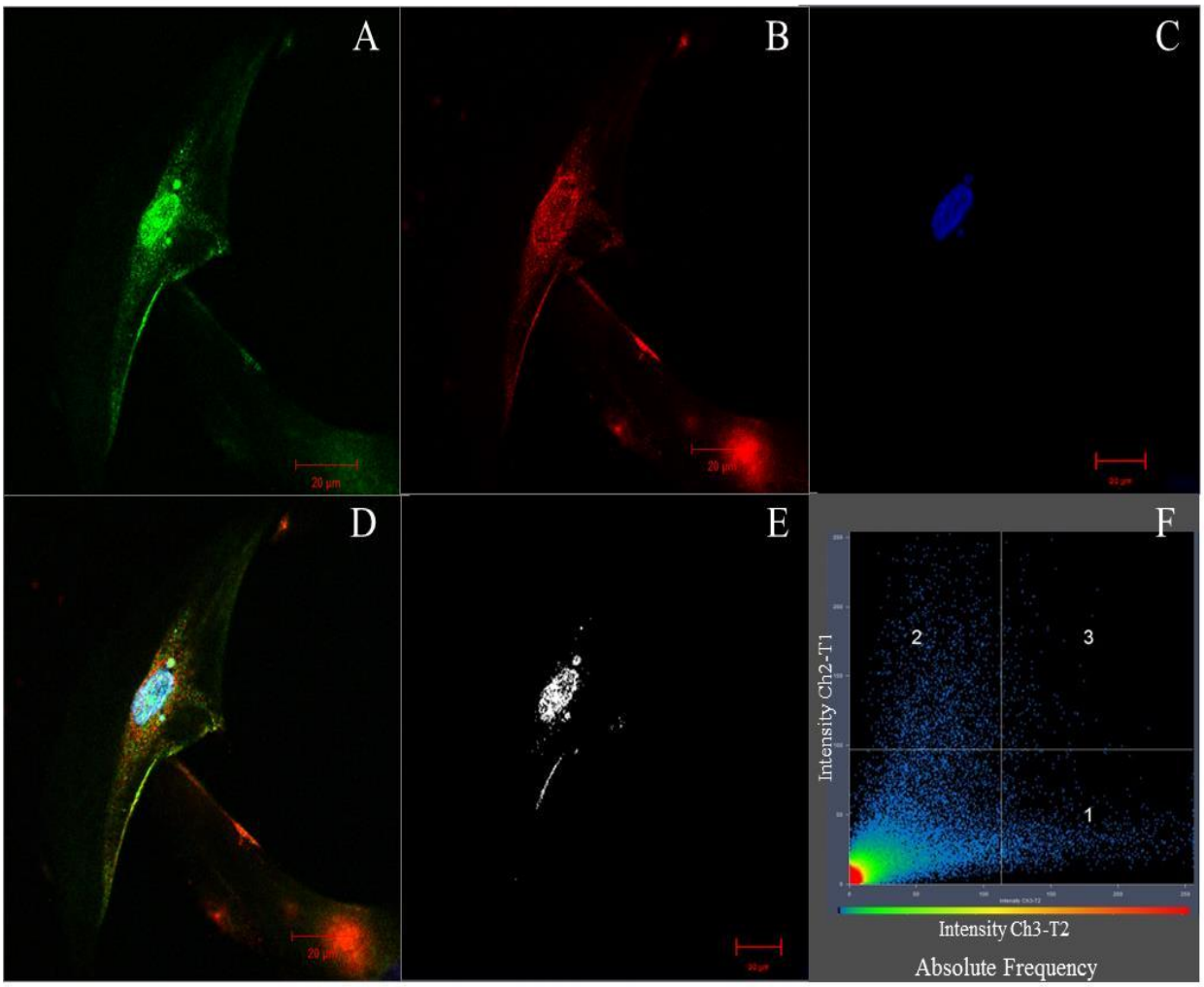

Figure 3.3: Fluorescent imaging and co-localization analysis of KCNE2 and CRYAB in differentiated H9C2 cardiomyocytes. The fluorescent imaging of (**A**) KCNE2 labeled with the rabbit polyclonal anti-KCNE2 primary antibody (Abcam: ab69376) as well as a donkey anti-rabbit Alexa 488 secondary antibody (Green). **B)** CRYAB labeled with the mouse monoclonal anti-Alpha B Crystallin primary antibody (Abcam: ab13496) as well donkey anti-mouse Cy3 secondary antibody (Red). **C**) Nucleus labeled with Hoechst H-33342 (blue). **D**) Overlay of images A-C. **E**) Co-localization of KCNE2 and CRYAB generated from merged images (white). **F**) Scatter diagram generated by co-localization analysis with quadrant three representing the degree of co-localization.

Table 3.7: Quantification of co-localization for the interaction between KCNE2 and CRYAB proteins

Weighted Co-localization Coefficient Channel 1 (Ch3-T2)	Weighted Co-localization Coefficient Channel 2 (Ch2-T1)	Overlap Coefficient	Correlation R	Correlation R x R
0.094	**0.195**	**0.563**	**0.062**	**0.093**

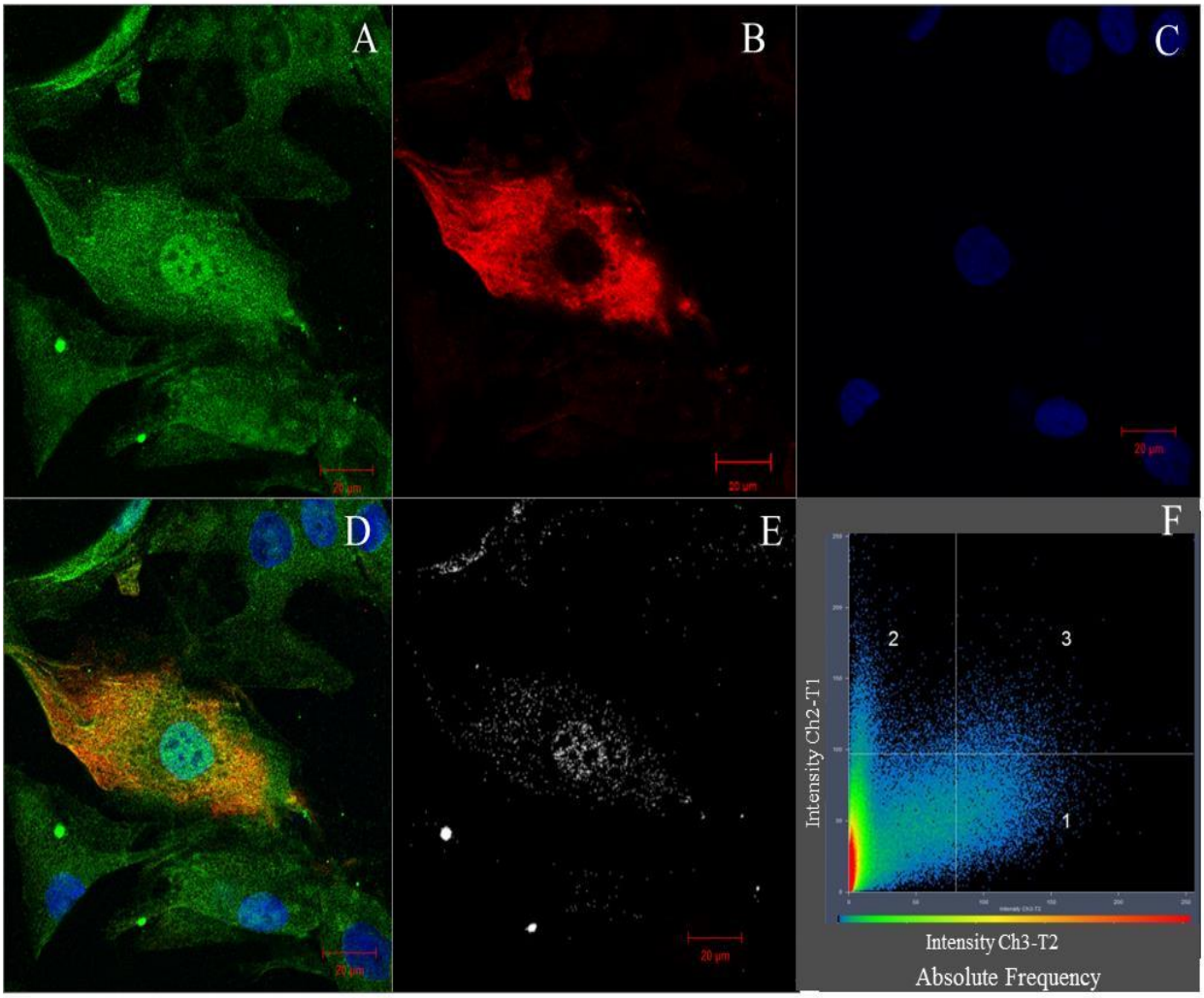

Figure 3.4: Fluorescent imaging and co-localization analysis of KCNE2 and FLNC in differentiated H9C2 cardiomyocytes. The fluorescent images of (**A**) KCNE2 labeled with the rabbit polyclonal anti-KCNE2 primary antibody (Abcam: ab69376) as well as a donkey anti-rabbit Alexa 488 secondary antibody (Green). **B)** FLNC labeled with the goat polyclonal anti-Filamin 2 primary antibody (Santa Cruz Biotechnology: sc-48496) as well as a donkey anti-goat Cy3 secondary antibody (Red). **C**) Nucleus labeled with Hoechst H-33342 (blue). **D**) Overlay of images A-C. **E**) Co-localization of KCNE2 and FLNC generated from merged images (white). **F**) Scatter diagram generated by co-localization analysis with quadrant three representing the degree of co-localization.

Table 3.8: Quantification of co-localization for the interaction between KCNE2 and FLNC proteins

Weighted Co-localization Coefficient Channel 1 (Ch3-T2)	Weighted Co-localization Coefficient Channel 2 (Ch2-T1)	Overlap Coefficient	Correlation R	Correlation R x R
0.361	**0.096**	**0.657**	**0.201**	**0.064**

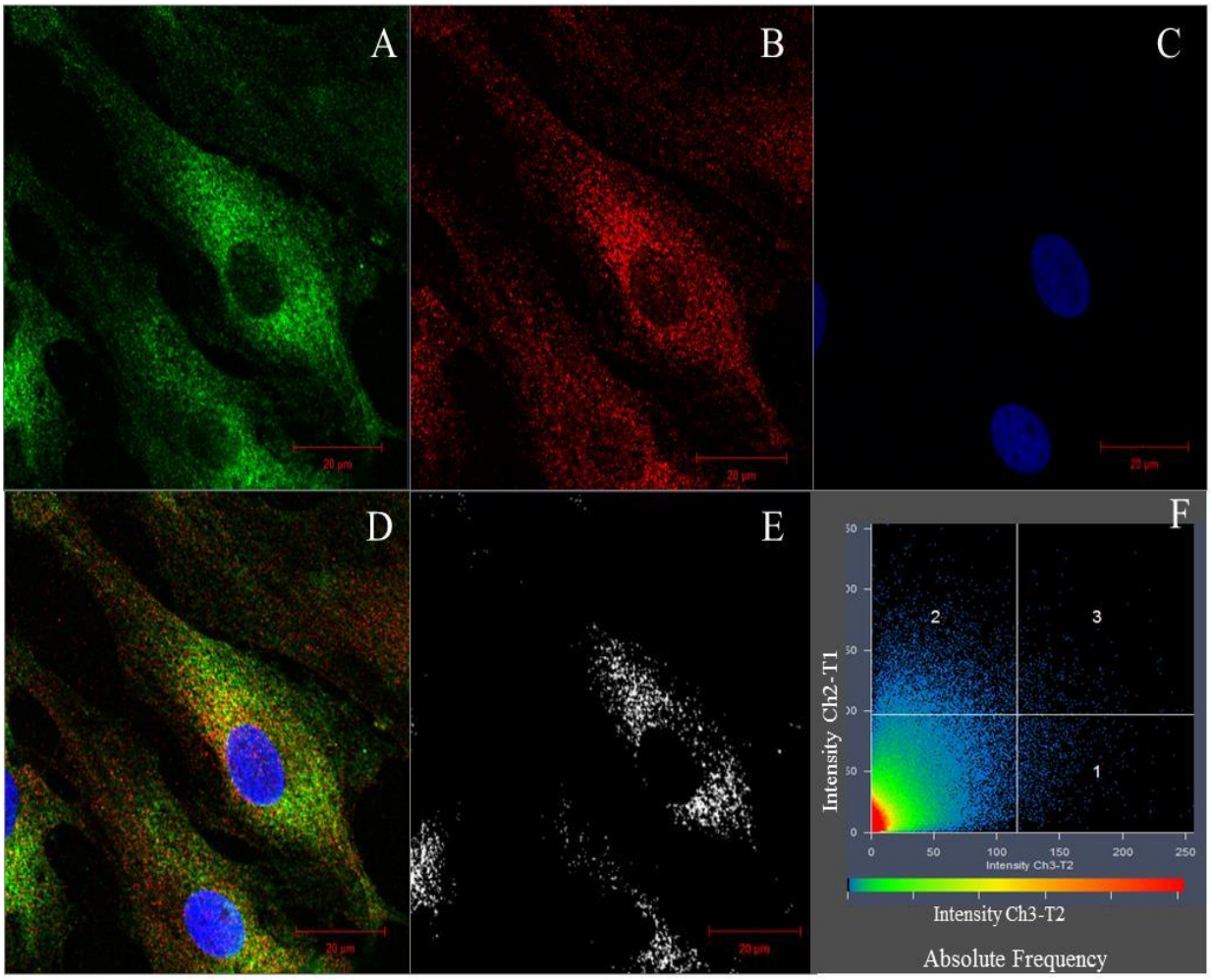

Figure 3.5: Fluorescent imaging and co-localization analysis of KCNE2 and VDAC1 in differentiated H9C2 cardiomyocytes. The fluorescent images of (**A**) KCNE2 labeled with the rabbit polyclonal anti-KCNE2 primary antibody (Abcam: ab69376) as well as a donkey anti-rabbit Alexa 488 secondary antibody (Green). **B)** VDAC1 labeled with the mouse monoclonal anti-VDAC1 primary antibody (Abcam: ab14734) as well as a donkey anti-mouse Cy3 secondary antibody (Red). **C**) Nucleus labeled with Hoechst H-33342 (blue). **D**) Overlay of images A-C. **E**) Co-localization of KCNE2 and VDAC1 generated from merged images (white). **F**) Scatter diagram generated by co-localization analysis with quadrant three representing the degree of co-localization.

Table 3.9: Quantification of co-localization for the interaction between KCNE2 and VDAC1 proteins

Weighted Co-localization Coefficient Channel 1 (Ch3-T2)	Weighted Co-localization Coefficient Channel 2 (Ch2-T1)	Overlap Coefficient	Correlation R	Correlation R x R
0.321	**0.041**	**0.602**	**0.086**	**0.029**

It should be noted that although co-localization offers proof that proteins occupy the same cellular space, it does not provide evidence of a physical interaction nor their functional relationship (Dunn et al. 2011). For this reason, it is important that other confirmatory analysis be done that will show a physical interaction between the proteins. In the present study, co-immunoprecipitation analysis was chosen for this purpose.

3.4 CO-IMMUNOPRECIPITATION (Co-IP) OF KCNE2 AND PUTATIVE Y2H INTERACTORS

Since autonomous activation of reporter genes and false positive interactor identifications are commonly observed with Y2H screens, it was necessary to verify bait-prey interactions. This was achieved by conducting co-immunoprecipitation experiments with the prey proteins (CRYAB, FLNC and VDAC1) and the KCNE2 bait protein (Section 2.15) (Figure 3.6). These assays were conducted with lysates from either normal or hypoxia treated differentiated H9C2 cardiomyocytes (Section 2.14) since both CRYAB and FLNC have been linked to cell stress response (Section 4.2.2) (Djabali et al. 1997; Kesner et al. 2010).

The results indicate that all three candidate interactors co-immunoprecipitated with KCNE2 (Figure 3.6, A). Two of the prey proteins (CRYAB and FLNC) co-immunoprecipitated with KCNE2 when using lysates from hypoxia treated cardiomyocytes (Figure 3.6, A, i and Figure 3.6, A, ii) (Section 2.14.1). The third prey protein (VDAC1) co-immunoprecipitated with KCNE2 when lysates from normal differentiated H9C2 cardiomyocytes were used (Figure 3.6, A, iii).

For comprehensiveness, reciprocal immunoprecipitation analyses were conducted. The results indicated that KCNE2 only immunoprecipitated with FLNC under hypoxic conditions (Figure 3.6, B, ii). No co-immunoprecipitation was observed for KCNE2 with either CRYAB or VDAC1 (Figure 3.6, B, i and Figure 3.6, B, iii).

Therefore, in the present study we have provided convincing evidence of the spatial (3D co-localization) and adequate proof of the physical (Co-IP) interaction between the KCNE2 proteins and three novel putative interacting proteins: CRYAB, FLNC and VDAC1.

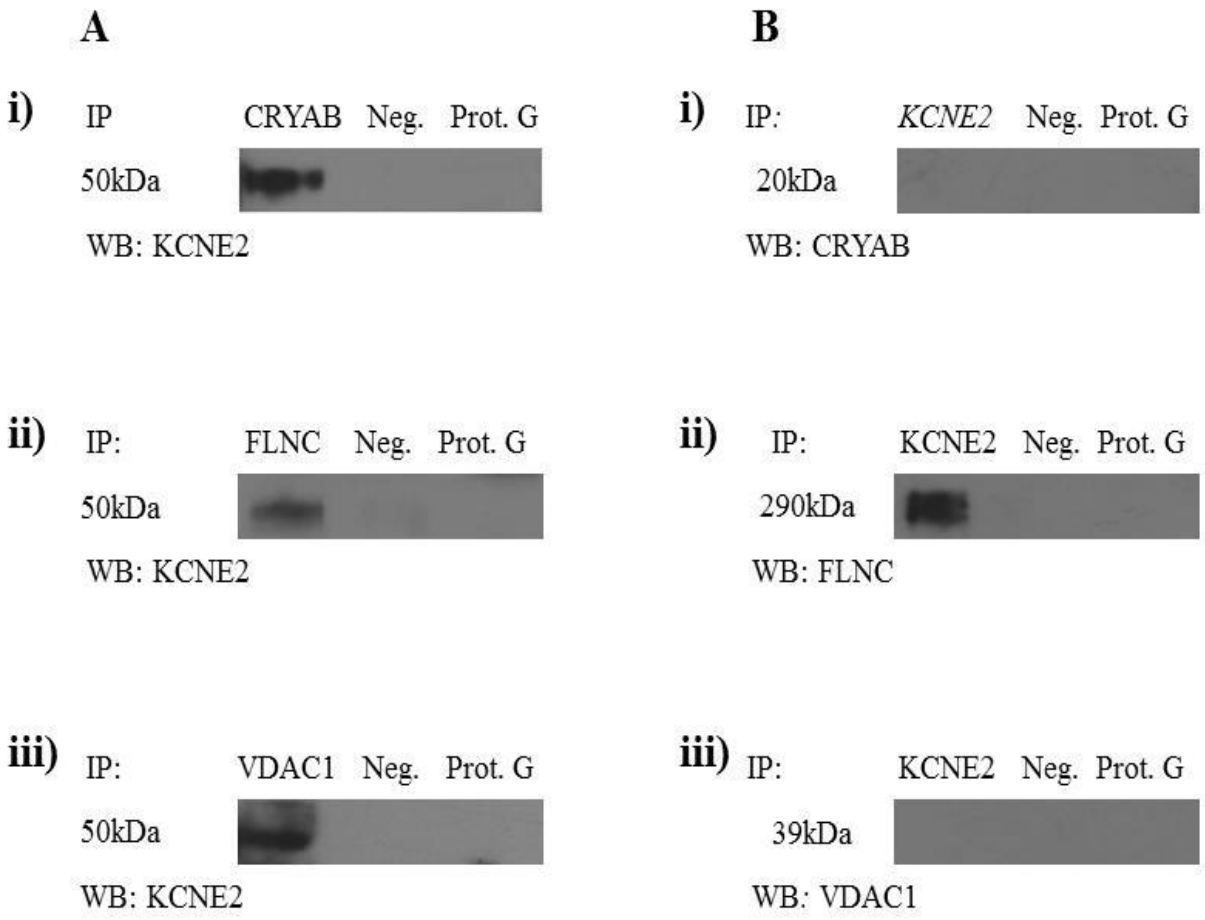

Figure 3.6: Co-immunoprecipitation of KCNE2 with prey proteins CRYAB, FLNC and VDAC1. A: CRYAB (i), FLNC (ii) and VDAC1 (iii) co-immunoprecipitated with KCNE2 in lysates of hypoxia treated differentiated H9C2 cardiomyocytes (i and ii) and standard lysates from differentiated H9C2 cardiomyocytes (iii). **B:** Reciprocal co-immunoprecipitations indicated that KCNE2 only co-immunoprecipitated with FLNC in lysates of differentiated H9C2 cardiomyocytes placed under hypoxic conditions (ii). No co-immunoprecipitation of KCNE2 was observed with CRYAB or VDAC1. Two negative controls, HA-probe and protein agarose G control, were included in all co-immunoprecipitation experiments. The clear HA-probe and protein agarose G control lanes indicate that these interactions are not false but rather a true physical interaction between the applicable proteins. Abbreviations: IP, immunoprecipitate; Neg., negative control; Prot G, protein agarose G control; WB, western blot.

Chapter 4

Discussion

Page

4.1 YEAST TWO-HYBRID ANALYSIS **91**

4.1.1 Y2H analysis to identify novel KCNE2 C-terminal domain interactors **92**

4.2 PUTATIVE PROTEIN ANALYSIS **93**

4.3 VERIFICATION STUDIES **94**

4.3.1 Three-dimensional Co-localization **94**

4.3.2 Co-immunoprecipitation **95**

4.4 PROTEINS IDENTIFIED AS KCNE2-PROTEIN LIGANDS **96**

4.4.1 Small heat-shock protein (CRYAB) **96**

4.4.2 Filamin (FLNC) **100**

4.4.3 Porin ion channel protein (VDAC1) **105**

4.5 IMPLICATIONS FOR KCNE2 **111**

4.6 STUDY LIMITATIONS **111**

4.6.1 Y2H analysis limitations **111**

4.6.2 Three-dimensional co-localization limitations **113**

4.6.3 Co-immunoprecipitation limitations **114**

4.7 FUTURE STUDIES **114**

4.8 CONCLUSION **115**

4.1 YEAST TWO-HYBRID ANALYSIS

LQTS is a cardiac repolarization disorder characterized by a prolonged QT interval on the ECG of affected individuals (Vicart et al. 1998; Schwartz et al. 2001). The symptoms of LQTS range from minor symptoms like dizziness and syncope to more severe symptoms such as seizures and SCD. Clinical features of LQTS are a result of the precipitations of Torsades de Pointes, which is a form of polymorphic ventricular tachycardia (Sanguinetti et al. 1995). A number of genetic forms of LQTS have been identified with more than 700 mutations in 12 different genes leading to disease pathogenesis. Of these known mutated genes, *KCNE2* is associated with LQT6. This gene encodes the β-subunit of potassium ion channels (Abbott et al. 1999; Abbott and Goldstein 2001; Eldstrom and Fedida 2011).

KCNE2 is a small transmembrane protein with an extracellular N-terminal and intracellular C-terminal domain (Section 1.5). This β-subunit protein assembles with voltage-gated potassium channel complex of pore-forming α-subunits to perform functions which included regulating heart rate, smooth muscle contraction and cell volume (McCrossan and Abbott 2004; www.genecards.org).

KCNE2 has been shown to associate with a number of different proteins such as HERG, KCNQ1-3 as well as HCN1 and HCN2 (Abbott et al. 1999; Tinel et al. 2000; Yu et al. 2001). Although several disease-causing mutations have been identified in *KCNE2* (many in the C-terminal domain of the protein), approximately 25% of patients with compelling LQTS have no genetic diagnosis (Napolitano 2005; Medeiros-Domingo et al. 2007b; Newton-Cheh et al. 2009). Therefore the present study aimed to identify plausible candidate genes for LQTS through searching for interactors of proteins encoded by known LQTS-causing genes.

We implemented an Y2H approach, using the C-terminal of KCNE2 as bait, to screen a cardiac cDNA library in order to identify novel protein ligands. Subsequently, we aim to screen the genes encoding novel protein interactors of KCNE2 in a South African LQTS cohort. This could possibly lead to the identification of novel disease-causing mutations or genetic modifier effects.

4.1.1 Y2H analysis to identify novel KCNE2 C-terminal domain interactors

Following successful transformation of the bait construct into yeast AH109, nutritional selection indicated that the pGBKT7-*KCNE2* construct did not autonomously activate transcription of the reporter genes. However, moderate growth was observed when colonies were streaked onto SD^{-}_{His} plates, suggesting leaky expression of the *HIS3* reporter gene. Thus, it was decided to add 10mM of 3-AT to the nutritional (Section 2.13.6) as well as colourimetric selection (Section 2.13.7) plates/media (Daniel et al. 2006). The 3-AT is a heterocyclic organic compound which acts as a competitive inhibitor of the product of the *HIS3* gene, which is an enzyme catalyzing the sixth step of histidine production. Thus, by adding 3-AT to the selection plates, cultures which are dependent on plasmids containing the *HIS3* gene to produce histidine, would have to produce higher levels of histidine in order for them to survive (Joung et al. 2000; Daniel et al. 2006; Bruckner et al. 2009).

According to the library mating efficiency calculations (Section 3.1.3.2) (Appendix III) approximately 3.066×10^5 pre-transformed cardiac cDNA clones were screened using the pGBKT7-*KCNE2* bait construct. Although this was an acceptable number of clones to be screened in the present study, it should be noted that it was much less than the calculated library titre of 2.9×10^8cfu/ml (Appendix III). This suggests that approximately 2.8×10^7 independent clones were not screened and that important ligands might have been overlooked.

Subsequently 379 clones were able to activate all the necessary reporter genes (*HIS3*, *ADE2* and *MEL1*) and were divided into primary and secondary clones (Table 3.3), based on their phenotype.

A number of different clones, encoding the same protein, were pulled out multiple times for example; NADH dehydrogenase subunit 1, ACTC1 (Appendix V) and others identified through restriction enzyme mapping (Section 2.6.2). This is not uncommon as Y2H have been shown to pull out different clones encoding the same protein yet; artefacts may perhaps exist and be the rationale behind multiple protein copies being identified.

4.2 PUTATIVE PROTEIN ANALYSIS

Thirty-nine primary clones and 44 secondary clones were selected for sequencing. Of these, 35 primary and 34 secondary clones were not selected for further investigation, as they were either duplicate clones or their open reading frames (ORF) did not match the ORFs predicted from the gene locus in either NCBI GenBank or Ensembl protein databases (Appendix V). Although the insert sequences of the clones had significant genomic matches in the NCBI database (http://www.ncbi.nlm.nih.gov), several of these inserts were not in-frame according to the ORF determined by the upstream GAL4 activation domain (AD). Subsequently, mismatch or non-significant proteins were translated (Appendix V). The reason for this could be the traditional methods used to generate libraries which are derived form oligo-dT primed cDNA. This causes one out of six cloned inserts to be in-frame with the transcription factor activation domain (Van Criekinge and Beyaert 1999). These mismatch peptides were too short and physiologically irrelevant and were therefore excluded from further analysis.

The remaining four primary clones (Table3.4) and 10 secondary clones (Table 3.5) were prioritized based on the following: subcellular location, function and likelihood of interaction.

It is safe to suggest that protein-protein interactions are unlikely to occur when proteins are separated by subcellular compartmentalization *in vivo*. Therefore, primary preys #122 (COL1A1) and #398 (NADH dehydrogenase subunit 1) and secondary prey #1880 (BCKDK) were eliminated from further analysis due to their subcellular location in the extracellular matrix of the cell, the mitochondrial inner membrane and the mitochondrial matrix, respectively (Table 3.4 and Table 3.5).

Primary prey #668 (PTPRK) as well as the three secondary preys; #18 (GAPDH), #64 (STON1) and #293 (NIT2) were excluded based on their functions. Although both PTPRK and STON1 are located at the cell membrane, their functions could not be related to those of KCNE2. Functions of PTPRK included cell growth control, tumour invasion, and metastasis, whereas STON1 is found to be involved in the endocytic machinery (www.genecards.org).

GAPDH is located in the cytoplasm and the nucleus and plays a role in glycolysis and nuclear related functions such as RNA transport and apoptosis while NIT2 is only present in the cytoplasm and has an omega-amidase activity (www.genecards.org). Taken together, these

functions are dissimilar from the known KCNE2 functions, indicating that these proteins are less likely to be ligands of the C-terminal of KCNE2 and were subsequently excluded from the study.

The primary prey #501 (FLNC) and the following secondary prey interactors; #15 (VDAC1), #22 (TTN), #93 (MYOM1), #95 (CRYAB), #250 (ACTC1) and #436 (POMP) were all good candidates for being true KCNE2 C-terminal ligands. Subsequently three proteins were selected for further verification analysis namely: CRYAB, FLNC and VDAC1.

In a parallel Y2H screen in our laboratory, focusing on novel KCNE1 interacting proteins, CRYAB was identified as a putative interactor and was therefore selected for further investigation. FLNC was selected based on a previous study that showed interaction between FLNC and KCND2; a protein functionally comparable and structurally similar to KCNE2. The voltage-dependent ion channel protein, VDAC1, was chosen for further verification because of its functional similarity to KCNE2 and plasma membrane localization. The four remaining putative interactor peptides, not selected for further analyses in the present study, will be screened in future studies.

4.3 VERIFICATION STUDIES

Given that post-translational modifications and protein folding may not occur adequately in the Y2H system, it was necessary to verify the three selected putative interactions using independent assays in mammalian cells. We chose to verify these putative interactions using 3D co-localization and co-immunoprecipitation analysis.

4.3.1 Three-dimensional co-localization

In previous years, older methods of co-localization were used to determine whether proteins share the same subcellular location by means of overlaying two-dimensional images captured from different colour channels (Costes et al. 2004). However, in the present study, the subcellular locations of the proteins were determined through the use of single images as well as z-stack analysis. The z-stack analysis reflects co-localization through the diameter of the cell making it a three dimensional application and therefore a much more powerful tool to assess co-localization. This 3D co-localization technique also assigns a value to the visual output; making this a quantitative method for the detection of co-localization

The present study made use of this 3D approach and convincingly showed that KCNE2 occupy the same subcellular space in differentiated H9C2 cardiomyocytes as CRYAB, FLNC and VDAC1.

4.3.2 Co-immunoprecipitation

As previously discussed (Section 3.3), significant co-localization was observed between the bait protein (KCNE2) and the three prey proteins (CRYAB, FLNC and VDAC1). Subsequently all three prey proteins were selected for further verification studies.

Following the identification of plausible interactions through the Y2H screen, Co-IP allowed for rapid assessment of protein-protein interactions. Co-IP analysis was selected as the technique to confirm the physical bait-prey protein interactions. This basic method is relatively easy to use, inexpensive, and proteins identified by Co-IP will be present in their native state and native concentrations (Phizicky and Fields 1995). This method provides conclusive evidence of the physical interactions between two or more proteins (highly specific) and is compatible with most downstream analysis methods (Miernyk and Thelen 2008). Finally, this technique has been well established in our laboratory and has proven to be a reliable method for protein-protein interaction verification.

Lysates used for Co-IP reactions initially originated from standard differentiated H9C2 cardiomyocytes. When the three prey proteins were co-immunoprecipitated with the bait protein (KCNE2), KCNE2 and VDAC1 indicated a relatively strong interaction (Figure 3.6, A, iii), KCNE2 and CRYAB a rather weak interaction and KCNE2 and FLNC showed no interaction at all (Figures not shown). However, several studies provided evidence that both CRYAB and FLNC have been linked to cell stress response (Djabali et al. 1997; Kesner et al. 2010), potentially explaining the weak or lack of interaction between these two proteins and KCNE2 under typical physiological conditions. Subsequently, differentiated H9C2 cardiomyocytes were subjected to stress by exposing the cells to hypoxic conditions for two hours (Section 2.14.1).

Thereafter, the Co-IP experiments were repeated using hypoxia lysates and results showed the positive interactions between the two putative prey proteins (CRYAB and FLNC) and KCNE2 (Figure 3.6, A, i and Figure 3.6, A, ii).

Furthermore, reciprocal Co-IP analyses were executed for completeness. The results indicated that KCNE2 was able to co-immunoprecipitate with FLNC (Figure 3.6, B, ii). No Co-IP was observed with either CRYAB (expected size of 20kDa) or VDAC1 (expected size of 39kDa) (Figure 3.6, B, i and Figure 3.6, B, iii). This could be explained by inadequate antibodies available for these two proteins i.e. antibodies that were not functionally tested for Co-IP analysis. Nonetheless, the present study provided suitable evidence of the interaction of KCNE2 with CRYAB and VDAC1 as well as irrefutable evidence for the spatial (3D co-localization) as well as physical (Co-IP) interaction between KCNE2 and FLNC (Appendix IV).

Included in each of the Co-IP experiments were two negative controls; lysate with HA-antibody and lysate with protein G agarose containing no antibody. These lanes were uncontaminated in all experiments and test antibodies did not bind non-specifically to protein G agarose in the absence of an antibody. Thus Co-IP analyses could proceed without any interference and were the reflection of true physical interactions.

4.4. PROTEINS IDENTIFIED AS KCNE2-PROTEIN LIGANDS

Three proteins, CRYAB, FLNC and VDAC1 were identified as KCNE2-interacting proteins in the present study. In the sections that follow, the functions of these proteins and the potential functional significance of their interactions with KNCE2 will be discussed.

4.4.1 Small heat-shock protein (CRYAB)

Alpha crystallins are known to exist as large soluble aggregates and contain two related subunits - αA (alpha-A crystallin or CRYAA) and αB (alpha-B crystallin or CRYAB) - that share a 55% amino acid sequence homology (Berry et al. 2001). These proteins form part of the small heat shock protein family (sHSPs) (Figure 4.1) and is characterized by an 80-100 amino acid conserved region. The latter region forms part of the homologous WDPF motifs (Tryptophan=W, Aspartic acid=D, Proline=P, Phenylalanine=F) and α-crystallin domains that connects the peptide to N- and C-terminal extensions (Boelens et al. 2001).

Both CRYAA and CRYAB consist of polar, flexible C-terminal domains (Figure 4.1) that are believed to be implicated in the chaperone-like activity of these proteins. When these crystallin subunits are subjected to post-translational modifications that includes deamination, glycation,

phosphorylation and truncation of the N-terminal and C-terminal regions; it decreases their chaperone activity (Berry et al. 2001).

Alpha-B crystallin (*CRYAB*) is highly expressed in vertebrate eye lens, skeletal and cardiac muscle and has been shown to form complexes with native proteins (alpha-A crystallin, Hsp27 and Hsp22) and interact with cytoskeletal proteins (actin, tubulin and intermediate filaments) (Boelens et al. 2001).

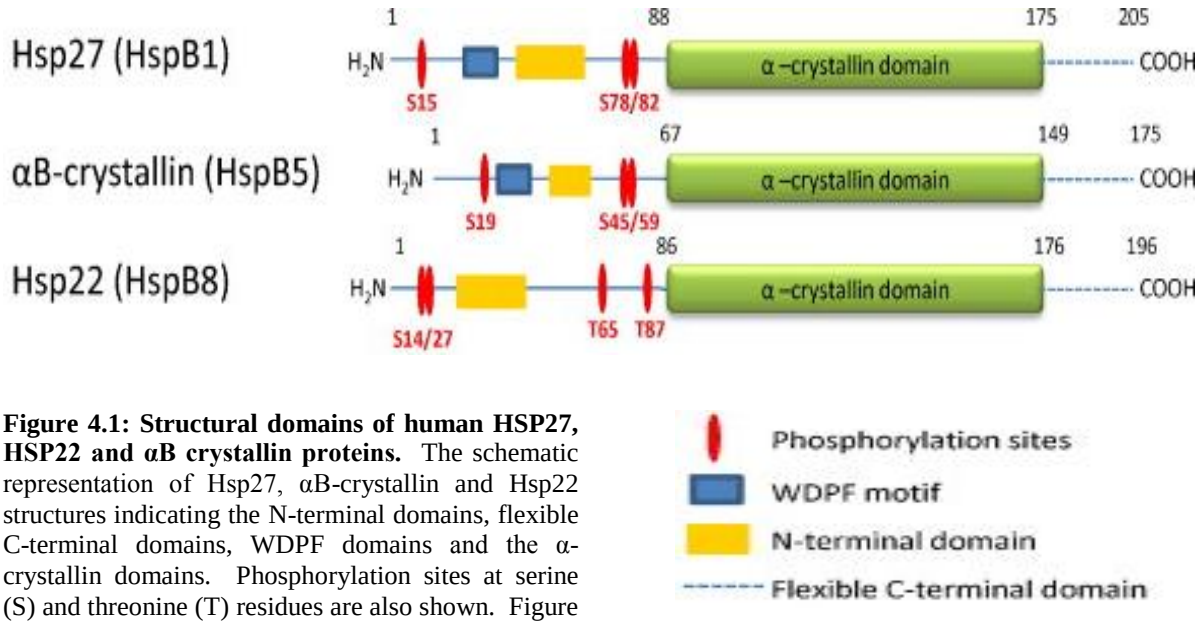

Figure 4.1: Structural domains of human HSP27, HSP22 and αB crystallin proteins. The schematic representation of Hsp27, αB-crystallin and Hsp22 structures indicating the N-terminal domains, flexible C-terminal domains, WDPF domains and the α-crystallin domains. Phosphorylation sites at serine (S) and threonine (T) residues are also shown. Figure taken from (Acunzo et al. 2012)

In cardiac muscle phosphorylated CRYAB binds to myofibrils under ischemic conditions as well as to titin - a large sarcomeric protein (Bullard 2003). These findings provide evidence of CRYAB being involved in the remodelling of the cytoskeleton and stabilizing/modulating filament assembly; assigning a protective function to this protein (Djabali et al. 1997; Boelens et al. 2001; Bullard 2003; Ghosh et al. 2007).

Crystallins function as chaperone-like molecules by preventing precipitation of denatured proteins and increasing the cells' tolerance to stress, even though they do not renature and release proteins as true chaperones would (Boelens et al 2001; Augusteyn 2004). Additionally, alpha crystallins are involved in regulating correct protein-folding, degradation and signalling (auto kinase activity) in the cell (Goldfarb et al. 2008).

Normally, CRYAB is located in the cytoplasm from where it is subsequently translocated and bound to an isolated region of the I-bands in the sarcomere (Bennardini et al. 1992; Bullard 2003; Ghosh et al. 2007). However, when stress is induced (specifically heat shock) the proteins are translocated to the nucleus where they reside in sub-nuclear structures (Klemenz et al. 1991). More recently though, it was found that CRYAB dissociates from filaments in order to interact with unfolding proteins in the cytoplasm, such as β- and gamma (γ)-crystallins, under these stress conditions (Ghosh et al. 2007). In our study, we found CRYAB to be located at both the plasma membrane as well as in the cytoplasm (Figure 3.3).

Another study found that the function and localization of CRYAB is largely dependent on its phosphorylation status (Clements et al. 2007). When CRYAB is not phosphorylated it is located in the cytoplasm where chaperone and signalling functions are executed. Then, with stress such as ischemia, CRYAB is phosphorylated and cellular protection is enhanced; translocating CRYAB to the sarcomere (Golenhofen et al. 2004; Clements et al. 2007).

Some variants in *CRYAB* (D109H and R157H) have previously been linked to late onset cardiomyopathy (Andley et al. 2011; Sacconi et al. 2012) which is a disease caused by conduction blocks, arrhythmias and chronic heart failure; causing patients to experience syncope and SCD (Goldfarb et al. 2008).

CRYAB has been shown to interact with several crystallins such as alpha-A crystallin (CRYAA) and beta-crystallin B2 (CRYBB2) (Fu and Liang 2002), also other heat shock proteins like heat shock protein beta-1 (HSPB1) (Figure 4.1) and heat shock protein beta-2 (HSPB2) (Fu and Liang 2002). CRYAB also interacts with other proteins such as cardiac titin (TTN) (Bullard 2003) filamin C (FLNC) (Kley et al. 2007), and voltage dependent anion-selective channel protein 1 (VDAC1) (Mitra et al. 2013) to name a few.

In a study by Kundu and colleagues, *KCNE2* was shown to be regulated by the estrogen hormone E2 (17- β-estradiol) in mice. This hormone exhibits a protective function, very similar to that of CRYAB, as it activates numerous protective signalling pathways during cellular stress. Estrogen has also been shown to regulate the expression of regulatory subunits of other cardiac K^+ channel genes such as *KCNE1* (Kundu et al. 2008). Additionally, high levels of estrogen have been shown to cause QT interval prolongation (Eghbali et al. 2005).

In the present study we focused on *KCNE2* - a LQTS causing gene - and identified CRYAB to be a putative interactor of KCNE2; mainly under stress (Section 2.14.1) (Figure 4.2). This was expected since CRYAB is a heat shock protein with known protective functions under stress conditions (Clements et al. 2007).

With normal/optimal physiological conditions, cardiomyocytes require a nutrient rich environment with a pH of approximately 7 (Fabiato and Fabiato 1978) and sufficient oxygen resources. Therefore, in the present study stress was induced by replacing enriched growth media with Esuni buffer (pH 6.4) and inducing hypoxia for two hours (Section 2.14.1). With the 3D co-localization analysis, a significant association was observed between CRYAB and KCNE2 (Section 3.3). However, with Co-IP analysis the physical interaction between these two proteins was only verified partially since (not confirmed with reciprocal experiments) (Section 3.4).

Nonetheless, we speculate that this interaction is true and that the location of this novel KCNE2/CRYAB interaction will most likely take place within the cytoplasm since this is where CRYAB is predominantly situated (Bennardini et al. 1992; Bullard 2003). In a previous study by Um and McDonald it was demonstrated that the intracellular trafficking of KCNE2 through the cytoplasm takes place before the protein reaches the plasma membrane (Um and McDonald 2007). This finding supports our hypothesis of cytoplasmic KCNE2/CRYAB interaction. We propose that this cytoplasmic interaction is necessary in order for CRYAB to regulate the correct conformational changes and folding of the KCNE2 protein before it reaches the cell membrane which would affect the subsequent functioning of KCNE2 K^+ channels.

However, it should also be considered that the novel KCNE2/CRYAB interaction might occur at the plasma membrane. This suggestion is reinforced with findings from a previous study by Clements and co-workers; showing the presence of CRYAB at the cell surface after stress was induced (Clements et al. 2007).

Taken together, these findings provide evidence of the possibility that both KCNE2 and CRYAB could be present in the same subcellular compartment at the same time under stress conditions; strengthening the findings of the present study (Figure 4.2).

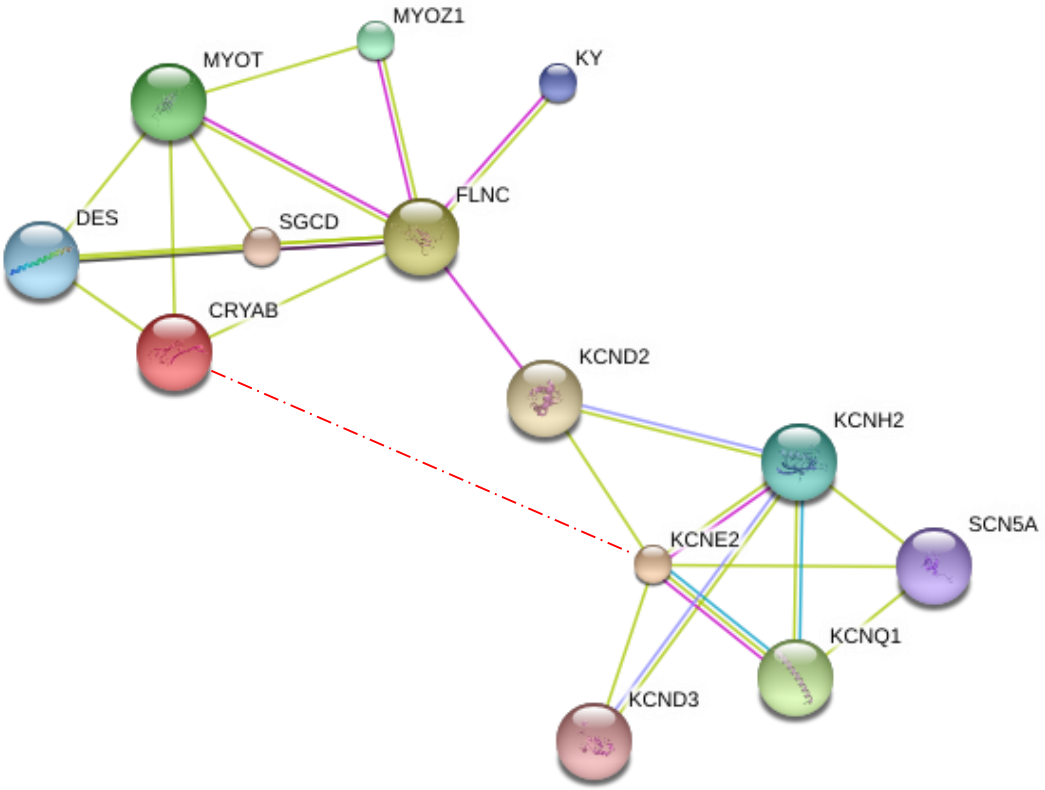

Figure 4.2: Predicted association between KCNE2 and CRYAB proteins. A schematic representation of known protein interactions indicated in green, blue and purple lines. The red dashed line indicates the proposed interaction between KCNE2 and CRYAB identified in the present study. Abbreviations: CRYAB, Alpha-B crystallin; DES, Desmin; FLNC, Filamin C; KCND2, potassium voltage-gated channel, Shal-related subfamily, member 2; KCND3, potassium voltage-gated channel, Shal-related subfamily, member 3; KCNE2, potassium voltage-gated channel, Isk-related family, member 2; KCNH2, potassium voltage-gated channel, subfamily H (eag-related), member 2; KCNQ1, potassium voltage-gated channel, KQT-like subfamily, member 1; KY, kyphoscoliosis peptidase; MYOT, Myotilin; MYOZ1, Myozenin 1; SGCD, Sarcoglycan, delta; SCN5A, sodium channel, voltage-gated, type V, alpha subunit. Figure adapted from: www.string-db.org.

4.4.2. Filamin (FLNC)

Filamins are characterized as elongated homodimeric proteins that crosslink filamentous actin (F-actin) in the cytoskeleton. They consist of a conserved actin-binding domain (ABD) at the N-terminal followed by an extended rod-like domain. With the ability to form dimers or tetramers, filamins are capable of bundling and crosslinking actin filaments into orthogonal networks and linking them to the cell membrane. Additionally, filamins are believed to act as scaffolding proteins that bind components of signalling pathways in order to enhance their activation (Murray et al. 2004; Popowicz et al. 2006).

The ABD consists of two tandem calponin domains whereas the rod regions of human filamin proteins are built by 24 immuno-globulin (Ig)-like repeats. Of these repeats, the last one is known to be responsible for dimerization of this protein (Figure 4.3). Furthermore, unique hinges are also located in the rod domain of filamins (Figure 4.3). This class of proteins is comprised of three members, filamin A (FLNA), filamin B (FLNB) and filamin C (FLNC) (Figure 4.3). These proteins share a 70% sequence homology (although the hinge regions are less homologous) and have been associated with diseases affecting the brain (periventricular nodular heterotopia or PVNH) and cardiovascular development (patent ductus arteriosus and aortic aneurysms) (Gariboldi et al. 1994; Robertson et al. 2003; Popowicz et al. 2006; Zhou et al. 2007).

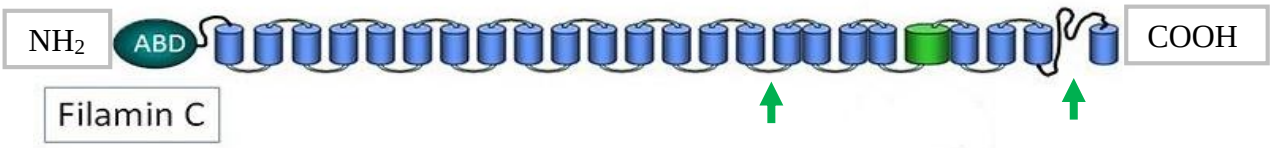

Figure 4.3: Structure of the human Filamin C protein. A schematic representation of the filamin C (FLNC) protein structure indicating the actin binding domain (ABD) at the N-terminal, 24 Ig-like repeat domains and two hinges (green arrows) in the rod region. Figure adapted from Linnemann et al. 2010.

The filamin protein is located in the cytoplasm at the Z-line, at the stress fibres in non-muscle cells (that consist of actin filaments and crosslinking proteins) as well as at the sarcolemmal membrane of muscle cells and is thought to be a signal transducer in a variety of systems (Kesner et al. 2010). Therefore, Thompson and colleagues hypothesized that FLNC may be involved in muscle maintenance by regulating and protecting the muscle during contraction (Thompson et al. 2000). This hypothesis is consistent with most filamin functions reported, such as being involved in actin polymerization (crosslinking). This process that is essential for regulating the contractile apparatus in skeletal and cardiac muscles, cell structure and organization of membrane receptors with signalling molecules. These processes are known to control cellular procedures including cell adhesion and migration, cell shape, growth, differentiation, apoptosis and survival (Thompson et al. 2000; Dalkilic et al. 2006; Popowicz et al. 2006).

Mutations identified in *FLNA* and *FLNB* largely impact human cortical development and results in skeletal muscle disorders, whereas mutations in *FLNC* cause skeletal and cardiac muscle

disorders since the expression of FLNC is restricted to muscle cells (Zhou et al. 2007; Gontier et al. 2013).

Mutations in the *FLNC* gene have previously been implicated in myofibrillar myopathy (MFM), which is characterized by the disruption of focal myofibrils and the abnormal accumulation of proteins in skeletal muscle fibres. The onset of MFM is variable and sudden death due to cardiovascular complications has previously been described. In a study by Kley and co-workers, it was found that approximately one third of patients with filamin-related myopathies had cardiac abnormalities including tachycardia, diastolic dysfunction and left ventricular hypertrophy. These investigators also found that FLNC interacts with CRYAB (Section 4.1.3.1) (Kley et al. 2007).

Moreover, mutations in *FLNC* have been associated with desminopathy, which is characterized by muscle weakness, conduction blocks, arrhythmias and chronic heart failure resulting in unexpected or sudden death (Goldfarb et al. 2008). This is of particular interest to the present study given that mutations in *KCNE2* have previously been associated with very similar symptoms i.e. arrhythmias, heart failure and SCD (Abbott et al. 1999; Gordon et al. 2007; Schwartz 2009).

In a previous study, FLNC was identified as an interactor of KCND2 (Petrecca et al. 2000). *KCND2* encodes the α-subunit of the voltage-gated potassium channel protein (also known as the Kv4.2 channel) located at the cell membrane and have been found to regulate heart rate and muscle contraction (Fiset and Giles 2006). Petrecca and co-workers proposed that FLNC mediates the direct link between KCND2 and the actin cytoskeleton and that this interaction is essential for the generation of appropriate KCND2 current densities (Petrecca et al. 2000). Following mapping studies, it was found that the C-terminal of FLNC interacted specifically with a four amino acid (aa) motif (PTPP) 30aa upstream of the C-terminus of KCND2 (Petrecca et al. 2000). The KCND2 ion channel conducts the fast transient outward current of cardiac action potential in the myocardium and has been associated with prolonged action potential as well as QT interval prolongation (LQTS) (Barry et al. 1998; Frank-Hansen et al. 2005).

In addition to the interaction with FLNC, Roepke and colleagues found KCND2 to interact with KCNE2 and revealed that KCNE2 regulate ventricular fast transient outward currents by

modulating KCND2 channels. Additionally it was discovered that targeted disruption of *KCNE2* leads to α-subunit targeting and impaired ventricular repolarization (Roepke et al. 2008).

In the present study FLNC was identified as a putative interactor of KCNE2. The protein structure of KCNE2 is similar to other FLNC interacting proteins identified by Thompson and colleagues i.e.; β1-integrins, γ-sarcoglycan and delta (δ)-sarcoglycan, apart from the fact that the sarcoglycans have intracellular N-terminal and extracellular C-terminal domains. These sarcoglycans are thought to be important components of structural support as well as signalling pathways in muscle cells (Thompson et al. 2000).

Furthermore, we observed the binding of the C-terminal of KCNE2 with the C-terminal of FLNC exclusively under conditions of stress, which is similar to results from a study by Kesner and co-workers. Here, in the last mentioned study, it was hypothesized that stress-induced conformational changes in filamins could have a direct effect on cell signalling through disruption of existing interactions or by presenting novel interactions (Kesner et al. 2010). It may therefore be possible that this stress-induced unfolding of FLNC is necessary for the interaction of FLNC with KCNE2.

The subcellular location of this novel KCNE2/FLNC interaction is thought to be either cytoplasmic or membrane associated. Depending on the phosphorylation state of FLNC, the protein can either be present at the membrane interacting with membrane associated proteins or it can be found in the cytoplasm interacting with the actin cytoskeleton (Thompson et al. 2000; Murray et al. 2004). At the membrane, FLNC has been shown to interact with the intracellular domains of γ-sarcoglycan, δ-sarcoglycan and β1-integrin proteins (Thompson et al. 2000) as well as with the C-terminal of KCND2 . Hence, with KCNE2 containing of a cytoplasmic domain, the newly identified interaction between FLNC and KCNE2 could possibly occur in a similar fashion as the previously identified FLNC/KCND2 interaction at the membrane.

Additionally, it is believed that although FLNC can be recruited to the membrane through a specific group of receptor signals, another group of signals could allow FLNC to translocate back to the actin cytoskeleton (Thompson et al. 2000). As explained previously in section 1.5.3, premature KCNE2 proteins are trafficked through the ER, Golgi apparatus and the cytoplasm to ultimately reach the cell membrane as mature proteins. The trafficking of both FLNC and

KCNE2 through the cytoplasm could be the alternative subcellular location for the novel interaction (Um and McDonald 2007).

In conclusion, literature research revealed several connections between FLNC and KCNE2 which strengthens the probability of their physical interaction *in vitro*. These overlaps include mutations in both genes causing similar symptoms (arrhythmia, conduction block, syncope and SCD) in different diseases (LQTS, RCM, and MFM); common interacting protein partners (KCND2) (Figure 4.2) as well as subcellular localization in cardiac muscle cells.

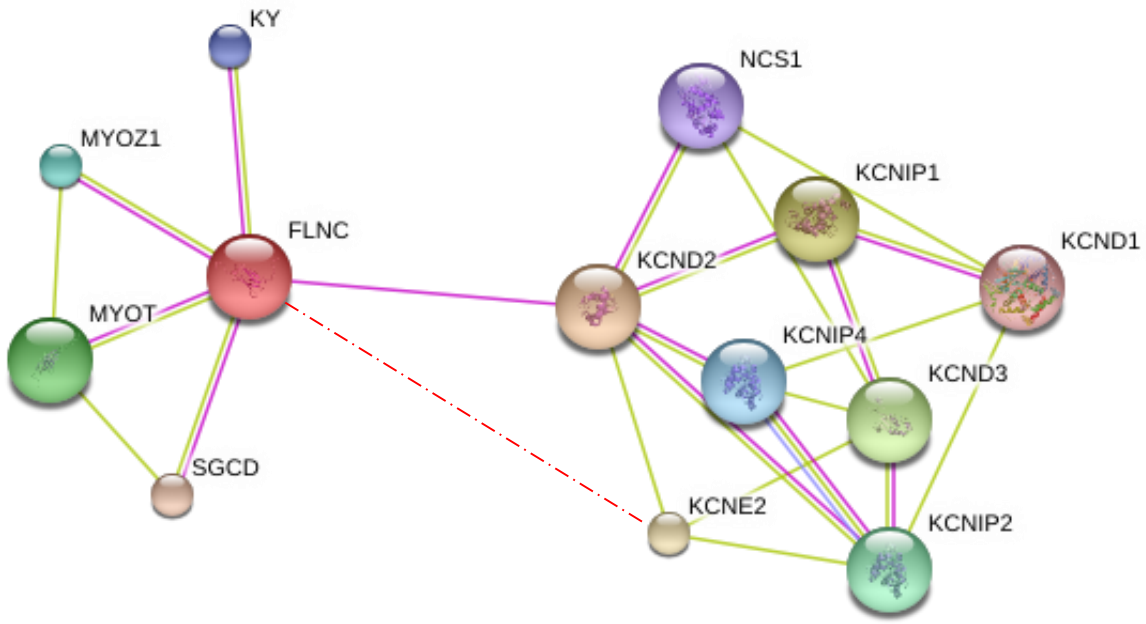

Figure 4.4: Predicted association between KCNE2 and FLNC proteins. A schematic representation of known protein interactions indicated with green, blue and purple lines. The red dashed line indicates the proposed interaction between KCNE2 and FLNC identified in the present study. Abbreviations: FLNC, Filamin C; KCND1, potassium voltage-gated channel, Shal-related subfamily, member1; KCND2, potassium voltage-gated channel, Shal-related subfamily, member 2; KCND3, potassium voltage-gated channel, Shal-related subfamily, member 3; KCNE2, potassium voltage-gated channel, Isk-related family, member 2; KCNIP1, Kv channel interacting protein 1; KCNIP2, Kv channel interacting protein 2; KCNIP4, Kv channel interacting protein 4; KY, kyphoscoliosis peptidase; MYOT, Myotilin; MYOZ1, Myozenin 1; NCS1, neuronal calcium sensor 1 SGCD, Sarcoglycan, delta. Figure adapted from: www.string-db.org.

We hypothesize that the interaction of FLNC with KCNE2 might be required for the membrane anchoring of the KCNE2 proteins and the subsequent functioning of these K^+ protein channels. Additionally, filamin have been shown, in a previous study, to mediate the direct link between KCND2 and the actin cytoskeleton and it is thought that the FLNC/KCND2 interaction is essential for the generation of appropriate current densities of KCND2 (Petrecca et al. 2000).

Accordingly, this can be extrapolated to the findings of the present study since KCNE2 and KCND2 are structurally and functionally related. We therefore propose that the KCNE2/FLNC interaction is important for the generation of proper KCNE2 current density and KCNE2-actin cytoskeleton association.

4.4.3 Porin ion channel protein (VDAC1)

The voltage-dependent anion-selective channel proteins (VDACs), also known as mitochondrial porins, have three known isoforms namely; VDAC1, VDAC2 and VDAC3. These proteins are mainly located on the outer mitochondrial membrane (OMM) (Sampson et al. 1997; Colombini 2004; De Pinto et al. 2010). VDAC1 and VDAC2 are characterized by their ability to form pores that allows diffusion of small hydrophilic solutes through the membrane whereas VDAC3 on the other hand, plays a more important physiological role by means of regulating functions of other proteins (Sampson et al. 1997; De Pinto et al. 2010).

At membrane potentials close to zero, these anion-selective channels are open. Once the voltage changes to values above +20mV or below -20mV, the pores close. Thus, previous studies have suggested that this protein is able to sense the membrane electrical potential and react to it accordingly (De Pinto et al. 2010).

VDACs consist of approximately 285 amino acid residues that contains 12 to 19 transmembrane β-strands and one α-helix situated at the N-terminal of the molecule (Figure 4.5) (Bay and Court 2002; Bayrhuber et al. 2008; Ujwal et al. 2008). The β-strands are connected by loops of different lengths (Figure 4.2) that play particular roles in gating of VDAC channels, pore size, ion selectivity as well as structural support of VDAC channels (Bay and Court 2002; Ujwal et al. 2008).

VDACs display a variety of functions including metabolite and energy interchange as well as cell volume control and apoptosis (Murphy 2004; De Pinto et al. 2010; Kerner et al. 2012). These functions have been shown to be dependent on interaction with other proteins and is regulated by the phosphorylation of VDACs (Kerner et al. 2012). VDAC proteins are expressed in a variety of tissue including the liver, kidney, heart and skeletal muscle (Kerner et al. 2012).

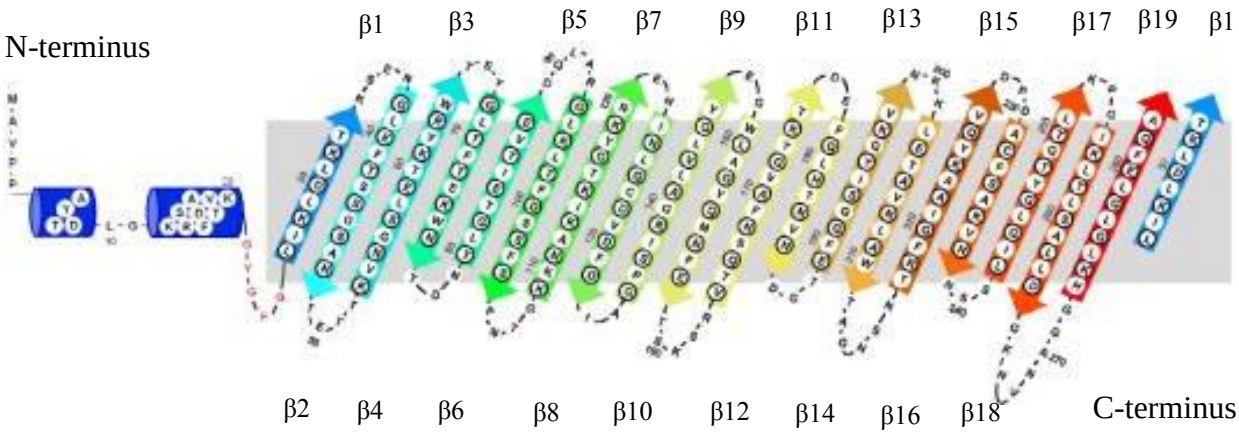

Figure 4.5: Secondary structure of VDAC1. The VDAC1 protein structure consists of transmembrane β-strands (up and down arrows) and one α-helix (blue cylinders) at the N-terminal. In the β-strands and the α-helix are the single-letter amino acid codes of VDAC1. β1 is mentioned again at the C-terminal to indicate that this is a closed barrel. Figure adapted from (Ujwal et al. 2008).

VDAC1 have been shown to interact with a number of proteins including BCL2-like 1(BCL2L1) a potent inhibitor of cell death (Shi et al. 2003) and Gelsolin (GSN) - an intracellular actin binding protein that also inhibits apoptosis through stabilizing the mitochondria (Koya 2000). Additionally, VDAC1 interact with CRYAB (Mitra et al. 2013); the small heat shock protein discussed in section 4.1.3.1 as well as tropomyosin 3 (TPM3); a protein that plays an essential role in the troponin complex and muscle contraction that has recently been identified as a possible biomarker for risk of arrhythmias (Rosengarten et al. 2013).

Diseases in which VDACs have been implicated include mitochondrial dysfunction diseases such as Alzheimer's disease, as well as other diseases such as Down syndrome (Yoo et al. 2001), cancer (Arbel and Shoshan-Barmatz 2010) type 2 diabetes mellitus, myocardial ischemia reperfusion and hypertension (Yuqi et al. 2009; Kerner et al. 2012). VDACs are also linked to hypertension, a major risk factor for coronary heart disease and congestive heart failure. Hypertension has been characterized as the risk factor responsible for the poor diagnosis in a range of cardiovascular diseases since it has been shown to mask the underlying illness (Yuqi et al. 2009).

In addition to the outer mitochondrial membrane (OMM) localization; VDAC1 was shown to be the porin protein most abundantly expressed at the plasma membrane (Kayser et al. 1989; Buettner et al. 2000; Okada et al. 2004; De Pinto et al. 2010; Kerner et al. 2012).

This protein has been studied extensively with previous studies implicating VDAC1 in the early stages of programmed cell death (Shimizu et al. 2001; Zheng et al. 2004).

Yuqi and co-workers investigated the effect of a mitochondrial transfer-RNA (tRNA) *A4263G* mutation on blood pressure in a family with maternally-inherited hypertension. Using lymphoblastoid cell lines from individuals carrying the mutation and control individuals, they showed an increase in VDAC1 expression and increased levels of apoptosis, while the mitochondrial potential significantly decreased. These results indicated that this specific *A4263G* mutation is associated with alterations in the expression of the VDAC1 protein, its localization as well as the level of apoptosis (Yuqi et al. 2009).

Apoptosis is accompanied by cell volume alterations. It was shown that certain ion channels, such as K^+ and Na^+ channels, activated during apoptosis are important in cell volume regulation (Bortner et al. 1997). The increase in K^+ efflux, associated with anion channel activation during rapid cell volume decrease, is important to sustain the electro neutrality of the membrane. This emphasizes the necessity for correct intracellular concentrations of cations as well as anions in order to regulate apoptosis. These apoptotic events cause activation of plasma membrane associated VDAC1 channels and subsequently the activation of K^+ channels (delayed rectified type) (Okada et al. 2004).

KCNE2, as discussed earlier (Section 1.5), is a voltage-gated K^+ channel situated at the plasma membrane that regulates the I_{Kr} current, which is the rapid delayed rectifier current, in the heart (Abbott et al. 1999). Functions of this channel include the regulation of heart rate, insulin secretion, muscle contraction and cell volume control (Yang et al. 2004; Yuqi et al. 2009; www.ncbi.nlm.nih.gov).

We identified the positive interaction between KCNE2 and VDAC1 through the Y2H screen of a cardiac cDNA library. This interaction took place under normal physiological conditions. However, when stress was induced through hypoxia (Section 2.14.1), no interaction was observed. This suggested that these two proteins do not interact under stress conditions.

In view of evidence from previous studies of both KCNE2 and VDAC1, one can deduce that the structure and functions of these proteins are relatively similar. This is supported by the fact that

both proteins are voltage-gated ion channels and form transmembrane pores at the plasma membrane (Figure 4.6) (Abbott et al. 1999; Okada et al. 2004; De Pinto et al. 2010).

Furthermore, KCNE2 and VDAC1 have similar functions including ion transport and cell volume control and have previously been associated with arrhythmic events and heart failure (Yang et al. 2004; Yuqi et al. 2009; www.ncbi.nlm.nih.gov).

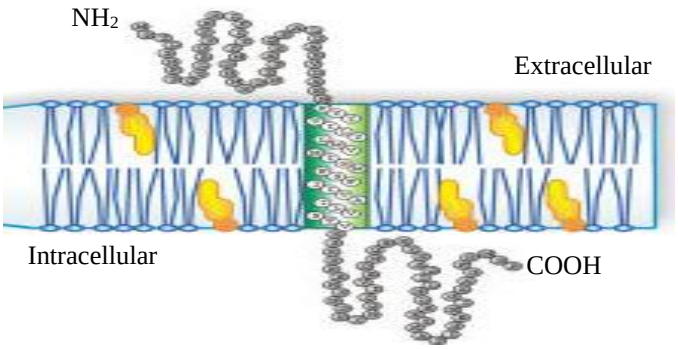

Figure 4.6: Schematic representation of KCNE2 transmembrane protein. In the diagram, KCNE2 is shown to stretch through the membrane with one pore forming region. KCNE2 has an extracellular N-terminal domain and an intracellular C-terminal domain. Figure adapted from: Um and McDonald 2007.

Interestingly, the KCND2 protein, previously shown to interact with KCNE2 (Zhang et al. 2001), was found to be even more similar to VDAC1. KCND2 is a voltage-gated ion channel (Figure 4.7) with six transmembrane spanning loops and an intracellular N-terminal domain (Isbrandt et al. 2000; Barros et al. 2012), almost identical to VDAC1 that contains approximately 19 transmembrane loops and an intracellular N-terminal domain (Figure 4.5) (Bay and Court 2002; Ujwal et al. 2008).

Through experimental procedures followed in the present study, the novel KCNE2/VDAC1 interaction was successfully confirmed through 3D co-localization analysis (Section 3.3) yet; Co-IP analysis could not provide conclusive evidence of the physical interaction between these proteins since reciprocal Co-IP results were inadequate (Section 3.4).

Even so, we hypothesize that this interaction is highly possible and that the subcellular localization of the novel KCNE2/VDAC1 association could occur at the plasma membrane. This is supported by previous studies detecting KCNE2 and, more recently, VDAC1 at the plasma membrane (Abbott et al. 1999; Okada et al. 2004; De Pinto et al. 2010).

On the other hand, mitochondria have been shown to be located throughout the cell's cytoplasm; depending on the energy requirements of the cell as well as the specific function of these

organelles and their role in cell survival (Frederick and Shaw 2007). Thus, we may speculate that membrane bound KCNE2 (more specifically the intracellular C-terminal of KCNE2) could associate with the intracellular OMM associated VDAC1 when mitochondria are located close to the plasma membrane.

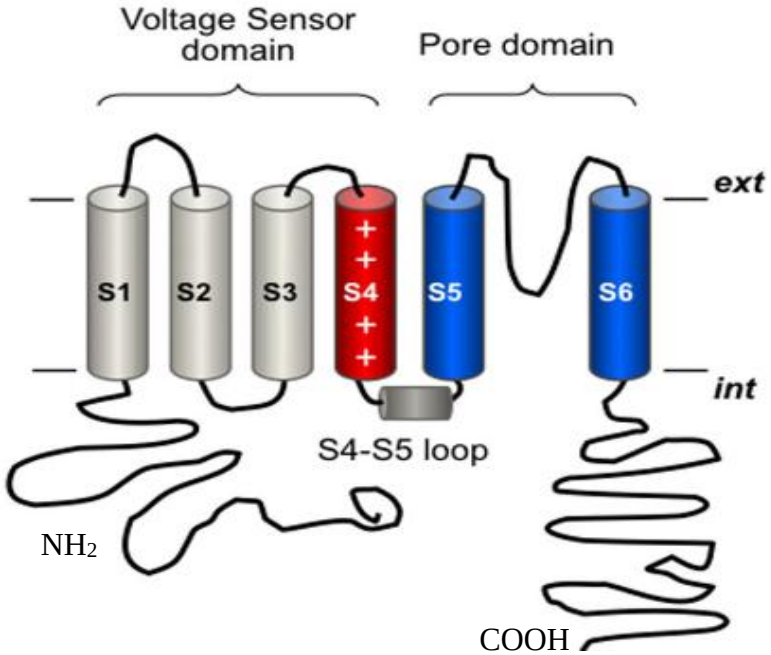

Figure 4.7: Schematic diagram of the Kv channel organization. This representation of a Kv channel, for example KCND2, indicates the six transmembrane regions (labeled S1-S6), the pore domain and the voltage sensor domain. Abbreviations: ext, extracellular; int, intracellular. It should be noted that this is a general representation of Kv channels and although uniformity exists in transmembrane and pore regions, large variability is found in the size and location of the N-terminal and C-terminal of different Kv channels. Figure adapted from: Barros et al. 2012.

Cytoplasmic localization of the novel KCNE2/VDAC1 interaction is another option to be explored. With mitochondria, containing VDAC1 on its outer membrane, situated and translocated within the cytoplasm (Frederick and Shaw 2007) and premature KCNE2 being trafficked through the ER and cytoplasm (Um and McDonald 2007) it is very possible that these proteins might associate here.

Numerous studies provided evidence that supports the finding of the present study; showing positive KCNE2/VDAC1 interaction. Particularly the study by Okada and colleagues who showed that the regulation of cell volume activates VDAC1 as well as delayed rectifier type K^+ channels (Okada et al. 2004) of which KCNE2 is one.

Taken together, we propose that the interaction between KCNE2 and VDAC1 might be necessary for the regulation of cell volume and apoptosis since both of these proteins are implicated in these processes. Additionally, the functions of VDAC1 channels have been shown to be dependent upon interactions with other proteins (Kerner et al. 2012). Consequently, we speculate that KCNE2 might be one of these proteins that control VDAC1 functions.

However, the opposite should also be considered since VDAC proteins were shown to regulate the functions of other proteins (De Pinto et al. 2010). Hence, we can also suggest that the KCNE2/VDAC1 interaction is necessary in order for VDAC1 to regulate KCNE2 functions at the plasma membrane. It could also be possible that this novel interaction is essential for the activation of KCNE2 and other K^+ channels during apoptosis (Okada et al. 2004).

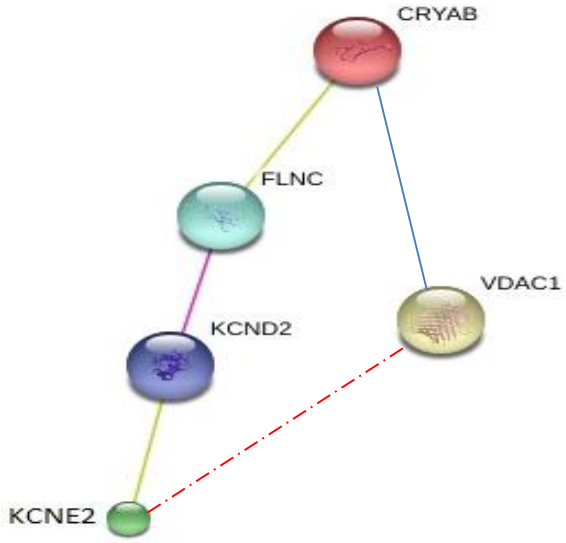

Figure 4.8: Predicted association between KCNE2 and VDAC1 proteins. A schematic representation of known protein interactions indicated with green, blue and purple lines. The red dashed line indicates the proposed interaction between KCNE2 and VDAC1 identified in the present study. Abbreviations: CRYAB, Alpha-B crystallin; FLNC, Filamin C; KCND2, potassium voltage-gated channel, Shal-related subfamily, member 2; KCNE2, potassium voltage-gated channel, Isk-related family, member 2; VDAC1, voltage-dependent anion channel 1. Figure adapted from www.string-db.org.

Three likely interaction sites/methods were proposed in the current study. Although, when looking at figure 3.5 it seems possible that the association of these proteins takes place at more than one of these suggested locations or in more than one way simultaneously i.e. in the cytoplasm as well as close to the cell surface.

Ultimately, we identified VDAC1 to be a novel putative interactor of the C-terminal domain of KCNE2 through 3D co-localization and Co-IP analysis. We also offered relevant evidence supporting the findings of the present study.

4.5 IMPLICATIONS FOR KCNE2

The Y2H system was used to identify novel interactors of the C-terminal of KCNE2 in order to elucidate additional functions or pathways in which KCNE2 might be involved. The putative interactors identified and verified in the present study include CRYAB, FLNC and VDAC1. This indicates that the C-terminal of KCNE2 is able to interact with at least three classes of proteins known as small heat-shock proteins, filamins and porin ion channels, respectively. Among these proteins identified, none to our knowledge have previously been proposed as interactors of the C-terminal of KCNE2, thus classifying them as novel interactions.

Following adequate research, it was established that the disruption of pathways in which all three interacting proteins are involved lead to cardiac dysfunction. Therefore, considering that only 75% of LQTS-causing mutations are known, the novel positive interacting proteins and other components of their respective pathways could be model candidates to be investigated for disease-causing or disease/phenotype modifiers.

4.6 STUDY LIMITATIONS

4.6.1 Y2H analysis limitations

The Y2H system is one of the most widely used and well established genetic techniques available to identify novel protein-protein interactions *in vivo* (Berggård et al. 2007). The Y2H system has proven to be relatively inexpensive, do not require special equipment and can easily be performed in any molecular laboratory with high efficacy and over the years, a myriad of interactions have successfully been identified using this technique. However, with the extreme application of this method a number of limitations have come to light (Bruckner et al. 2009).

When using a classic cDNA library Y2H screen, as was done in the present study, the aim is to search for pairwise interactions between bait and prey proteins that have been pooled. This means that the pooled prey library do not only contain full length ORFs but small DNA fragments as well leading to false positives being identified due to non-specific interactions (Van Criekinge and Beyaert 1999).

Moreover, since Y2H relies on the reconstitution of a transcription factor and the expression of reporter genes, all interaction in this assay takes place within the nucleus of the yeast cell (Fields

and Song 1989; Bruckner et al. 2009). This, of course does not represent the true cellular compartments where interacting proteins reside *in vivo.* Therefore interactions may be detected in Y2H analysis that cannot take place *in vivo* because the putative interacting proteins are located in cellular compartments that makes it impossible for them to interact. Furthermore, certain proteins may become toxic to the host cell when expressed or could degrade vital yeast proteins or proteins necessary for the assay (Van Criekinge and Beyaert 1999).

One should also be aware that Y2H is notorious for producing false positive interactions, i.e. showing reporter gene activation where no bait-prey interaction has taken place. This could be due to the bait construct being able to autonomously activate the transcription of reporter genes (auto activation) (Cusick et al. 2005; Lalonde et al. 2008; Bruckner et al. 2009). In the present study, the *KCNE2*-bait construct was unable to act as an auto-activator of reporter gene transcription.

The detection of false negative interactions is also a possibility when performing an Y2H screen. This happens when the interaction between the bait and prey was facilitated by a fusion or anchor protein; leading to the prevention of interaction due to a change in molecular structure (Van Criekinge and Beyaert 1999). Moreover, false negatives may also be caused by interactions that require specific post-translational modifications and unless the enzymes responsible for these modifications are present in the yeast, no interaction will be detected (Cusick et al. 2005; Bruckner et al. 2009).

Additionally, Y2H screening only identifies defined binary interactions in a complex and not all the components of a larger complex which could lead to certain protein interactions being overlooked (Berggård at al. 2007; Bruckner et al. 2009).

Another limitation of this system can be ascribed to the bait and prey proteins fusing to the DNA binding domain. This fusion of proteins might change the conformation of the bait and/or prey proteins and could influence their functions and binding properties (Fields and Song 1989; Bruckner et al. 2009).

When taking the above mentioned limitations into consideration, it is evident that independent verification of protein-protein interaction is crucial. Thus, in order to address this matter, a co-

localization assay was selected to determine whether the interacting proteins are located in the same subcellular compartment at any given time.

However, although co-localization of proteins provides evidence of spatial closeness and the presence of two or more proteins in the same cellular compartment, it does not offer prove of a physical interaction between these proteins (Dunn et al. 2011). Therefore, an additional verification technique is necessary to determine if the interaction is a true specific binary protein interaction. In the present study we used a co-immunoprecipitation (Co-IP) assay to confirm this.

4.6.2 Three-dimensional co-localization limitations

Some of the limitations identified throughout the use of 3D co-localization are as follows: The use of highly specific primary antibodies raised against the proteins of interest and fluorophore-labeled secondary antibodies required a great deal of optimization to determine the adequate concentration for each antibody to be used. This was necessary in order to acquire suitable images for analysis which proved to be somewhat time consuming. Additionally, when investigating endogenous proteins (like in the present study), components of the protein complex may not be expressed sufficiently in the cell line studied (Berggård et al. 2007).

Finally, when using conventional light microscopy the resolution is limited to approximately 200nm by the diffraction of light, causing objects closer than 200nm to each other to appear as a single object (Lalonde et al. 2008). However, the method used in the present study allowed z-stack images to be taken roughly 260nm (0.26µm) apart, suggesting that this distance may separate proteins that appear co-localized by fluorescence microscopy. As a result it is possible to determine whether two proteins share the same subcellular space yet, no conclusive evidence can be given regarding physical association between the proteins of interest.

This 3D co-localization method should therefore be considered as one technique that could be used in conjunction with other techniques - such as Co-IP - in order to verify physical protein-protein interactions.

4.6.3 Co-immunoprecipitation limitations

Some Co-IP limitations were encountered during the course of this study. The predicted size of KCNE2 has been estimated between 14kDa and 20kDa however, the size of KCNE2 detected throughout all the Co-IP and WB experiments in the present study were approximately 40kDa - 50kDa. This matter was addressed by conducting experiments with three different KCNE2-specific antibodies from three different manufacturers, yet all yielded similar results of lysates producing an intense protein band at approximately 50kDa.

Another possible explanation for the bigger protein band of KCNE2 could be attributed to complex formation of the protein (Um and McDonald 2007). Um and McDonald also reported a 40kDa protein fragment on western blots for the KCNE2 protein. They analysed the band and found that it represented the correct KCNE2 fragment. Further analysis indicated that the 40kDa fragment resulted from the dimerization of KCNE2 proteins (Um and McDonald 2007). Subsequently, this provided support for the results presented in the current study.

4.7 FUTURE STUDIES

The three novel interactors of the C-terminal of KCNE2 identified and verified in the present study demands further investigation to elucidate the true nature of their interaction and physiological relevance to KCNE2 and LQTS.

Therefore, genes encoding these novel interacting proteins should be considered as good candidates to screen for mutations, especially in our SA cohort of LQTS patients. With the identification of novel disease-causing mutations in patients (possibly segregating in the family) and the absence of these mutations in control subjects, functional studies should be considered to establish the effect of these mutations on disease phenotype. This would include the deletion or inhibition of gene expression (Knockout experiments) as well as mutagenesis experiments in order to elucidate the precise mechanism of function of these mutations and the effect they have on K^+ flow and general functioning of KCNE2 K^+ channels in cardiac muscle cells.

Through the identification of the three prey interactors, additional pathways were identified in which KCNE2 might be implicated. Therefore it will be interesting to investigate these pathways in terms of their contribution to cardiac conduction disorders and heart failure.

Furthermore, future studies should include the investigation of the four putative interactors that fell outside the scope of the present study (ACTC1, MYOM1, POMP and TTN).

4.8 CONCLUSION

In this investigation of the C-terminal of KCNE2, seven putative interactors were identified by means of Y2H analysis. Three of these interactors were selected for further investigation and were subsequently subjected to direct Y2H protein-protein interaction verification assays namely; 3D co-localization and co-immunoprecipitation (Co-IP) analysis. Although some difficulty was experienced with reciprocal Co-IP verification experiments, it is still considered that CRYAB and VDAC1 are true KCNE2 C-terminal ligands due to positive co-localization and partially positive Co-IP data. Both protein interaction techniques used for the verification of the KCNE2/FLNC interaction provided irrefutable evidence of the subcellular localization as well as physical association between these two proteins.

All three of the putative positive interactors identified in this study are novel and should provide new understanding and insight into the mechanisms in which *KCNE2* is involved and how it contributes to disease pathogenesis. By means of identifying novel KCNE2 interacting proteins, different pathways and targets could be revealed. With investigation of these new targets and pathways the mechanism by which *KCNE2* mutations induce cardiac dysfunction, can possibly be elucidated. In conclusion, this study identified interesting and novel interactors that will contribute to our current knowledge of *KCNE2*.

References

Abbott, G W, and S A Goldstein. 2001. "Potassium Channel Subunits Encoded by the KCNE Gene Family: Physiology and Pathophysiology of the MinK-related Peptides (MiRPs)." *Molecular Interventions* 1 (2) (June): 95–107.

Abbott, G W, B Ramesh, and S K S Srai. 2008. "Secondary Structure of the MiRP1 (KCNE2) Potassium Channel Ancillary Subunit." *Protein and Peptide Letters* 15 (1): 63–75.

Abbott, Geoffrey W, Federico Sesti, Igor Splawski, Marianne E Buck, Michael H Lehmann, Katherine W Timothy, Mark T Keating, and Steve A.N Goldstein. 1999. "MiRP1 Forms IKr Potassium Channels with HERG and Is Associated with Cardiac Arrhythmia." *Cell* 97 (2) (April 16): 175–187. doi:10.1016/S0092-8674(00)80728-X.

Ackerman, M.J., and D.E. Clapham. 1997. "Mechanisms of Disease: Ion Channels - Basic Science and Clinical Disease." *New England Journal of Medicine* 336 (22): 1575–1586.

Ackerman, Michael J., Silvia G. Priori, Stephan Willems, Charles Berul, Ramon Brugada, Hugh Calkins, A. John Camm, et al. 2011. "HRS/EHRA Expert Consensus Statement on the State of Genetic Testing for the Channelopathies and Cardiomyopathies This Document Was Developed as a Partnership Between the Heart Rhythm Society (HRS) and the European Heart Rhythm Association (EHRA)." *Europace* 13 (8) (August 1): 1077–1109. doi:10.1093/europace/eur245.

Acunzo, Julie, Maria Katsogiannou, and Palma Rocchi. 2012. "Small Heat Shock Proteins HSP27 (HspB1), αB-crystallin (HspB5) and HSP22 (HspB8) as Regulators of Cell Death." *The International Journal of Biochemistry & Cell Biology* 44 (10) (October): 1622–1631. doi:10.1016/j.biocel.2012.04.002.

Andley, Usha P., Paul D. Hamilton, Nathan Ravi, and Conrad C. Weihl. 2011. "A Knock-In Mouse Model for the R120G Mutation of αB-Crystallin Recapitulates Human Hereditary Myopathy and Cataracts." *PLoS ONE* 6 (3) (March 18): e17671. doi:10.1371/journal.pone.0017671.

Arbel, Nir, and Varda Shoshan-Barmatz. 2010. "Voltage-dependent Anion Channel 1-based Peptides Interact with Bcl-2 to Prevent Antiapoptotic Activity." *Journal of Biological Chemistry* 285 (9) (February 26): 6053–6062. doi:10.1074/jbc.M109.082990.

Augusteyn, Robert C. 2004. "Alpha-crystallin: a Review of Its Structure and Function." *Clinical & Experimental Optometry: Journal of the Australian Optometrical Association* 87 (6) (November): 356–366.

Barros, Francisco, Pedro Domínguez, and Pilar de la Peña. 2012. "Cytoplasmic Domains and Voltage-dependent Potassium Channel Gating." *Frontiers in Pharmacology of Ion Channels and Channelopathies* 3: 49. doi:10.3389/fphar.2012.00049.

Barry, D M, H Xu, R B Schuessler, and J M Nerbonne. 1998. "Functional Knockout of the Transient Outward Current, long-QT Syndrome, and Cardiac Remodeling in Mice

Expressing a Dominant-negative Kv4 Alpha Subunit." *Circulation Research* 83 (5) (September 7): 560–567.

Bay, Denice C, and Deborah A Court. 2002. "Origami in the Outer Membrane: The Transmembrane Arrangement of Mitochondrial Porins." *Biochemistry and Cell Biology = Biochimie et Biologie Cellulaire* 80 (5): 551–562.

Bayrhuber, Monika, Thomas Meins, Michael Habeck, Stefan Becker, Karin Giller, Saskia Villinger, Clemens Vonrhein, Christian Griesinger, Markus Zweckstetter, and Kornelius Zeth. 2008. "Structure of the Human Voltage-dependent Anion Channel." *Proceedings of the National Academy of Sciences* 105 (40) (October 7): 15370–15375. doi:10.1073/pnas.0808115105.

Becker, Daniel E. 2006. "Fundamentals of Electrocardiography Interpretation." *Anesthesia Progress* 53 (2): 53–64. doi:10.2344/0003-3006(2006)53[53:FOEI]2.0.CO;2.

Bendahhou, Saïd, Céline Marionneau, Karinne Haurogne, Marie-Madeleine Larroque, Renaud Derand, Viktoria Szuts, Denis Escande, Sophie Demolombe, and Jacques Barhanin. 2005. "In Vitro Molecular Interactions and Distribution of KCNE Family with KCNQ1 in the Human Heart." *Cardiovascular Research* 67 (3) (August 15): 529–538. doi:10.1016/j.cardiores.2005.02.014.

Bennardini, F, A Wrzosek, and M Chiesi. 1992. "Alpha B-crystallin in Cardiac Tissue. Association with Actin and Desmin Filaments." *Circulation Research* 71 (2) (August): 288–294.

Berggård, Tord, Sara Linse, and Peter James. 2007. "Methods for the Detection and Analysis of Protein-protein Interactions." *Proteomics* 7 (16) (August): 2833–2842. doi:10.1002/pmic.200700131.

Berry, Vanita, Peter Francis, M. Ashwin Reddy, Dean Collyer, Eranga Vithana, Ian MacKay, Gary Dawson, et al. 2001. "Alpha-B Crystallin Gene (CRYAB) Mutation Causes Dominant Congenital Posterior Polar Cataract in Humans." *American Journal of Human Genetics* 69 (5) (November): 1141–1145.

Boelens, Wilbert C., Yvonne Croes, and Wilfried W. de Jong. 2001. "Interaction Between αB-crystallin and the Human 20S Proteasomal Subunit C8/α7." *Biochimica et Biophysica Acta (BBA) - Protein Structure and Molecular Enzymology* 1544 (1–2) (January 12): 311–319. doi:10.1016/S0167-4838(00)00243-0.

Bortner, C D, F M Hughes Jr, and J A Cidlowski. 1997. "A Primary Role for K+ and Na+ Efflux in the Activation of Apoptosis." *The Journal of Biological Chemistry* 272 (51) (December 19): 32436–32442.

Brink, P. A., and V. A. Corfield. 2009. "The Long QT Syndrome in South Africa." *SA Heart Journal* 5 (4) (August 2): 160–163.

Brink, Paul A., Lia Crotti, Valerie Corfield, Althea Goosen, Glenda Durrheim, Paula Hedley, Marshall Heradien, et al. 2005. "Phenotypic Variability and Unusual Clinical Severity of Congenital Long-QT Syndrome in a Founder Population." *Circulation* 112 (17) (October 25): 2602–2610. doi:10.1161/CIRCULATIONAHA.105.572453.

Bruckner, Anna, Cecile Polge, Nicolas Lentze, Daniel Auerbach, and Uwe Schlattner. 2009. "Yeast Two-Hybrid, a Powerful Tool for Systems Biology." *International Journal of Molecular Sciences* 10 (6) (June 18): 2763–2788. doi:10.3390/ijms10062763.

Buettner, Reinhard, Georg Papoutsoglou, Eliana Scemes, David C. Spray, and Rolf Dermietzel. 2000. "Evidence for Secretory Pathway Localization of a Voltage-dependent Anion Channel Isoform." *Proceedings of the National Academy of Sciences* 97 (7) (March 28): 3201–3206. doi:10.1073/pnas.97.7.3201.

Bullard, B. 2003. "Association of the Chaperone B-crystallin with Titin in Heart Muscle." *Journal of Biological Chemistry* 279 (9) (December 16): 7917–7924. doi:10.1074/jbc.M307473200.

Chandrasekhar, Kshama D., Tuba Bas, and William R. Kobertz. 2006. "KCNE1 Subunits Require Co-assembly with K+ Channels for Efficient Trafficking and Cell Surface Expression." *Journal of Biological Chemistry* 281 (52) (December 29): 40015–40023. doi:10.1074/jbc.M604398200.

Cheng, Ching-Feng, Hai-Chien Kuo, and Kenneth R Chien. 2003. "Genetic Modifiers of Cardiac Arrhythmias." *Trends in Molecular Medicine* 9 (2) (February): 59–66. doi:10.1016/S1471-4914(03)00004-2.

Clancy, C. E. 2005. "Inherited and Acquired Vulnerability to Ventricular Arrhythmias: Cardiac Na+ and K+ Channels." *Physiological Reviews* 85 (1) (January 1): 33–47. doi:10.1152/physrev.00005.2004.

Clements, Richard T., Neel R. Sodha, Jun Feng, Shigetoshi Mieno, Munir Boodhwani, Basel Ramlawi, Cesario Bianchi, and Frank W. Sellke. 2007. "Phosphorylation and Translocation of Heat Shock Protein 27 and αB-crystallin in Human Myocardium after Cardioplegia and Cardiopulmonary Bypass." *The Journal of Thoracic and Cardiovascular Surgery* 134 (6) (December): 1461–1470.e3. doi:10.1016/j.jtcvs.2007.06.026.

Colombini, Marco. 2004. "VDAC: The Channel at the Interface Between Mitochondria and the Cytosol." *Molecular and Cellular Biochemistry* 256-257 (1-2) (February): 107–115.

Costes, Sylvain V., Dirk Daelemans, Edward H. Cho, Zachary Dobbin, George Pavlakis, and Stephen Lockett. 2004. "Automatic and Quantitative Measurement of Protein-Protein Colocalization in Live Cells." *Biophysical Journal* 86 (6) (June): 3993–4003. doi:10.1529/biophysj.103.038422.

Crotti, Lia, Giuseppe Celano, Federica Dagradi, and Peter J Schwartz. 2008. "Congenital Long QT Syndrome." *Orphanet Journal of Rare Diseases* 3: 18. doi:10.1186/1750-1172-3-18.

Crotti, Lia, Andrew L. Lundquist, Roberto Insolia, Matteo Pedrazzini, Chiara Ferrandi, Gaetano M. De Ferrari, Alessandro Vicentini, et al. 2005. "KCNH2-K897T Is a Genetic Modifier of Latent Congenital Long-QT Syndrome." *Circulation* 112 (9) (August 30): 1251–1258. doi:10.1161/CIRCULATIONAHA.105.549071.

Crotti, Lia, Maria Cristina Monti, Roberto Insolia, Anna Peljto, Althea Goosen, Paul A Brink, David A Greenberg, Peter J Schwartz, and Alfred L George Jr. 2009. "NOS1AP Is a Genetic Modifier of the long-QT Syndrome." *Circulation* 120 (17) (October 27): 1657–1663. doi:10.1161/CIRCULATIONAHA.109.879643.

Cusick, Michael E, Niels Klitgord, Marc Vidal, and David E Hill. 2005. "Interactome: Gateway into Systems Biology." *Human Molecular Genetics* 14 Spec No. 2 (October 15): R171–181. doi:10.1093/hmg/ddi335.

Dalkilic, I., J. Schienda, T. G. Thompson, and L. M. Kunkel. 2006. "Loss of FilaminC (FLNc) Results in Severe Defects in Myogenesis and Myotube Structure." *Molecular and Cellular Biology* 26 (17) (September 1): 6522–6534. doi:10.1128/MCB.00243-06.

Daniel, Jewel A., Jiyoun Yoo, Blaine T. Bettinger, David C. Amberg, and Daniel J. Burke. 2006. "Eliminating Gene Conversion Improves High-Throughput Genetics in Saccharomyces Cerevisiae." *Genetics* 172 (1) (January 1): 709–711. doi:10.1534/genetics.105.047662.

De Pinto, Vito, Angela Messina, Darius J R Lane, and Alfons Lawen. 2010. "Voltage-dependent Anion-selective Channel (VDAC) in the Plasma Membrane." *FEBS Letters* 584 (9) (May 3): 1793–1799. doi:10.1016/j.febslet.2010.02.049.

Djabali, K, B de Néchaud, F Landon, and M M Portier. 1997. "AlphaB-crystallin Interacts with Intermediate Filaments in Response to Stress." *Journal of Cell Science* 110 (Pt 21) (November): 2759–2769.

Drago, Antonio, Fabrizio De Ponti, Giuseppe Boriani, Diana De Ronchi, and Alessandro Serretti. 2008. "Strategy for a Genetic Assessment of Antipsychotic and Antidepressant-related Proarrhythmia." *Current Medicinal Chemistry* 15 (24): 2472–2517.

Dunn, Kenneth W., Malgorzata M. Kamocka, and John H. McDonald. 2011. "A Practical Guide to Evaluating Colocalization in Biological Microscopy." *American Journal of Physiology - Cell Physiology* 300 (4) (April): C723–C742. doi:10.1152/ajpcell.00462.2010.

Eghbali, Mansoureh, Rupal Deva, Abderrahmane Alioua, Tamara Y Minosyan, Hongmei Ruan, Yibin Wang, Ligia Toro, and Enrico Stefani. 2005. "Molecular and Functional Signature of Heart Hypertrophy During Pregnancy." *Circulation Research* 96 (11) (June 10): 1208–1216. doi:10.1161/01.RES.0000170652.71414.16.

Eldstrom, Jodene, and David Fedida. 2011. "The Voltage-gated Channel Accessory Protein KCNE2: Multiple Ion Channel Partners, Multiple Ways to Long QT Syndrome." *Expert Reviews in Molecular Medicine* 13 (December 14). doi:10.1017/S1462399411002092. http://www.journals.cambridge.org/abstract_S1462399411002092.

Elliott, Perry, Bert Andersson, Eloisa Arbustini, Zofia Bilinska, Franco Cecchi, Philippe Charron, Olivier Dubourg, et al. 2008. "Classification of the Cardiomyopathies: a Position Statement from the European Society of Cardiology Working Group on Myocardial and Pericardial Diseases." *European Heart Journal* 29 (2) (January 1): 270–276. doi:10.1093/eurheartj/ehm342.

Fabiato, A, and F Fabiato. 1978. "Effects of pH on the Myofilaments and the Sarcoplasmic Reticulum of Skinned Cells from Cardiace and Skeletal Muscles." *The Journal of Physiology* 276 (March): 233–255.

Feldman, Arthur M., and Dennis McNamara. 2000. "Myocarditis." *New England Journal of Medicine* 343 (19): 1388–1398. doi:10.1056/NEJM200011093431908.

Fields, S, and O Song. 1989. "A Novel Genetic System to Detect Protein-protein Interactions." *Nature* 340 (6230) (July 20): 245–246. doi:10.1038/340245a0.

Fiset, Céline, and Wayne R. Giles. 2006. "Transmural Gradients of Repolarization and Excitation–Contraction Coupling in Mouse Ventricle." *Circulation Research* 98 (10) (May 26): 1237–1239. doi:10.1161/01.RES.0000225859.82676.ba.

Frank-Hansen, Rune, Lars Allan Larsen, Paal Andersen, Cathrine Jespersgaard, and Michael Christiansen. 2005. "Mutations in the Genes KCND2 and KCND3 Encoding the Ion Channels Kv4.2 and Kv4.3, Conducting the Cardiac Fast Transient Outward Current (ITO,f), Are Not a Frequent Cause of Long QT Syndrome." *Clinica Chimica Acta* 351 (1–2) (January): 95–100. doi:10.1016/j.cccn.2004.08.017.

Frederick, Rebecca L, and Janet M Shaw. 2007. "Moving Mitochondria: Establishing Distribution of an Essential Organelle." *Traffic (Copenhagen, Denmark)* 8 (12) (December): 1668–1675. doi:10.1111/j.1600-0854.2007.00644.x.

Friedlander, Y, M Vatta, N Sotoodehnia, R Sinnreich, H Li, O Manor, J A Towbin, D S Siscovick, and J D Kark. 2005. "Possible Association of the Human KCNE1 (minK) Gene and QT Interval in Healthy Subjects: Evidence from Association and Linkage Analyses in Israeli Families." *Annals of Human Genetics* 69 (Pt 6) (November): 645–656. doi:10.1046/j.1529-8817.2005.00182.x.

Fu, Ling, and Jack J.-N. Liang. 2002. "Detection of Protein-Protein Interactions Among Lens Crystallins in a Mammalian Two-hybrid System Assay." *Journal of Biological Chemistry* 277 (6) (February 8): 4255–4260. doi:10.1074/jbc.M110027200.

Gariboldi, Manuela, Elena Maestrini, Federico Canzian, Giacomo Manenti, Laura De Gregorio, Stefano Rivella, Aurobindo Chatterjee, et al. 1994. "Comparative Mapping of the Actin-Binding Protein 280 Genes in Human and Mouse." *Genomics* 21 (2) (May 15): 428–430. doi:10.1006/geno.1994.1288.

Ghosh, Joy G., Scott A. Houck, and John I. Clark. 2007. "Interactive Sequences in the Stress Protein and Molecular Chaperone Human ?B Crystallin Recognize and Modulate the

Assembly of Filaments." *The International Journal of Biochemistry & Cell Biology* 39 (10): 1804–1815. doi:10.1016/j.biocel.2007.04.027.

Gima, Kazutaka, and Yoram Rudy. 2002. "Ionic Current Basis of Electrocardiographic Waveforms: a Model Study." *Circulation Research* 90 (8) (May 3): 889–896.

Glaaser, Ian W, Robert S Kass, and Colleen E Clancy. 2003. "Mechanisms of Genetic Arrhythmias: From DNA to ECG." *Progress in Cardiovascular Diseases* 46 (3) (November): 259–270. doi:10.1016/S0033-0620(03)00073-2.

Goldenberg, Ilan, Arthur J Moss, Wojciech Zareba, Scott McNitt, Jennifer L Robinson, Ming Qi, Jeffrey A Towbin, Michael J Ackerman, and Laura Murphy. 2006. "Clinical Course and Risk Stratification of Patients Affected with the Jervell and Lange-Nielsen Syndrome." *Journal of Cardiovascular Electrophysiology* 17 (11) (November): 1161–1168. doi:10.1111/j.1540-8167.2006.00587.x.

Goldenberg, Ilan, Wojciech Zareba, and Arthur J. Moss. 2008. "Long QT Syndrome." *Current Problems in Cardiology* 33 (11) (November): 629–694. doi:10.1016/j.cpcardiol.2008.07.002.

Goldfarb, Lev G, Montse Olivé, Patrick Vicart, and Hans H Goebel. 2008. "Intermediate Filament Diseases: Desminopathy." *Advances in Experimental Medicine and Biology* 642: 131–164.

Golenhofen, Nikola, Ming Der Perng, Roy A. Quinlan, and Detlev Drenckhahn. 2004. "Comparison of the Small Heat Shock Proteins ?B-crystallin, MKBP, HSP25, HSP20, and cvHSP in Heart and Skeletal Muscle." *Histochemistry and Cell Biology* 122 (5) (October 12): 415–425. doi:10.1007/s00418-004-0711-z.

Gontier, Yves, Anu Taivainen, Lionel Fontao, Arnoud Sonnenberg, Arjan van der Flier, Olli Carpen, Georgine Faulkner, and Luca Borradori. 2013. "The Z-disc Proteins Myotilin and FATZ-1 Interact with Each Other and Are Connected to the Sarcolemma via Muscle-specific Filamins." Accessed July 15. http://jcs.biologists.org.

Gordon, E., G. Panaghie, L. Deng, K. J. Bee, T. K. Roepke, T. Krogh-Madsen, D. J. Christini, et al. 2007. "A KCNE2 Mutation in a Patient with Cardiac Arrhythmia Induced by Auditory Stimuli and Serum Electrolyte Imbalance." *Cardiovascular Research* 77 (1) (September 19): 98–106. doi:10.1093/cvr/cvm030.

Gorre, Frauke, and Hans Vandekerckhove. 2010. "Beta-blockers: Focus on Mechanism of Action. Which Beta-blocker, When and Why?" *Acta Cardiologica* 65 (5) (October): 565–570.

Harper, J W, G R Adami, N Wei, K Keyomarsi, and S J Elledge. 1993. "The P21 Cdk-interacting Protein Cip1 Is a Potent Inhibitor of G1 Cyclin-dependent Kinases." *Cell* 75 (4) (November 19): 805–816.

Heradien, M., A. Goosen, J. C. Moolman-Smook, and P. A. Brink. 2007. "Race and Gender Representation of Hypertrophic Cardiomyopathy or Long QT Syndrome Cases in a South African Research Setting" (October). http://scholar.sun.ac.za/handle/10019.1/19317.

Hibino, Hiroshi, Atsushi Inanobe, Kazuharu Furutani, Shingo Murakami, Ian Findlay, and Yoshihisa Kurachi. 2010. "Inwardly Rectifying Potassium Channels: Their Structure, Function, and Physiological Roles." *Physiological Reviews* 90 (1) (January 1): 291–366. doi:10.1152/physrev.00021.2009.

Hofman, Nynke, Hanno L Tan, Marielle Alders, Irene M van Langen, and Arthur A M Wilde. 2010. "Active Cascade Screening in Primary Inherited Arrhythmia Syndromes: Does It Lead to Prophylactic Treatment?" *Journal of the American College of Cardiology* 55 (23) (June 8): 2570–2576. doi:10.1016/j.jacc.2009.12.063.

Houlston, R S, and I P Tomlinson. 1998. "Modifier Genes in Humans: Strategies for Identification." *European Journal of Human Genetics: EJHG* 6 (1) (January): 80–88. doi:10.1038/sj.ejhg.5200156.

Isbrandt, D, T Leicher, R Waldschütz, X Zhu, U Luhmann, U Michel, K Sauter, and O Pongs. 2000. "Gene Structures and Expression Profiles of Three Human KCND (Kv4) Potassium Channels Mediating A-type Currents I(TO) and I(SA)." *Genomics* 64 (2) (March 1): 144–154. doi:10.1006/geno.2000.6117.

Isbrandt, Dirk, Patrick Friederich, Anna Solth, Wilhelm Haverkamp, Andreas Ebneth, Martin Borggrefe, Harald Funke, et al. 2002. "Identification and Functional Characterization of a Novel KCNE2 (MiRP1) Mutation That Alters HERG Channel Kinetics." *Journal of Molecular Medicine* 80 (8) (August 1): 524–532. doi:10.1007/s00109-002-0364-0.

James, Jeanne, Hanna Osinska, Timothy E. Hewett, Thomas Kimball, Raisa Klevitsky, Sandra Witt, D. Greg Hall, James Gulick, and Jeffrey Robbins. 1999. "Transgenic Over-Expression of a Motor Protein at High Levels Results in Severe Cardiac Pathology." *Transgenic Research* 8 (1) (February 1): 9–22. doi:10.1023/A:1008894507995.

Jeff, Janina M., Kristin Brown-Gentry, Sarah G. Buxbaum, Daniel F. Sarpong, Herman A. Taylor, Alfred L. George, Dan M. Roden, and Dana C. Crawford. 2011. "SCN5A Variation Is Associated With Electrocardiographic Traits in the Jackson Heart Study." *Circulation: Cardiovascular Genetics* 4 (2) (April 1): 139–144. doi:10.1161/CIRCGENETICS.110.958124.

Jervell, Anton, and Fred Lange-Nielsen. 1957. "Congenital Deaf-mutism, Functional Heart Disease with Prolongation of the Q-T Interval, and Sudden Death." *American Heart Journal* 54 (1) (July): 59–68. doi:10.1016/0002-8703(57)90079-0.

Jiang, M., M. Zhang, D.G. Tang, H.F. Clemo, J. Liu, D. Holwitt, V. Kasirajan, A.L. Pond, E. Wettwer, and G.-N. Tseng. 2004. "KCNE2 Protein Is Expressed in Ventricles of Different Species, and Changes in Its Expression Contribute to Electrical Remodeling in Diseased Hearts." *Circulation* 109 (14): 1783–1788.

Jiang, Min, Xulin Xu, Yuhong Wang, Futoshi Toyoda, Xian-Sheng Liu, Mei Zhang, Richard B. Robinson, and Gea-Ny Tseng. 2009. "Dynamic Partnership Between KCNQ1 and KCNE1 and Influence on Cardiac IKs Current Amplitude by KCNE2." *Journal of Biological Chemistry* 284 (24) (June 12): 16452–16462. doi:10.1074/jbc.M808262200.

Joung, J. Keith, Elizabeth I. Ramm, and Carl O. Pabo. 2000. "A Bacterial Two-hybrid Selection System for Studying protein–DNA and Protein–protein Interactions." *Proceedings of the National Academy of Sciences* 97 (13) (June 20): 7382–7387. doi:10.1073/pnas.110149297.

Kannankeril, Prince, Dan M. Roden, and Dawood Darbar. 2010. "Drug-Induced Long QT Syndrome." *Pharmacological Reviews* 62 (4) (December 1): 760–781. doi:10.1124/pr.110.003723.

Kato, K., H. Shinohara, S. Goto, Y. Inaguma, R. Morishita, and T. Asano. 1992. "Copurification of Small Heat Shock Protein with Alpha B Crystallin from Human Skeletal Muscle." *Journal of Biological Chemistry* 267 (11) (April 15): 7718–7725.

Kayser, H, H D Kratzin, F P Thinnes, H Götz, W E Schmidt, K Eckart, and N Hilschmann. 1989. "[Identification of human porins. II. Characterization and primary structure of a 31-lDa porin from human B lymphocytes (Porin 31HL)]." *Biological chemistry Hoppe-Seyler* 370 (12) (December): 1265–1278.

Keating, M T, and M C Sanguinetti. 2001. "Molecular and Cellular Mechanisms of Cardiac Arrhythmias." *Cell* 104 (4) (February 23): 569–580.

Kelsell, David P., John Dunlop, and Malcolm B. Hodgins. 2001. "Human Diseases: Clues to Cracking the Connexin Code?" *Trends in Cell Biology* 11 (1) (January 1): 2–6. doi:10.1016/S0962-8924(00)01866-3.

Kerner, Janos, Kwangwon Lee, Bernard Tandler, and Charles L Hoppel. 2012. "VDAC Proteomics: Post-translation Modifications." *Biochimica et Biophysica Acta* 1818 (6) (June): 1520–1525. doi:10.1016/j.bbamem.2011.11.013.

Kesner, Barry A., Feng Ding, Brenda R. Temple, and Nikolay V. Dokholyan. 2010. "N-terminal Strands of Filamin Ig Domains Act as a Conformational Switch Under Biological Forces." *Proteins* 78 (1) (January): 12–24. doi:10.1002/prot.22479.

Klemenz, R., E. Fröhli, R. H. Steiger, R. Schäfer, and A. Aoyama. 1991. "Alpha B-crystallin Is a Small Heat Shock Protein." *Proceedings of the National Academy of Sciences* 88 (9) (May 1): 3652–3656. doi:10.1073/pnas.88.9.3652.

Kley, Rudolf A., Yorck Hellenbroich, Peter F. M. van der Ven, Dieter O. Fürst, Angela Huebner, Vera Bruchertseifer, Sören A. Peters, et al. 2007. "Clinical and Morphological Phenotype of the Filamin Myopathy: a Study of 31 German Patients." *Brain* 130 (12) (December 1): 3250–3264. doi:10.1093/brain/awm271.

Koya, R. C. 2000. “Gelsolin Inhibits Apoptosis by Blocking Mitochondrial Membrane Potential Loss and Cytochrome c Release.” *Journal of Biological Chemistry* 275 (20) (May 12): 15343–15349. doi:10.1074/jbc.275.20.15343.

Kubota, T, W Shimizu, S Kamakura, and M Horie. 2000. “Hypokalemia-induced Long QT Syndrome with an Underlying Novel Missense Mutation in S4-S5 Linker of KCNQ1.” *Journal of Cardiovascular Electrophysiology* 11 (9) (September): 1048–1054.

Kundu, Pallob, Andrea Ciobotaru, Sina Foroughi, Ligia Toro, Enrico Stefani, and Mansoureh Eghbali. 2008. “Hormonal Regulation of Cardiac KCNE2 Gene Expression.” *Molecular and Cellular Endocrinology* 292 (1-2) (September 24): 50–62. doi:10.1016/j.mce.2008.06.003.

Lahtinen, Annukka M., Annukka Marjamaa, Heikki Swan, and Kimmo Kontula. 2011. “KCNE1 D85N Polymorphism — a Sex-specific Modifier in Type 1 Long QT Syndrome?” *BMC Medical Genetics* 12 (1) (January 18): 11. doi:10.1186/1471-2350-12-11.

Laitinen, Päivi, Heidi Fodstad, Kirsi Piippo, Heikki Swan, Lauri Toivonen, Matti Viitasalo, Jaakko Kaprio, and Kimmo Kontula. 2000. “Survey of the Coding Region of the HERG Gene in Long QT Syndrome Reveals Six Novel Mutations and an Amino Acid Polymorphism with Possible Phenotypic Effects.” *Human Mutation* 15 (6): 580–581. doi:10.1002/1098-1004(200006)15:6<580::AID-HUMU16>3.0.CO;2-0.

Lalonde, Sylvie, David W Ehrhardt, Dominique Loqué, Jin Chen, Seung Y Rhee, and Wolf B Frommer. 2008. “Molecular and Cellular Approaches for the Detection of Protein-protein Interactions: Latest Techniques and Current Limitations.” *The Plant Journal: For Cell and Molecular Biology* 53 (4) (February): 610–635. doi:10.1111/j.1365-313X.2007.03332.x.

Lehnart, S.E., M.J. Ackerman, D.W. Benson, R. Brugada, C.E. Clancy, J.K. Donahue, A.L. George, et al. 2007. “Inherited Arrhythmias: A National Heart, Lung, and Blood Institute and Office of Rare Diseases Workshop Consensus Report About the Diagnosis, Phenotyping, Molecular Mechanisms, and Therapeutic Approaches for Primary Cardiomyopathies of Gene Mutations Affecting Ion Channel Function.” *Circulation* 116 (20): 2325–2345.

Lewis, Anthony, Zoe A. McCrossan, and Geoffrey W. Abbott. 2004. “MinK, MiRP1, and MiRP2 Diversify Kv3.1 and Kv3.2 Potassium Channel Gating.” *Journal of Biological Chemistry* 279 (9) (February 27): 7884–7892. doi:10.1074/jbc.M310501200.

Linnemann, Anja, Peter F.M. van der Ven, Padmanabhan Vakeel, Britta Albinus, Dirk Simonis, Gerd Bendas, Jörg A. Schenk, Burkhard Micheel, Rudolf A. Kley, and Dieter O. Fürst. 2010. “The Sarcomeric Z-disc Component Myopodin Is a Multiadapter Protein That Interacts with Filamin and A-actinin.” *European Journal of Cell Biology* 89 (9) (September): 681–692. doi:10.1016/j.ejcb.2010.04.004.

Lu, Y., M. P Mahaut-Smith, C. L-H Huang, and J. I Vandenberg. 2003. “Mutant MiRP1 Subunits Modulate HERG K+ Channel Gating: a Mechanism for Pro-arrhythmia in Long

QT Syndrome Type 6." *The Journal of Physiology* 551 (1) (August 14): 253–262. doi:10.1113/jphysiol.2003.046045.

Marbán, Eduardo. 2002. "Cardiac Channelopathies." *Nature* 415 (6868) (January 10): 213–218. doi:10.1038/415213a.

McCrossan, Zoe A, and Geoffrey W Abbott. 2004. "The MinK-related Peptides." *Neuropharmacology* 47 (6) (November): 787–821. doi:10.1016/j.neuropharm.2004.06.018.

McCrossan, Zoe A., Torsten K. Roepke, Anthony Lewis, Gianina Panaghie, and Geoffrey W. Abbott. 2009. "Regulation of the Kv2.1 Potassium Channel by MinK and MiRP1." *Journal of Membrane Biology* 228 (1) (February 14): 1–14. doi:10.1007/s00232-009-9154-8.

McDonald, T V, Z Yu, Z Ming, E Palma, M B Meyers, K W Wang, S A Goldstein, and G I Fishman. 1997. "A minK-HERG Complex Regulates the Cardiac Potassium Current I(Kr)." *Nature* 388 (6639) (July 17): 289–292. doi:10.1038/40882.

McMichael, J. 1982. "History of Atrial Fibrillation 1628-1819 Harvey - de Senac - La?nnec." *British Heart Journal* 48 (3) (September): 193–197.

Medeiros-Domingo, Argelia, Pedro Iturralde-Torres, and Michael J. Ackerman. 2007a. "Clinical and Genetic Characteristics of Long QT Syndrome." *Revista Española de Cardiología (English Edition)* 60 (7): 739–752. doi:10.1016/S1885-5857(08)60010-9.

Medeiros-Domingo, Argelia, Toshihiko Kaku, David J. Tester, Pedro Iturralde-Torres, Ajit Itty, Bin Ye, Carmen Valdivia, et al. 2007b. "SCN4B-Encoded Sodium Channel B4 Subunit in Congenital Long-QT Syndrome." *Circulation* 116 (2) (July 10): 134–142. doi:10.1161/CIRCULATIONAHA.106.659086.

Miernyk, Jan A, and Jay J Thelen. 2008. "Biochemical Approaches for Discovering Protein-protein Interactions." *The Plant Journal: For Cell and Molecular Biology* 53 (4) (February): 597–609. doi:10.1111/j.1365-313X.2007.03316.x.

Mitra, A., T. Basak, K. Datta, S. Naskar, S. Sengupta, and S. Sarkar. 2013. "Role of A-crystallin B as a Regulatory Switch in Modulating Cardiomyocyte Apoptosis by Mitochondria or Endoplasmic Reticulum During Cardiac Hypertrophy and Myocardial Infarction." *Cell Death & Disease* 4 (4) (April 4): e582. doi:10.1038/cddis.2013.114.

Moric-Janiszewska, Ewa. 2012. "Non Genetic Risk Factors of long-QT Syndrome." *Open Journal of Genetics* 02 (01): 56–61. doi:10.4236/ojgen.2012.21007.

Moss, A J, W Zareba, W J Hall, P J Schwartz, R S Crampton, J Benhorin, G M Vincent, et al. 2000. "Effectiveness and Limitations of Beta-blocker Therapy in Congenital long-QT Syndrome." *Circulation* 101 (6) (February 15): 616–623.

Moss, Arthur J, Wojciech Zareba, Elizabeth S Kaufman, Eric Gartman, Derick R Peterson, Jesaia Benhorin, Jeffrey A Towbin, et al. 2002. "Increased Risk of Arrhythmic Events in long-QT Syndrome with Mutations in the Pore Region of the Human Ether-a-go-go-related Gene Potassium Channel." *Circulation* 105 (7) (February 19): 794–799.

Murphy, Elizabeth. 2004. "Primary and Secondary Signaling Pathways in Early Preconditioning That Converge on the Mitochondria to Produce Cardioprotection." *Circulation Research* 94 (1) (January 9): 7–16. doi:10.1161/01.RES.0000108082.76667.F4.

Murray, James T., David G. Campbell, Mark Peggie, Alfonso Mora, and Philip Cohen. 2004. "Identification of Filamin C as a New Physiological Substrate of PKBα Using KESTREL." *Biochemical Journal* 384 (3) (December 15): 489. doi:10.1042/BJ20041058.

Napolitano, C, P J Schwartz, A M Brown, E Ronchetti, L Bianchi, A Pinnavaia, G Acquaro, and S G Priori. 2000. "Evidence for a Cardiac Ion Channel Mutation Underlying Drug-induced QT Prolongation and Life-threatening Arrhythmias." *Journal of Cardiovascular Electrophysiology* 11 (6) (June): 691–696.

Napolitano, C. 2005. "Genetic Testing in the Long QT Syndrome: Development and Validation of an Efficient Approach to Genotyping in Clinical Practice." *JAMA (Chicago, Ill.)* 294 (23): 2975–2980. doi:10.1001/jama.294.23.2975.

Newton-Cheh, Christopher, Mark Eijgelsheim, Kenneth M Rice, Paul I W de Bakker, Xiaoyan Yin, Karol Estrada, Joshua C Bis, et al. 2009. "Common Variants at Ten Loci Influence QT Interval Duration in the QTGEN Study." *Nature Genetics* 41 (4) (April): 399–406. doi:10.1038/ng.364.

Newton-Cheh, Christopher, Chao-Yu Guo, Martin G. Larson, Stacy L. Musone, Aarti Surti, Amy L. Camargo, Jared A. Drake, et al. 2007. "Common Genetic Variation in KCNH2 Is Associated With QT Interval Duration The Framingham Heart Study." *Circulation* 116 (10) (September 4): 1128–1136. doi:10.1161/CIRCULATIONAHA.107.710780.

Okada, Seiko F, Wanda K O'Neal, Pingbo Huang, Robert A Nicholas, Lawrence E Ostrowski, William J Craigen, Eduardo R Lazarowski, and Richard C Boucher. 2004. "Voltage-dependent Anion Channel-1 (VDAC-1) Contributes to ATP Release and Cell Volume Regulation in Murine Cells." *The Journal of General Physiology* 124 (5) (November): 513–526. doi:10.1085/jgp.200409154.

Parmacek, Michael S, and R John Solaro. 2004. "Biology of the Troponin Complex in Cardiac Myocytes." *Progress in Cardiovascular Diseases* 47 (3) (December): 159–176.

Peer, Wendy Ann. 2011. "Plasma Membrane Protein Trafficking." In *The Plant Plasma Membrane*, edited by Angus S. Murphy, Burkhard Schulz, and Wendy Peer, 19:31–56. Berlin, Heidelberg: Springer Berlin Heidelberg. http://link.springer.com/10.1007/978-3-642-13431-9_2.

Petrecca, K, D M Miller, and A Shrier. 2000. "Localization and Enhanced Current Density of the Kv4.2 Potassium Channel by Interaction with the Actin-binding Protein Filamin." *The Journal of Neuroscience: The Official Journal of the Society for Neuroscience* 20 (23) (December 1): 8736–8744.

Phizicky, E M, and S Fields. 1995. "Protein-protein Interactions: Methods for Detection and Analysis." *Microbiological Reviews* 59 (1) (March): 94–123.

Pinnell, Jeremy, Simon Turner, and Simon Howell. 2007. "Cardiac Muscle Physiology." *Continuing Education in Anaesthesia, Critical Care & Pain* 7 (3) (June 1): 85–88. doi:10.1093/bjaceaccp/mkm013.

Popowicz, Grzegorz M., Michael Schleicher, Angelika A. Noegel, and Tad A. Holak. 2006. "Filamins: Promiscuous Organizers of the Cytoskeleton." *Trends in Biochemical Sciences* 31 (7) (July): 411–419. doi:10.1016/j.tibs.2006.05.006.

Priori, S G, D W Mortara, C Napolitano, L Diehl, V Paganini, F Cantù, G Cantù, and P J Schwartz. 1997. "Evaluation of the Spatial Aspects of T-wave Complexity in the long-QT Syndrome." *Circulation* 96 (9) (November 4): 3006–3012.

Rastogi, V. B. 1997. *Modern Biology*. Pitambar Publishing.

Robertson, Stephen P, Stephen R F Twigg, Andrew J Sutherland-Smith, Valérie Biancalana, Robert J Gorlin, Denise Horn, Susan J Kenwrick, et al. 2003. "Localized Mutations in the Gene Encoding the Cytoskeletal Protein Filamin A Cause Diverse Malformations in Humans." *Nature Genetics* 33 (4) (April): 487–491. doi:10.1038/ng1119.

Roepke, Torsten K., Andrianos Kontogeorgis, Christopher Ovanez, Xianghua Xu, Jeffrey B. Young, Kerry Purtell, Peter A. Goldstein, et al. 2008. "Targeted Deletion of Kcne2 Impairs Ventricular Repolarization via Disruption of IK,slow1 and Ito,f." *The FASEB Journal* 22 (10) (October 1): 3648–3660. doi:10.1096/fj.08-110171.

Romano, C, G Gemme, and R pongiglione. 1963. "[Rare cardiac arrythmias of the pediatric age. ii. syncopal attacks due to paroxysmal ventricular fibrillation. (Presentation of 1st case in italian pediatric literature)]." *La Clinica Pediatrica* 45 (September): 656–683.

Rosengarten, J. A., P. A. Scott, S. E. Larkin, S. Garbis, N. P. Curzen, P. A. Townsend, J. M. Morgan, et al. 2013. "Main Session: Molecular Mechanisms in Cardiomyopathies." *Europace* 15 (suppl 2) (June 1): ii11–ii11. doi:10.1093/europace/eut194.

Sacconi, Sabrina, Léonard Féasson, Jean Christophe Antoine, Christophe Pécheux, Rafaelle Bernard, Ana Maria Cobo, Alberto Casarin, Leonardo Salviati, Claude Desnuelle, and Andoni Urtizberea. 2012. "A Novel CRYAB Mutation Resulting in Multisystemic Disease." *Neuromuscular Disorders: NMD* 22 (1) (January): 66–72. doi:10.1016/j.nmd.2011.07.004.

Sampson, M J, R S Lovell, and W J Craigen. 1997. "The Murine Voltage-dependent Anion Channel Gene Family. Conserved Structure and Function." *The Journal of Biological Chemistry* 272 (30) (July 25): 18966–18973.

Sanguinetti, M C, C Jiang, M E Curran, and M T Keating. 1995. "A Mechanistic Link Between an Inherited and an Acquired Cardiac Arrhythmia: HERG Encodes the IKr Potassium Channel." *Cell* 81 (2) (April 21): 299–307.

Satwani, Shiyam, G. William Dec, and Jagat Narula. 2004. "β-Adrenergic Blockers in Heart Failure: Review of Mechanisms of Action and Clinical Outcomes." *Journal of Cardiovascular Pharmacology and Therapeutics* 9 (4) (October 1): 243–255. doi:10.1177/107424840400900404.

Schulze Bahr, E. 2012. "Long QT Syndromes: Genetic Basis." *Cardiac Electrophysiology Clinics* 4 (1): 1–16. doi:10.1016/j.ccep.2012.01.001.

Schwartz, P J, S G Priori, C Spazzolini, A J Moss, G M Vincent, C Napolitano, I Denjoy, et al. 2001. "Genotype-phenotype Correlation in the long-QT Syndrome: Gene-specific Triggers for Life-threatening Arrhythmias." *Circulation* 103 (1) (January 2): 89–95.

Schwartz, P. J. 1993. "Diagnostic Criteria for the Long QT Syndrome: An Update." *Circulation* 88 (2): 782–784.

Schwartz, P. J. 2009. "Prevalence of the Congenital Long-qt Syndrome." *Circulation* 120 (18): 1761–1767. doi:10.1161/CIRCULATIONAHA.109.863209.

Schwartz, P. J. 2012. "Genetic Testing for the Long QT Syndrome: Who and Why? Insights for Clinical Management." *SA Heart Journal* 9 (2) (May 31): 100–104.

Schwartz, P. J., Carla Spazzolini, Lia Crotti, Jørn Bathen, Jan P. Amlie, Katherine Timothy, Maria Shkolnikova, et al. 2006. "The Jervell and Lange-Nielsen Syndrome Natural History, Molecular Basis, and Clinical Outcome." *Circulation* 113 (6) (February 14): 783–790. doi:10.1161/CIRCULATIONAHA.105.592899.

Schwartz, P. J., Emilio Vanoli, Lia Crotti, Carla Spazzolini, Chiara Ferrandi, Althea Goosen, Paula Hedley, et al. 2008. "Neural Control of Heart Rate Is an Arrhythmia Risk Modifier in Long QT Syndrome." *Journal of the American College of Cardiology* 51 (9) (March): 920–929. doi:10.1016/j.jacc.2007.09.069.

Shi, Yong, Jianjun Chen, Changjiang Weng, Rui Chen, Yanhua Zheng, Quan Chen, and Hong Tang. 2003. "Identification of the Protein-protein Contact Site and Interaction Mode of Human VDAC1 with Bcl-2 Family Proteins." *Biochemical and Biophysical Research Communications* 305 (4) (June 13): 989–996.

Shimizu, S, Y Matsuoka, Y Shinohara, Y Yoneda, and Y Tsujimoto. 2001. "Essential Role of Voltage-dependent Anion Channel in Various Forms of Apoptosis in Mammalian Cells." *The Journal of Cell Biology* 152 (2) (January 22): 237–250.

Shimizu, Wataru, and Charles Antzelevitch. 1997. “Sodium Channel Block With Mexiletine Is Effective in Reducing Dispersion of Repolarization and Preventing Torsade de Pointes in LQT2 and LQT3 Models of the Long-QT Syndrome.” *Circulation* 96 (6) (September 16): 2038–2047. doi:10.1161/01.CIR.96.6.2038.

Shimizu and Antzelevitch. 1999. “Cellular Basis for Long QT, Transmural Dispersion of Repolarization, and Torsade de Pointes in the Long QT Syndrome.” *Journal of Electrocardiology* 32: 177–184.

Shimizu, Wataru, Minoru Horie, Seiko Ohno, Kotoe Takenaka, Masato Yamaguchi, Masami Shimizu, Takashi Washizuka, et al. 2004. “Mutation Site-specific Differences in Arrhythmic Risk and Sensitivity to Sympathetic Stimulation in the LQT1 Form of Congenital Long QT Syndrome: Multicenter Study in Japan.” *Journal of the American College of Cardiology* 44 (1) (July 7): 117–125. doi:10.1016/j.jacc.2004.03.043.

Shoshan-Barmatz, V, and M Golan. 2012. “Mitochondrial VDAC1: Function in Cell Life and Death and a Target for Cancer Therapy.” *Current Medicinal Chemistry* 19 (5): 714–735.

Spach, M.S., and C.F. Starmer. 1995. “Altering the Topology of Gap Junctions: A Major Therapeutic Target for Atrial Fibrillation.” *Cardiovascular Research* 30 (3): 337–344.

Splawski, I, M Tristani-Firouzi, M H Lehmann, M C Sanguinetti, and M T Keating. 1997. “Mutations in the hminK Gene Cause Long QT Syndrome and Suppress IKs Function.” *Nature Genetics* 17 (3) (November): 338–340. doi:10.1038/ng1197-338.

Splawski, I., J. Shen, K. W. Timothy, M. H. Lehmann, S. Priori, J. L. Robinson, A. J. Moss, et al. 2000. “Spectrum of Mutations in Long-QT Syndrome Genes : KVLQT1, HERG, SCN5A, KCNE1, and KCNE2.” *Circulation* 102 (10) (September 5): 1178–1185. doi:10.1161/01.CIR.102.10.1178.

Starr, Cecie, Christine A. Evers, and Lisa Starr. 2010. *Biology: Concepts and Applications*. Cengage Learning.

Stein, M. 2008. “Conduction Reserve: Phenomenon and Underlying Mechanism” (April 10). http://igitur-archive.library.uu.nl/dissertations/2008-0409-200412/UUindex.html.

Tan, H L, M T Bink-Boelkens, C R Bezzina, P C Viswanathan, G C Beaufort-Krol, P J van Tintelen, M P van den Berg, A A Wilde, and J R Balser. 2001. “A Sodium-channel Mutation Causes Isolated Cardiac Conduction Disease.” *Nature* 409 (6823) (February 22): 1043–1047. doi:10.1038/35059090.

Tester, David J., Melissa L. Will, Carla M. Haglund, and Michael J. Ackerman. 2006. “Effect of Clinical Phenotype on Yield of Long QT Syndrome Genetic Testing.” *Journal of the American College of Cardiology* 47 (4) (February 21): 764–768. doi:10.1016/j.jacc.2005.09.056.

Thompson, Terri G., Yiu-Mo Chan, Andrew A. Hack, Melissa Brosius, Michael Rajala, Hart G. W. Lidov, Elizabeth M. McNally, Simon Watkins, and Louis M. Kunkel. 2000. “Filamin

2 (FLN2): A Muscle-specific Sarcoglycan Interacting Protein." *The Journal of Cell Biology* 148 (1) (January 10): 115–126. doi:10.1083/jcb.148.1.115.

Tinel, Norbert, Sylvie Diochot, Inger Lauritzen, Jacques Barhanin, Michel Lazdunski, and Marc Borsotto. 2000. "M-type KCNQ2–KCNQ3 Potassium Channels Are Modulated by the KCNE2 Subunit." *FEBS Letters* 480 (2–3) (September 1): 137–141. doi:10.1016/S0014-5793(00)01918-9.

Towbin, Jeffrey A, and Matteo Vatta. 2001. "Molecular Biology and the Prolonged QT Syndromes." *The American Journal of Medicine* 110 (5) (April 1): 385–398. doi:10.1016/S0002-9343(00)00715-4.

Ujwal, Rachna, Duilio Cascio, Jacques-Philippe Colletier, Salem Faham, Jun Zhang, Ligia Toro, Peipei Ping, and Jeff Abramson. 2008. "The Crystal Structure of Mouse VDAC1 at 2.3 A Resolution Reveals Mechanistic Insights into Metabolite Gating." *Proceedings of the National Academy of Sciences of the United States of America* 105 (46) (November 18): 17742–17747. doi:10.1073/pnas.0809634105.

Um, Sung Yon, and Thomas V. McDonald. 2007. "Differential Association Between HERG and KCNE1 or KCNE2." *PLoS ONE* 2 (9) (September 26): e933. doi:10.1371/journal.pone.0000933.

Van Criekinge, Wim, and Rudi Beyaert. 1999. "Yeast Two-Hybrid: State of the Art." *Biological Procedures Online* 2 (October 4): 1–38. doi:10.1251/bpo16.

Vicart, P, A Caron, P Guicheney, Z Li, M C Prévost, A Faure, D Chateau, et al. 1998. "A Missense Mutation in the alphaB-crystallin Chaperone Gene Causes a Desmin-related Myopathy." *Nature Genetics* 20 (1) (September): 92–95. doi:10.1038/1765.

Vicart, Patrick, Anne Caron, Pascale Guicheney, Zhenlin Li, Marie-Christine Prévost, Armelle Faure, Danielle Chateau, et al. 1998. "A Missense Mutation in the αB-crystallin Chaperone Gene Causes a Desmin-related Myopathy." *Nature Genetics* 20 (1): 92–95. doi:10.1038/1765.

Vincent, G M. 1998. "The Molecular Genetics of the Long QT Syndrome: Genes Causing Fainting and Sudden Death." *Annual Review of Medicine* 49: 263–274. doi:10.1146/annurev.med.49.1.263.

Wang, Q, J Shen, I Splawski, D Atkinson, Z Li, J L Robinson, A J Moss, J A Towbin, and M T Keating. 1995. "SCN5A Mutations Associated with an Inherited Cardiac Arrhythmia, Long QT Syndrome." *Cell* 80 (5) (March 10): 805–811.

Ward, O C. 1964. "A new familial cardiac syndrome in children." *Journal of the Irish Medical Association* 54 (April): 103–106.

Weerapura, Manjula, Stanley Nattel, Denis Chartier, Ricardo Caballero, and Terence E Hébert. 2002. "A Comparison of Currents Carried by HERG, with and Without Coexpression of

MiRP1, and the Native Rapid Delayed Rectifier Current. Is MiRP1 the Missing Link?" *The Journal of Physiology* 540 (Pt 1) (April 1): 15–27.

Xu, Ning. 2013. "On the Concept of Resting Potential—Pumping Ratio of the Na+/K+ Pump and Concentration Ratios of Potassium Ions Outside and Inside the Cell to Sodium Ions Inside and Outside the Cell." *The Journal of Membrane Biology* 246 (1) (January 1): 75–90. doi:10.1007/s00232-012-9507-6.

Yang, P., H. Kanki, B. Drolet, T. Yang, J. Wei, P.C. Viswanathan, S.H. Hohnloser, et al. 2002. "Allelic Variants in long-QT Disease Genes in Patients with Drug-associated Torsades de Pointes." *Circulation* 105 (16): 1943–1948.

Yang, Yiqing, Min Xia, Qingfeng Jin, Said Bendahhou, Jingyi Shi, Yiping Chen, Bo Liang, et al. 2004. "Identification of a KCNE2 Gain-of-Function Mutation in Patients with Familial Atrial Fibrillation." *American Journal of Human Genetics* 75 (5) (November): 899–905.

Ying, Shui-Wang, Vikram A. Kanda, Zhaoyang Hu, Kerry Purtell, Elizabeth C. King, Geoffrey W. Abbott, and Peter A. Goldstein. 2012. "Targeted Deletion of Kcne2 Impairs HCN Channel Function in Mouse Thalamocortical Circuits." *PLoS ONE* 7 (8) (August 3): e42756. doi:10.1371/journal.pone.0042756.

Yoo, B C, M Fountoulakis, N Cairns, and G Lubec. 2001. "Changes of Voltage-dependent Anion-selective Channel Proteins VDAC1 and VDAC2 Brain Levels in Patients with Alzheimer's Disease and Down Syndrome." *Electrophoresis* 22 (1) (January): 172–179. doi:10.1002/1522-2683(200101)22:1<172::AID-ELPS172>3.0.CO;2-P.

Yu, H., J. Wu, I. Potapova, R. T. Wymore, B. Holmes, J. Zuckerman, Z. Pan, et al. 2001. "MinK-Related Peptide 1 A β Subunit for the HCN Ion Channel Subunit Family Enhances Expression and Speeds Activation." *Circulation Research* 88 (12) (June 22): e84–e87. doi:10.1161/hh1201.093511.

Yu, W, F Zhang, W Hu, R Zhang, C Wang, J Lu, F Jiang, et al. 2013. "Association Between KCNQ1 Genetic Variants and QT Interval in a Chinese Population." *Diabetic Medicine: a Journal of the British Diabetic Association* (May 22). doi:10.1111/dme.12237.

Yuqi, Liu, Gao Lei, Li Yang, Li Zongbin, Xu Hua, Wang Lin, Chen Rui, et al. 2009. "Voltage-dependent Anion Channel (VDAC) Is Involved in Apoptosis of Cell Lines Carrying the Mitochondrial DNA Mutation." *BMC Medical Genetics* 10 (1) (November 9): 114. doi:10.1186/1471-2350-10-114.

Zhang, M., M. Jiang, and G.-N. Tseng. 2001. "MinK-Related Peptide 1 Associates With Kv4.2 and Modulates Its Gating Function : Potential Role as Subunit of Cardiac Transient Outward Channel?" *Circulation Research* 88 (10) (May 10): 1012–1019. doi:10.1161/hh1001.090839.

Zhang, Mei, Yuhong Wang, Min Jiang, Dimitar P. Zankov, Sabeeha Chowdhury, Vigneshwar Kasirajan, and Gea-Ny Tseng. 2012. "KCNE2 Protein Is More Abundant in Ventricles Than in Atria and Can Accelerate hERG Protein Degradation in a Phosphorylation-

dependent Manner." *American Journal of Physiology - Heart and Circulatory Physiology* 302 (4) (February 15): H910–H922. doi:10.1152/ajpheart.00691.2011.

Zheng, Yanhua, Yong Shi, Changhai Tian, Chunsun Jiang, Haijing Jin, Jianjun Chen, Alex Almasan, Hong Tang, and Quan Chen. 2004. "Essential Role of the Voltage-dependent Anion Channel (VDAC) in Mitochondrial Permeability Transition Pore Opening and Cytochrome c Release Induced by Arsenic Trioxide." *Oncogene* 23 (6) (February 12): 1239–1247. doi:10.1038/sj.onc.1207205.

Zhou, Xianghua, Jan Borén, and Levent M Akyürek. 2007. "Filamins in Cardiovascular Development." *Trends in Cardiovascular Medicine* 17 (7) (October): 222–229. doi:10.1016/j.tcm.2007.08.001.

Zinchuk, Vadim, Olga Zinchuk, and Teruhiko Okada. 2007. "Quantitative Colocalization Analysis of Multicolor Confocal Immunofluorescence Microscopy Images: Pushing Pixels to Explore Biological Phenomena." *Acta Histochemica et Cytochemica* 40 (4) (August 30): 101–111. doi:10.1267/ahc.07002.

URL Reference List

http://www.mindcreators.com/neuronbasics.htm

http://biology-forums.com/gallery/.jpeg

http://kakistudy.blogspot.com/2011/03/heartbeat-mechanism.html

https://en.wikipedia.org/wiki/QRS_complex

http://www.genedx.com/wp-content/uploads/2010/12/LQT.jpg

http://www.mrc.ac.za/annualreport/annualreport1112.pdf

http://journals.cambridge.org/fulltext_content/ERM/ERM1_19/S1462399499001349sup022.gif

http://www.ensembl.org

http://eu.idtdna.com/analyzer/applications/oligoanalyzer/

http://www.ncbi.nlm.nih.gov/Entrez

http://www.ncbi.nlm.nih.gov/BLAST

http://www.clontech.com/

http://www.genecards.org/

http://www.nextprot.org/

http://www.scq.ubc.ca/the-yeast-two-hybrid-assay-an-exercise-in-experimental-eloquence/

http://www.swtafe.vic.edu.au/toolbox/lab_ops/laboratory/studynotes/SNHaemo.htm

http://microscopy.zeiss.com/microscopy/en_de/downloads/zen.html

Appendix I

Reagents

1. SOLUTION USED IN GENERATION OF COMPETENT CELLS

CAP buffer:

60mM $CaCl_2$	2.21g
15% glycerol	37.5ml
10mM PIPES	0.76g

ddH_2O up to 250ml. pH 7.0. Keep in fridge

2. BACTERIAL MEDIA

Luria-Bertani (LB) Media

Bacto tryptone	5g
Yeast extract	2.5g
NaCl	5g
Agar	8g

ddH_2O to final volume of 500ml

Autoclave for 20 minutes at 121ºC and add appropriate antibiotic to media when the temperature has reached ±55ºC (Ampicillin, 50mg/ml and Kanamycin 100mg/ml).

LB Agar Plates

Bacto tryptone	5g
Yeast extract	2.5g
NaCl	5g
Agar	8g

ddH_2O to final volume of 500ml

Autoclave for 20 minutes at 121ºC and add appropriate antibiotic to media when the temperature has reached ±55ºC, prior to pouring plates (Ampicillin, 50mg/ml and Kanamycin 100mg/ml).

3. YEAST MEDIA

YPDA Media

Difco peptone	10g
Yeast extract	5g
Glucose	10g
L-adenine hemisulphate (0.2% stock)	7.5ml

ddH_2O to a final volume of 500ml; Autoclave at 121ºC for 15 minutes

2X YPDA Media

Difco peptone	12g
Yeast extract	6g
Glucose	12g
L-adenine hemisulphate (0.2% stock)	9ml

ddH_2O to a final volume of 500ml; Autoclave at 121ºC for 15 minutes

YPDA Agar

Difco peptone	10g
Yeast extract	5g
Glucose	10g
Bacto agar	10g
L-adenine hemisulphate (0.2% stock)	7.5ml

ddH_2O to a final volume of 500ml; Autoclave at 121ºC for 15 minutes

4. YEAST TRANSFORMATION REAGENTS

1M Lithium Acetate (LiAc)

LiAc	5.1g

ddH_2O to a final volume of 50ml

100mM LiAc

1M LiAc	5ml

ddH_2O to a final volume of 50ml

50% PEG 4000

PEG 4000	25g
ddH_2O to a final volume of 50ml	

Herring Sperm

Herring Sperm	50mg
ddH_2O to a final volume of 50ml	

5. SINGLE DROPOUT MEDIA

SD^{-Trp} Media

Glucose	12g
Yeast nitrogen base without amino acids	4g
SD^{-Trp} amino acid supplement	0.4g
0.2% adenine hemisulphate	9ml
ddH_2O to a final volume of 600ml; Autoclave at 121ºC for 15 minutes	

SD^{-Trp} Agar Plates

Glucose	12g
Yeast nitrogen base without amino acids	4g
SD^{-Trp} amino acid supplement	0.4g
Bacto agar	12g
0.2% adenine hemisulphate	9ml
ddH_2O to a final volume of 600ml; Autoclave at 121ºC for 15 minutes	

SD^{-Leu} Media

Glucose	12g
Yeast nitrogen base without amino acids	4g
SD^{-Leu} amino acid supplement	0.4g
0.2% adenine hemisulphate	9ml
ddH_2O to a final volume of 600ml; Autoclave at 121ºC for 15 minutes	

SD^{-Leu} Agar Plates

Glucose	12g
Yeast nitrogen base without amino acids	4g
SD^{-Leu} amino acid supplement	0.4g
Bacto agar	12g
0.2% adenine hemisulphate	9ml

ddH$_2$O to a final volume of 600ml; Autoclave at 121ºC for 15 minutes

SD$^{-Trp/-Leu}$ Media

Glucose	12g
Yeast nitrogen base without amino acids	4g
SD$^{-Trp/-Leu}$ amino acid supplement	0.4g
0.2% adenine hemisulphate	9ml

ddH$_2$O to a final volume of 600ml; Autoclave at 121ºC for 15 minutes

SD$^{-Trp/-Leu}$ Agar Plates

Glucose	12g
Yeast nitrogen base without amino acids	4g
SD$^{-Trp/-Leu}$ amino acid supplement	0.4g
0.2% adenine hemisulphate	9ml
Bacto agar	12g

ddH$_2$O to a final volume of 600ml; Autoclave at 121ºC for 15 minutes

TDO Media

Glucose	12g
Yeast nitrogen base without amino acids	4g
SD$^{-Trp-Leu-His}$ amino acid supplement	0.4g

ddH$_2$O to a final volume of 600ml; pH 5.8; Autoclave at 121ºC for 15 minutes

TDO Agar Plates

Glucose	12g
Bacto agar	12g
Yeast nitrogen base without amino acids	4g
$SD^{-Trp-Leu-His}$ amino acid supplement	0.4g

ddH_2O to a final volume of 600ml; pH 5.8; Autoclave at 121ºC for 15 minutes

QDO Media

Glucose	12g
Yeast nitrogen base without amino acids	4g
$SD^{-Trp-Leu-His-Ade}$ amino acid supplement	0.4g

ddH_2O to a final volume of 600ml; pH 5.8; Autoclave at 121ºC for 15 minutes

QDO Agar Plates

Glucose	12g
Bacto agar	12g
Yeast nitrogen base without amino acids	4g
$SD^{-Trp-Leu-His-Ade}$ amino acid supplement	0.4g

ddH_2O to a final volume of 600ml; pH 5.8; Autoclave at 121ºC for 15 minutes

X-α-galactosidase Solutions (20mg/ml)

x-α-galactosidase	250mg
Dimethylformamide (DMF)	12.5ml

3-Amino-1,2,4-triazole (3-AT) (10mM)

3-AT	0.84g

ddH_2O to a final volume of 1L

Add 6ml 3-AT solution and 1ml X-α-Galactosidase solution to TDO and QDO plates when agar temperature has reached ± 55ºC

Note: All media or plates containing glucose were autoclaved for 15 minutes to avoid crystallisation

6. ELECTROPHORESIS SOLUTIONS

SB Buffer (20X stock)

Di-sodium tetraborate decahydrate	38.137g/mol
ddH_2O to a final volume of 1L	

SDS-PAGE Running buffer (10X)

Tris base	30g
Glycine	144g
10% SDS	100ml
ddH_2O to a final volume of 1L	

7. GELS

1 % Agarose Gel

Agarose	1g
SB Buffer (1X)	100ml

Microwave for 2-3 minutes; add 5µl ethidium bromide (10mglml) when temperature reaches ± 55ºC

8. LOADING DYES

Ethidium bromide stock (10mg/ml)

Ethidium bromide (Sigma)	500mg
ddH_2O	50ml

Stir for 4 hours using magnetic stirrer and store in dark container at 4ºC

Bromophenol Blue loading dye

Bromophenol blue	1% (w/v)
ddH_2O to a final volume of 100ml; store at 4ºC	

SDS Loading Dye

Laemmli sample buffer (Bio-Rad)	950µl
β-mercapto-ethanol	50µl

9. CO-IP REAGENTS

Lysis buffer

Hepes	10ml
5M NaCl	4ml
0.5M EDTA	4ml
Triton X-100	2ml
10mM Nappi	80ml
1M Na_3VO_4	400µl

ddH_2O to final volume of 200ml

- $^1/_4$ tablet protease inhibitor and 100µl PMSF freshly added to 5ml lysis buffer for Co-IP experiment

TBST (pH7.6)

5M NaCl	60ml
1M Tris base	40ml
0.1% Tween-20	2ml

ddH_2O to a final volume of 2L

Membrane blocking solution

Powder milk	7.5g
Tween-20	15µl
TBST solution	150ml

Esuni Buffer

NaCl	8.1g
KCl	0.9g
$MgCl_2$	0.1g
$CaCl_2.H_2O$	0.13g
Hepes	0.95g

ddH_2O to a final volume of 1L; pH6.2;

Metabolic inhibition with 2DG	3.28g
ddH_2O to a final volume of 1L; pH6.4	

10. CO-LOCALIZATION REAGENTS

Phosphate buffered saline (PBS)

1 PBS Tablet	
ddH_2O to a final volume of 200ml	

1% Bovine Serum Albumin (BSA)

BSA	0.5g
PBS solution	50ml

Cell mounting solution

Mowiol	1ml
Anti-fade	<0.01g
Heat for 1hour at 55ºC; spin tube down before use	

11. EUKARYOTIC CELL CULTURE MEDIA

Growth Media

DMEM (4.5g/L glucose, with L-glutamine)	500ml
Foetal Bovine Serum	50ml
Penicillin/Streptomycin	5ml
Pre-warm to 37ºC before use	

Differentiation Media

DMEM (4.5g/L glucose, with L-glutamine)	500ml
Horse Serum	5ml
Penicillin/Streptomycin	5ml
Pre-warm to 37ºC before use	

Appendix II
Vectors

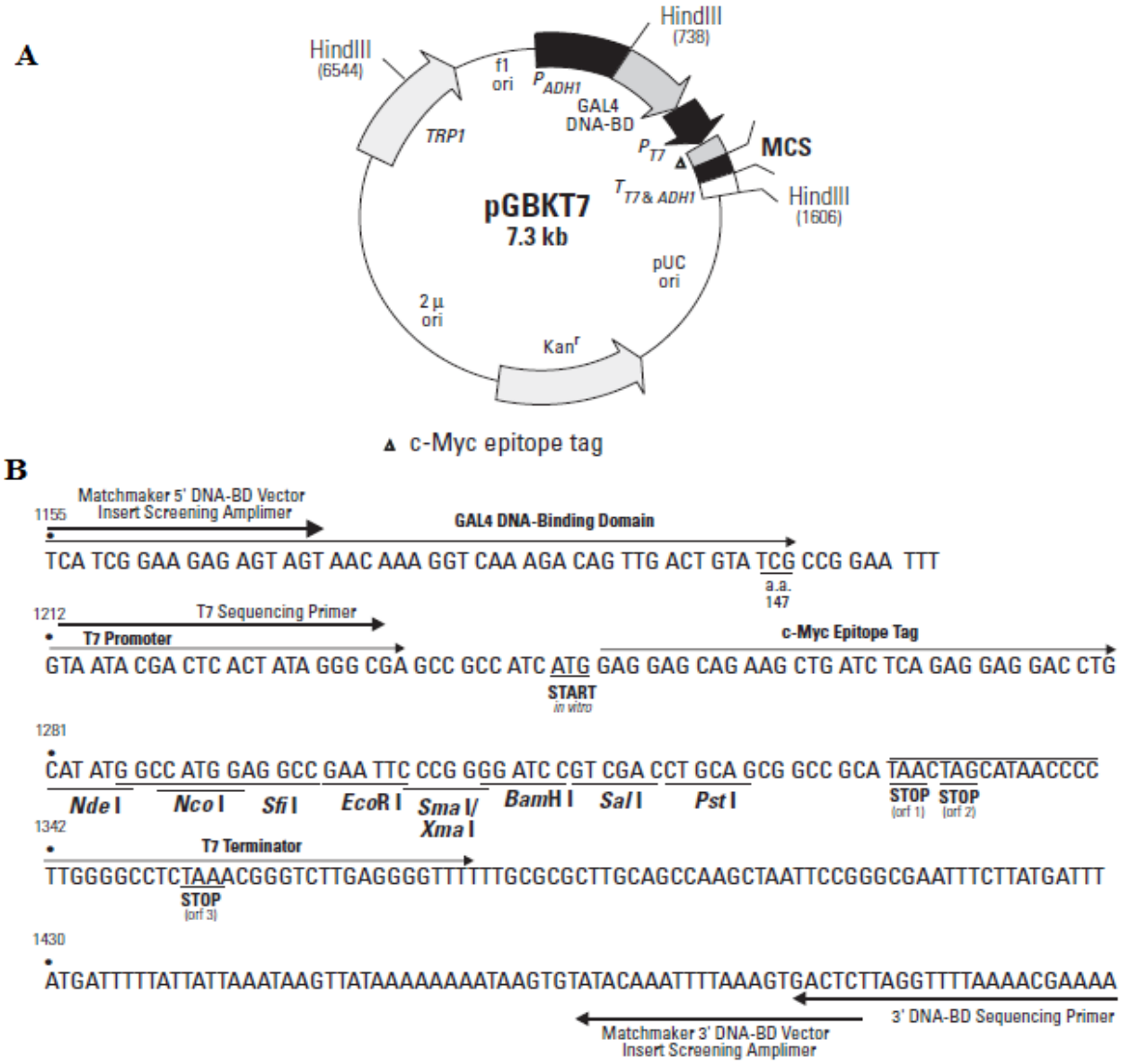

Restriction map and Multiple Cloning Site (MCS) of pGBKT7 Y2H vector. A) The positions of the Kanamycin resistance gene (*Kan*^{r}), the trypsin (*TRP*1) nutritional marker for selection in yeast, *GAL4*-BD coding sequences, f1 bacteriophage and pUC origins of replication, the truncated *S.cerevisiae ADH1* promoter sequence (P_{ADH1}) and the MCS. B) The nucleotide sequence of the pGBKT7 MCS. The sequence indicated the positions of all the unique restriction enzyme recognition sequences, stop codons in the T7 termination sequence, *GAL*4-BD coding sequence, T7 promoter sequence, c-Myc epitope tag, position of screening and sequencing primers. (Adapted from pGBKT7 vector information datasheet, Clontech)

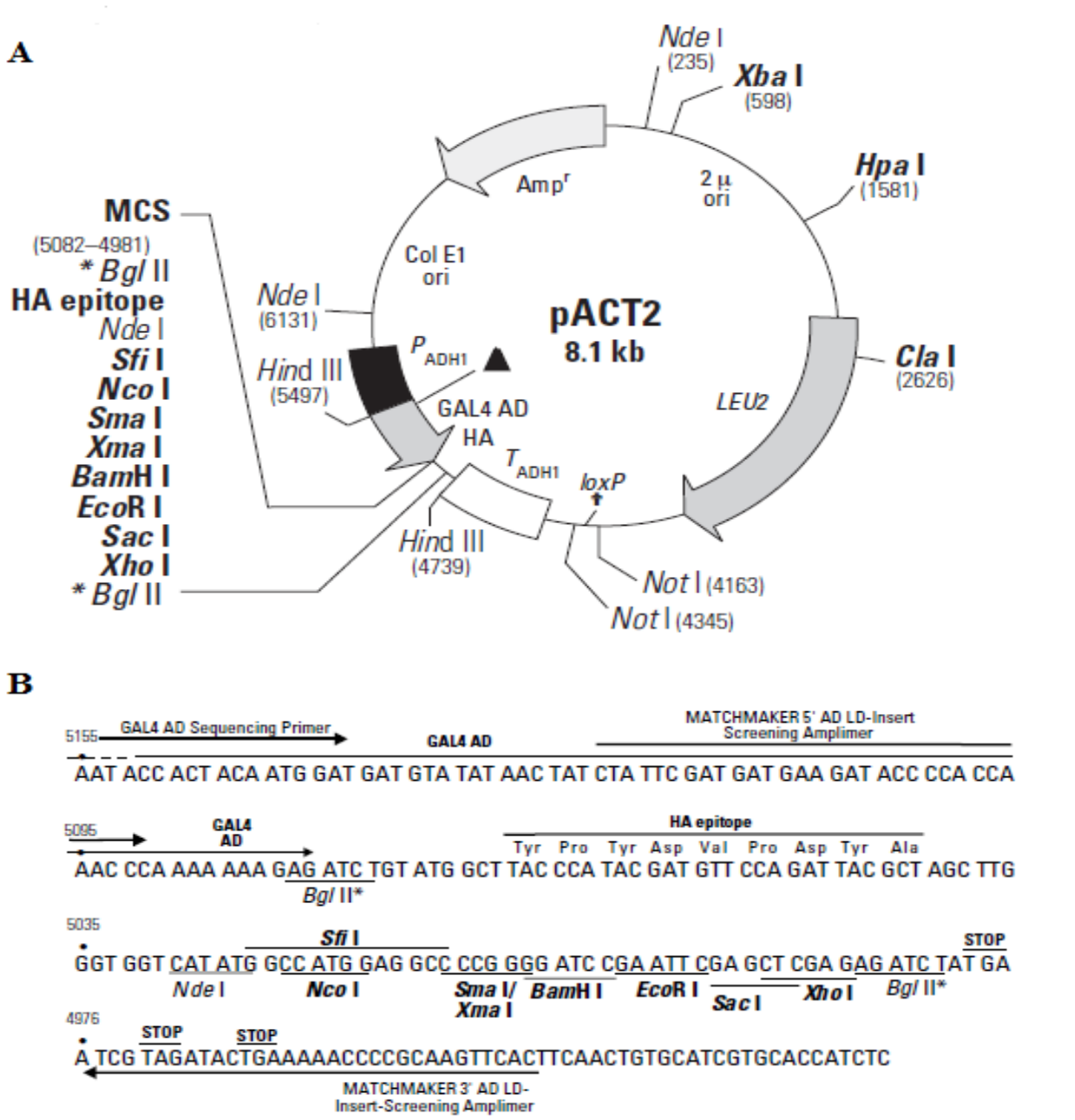

Restriction map and Multiple Cloning Site (MCS) of pACT2 Y2H prey vector. A) Shows the positions of unique restriction enzyme sites indicated in bold font as well as the positions of the Ampicillin resistance gene (*Amp*^{r}), the leucine (*LEU2*) nutritional marker, *GAL*4-BD coding sequence, 2µ and pBR322 plasmid origin of replication, the *S.cerevisiae ADH1* promoter, *S.cerevisiae ADH1* termination sequence, Lox sites (Lox 1 and Lox 2), the haemagglutinin (HA) epitope tag and the MCS. B) The nucleotide sequence of the pACT2 MCS. The position of restriction enzyme sites, stop codons, *GAL*4-BD coding sequence, HA epitope tag and the positions of the pACT2-F and pACT2-R primer sequences. (Adapted from pACT2 vector information datasheet, Clontech)

Appendix III
Calculations

CALCULATING YEAST MATING EFFICIENCY

- Count number of colonies on all plates with 30-300 colonies after 4 days

$$\#\text{colony forming units (cfu)/ml} = \frac{\#\text{cfu} \times 1000\mu\text{l/ml}}{\text{Volume plated } (\mu\text{l}) \times \text{dilution factor}}$$

1. #cfu/ml on SD^{-Leu} plates = viability of prey partner
2. #cfu/ml on SD^{-Trp} plates = viability of bait partner
3. #cfu/ml on $SD^{-Leu-Trp}$ plates = viability of diploids
4. Lowest #cfu/ml of SD^{-Leu} plates or SD^{-Trp} plates = indication of limiting partner

$$5.\ \text{Mating efficiency} = \frac{\#\text{cfu/ml of diploids} \times 100}{\#\text{cfu/ml of limiting partner}}$$

Library titre:

- Count number of colonies on all plates with 30-300 colonies after 4 days

$$\#\text{cfu/ml} = \frac{\#\text{colonies}}{\text{Volume plated } (\mu\text{l}) \times \text{dilution factor}}$$

Number of clones screened:
#cfu/ml x final resuspension concentration

HAEMOCYTOMETRIC CELL COUNT

In order to determine the number of cells per millilitre (ml), the number of cells in each of the five larger square blocks was counted. The amount of the cells in these five squares was added together and divided by five to get an average number of cells for each of the 25 large squares of the central quadrant of the haemocytometer (See figure 2.2). The average number of cells was subsequently multiplied by 25 to get an estimated average number of cells within the large central quadrant. The formula used to determine the number of cells/ml is as follows:

$\#\ \text{cells/ml} = \#\ \text{cells} \times \text{dilution factor} \times 10^4$ (because the depth of the counting chamber is 0.1mm)

Appendix IV
Aligned sequence of KCNE2

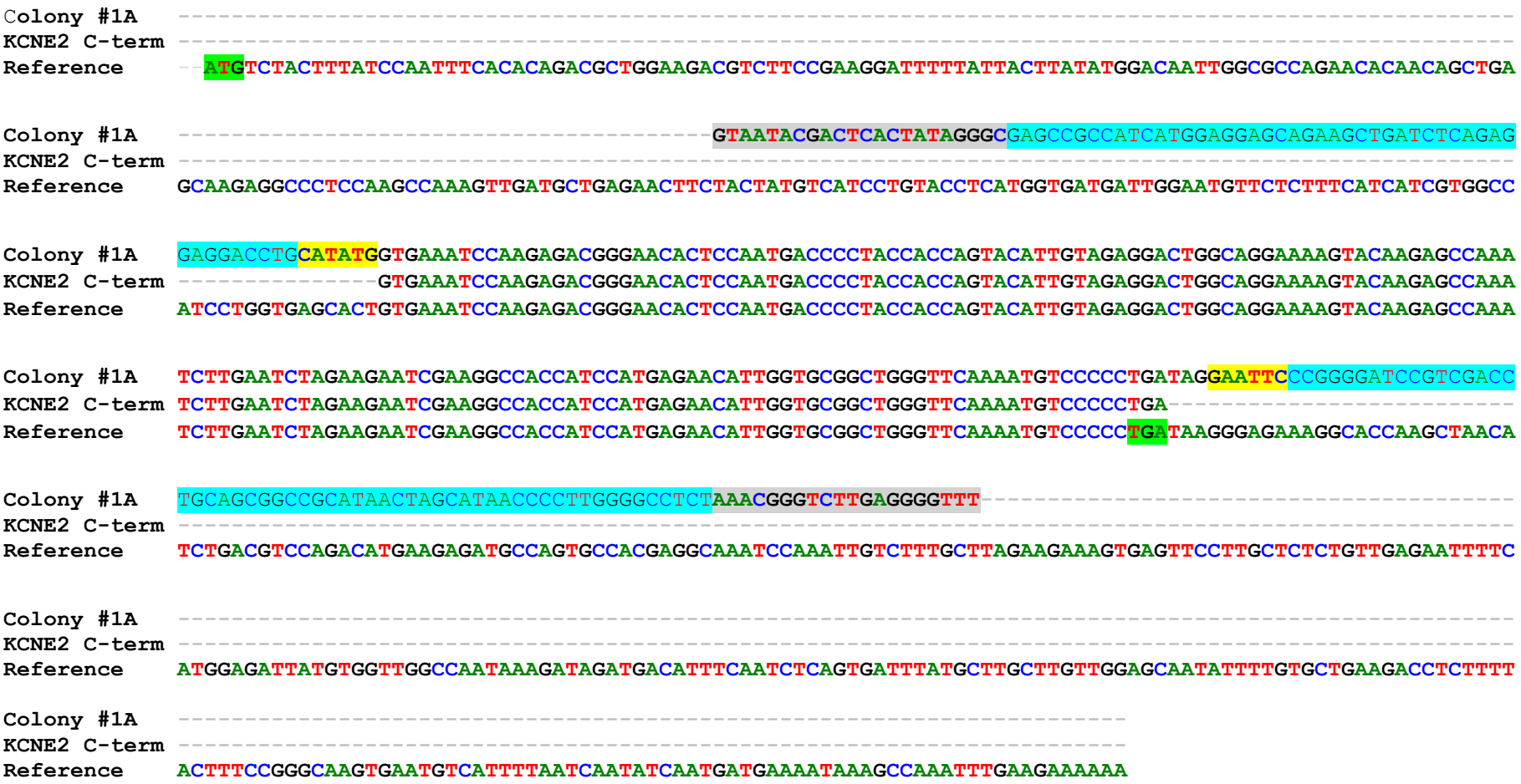

Figure 1: Sequence analysis of the pGBKT7-*KCNE2* construct. Sequence homology alignment of colony #1A with the C-terminal encoding sequence of *KCNE2* in the pGBKT7 vector as well as the reference sequence for *KCNE2* (GenBank: http://www.ncbi.nlm.nih.gov/Entrez) (NM_172201.1). The primer nucleotide sequences of the pGBKT7 vector are shade grey; the pBGKT7 vector sequences are in the turquoise boxes and the restriction enzyme recognition sequences are shaded yellow. The start and stop codons of the *KCNE2* reference sequence are indicated in the green shaded boxes respectively.

Appendix V
Tables of primary and secondary clones

Table 1.1: Activation of nutritional and colourimetric reporter genes of the 427 clones.

Colony #	Growth on TD0 with 3-AT (*HIS*3 activation)	Growth on QDO with 3-AT (*ADE*2 activation)	X-α-Galactosidase assay (Colour) (*MEL*1 activation)
4	+++	+++	++ (light blue)
5	+++	++	++(light blue)
8	+++	+++	++(light blue)
9	+++	+++	+++ (dark blue)
10	+++	+++	+++(dark blue)
11	+++	++	+++(dark blue)
15	+++	+++	++(light blue)
16	+++	+++	+++(dark blue)
17	+++	++	++(light blue)
18	+++	++	++(light blue)
22	+++	++	++(light blue)
23	+++	+++	+++(dark blue)
24	+++	++	+++(dark blue)
26	+++	++	+ (no blue)
28	+++	++	+(no blue)
29	+++	+++	++(light blue)
30	+++	+++	++(light blue)
38	+++	++	++(light blue)
41	+++	++	++(light blue)
42	+++	+++	- (no growth)
46	+++	+++	+++(dark blue)
48	+++	+++	++(light blue)
53	+++	+++	++(light blue)
56	+++	+++	+++(dark blue)
57	+++	++	++(light blue)
61	+++	+++	++(light blue)
64	+++	++	++(light blue)
65	+++	+++	+(no blue)
66	+++	+++	++(light blue)
67	+++	+++	++(light blue)
68	+++	+++	+++(dark blue)
72	+++	++	++(light blue)
73	+++	++	- (no growth)
74	+++	+++	+(no blue)

Colony #	Growth on TD0 with 3-AT (*HIS*3 activation)	Growth on QDO with 3-AT (*ADE*2 activation)	X-α-Galactosidase assay (Colour) (*MEL*1 activation)
79	+++	+++	+++(dark blue)
81	+++	+++	- (no growth)
82	+++	+++	+++(dark blue)
84	+++	+++	+(no blue)
89	+++	+++	- (no growth)
92	+++	+++	++(light blue)
95	+++	+++	++(light blue)
96	+++	+++	+++(dark blue)
97	+++	+++	++(light blue)
98	+++	+++	++(light blue)
101	+++	+++	++(light blue)
102	+++	+++	+++(dark blue)
103	+++	++	++(light blue)
105	+++	+++	++(light blue)
106	+++	+++	++(light blue)
107	+++	+++	+(no blue)
108	+++	+++	+(no blue)
111	+++	+++	++(light blue)
112	+++	+++	+++(dark blue)
113	+++	+++	+++(dark blue)
114	+++	++	- (no growth)
116	+++	+++	++(light blue)
118	+++	+++	++(light blue)
120	+++	++	++(light blue)
121	+++	+++	++(light blue)
93	+++	+++	++(light blue)
124	+++	++	- (no growth)
125	+++	+++	+++(dark blue)
127	+++	++	++(light blue)
128	+++	++	++(light blue)
129	+++	+++	+(no blue)
131	+++	++	- (no growth)
132	+++	++	+(no blue)
134	+++	+++	+(no blue)
135	+++	++	++(light blue)
137	+++	+++	+++(dark blue)
138	+++	++	- (no growth)

Colony #	Growth on TD0 with 3-AT (*HIS*3 activation)	Growth on QDO with 3-AT (*ADE*2 activation)	X-α-Galactosidase assay (Colour) (*MEL*1 activation)
139	+++	++	++(light blue)
142	+++	++	++(light blue)
143	+++	+++	+++(dark blue)
144	+++	+++	++(light blue)
145	+++	+++	++(light blue)
146	+++	++	++(light blue)
148	+++	+++	++(light blue)
149	+++	+++	++(light blue)
155	+++	+++	++(light blue)
157	+++	+++	++(light blue)
158	+++	+++	++(light blue)
160	+++	+++	++(light blue)
162	+++	++	++(light blue)
163	+++	+++	++(light blue)
165	+++	+++	++(light blue)
170	+++	+++	++(light blue)
171	+++	++	+(no blue)
174	+++	++	++(light blue)
175	+++	+++	++(light blue)
176	+++	++	+(no blue)
180	+++	++	+(no blue)
181	+++	++	+(no blue)
182	+++	++	+(no blue)
185	+++	+++	++(light blue)
186	+++	++	- (no growth)
191	+++	++	+(no blue)
192	+++	++	++(light blue)
193	+++	+++	++(light blue)
194	+++	++	++(light blue)
196	+++	++	+(no blue)
197	+++	+++	++(light blue)
198	+++	+++	++(light blue)
199	+++	+++	- (no growth)
202	+++	+++	++(light blue)
203	+++	+++	+(no blue)
205	+++	+++	++(light blue)
206	+++	++	+(no blue)

Colony #	Growth on TD0 with 3-AT (*HIS*3 activation)	Growth on QDO with 3-AT (*ADE*2 activation)	X-α-Galactosidase assay (Colour) (*MEL*1 activation)
209	+++	+++	+(no blue)
211	+++	++	+(no blue)
212	+++	++	+(no blue)
214	+++	+++	++(light blue)
216	+++	+++	++(light blue)
217	+++	+++	+++(dark blue)
218	+++	+++	+++(dark blue)
219	+++	+++	+(no blue)
222	+++	+++	++(light blue)
223	+++	++	+(no blue)
226	+++	++	++(light blue)
227	+++	++	- (no growth)
228	+++	+++	++(light blue)
229	+++	++	++(light blue)
230	+++	+++	+++(dark blue)
233	+++	++	++(light blue)
234	+++	+++	++(light blue)
236	+++	++	++(light blue)
237	+++	+++	++(light blue)
238	+++	+++	+++(dark blue)
239	+++	++	++(light blue)
242	+++	+++	+++(dark blue)
243	+++	++	+(no blue)
244	+++	++	++(light blue)
247	+++	+++	+++(dark blue)
248	+++	+++	++(light blue)
250	+++	+++	++(light blue)
251	+++	+++	+++(dark blue)
252	+++	+++	++(light blue)
257	+++	+++	++(light blue)
259	+++	+++	++(light blue)
261	+++	+++	++(light blue)
262	+++	++	++(light blue)
264	+++	++	++(light blue)
265	+++	+++	++(light blue)
271	+++	+++	++(light blue)
272	+++	+++	++(light blue)

Colony #	Growth on TD0 with 3-AT (*HIS*3 activation)	Growth on QDO with 3-AT (*ADE*2 activation)	X-α-Galactosidase assay (Colour) (*MEL*1 activation)
278	+++	+++	++(light blue)
279	+++	+++	++(light blue)
281	+++	+++	+++(dark blue)
283	+++	+++	+++(dark blue)
285	+++	++	++(light blue)
290	+++	++	+(no blue)
291	+++	++	++(light blue)
293	+++	++	++(light blue)
295	+++	+++	++(light blue)
296	+++	++	++(light blue)
297	+++	++	+(no blue)
299	+++	++	++(light blue)
302	+++	+++	+++(dark blue)
303	+++	+++	+++(dark blue)
305	+++	++	++(light blue)
307	+++	++	++(light blue)
309	+++	+++	+(no blue)
317	+++	+++	++(light blue)
319	+++	+++	++(light blue)
321	+++	++	++(light blue)
323	+++	++	++(light blue)
328	+++	+++	++(light blue)
329	+++	++	++(light blue)
330	+++	+++	++(light blue)
331	+++	+++	++(light blue)
333	+++	+++	++(light blue)
334	+++	+++	+(no blue)
335	+++	+++	++(light blue)
336	+++	++	++(light blue)
338	+++	+++	++(light blue)
340	+++	+++	+(no blue)
343	+++	+++	++(light blue)
349	+++	+++	+++(dark blue)
351	+++	+++	++(light blue)
355	+++	+++	+++(dark blue)
358	+++	++	++(light blue)
359	+++	++	++(light blue)

Colony #	Growth on TD0 with 3-AT (*HIS*3 activation)	Growth on QDO with 3-AT (*ADE*2 activation)	X-α-Galactosidase assay (Colour) (*MEL*1 activation)
360	+++	+++	+++(dark blue)
368	+++	++	+++(dark blue)
371	+++	+++	+++(dark blue)
375	+++	++	++(light blue)
380	+++	+++	++(light blue)
383	+++	+++	+++(dark blue)
395	+++	+++	+++(dark blue)
396	+++	+++	++(light blue)
398	+++	+++	+++(dark blue)
403	+++	+++	++(light blue)
406	+++	++	++(light blue)
407	+++	+++	+++(dark blue)
409	+++	+++	++(light blue)
412	+++	++	+++(dark blue)
414	+++	+++	++(light blue)
416	+++	+++	+++(dark blue)
417	+++	++	+++(dark blue)
418	+++	+++	+++(dark blue)
419	+++	+++	+(no blue)
420	+++	+++	++(light blue)
423	+++	++	++(light blue)
424	+++	++	++(light blue)
425	+++	+++	++(light blue)
426	+++	+++	++(light blue)
427	+++	+++	++(light blue)
428	+++	+++	++(light blue)
430	+++	+++	++(light blue)
431	+++	+++	++(light blue)
432	+++	+++	++(light blue)
433	+++	+++	++(light blue)
434	+++	++	++(light blue)
435	+++	+++	++(light blue)
436	+++	+++	++(light blue)
437	+++	+++	++(light blue)
439	+++	+++	++(light blue)
440	+++	++	++(light blue)
441	+++	++	++(light blue)

Colony #	Growth on TD0 with 3-AT (*HIS*3 activation)	Growth on QDO with 3-AT (*ADE*2 activation)	X-α-Galactosidase assay (Colour) (*MEL*1 activation)
442	+++	+++	++(light blue)
443	+++	+++	++(light blue)
445	+++	++	++(light blue)
446	+++	+++	++(light blue)
448	+++	+++	++(light blue)
451	+++	+++	++(light blue)
452	+++	+++	+++(dark blue)
453	+++	+++	++(light blue)
456	+++	++	++(light blue)
459	+++	++	++(light blue)
461	+++	++	++(light blue)
462	+++	++	++(light blue)
464	+++	+++	+++(dark blue)
470	+++	++	++(light blue)
475	+++	+++	++(light blue)
477	+++	++	++(light blue)
479	+++	+++	++(light blue)
480	+++	+++	++(light blue)
481	+++	++	++(light blue)
484	+++	+++	+++(dark blue)
487	+++	+++	++(light blue)
490	+++	++	+(no blue)
493	+++	++	++(light blue)
494	+++	+++	++(light blue)
495	+++	+++	++(light blue)
496	+++	++	+(no blue)
501	+++	+++	+++(dark blue)
503	+++	++	++(light blue)
506	+++	+++	++(light blue)
507	+++	+++	++(light blue)
508	+++	+++	++(light blue)
510	+++	+++	+++(dark blue)
514	+++	+++	+++(dark blue)
515	+++	+++	++(light blue)
520	+++	++	++(light blue)
521	+++	+++	++(light blue)
523	+++	++	++(light blue)

Colony #	Growth on TD0 with 3-AT (*HIS*3 activation)	Growth on QDO with 3-AT (*ADE*2 activation)	X-α-Galactosidase assay (Colour) (*MEL*1 activation)
525	+++	++	++(light blue)
526	+++	+++	++(light blue)
534	+++	++	++(light blue)
537	+++	+++	++(light blue)
538	+++	++	++(light blue)
540	+++	++	++(light blue)
543	+++	++	++(light blue)
546	+++	+++	+++(dark blue)
550	+++	++	++(light blue)
553	+++	++	+++(dark blue)
554	+++	++	++(light blue)
564	+++	+++	++(light blue)
578	+++	++	++(light blue)
579	+++	++	++(light blue)
589	+++	++	+(no blue)
590	+++	++	++(light blue)
594	+++	++	++(light blue)
598	+++	++	++(light blue)
601	+++	++	++(light blue)
610	+++	+++	+++(dark blue)
615	+++	++	++(light blue)
616	+++	++	++(light blue)
617	+++	++	++(light blue)
619	+++	++	++(light blue)
623	+++	++	++(light blue)
627	+++	++	++(light blue)
630	+++	++	++(light blue)
634	+++	++	+(no blue)
635	+++	+++	++(light blue)
636	+++	++	++(light blue)
639	+++	++	++(light blue)
640	+++	++	++(light blue)
645	+++	++	++(light blue)
649	+++	++	+++(dark blue)
655	+++	++	++(light blue)
665	+++	++	++(light blue)
668	+++	++	+++(dark blue)

Colony #	Growth on TD0 with 3-AT (*HIS*3 activation)	Growth on QDO with 3-AT (*ADE*2 activation)	X-α-Galactosidase assay (Colour) (*MEL*1 activation)
669	+++	++	++(light blue)
684	+++	++	+++(dark blue)
686	+++	++	++(light blue)
687	+++	+++	+++(dark blue)
689	+++	++	++(light blue)
691	+++	+++	++(light blue)
693	+++	+++	+++(dark blue)
695	+++	++	++(light blue)
696	+++	++	++(light blue)
698	+++	+++	++(light blue)
700	+++	++	++(light blue)
701	+++	+++	++(light blue)
706	+++	++	++(light blue)
710	+++	++	++(light blue)
711	+++	++	++(light blue)
712	+++	++	++(light blue)
713	+++	++	++(light blue)
718	+++	+++	+++(dark blue)
724	+++	++	++(light blue)
726	+++	++	++(light blue)
727	+++	++	++(light blue)
749	+++	++	++(light blue)
750	+++	++	++(light blue)
753	+++	++	++(light blue)
759	+++	++	++(light blue)
760	+++	++	++(light blue)
770	+++	++	++(light blue)
771	+++	++	++(light blue)
774	+++	++	+++(dark blue)
775	+++	++	+++(dark blue)
776	+++	++	+++(dark blue)
777	+++	++	+++(dark blue)
780	+++	++	++(light blue)
781	+++	++	++(light blue)
782	+++	++	++(light blue)
784	+++	++	++(light blue)
785	+++	++	++(light blue)

Colony #	Growth on TD0 with 3-AT (*HIS*3 activation)	Growth on QDO with 3-AT (*ADE*2 activation)	X-α-Galactosidase assay (Colour) (*MEL*1 activation)
787	+++	++	++(light blue)
789	+++	++	++(light blue)
790	+++	++	++(light blue)
798	+++	++	++(light blue)
802	+++	++	+++(dark blue)
817	+++	+++	+++(dark blue)
818	+++	++	+++(dark blue)
819	+++	++	++(light blue)
823	+++	++	++(light blue)
832	+++	++	++(light blue)
836	+++	++	++(light blue)
841	+++	++	++(light blue)
842	+++	++	++(light blue)
846	+++	++	++(light blue)
847	+++	++	++(light blue)
852	+++	++	++(light blue)
855	+++	++	++(light blue)
861	+++	+++	++(light blue)
864	+++	++	++(light blue)
869	+++	++	++(light blue)
870	+++	++	+++(dark blue)
872	+++	+++	+++(dark blue)
875	+++	++	++(light blue)
876	+++	++	+++(dark blue)
881	+++	++	++(light blue)
883	+++	++	++(light blue)
887	+++	++	+++(dark blue)
890	+++	++	++(light blue)
893	+++	++	+++(dark blue)
1008	+++	++	++(light blue)
1020	+++	++	+(no blue)
1340	+++	+++	+++(dark blue)
1363	+++	++	++(light blue)
1451	+++	++	++(light blue)
1482	+++	+++	+++(dark blue)
1569	+++	++	++(light blue)
1596	+++	++	++(light blue)

Colony #	Growth on TD0 with 3-AT (*HIS*3 activation)	Growth on QDO with 3-AT (*ADE*2 activation)	X-α-Galactosidase assay (Colour) (*MEL*1 activation)
1649	+++	++	++(light blue)
1661	+++	+++	+++(dark blue)
1728	+++	+++	+++(dark blue)
1808	+++	++	++(light blue)
1830	+++	++	+++(dark blue)
1848	+++	++	++(light blue)
1857	+++	++	++(light blue)
1859	+++	++	++(light blue)
1860	+++	++	++(light blue)
1880	+++	++	++(light blue)
1940	+++	++	++(light blue)
1951	+++	++	++(light blue)
1962	+++	++	++(light blue)
2011	+++	++	++(light blue)
2102	+++	++	++(light blue)
2138	+++	++	++(light blue)
2180	+++	++	++(light blue)
2189	+++	++	++(light blue)
2222	+++	++	++(light blue)
2223	+++	++	++(light blue)
2264	+++	++	++(light blue)
2322	+++	++	++(light blue)
2358	+++	++	++(light blue)
2391	+++	++	++(light blue)
2393	+++	++	++(light blue)
2641	+++	++	++(light blue)
2736	+++	++	++(light blue)
2753	+++	++	+++(dark blue)
2764	+++	+++	+++(dark blue)
2792	+++	+++	+++(dark blue)
2948	+++	++	++(light blue)
3005	+++	++	++(light blue)
3006	+++	++	+++(dark blue)
3040	+++	++	++(light blue)
3066	+++	++	++(light blue)
3074	+++	++	++(light blue)
3103	+++	++	++(light blue)

Colony #	Growth on TD0 with 3-AT (*HIS*3 activation)	Growth on QDO with 3-AT (*ADE*2 activation)	X-α-Galactosidase assay (Colour) (*MEL*1 activation)
3135	+++	++	++(light blue)
3167	+++	++	++(light blue)
3204	+++	+++	+++(dark blue)
3325	+++	++	++(light blue)
3375	+++	+++	+++(dark blue)
3404	+++	+++	+(no blue)
3441	+++	++	++(light blue)
3445	+++	+++	++(light blue)
3458	+++	+++	+++(dark blue)
3481	+++	++	++(light blue)
3483	+++	++	++(light blue)
3496	+++	+++	+++(dark blue)
3507	+++	++	++(light blue)
3512	+++	++	++(light blue)
3542	+++	++	++(light blue)
3547	+++	++	++(light blue)
3570	+++	++	++(light blue)
3573	+++	++	++(light blue)
3605	+++	+++	+++(dark blue)
3610	+++	+++	+++(dark blue)
3624	+++	++	++(light blue)
3628	+++	+++	+++(dark blue)
3640	+++	++	++(light blue)

Colonies in blue bars were able to activate *HIS3*, *ADE2* and *MEL1* reporter genes. TDO = $SD^{-Leu-Trp-His}$ plates; QDO = $SD^{-Leu-Trp-His-Ade}$ plates. Growth on solid media: +++ = very good; ++ = good, + = weak; - = no growth. Dark blue = primary clones; light blue = secondary clones

Table 1.2: Interaction of primary prey clones with heterologous baits in specificity tests

Clone #	x pGBKT-KCNE2 TDO	x pGBKT7-KCNE2 QDO	x pGBKT7 TDO	x pGBKT7 QDO	x pGBKT-53 TDO	x pGBKT-53 QDO	x WFS1 TDO	x WFS1 QDO
9	+++	+++	+++	++	+++	+++	+++	++
10	++	-	++	-	++	-	++	-
*11	+++	+++	+++	+++	+++	-	+++	-
*16	+++	+++	++	+++	+++	-	+++	-
23	+	-	+	-	+	-	+	-
*24	+++	+++	+++	+++	+++	-	++	-
46	+	-	+	-	+	-	+	-
56	+++	-	+++	-	+++	-	++	-
*68	++	-	++	-	++	-	++	-
*79	+++	+++	+++	++	++	+	-	-
*82	+++	+++	++	+++	++	+	++	-
96	+	-	+	-	+	-	+	-
102	+++	-	+++	-	+++	-	++	-
*112	+++	+++	+++	++	+++	+	+++	+
113	-	-	-	-	-	-	-	-
125	+++	+++	+++	+++	+++	+++	+++	+++
*137	+++	+++	+++	+++	+++	-	+	-
*143	+++	+++	+++	++	+	+	+	-
217	+++	+++	+++	+++	+++	+++	++	+++
*218	+++	-	++	-	++	-	+++	-
230	+++	+++	+++	+++	+++	+	+++	+++
238	+++	+++	+++	+++	+++	+++	+++	++
242	+	-	+	-	+	-	+	-
247	+++	+++	+++	+++	++	++	+	-
*251	++	+++	++	++	++	-	+	-
*281	+++	+++	++	++	+	-	+	-
283	++	-	++	-	++	-	+	-
302	+	-	+	-	++	-	++	-

Clone #	x pGBKT-KCNE2 TDO	x pGBKT7-KCNE2 QDO	x pGBKT7 TDO	x pGBKT7 QDO	x pGBKT-53 TDO	x pGBKT-53 QDO	x WFS1 TDO	x WFS1 QDO
*303	+++	+++	+++	++	+++	-	++	-
*349	+++	+++	+++	+++	+++	++	+++	-
*355	+++	+++	+++	++	++	-	++	-
360	+++	+++	+++	+++	++	+++	++	+++
368	+	-	++	-	++	-	+	-
371	+++	+++	+++	+++	+++	+++	+	-
383	+++	+++	+++	+++	+++	+++	++	-
*395	+++	+++	+++	++	+++	+	++	-
*398	++	++	+++	-	+++	-	++	-
407	++	-	+	-	+	-	+	-
412	++	-	++	-	++	-	++	-
416	++	-	++	-	++	-	+++	-
417	+++	+++	+++	+++	+++	+++	++	-
*418	+++	+++	+++	+	+++	-	++	-
*452	++	+++	+++	+	+++	+	++	-
*464	+++	-	++	-	+++	-	++	-
*484	+++	+++	++	+++	++	+	+	-
*501	+++	+++	+++	+++	+++	+	++	-
510	+++	+++	++	++	++	++	++	-
514	+++	+++	+++	+++	+++	+++	-	-
546	+++	+++	+++	+++	+++	++	+++	-
*553	+++	+++	+++	++	+++	++	+++	-
610	+++	+++	+++	+++	+++	++	++	-
649	+++	+++	+++	+++	+++	+++	+++	+
*668	+++	+++	+++	+++	+++	++	++	-
684	+++	+++	+++	+++	+++	+++	++	-
*687	+++	+++	++	++	++	-	++	-
*693	+++	+++	++	++	+++	+	+++	-
*718	+++	+++	+++	++	+++	+	+++	-

Clone #	x pGBKT-KCNE2 TDO	x pGBKT7-KCNE2 QDO	x pGBKT7 TDO	x pGBKT7 QDO	x pGBKT-53 TDO	x pGBKT-53 QDO	x WFS1 TDO	x WFS1 QDO
774	+++	+++	++	++	+++	++	+++	+
775	++	-	+++	-	+++	-	++	-
776	++	-	++	-	++	-	++	-
*777	+++	+++	+++	+++	++	++	++	-
*802	+++	+++	++	++	+++	++	+++	+
817	+++	+++	+++	+++	+++	+++	++	-
818	+++	+++	+++	+++	+++	+++	+++	+
870	+++	+++	+++	+++	+++	+++	+++	-
872	+++	+++	++	++	+++	++	-	+
876	+++	+++	+++	+++	+++	++	++	-
887	+++	+++	+++	+++	+++	+++	++	+
893	+++	+++	+++	+	+++	-	-	-
1340	+++	-	+++	-	+++	-	+++	-
1482	++	-	++	-	+++	-	++	-
1661	++	-	++	-	+++	-	+++	-
1728	++	-	++	-	++	-	++	-
1830	++	-	++	-	++	-	++	-
*2753	+++	+++	+++	+++	++	++	-	-
*2764	+++	+++	+++	++	+++	-	+++	-
2792	++	-	+++	-	+++	-	+++	-
*3006	+++	+++	+++	+	+++	++	-	-
3204	++	-	++	-	++	-	+++	-
3375	++	-	++	-	++	-	++	-
3458	++	-	++	-	+++	-	+++	-
*3496	+++	+++	+++	+++	+++	++	+++	+
*3605	+++	+++	+++	+++	+++	++	+++	-
*3610	++	+	++	-	++	-	++	-
*3628	++	++	+++	-	+++	-	++	-

TDO = $SD^{-Leu-Trp-His}$ plates; QDO = $SD^{-Leu-Trp-His-Ade}$ plates. Growth of colonies: +++ = very good; ++ = good; + = weak; - = no growth. * = Clones selected for sequencing.

Table 1.3: Interaction of secondary prey clones with heterologous baits in specificity tests

Clone #	x pGBKT-KCNE2 TDO	x pGBKT7-KCNE2 QDO	x pGBKT7 TDO	x pGBKT7 QDO	x pGBKT-53 TDO	x pGBKT-53 QDO	x WFS1 TDO	x WFS1 QDO
4	++	-	-	-	-	-	-	-
5	+++	+++	+++	+++	+++	+++	-	+++
8	+++	+++	++	+	++	++	++	++
*15	+++	+++	+++	-	++	-	-	-
17	+++	-	++	-	++	-	++	-
*18	+++	+++	++	-	-	-	+	-
*22	+++	++	++	-	++	-	+++	-
29	+++	+++	+++	++	+++	++	++	+
*30	+++	+++	+++	+	++	-	++	-
38	+++	+++	+++	++	+++	+++	+++	++
41	+	-	-	-	-	-	-	-
48	+++	+++	+++	+++	+++	+++	+++	+
53	+++	+++	+++	+++	+++	+++	+++	+++
57	+++	+++	+++	++	+++	+++	-	-
61	+++	+++	+++	+++	+++	+++	++	-
*64	+++	+++	+++	++	++	-	+	-
66	+++	+++	+++	+++	+++	+++	++	-
67	+++	+++	+++	+++	++	+	+	-
*72	+++	+++	+++	-	++	-	++	-
92	+++	+++	+++	+++	+++	+++	+++	++
*93	+++	+++	++	++	+++	+	++	+
*95	+++	+++	+++	+++	+++	-	+	-
97	++	+++	+++	-	-	-	++	-
98	+++	+++	+++	+++	+++	+++	++	-
*101	+++	+++	+++	+	-	-	-	-
103	++	-	-	-	-	-	-	-
105	+++	+++	+++	+++	+++	++	++	+++
111	+++	+++	+++	++	+++	++	-	-
118	+++	+++	+++	++	+++	+++	+++	+

Clone #	x pGBKT-KCNE2 TDO	x pGBKT7-KCNE2 QDO	x pGBKT7 TDO	x pGBKT7 QDO	x pGBKT-53 TDO	x pGBKT-53 QDO	x WFS1 TDO	x WFS1 QDO
120	+++	+++	+++	++	+++	++	+	++
121	++	-	-	-	-	-	-	-
127	+++	+++	+++	+++	-	+	-	-
128	+++	+++	+++	+++	+++	++	-	-
135	+++	+++	+++	++	+++	++	+	-
139	+++	+++	+++	+++	+++	+++	+++	+
142	+++	+++	+++	++	+++	++	+++	+
*144	+++	+++	+++	+	++	-	-	-
145	+++	+++	+++	++	++	+	-	-
149	+++	+++	+++	+++	+++	+++	-	-
157	+++	+++	+++	++	+++	+++	+++	++
160	++	-	-	-	-	-	-	-
*162	+++	+++	+++	-	+	-	-	-
163	+++	+++	+++	+++	+++	+	+++	+++
174	+++	+++	+++	++	+++	+++	++	-
175	+++	+++	+++	++	+++	+++	+++	-
185	+++	+++	+++	-	+++	+++	+++	++
*192	+++	+++	+++	-	+++	-	++	-
193	+++	+++	+++	++	+++	+++	+	-
*194	+++	+++	+++	-	+++	-	-	-
*197	+++	+++	+++	++	+++	++	-	-
202	+++	+++	+++	+++	+++	+++	+++	+
205	+++	+++	+++	+	+++	+++	+++	+++
216	+++	+++	+++	+++	+++	++	+	-
222	+++	+++	+++	++	+++	+++	+++	-
228	+++	+++	+++	+	+++	++	+++	++
229	+++	+++	+++	+	+++	+++	+++	+++
233	+++	+++	+++	-	+++	+++	-	-
*236	+++	+++	+++	+	+	-	-	-
244	+++	+++	+++	-	+++	+++	+	-

Clone #	x pGBKT-KCNE2 TDO	x pGBKT7-KCNE2 QDO	x pGBKT7 TDO	x pGBKT7 QDO	x pGBKT-53 TDO	x pGBKT-53 QDO	x WFS1 TDO	x WFS1 QDO
248	+++	+++	+++	-	+++	+++	+++	-
*250	+++	+++	+++	-	++	-	++	-
252	+++	+++	+++	+	++	+	-	-
*257	+++	+++	+++	+	++	++	-	-
*259	+++	+++	+++	-	++	+	-	-
261	+++	++	+++	-	++	-	-	-
*262	+++	+++	+++	-	-	-	+	-
265	+++	+++	+++	+	+++	+++	+++	-
*272	+++	+++	+++	++	++	+	-	-
278	+++	+++	+++	++	+++	+++	+++	-
279	+++	+++	+++	++	+	-	++	+
*285	+++	+++	++	-	++	+	-	-
*291	+++	+++	++	++	-	-	-	-
*293	+++	+++	++	+	+	-	+	-
295	+++	+++	+++	++	++	+++	++	+
296	+++	+++	+++	+	+++	+++	+++	+
299	+++	+++	++	+	+++	++	+++	++
*307	+++	+++	-	+	++	-	-	-
*321	+++	+++	+++	-	++	-	++	-
323	+++	+++	+++	+++	+++	+++	+++	+++
328	+	-	-	-	-	-	-	-
329	+++	+++	+++	++	+++	++	+++	-
330	+++	+++	++	++	+++	+++	++	-
331	+++	+++	++	++	+++	+++	++	++
333	++	-	-	-	-	-	-	-
336	+++	+++	+++	++	+++	++	-	-
358	+++	+++	+++	+++	+++	-	+++	+++
359	+++	+++	+++	++	+++	+	+++	+++
375	+++	+++	+++	+++	++	+	+++	+++
380	+++	+++	++	+++	+++	++	+	-

Clone #	x pGBKT-KCNE2 TDO	x pGBKT7-KCNE2 QDO	x pGBKT7 TDO	x pGBKT7 QDO	x pGBKT-53 TDO	x pGBKT-53 QDO	x WFS1 TDO	x WFS1 QDO
395	+++	+++	++	+++	+++	+++	+++	+++
414	+++	+++	++	++	++	-	++	++
424	+++	+++	+++	++	++	-	+++	+++
426	+++	+++	+++	-	+++	+++	+++	-
427	+++	+++	+++	+++	+++	+++	++	-
431	++	-	-	-	-	-	-	-
432	+++	+++	+++	++	+++	+++	-	-
433	+++	+++	++	++	+++	++	+++	-
434	+++	+++	+++	+++	+++	-	+++	-
*436	+++	+++	+	-	++	-	+++	-
439	-	-	-	-	-	-	-	-
440	-	-	-	-	-	-	-	-
*441	+++	+++	++	-	++	+	+++	-
445	+++	++	+++	-	++	-	+++	-
446	+++	+++	+++	-	+++	+++	+++	-
453	++	-	++	-	-	-	-	-
457	+++	+++	+++	-	+++	++	+++	++
*459	+++	+++	+++	-	+++	-	+++	-
461	+++	+++	+++	+	+++	+	+++	++
470	+++	-	-	-	-	-	-	-
475	+++	+	+++	-	+++	+	+	-
480	+++	+++	+++	-	+++	+++	-	-
481	+++	+++	+++	++	+++	-	+++	+++
*495	+++	++	+++	-	++	-	-	-
503	++	-	-	-	+	-	+	-
507	+++	+++	+++	++	+++	+++	+++	+++
515	+++	+++	+++	+++	+++	++	+++	+++
520	+++	+++	+++	++	++	+++	+++	+++
521	+++	+++	++	+	+++	+++	+++	+++
523	++	+++	++	+	+	+	+++	+++

Clone #	x pGBKT-KCNE2 TDO	x pGBKT7-KCNE2 QDO	x pGBKT7 TDO	x pGBKT7 QDO	x pGBKT-53 TDO	x pGBKT-53 QDO	x WFS1 TDO	x WFS1 QDO
525	+++	+++	+++	+	++	+++	++	-
*526	+++	+++	++	+	++	+	-	-
534	+++	+++	+++	++	+++	++	-	-
537	+++	+++	++	+++	+++	++	+	-
538	+++	+++	+++	+++	++	++	+	+
540	++	+++	+++	+++	-	-	+++	+++
543	++	-	-	-	-	-	-	-
550	+++	+++	+++	+	+++	++	++	-
554	+++	+++	+++	+	+++	++	++	-
578	+++	+++	+++	+	++	++	-	-
579	+++	+++	+++	++	++	+	-	-
*590	+++	+++	+++	+	++	+	-	-
594	+++	+++	+++	++	++	+	+	-
598	+++	+++	+++	+	+++	+++	-	-
*601	++	++	+	-	-	-	-	-
616	+++	+++	+++	++	++	+	-	-
*623	+++	+++	+++	+	-	-	++	-
630	+++	+++	+++	++	+++	+++	+++	++
645	++	-	-	-	-	-	-	-
*665	+++	+++	+++	+	-	+	-	-
669	+++	+++	+++	++	+++	++	++	-
*686	++	+++	++	-	++	+	-	-
691	+++	+++	+++	+	+++	-	-	-
695	+++	+++	+++	+	+++	+++	-	-
*696	+++	+++	+++	++	+++	-	-	-
698	+++	+++	+++	-	+++	+++	+++	++
700	+++	+++	+++	++	+	-	+++	+++
701	+++	++	+++	-	+++	-	+++	-
706	+++	+++	+++	+++	+++	+++	+++	+
710	+++	+++	+++	++	+++	+++	+++	++

Clone #	x pGBKT-KCNE2 TDO	x pGBKT7-KCNE2 QDO	x pGBKT7 TDO	x pGBKT7 QDO	x pGBKT-53 TDO	x pGBKT-53 QDO	x WFS1 TDO	x WFS1 QDO
711	++	-	-	-	-	-	-	-
712	+++	+++	+++	+	++	+	++	++
*713	+++	+++	+++	+	+++	++	+++	-
724	+++	+++	+++	+	+++	+++	++	-
726	+++	+++	+++	-	+++	++	+++	+
727	+++	+++	+++	+++	+++	+++	+++	+++
749	+++	+++	+++	+	+++	+++	++	-
750	+++	+++	+++	++	+++	-	+++	+++
753	++	-	++	-	++	-	++	-
759	+++	+++	+++	+	+++	+++	-	-
770	+	-	-	-	-	-	-	-
781	+++	+++	+++	-	+++	+++	+++	-
787	++	-	-	-	-	-	-	-
790	+++	+++	+++	-	+++	+++	-	-
798	+++	+++	+++	+	+++	+++	-	-
819	+++	+++	+++	+	+++	+++	-	-
823	+	-	-	-	-	-	-	-
836	+++	+++	+++	+	+++	+++	+++	+++
846	+	-	-	-	-	-	-	-
847	+++	+++	+++	++	++	++	++	-
852	++	-	-	-	-	-	-	-
861	+++	+++	+++	-	+++	+++	-	-
864	+++	+++	+++	-	+++	+++	+	++
869	-	-	-	-	-	-	-	-
881	+++	+++	+++	+	-	-	+++	+++
883	+++	+++	+++	++	+++	+++	+++	-
*1008	+++	+++	+++	+	++	++	-	-
1363	+++	+	+++	-	++	-	++	-
1451	+	-	-	-	-	-	-	-
1569	++	-	-	-	-	-	-	-

Clone #	x pGBKT-KCNE2 TDO	x pGBKT7-KCNE2 QDO	x pGBKT7 TDO	x pGBKT7 QDO	x pGBKT-53 TDO	x pGBKT-53 QDO	x WFS1 TDO	x WFS1 QDO
1596	+++	+++	+++	+	+++	+++	+++	-
1649	+++	+++	+++	+++	+++	+++	+++	++
*1808	++	+++	-	-	-	-	-	-
*1857	+++	+++	+++	-	++	-	+	-
1859	+	-	-	-	-	-	-	-
1860	+++	+++	+++	++	+++	+++	++	-
*1880	+++	+++	+++	-	++	-	-	-
1940	++	-	-	-	-	-	-	-
1962	+++	+++	+++	++	+++	+++	+++	-
*2011	+++	+++	+++	-	+++	-	+++	++
2102	+++	+++	+++	-	+++	+++	-	-
2138	+++	++	+++	-	++	++	-	-
2180	++	-	-	-	-	-	-	-
*2189	+++	+++	+++	++	+	++	-	-
2264	+++	++	+++	-	+++	++	-	-
2322	++	-	-	-	-	-	-	-
2391	+++	+++	+++	-	++	+++	+	++
2641	+++	+++	+++	+++	++	+	-	-
2736	+++	+++	+++	-	+++	+++	+++	+++
3066	+++	+++	+++	+++	+++	-	+++	+++
3074	+++	+++	+++	+++	+++	+++	+++	+++
3135	+++	-	++	-	++	-	+++	-
3167	++	-	++	-	+	-	+++	-
3441	+++	+++	+++	+++	+++	+++	+++	+++
3481	+++	++	++	-	++	-	++	-
3483	+++	-	+++	-	++	-	++	-
3507	+++	++	+++	-	++	-	+++	-
3512	++	-	+	-	-	-	-	-
3542	+++	-	+++	-	++	-	+++	-

Clone #	x pGBKT-KCNE2 TDO	x pGBKT7-KCNE2 QDO	x pGBKT7 TDO	x pGBKT7 QDO	x pGBKT-53 TDO	x pGBKT-53 QDO	x WFS1 TDO	x WFS1 QDO
3547	+++	+++	+++	+++	+++	+++	+++	+++
3570	++	-	-	-	-	-	-	-
*3640	+++	+++	+++	-	+	-	-	-

TDO = SD$^{-Leu-Trp-His}$ plates; QDO = SD$^{-Leu-Trp-His-Ade}$ plates. Growth of colonies: +++ = very good; ++ = good; + = weak; - = no growth. * *Clones selected for sequencing.

Table 1.4: Identification of primary putative KCNE2 interactor clones from the Y2H cardiac cDNA library screen

Clone #	Identity BLASTn	BLASTp	Accession # e-value	Accession # e-value	Cellular location
11	*Homo sapiens* arginine and glutamate rich 1 (ARGLU1), mRNA	dihydrolipoamide succinyltransferase [Streptomyces sviceus ATCC 29083]	NM_018011.3 (0.0)	ZP_06916558.1 (0.33)	n/a
16	*Homo sapiens* ATP synthase, H+ transporting, mitochondrial F1 complex, beta polypeptide (ATP5B), nuclear gene encoding mitochondrial protein, mRNA	hypothetical protein Ajs_0177	NM_001686.3 (0.0)	YP_984508.1 (7.2)	n/a
24	*Homo sapiens* interleukin 1 receptor, type I (IL1R1), mRNA	RecName: Full=Probable beta-1,3-galactosyltransferase 12	NM_000877.2 (0.0)	Q66GS2.1 (8)	Golgi apparatus membrane
68	*Homo sapiens* tropomyosin 1 (alpha) (TPM1), transcript variant 1,mRNA	No significant similarity	NM_001018005.1 (0.0)	n/a	n/a
79	*Homo sapiens* chromosome 8 genomic contig, alternate assembly whole genome shotgun sequence	No significant similarity	NW_001839132.1 (0.0)	n/a	n/a
82	*Homo sapiens* mitochondrion, complete genome	NADH dehydrogenase subunit 1 [*Homo sapiens*]	NC_012920.1 (0.0)	ADB44568.1 (2E-11)	Mitochondria
112	*Homo sapiens* collagen, type I, alpha 1 (COL1A1), mRNA	collagen, type I, alpha 1, isoform CRA_a [*Homo sapiens*]	NM_000088.3 (0.0)	EAW94630.1 (7E-157)	Extracellular matrix
137	*Homo sapiens* mitochondrion, complete genome	cytochrome oxidase subunit II [*Homo sapiens*]	NC_012920.1 (0.0)	ABG27224.1 (3E-22)	Mitochondria

Clone #	Identity BLASTn	BLASTp	Accession # e-value	Accession # e-value	Cellular location
143	*Homo sapiens* mitochondrion, complete genome	NADH dehydrogenase subunit 1 [*Homo sapiens*]	NC_012920.1 (0.0)	AAN77914.1 (2E-15)	Mitochondria
218	*Homo sapiens* tropomyosin 1 (alpha) (TPM1), transcript variant 1, mRNA	No significant similarity	NM_001018005.1 (0.0)	n/a	n/a
251	*Homo sapiens* mitochondrion, complete genome	NADH dehydrogenase subunit 1 [*Homo sapiens*]	NC_012920.1 (0.0)	ADB44568.1 (2E-21)	Mitochondria
281	*Homo sapiens* mitochondrion, complete genome	hypothetical protein [Tuber melanosporum Mel28]	NC_012920.1 (0.0)	XP_002841996.1 (0.54)	n/a
303	*Homo sapiens* aspartyl-tRNA synthetase (DARS), mRNA	RecName: Full=Putative uncharacterized mitochondrial protein NCU16001	NM_001349.2 (0.0)	Q35137.2 (0.21)	Mitochondria
349	*Homo sapiens* protein kinase, AMP-activated, alpha 2 catalytic subunit (PRKAA2), mRNA	hypothetical protein HMPREF9473_04582 [Clostridium hathewayi]	NM_006252.3 (0.0)	ZP_09152519.1 (2.8)	n/a
355	*Homo sapiens* mitochondrion, complete genome	cytochrome oxidase I [Pteropus temminckii]	NC_012920.1 (0.0)	AAA32045.2 (5E-12)	Mitochondria
395	*Homo sapiens* myotubularin related protein 4 (MTMR4), mRNA	NADH dehydrogenase subunit 1 [*Homo sapiens*]	NM_004687.4 (0.0)	ADB44568.1 0.000000002	Mitochondria
398	*Homo sapiens* mitochondrion, complete genome	NADH dehydrogenase subunit 1 [*Homo sapiens*]	NC_012920.1 (0.0)	ADB44568.1 6E-17	Mitochondria
418	*Homo sapiens* mitochondrion, complete genome	unnamed protein product [Bacillus pseudofirmus OF4]	NC_012920.1 (0.0)	YP_003425713.1 8.6	n/a
452	*Homo sapiens* mitochondrion, complete genome	NADH dehydrogenase subunit 1 [*Homo sapiens*]	NC_012920.2 (0.0)	AAN77914.1 2E-15	Mitochondria
464	*Homo sapiens* tropomyosin 1 (alpha) (TPM1), transcript variant 1,mRNA	No significant similarity	NM_001018005.1 (0.0)	n/a	n/a
484	*Homo sapiens* mitochondrion, complete genome	NADH dehydrogenase subunit 1 [*Homo sapiens*]	NC_012920.1 (0.0)	ADB44568.1 1E-13	Mitochondria
*501	*Homo sapiens* filamin C, gamma (FLNC), transcript variant 2, mRNA	Chain A, Dimerization Of Human Filamin C: Crystal Structure Of the domain 24	NM_001127487.1 (0.0)	1V05_A 2E-57	Cytoplasm, Membrane, Sarcomere, Myofibril

Clone #	Identity		Accession # e-value	Accession # e-value	Cellular location
	BLASTn	BLASTp			
553	*Homo sapiens* mitochondrion, complete genome	No significant similarity	NC_012920.1 (0.0)	n/a	n/a
668	*Homo sapiens* protein tyrosine phosphatase, receptor type, K (PTPRK),transcript variant 2, mRNA	protein tyrosine phosphatase, receptor type, K, isoform CRA_e	NM_002844.3 (0.0)	EAW48088.1 1E-106	Cell membrane, Cell junction
687	*Homo sapiens* mitochondrion, complete genome	NADH dehydrogenase subunit 1 [*Homo sapiens*]	NC_012920.1 (0.0)	ADB44568.1 6E-10	Mitochondria
693	*Homo sapiens* mitochondrion, complete genome	NADH dehydrogenase subunit 1 [*Homo sapiens*]	NC_012920.1 (0.0)	AAN77914.1 2E-15	Mitochondria
718	*Homo sapiens* mitochondrion, complete genome	NADH dehydrogenase subunit 1 [*Homo sapiens*]	NC_012920.1 (0.0)	ADB44568.1 1E-13	Mitochondria
777	*Homo sapiens* metastasis associated lung adenocarcinoma transcript	hypothetical protein, unlikely [Trypanosoma vivax Y486]	NR_002819.2 (0.0)	CCC51287.1 1.5	n/a
802	*Homo sapiens* mitochondrion, complete genome	No significant similarity	NC_012920.1 (0.0)	n/a	n/a
872	*Homo sapiens* mitochondrion, complete genome	No significant similarity	NC_012920.2 (0.0)	n/a	n/a
876	*Homo sapiens* yippee-like 5 (Drosophila)(YPEL5), transcript variant 3,mRNA	unnamed protein product [Desulfosporosinus orientis DSM 765]	NM_001127399.1 (0.0)	YP_004972419. 1 (4)	n/a
893	*Homo sapiens* chromosome 10 genomic contig, GRCh37.p5 Primary Assembly	unnamed protein product [Tetraodon nigroviridis]	NT_030059.13 (0.0)	CAF87655.1 0.14	n/a
2753	*Homo sapiens* MT-RNR2-like 1 (MTRNR2L1), mRNA	Fe(3+) ions import ATP-binding protein FbpC [Pseudoalteromonas]	NM_001190452.1 (0.0)	ZP_09239936.1 3.6	Cell membrane
2764	*Homo sapiens* mitochondrion, complete genome	2-octaprenyl-6-methoxyphenol hydroxylase [Collimonas fungivorans]	NC_012920.1 (0.0)	YP_004754278. 1 45	Mitochondria
3006	*Homo sapiens* chromosome 2 genomic contig, GRCh37.p5 Primary Assembly	hypothetical protein TREAZ_2861	NT_022184.15 (0.0)	YP_004528574. 1 22	n/a
3496	*Homo sapiens* mitochondrion, complete genome	NADH dehydrogenase subunit 1 [*Homo sapiens*]	NC_012920.1 (0.0)	AAN77914.12E-15	Mitochondria
3605	*Homo sapiens* mitochondrion, complete genome	NADH dehydrogenase subunit 1 [*Homo sapiens*]	NC_012920.2 (0.0)	AAN77914.12E-15	Mitochondria

Clone #	Identity BLASTn	BLASTp	Accession # e-value	Accession # e-value	Cellular location
3610	n/a	n/a	n/a	n/a	n/a
3628	*Homo sapiens* S-phase kinase-associated protein 1 (SKP1), transcript	hypothetical protein HMPREF9074_05118 [Capnocytophaga sp. oral]	NM_170679.2 (0.0)	ZP_08449328.1 486	n/a

***** = Clones selected for further investigation in the present study

Table 1.5: Identification of primary putative KCNE2 interactor clones from the Y2H cardiac cDNA library screen

Clone #	Identity BLASTn	BLASTp	Accession # e-value	Accession # e-value	Cellular location
*15	Homo sapiens voltage-dependent anion channel 1 (VDAC1),	voltage-dependent anion-selective channel protein 1	NR_036625.1 (0)	NP_003365.1 (0)	Mitochondrial outer membrane, Cell membrane
18	Homo sapiens glyceraldehyde-3-phosphate dehydrogenase (GAPDH)	glyceraldehyde-3-phosphate dehydrogenase isoform 2	NM_002046.3 (0)	NP_001243728.1 (6E-153)	Cytoplasm, Nucleus
22	Homo sapiens titin (TTN), transcript variant novex-3, mRNA	Novex-3 Titin Isoform	NM_133379.3 (0)	CAD12458.1 (2E-76)	Cytoplasm, Nucleus
30	Homo sapiens titin (TTN), transcript variant N2-B, mRNA	putative regulatory protein NosR	NM_003319.4 (2.00E-139)	ZP_01737051.1 (4.1)	n/a
64	Homo sapiens stonin 1 (STON1), transcript variant 2, mRNA	STON1 protein [Homo sapiens]	NM_006873.3 (0)	AFE71436.1 (1E-46)	Cytoplasm, Cell membrane
72	Homo sapiens glucan (1,4-alpha-), branching enzyme 1 (GBE1),	dsDNA-dependent ATPase (Rad54b),	NM_000158.3 (0)	XP_001268743.1 (6.7)	n/a
93	Homo sapiens myomesin 1, 185kDa (MYOM1), transcript variant 2	myomesin-1 isoform b [Homo sapiens]	NM_019856.1 (0)	NP_062830.1 (2E-56)	Sarcomere, M-band
*95	Homo sapiens crystallin, alpha B (CRYAB), mRNA	crystallin, alpha B, isoform CRA_c	NM_001885.1 (0)	EAW67166.1 (6E-55)	Cytoplasm, Nucleus

Clone #	Identity		Accession # e-value	Accession # e-value	Cellular location
	BLASTn	BLASTp			
101	Homo sapiens mitochondrion, complete genome	cytochrome c oxidase subunit I [Sarcocystis neurona]	NC_012920.1 (0)	AAZ39838.1 (3E-11)	n/a
144	Homo sapiens ring finger protein 145 (RNF145), transcript variant 4	n/a	NM_001199382.1 (0)	n/a	n/a
162	Homo sapiens actin, alpha 2, smooth muscle, aorta (ACTA2),transcript variant 1	actin, alpha, cardiac muscle, isoform CRA_b	NM_001141945.1 (0)	EAW92317.1 (1E-117)	Cytoplasm, Cytoskeleton
192	Homo sapiens family with sequence similarity 100, member A (FAM100A)	uncharacterized protein LOC100982856	NM_145253.2 (0)	XP_003815203.1 (3E-75)	n/a
194	Homo sapiens mitochondrion, complete genome	PDK repeat-containing protein	NC_012920.1 (0)	YP_004988500.1 (1.9)	n/a
197	Homo sapiens chromosome 6 genomic contig	hypothetical protein LOC100426450	NT_007592.15 (0)	XP_002803747.1 (1.00E-07)	n/a
236	n/a	n/a	n/a	n/a	n/a
250	Homo sapiens actin, alpha, cardiac muscle 1 (ACTC1), mRNA	cardiac actin ACTC1	NM_005159.4 (0)	EAW92317.1 (1E-117)	Cytoplasm, Cytoskeleton
257	Homo sapiens chromosome 2 genomic contig	n/a	NT_005334.16 (2E-146)	n/a	n/a
259	Homo sapiens ral guanine nucleotide dissociation stimulator-like	hypothetical protein SNOG_12038	NR_028387.1 (5.00E-41)	XP_001802270.1 (12)	n/a
262	Homo sapiens actin, alpha, cardiac muscle 1 (ACTC1), mRNA	cardiac actin ACTC1	NM_005159.4 (0)	EAW92317.1 (1E-117)	Cytoplasm, Cytoskeleton
272	Homo sapiens chromosome 14 open reading frame 126 (C14orf126	unknown [Pongo pygmaeus]	NM_080664.2 (6E-85)	AAY51665.1 (8.1)	n/a
285	Homo sapiens KIAA1191 (KIAA1191), transcript variant 3, mRNA	PREDICTED: similar to AGAP008389-PA [Tribolium castaneum]	NM_001079685.1 (0)	XP_001815332.1 (1.4)	n/a
291	Homo sapiens chromosome 1 genomic contig	n/a	NT_004487.19 (6.00E-90)	n/a	n/a

Clone #	Identity BLASTn	BLASTp	Accession # e-value	Accession # e-value	Cellular location
293	Nitrilase family member 2 (NIT2)	Nitrilase family member 2 (NIT2)	NM_020202.4 (0)	BAG57372.1 (8E-106)	Cytoplasm
307	Homo sapiens inositol(myo)-1(or 4)-monophosphatase 1 (IMPA1)	hypothetical protein HMPREF1063_00697	NM_005536.3 (0)	EIY30101.1 (5)	n/a
321	Homo sapiens family with sequence similarity 46, member A (FAM46A),	family with sequence similarity 46, member A	NM_017633.2 (8.00E-170)	CAI23545.1 (3E-72)	n/a
436	Homo sapiens proteasome maturation protein (POMP), mRNA	proteosome maturation protein	NM_015932.5 (0)	NP_057016.1 (6E-96)	Cytoplasm, Nucleus, Microsome membrane
441	Homo sapiens lipoprotein lipase (LPL), mRNA	n/a	NM_000237.2 (0)	n/a	n/a
459	Homo sapiens AT rich interactive domain 1B (SWI1-like) (ARID1B)	novel protein ,AT rich interactive domain 1B (SWI1-like)	NM_017519.2 (0)	CAI42305.1 (1E-145)	n/a
495	Homo sapiens chromosome 3 genomic contig, GRCh37.p5	hypothetical protein DDB_G0276853	NT_005612.16 (0)	XP_642945.1 (13)	n/a
526	Homo sapiens tropomyosin 1 (alpha) (TPM1)	n/a	NM_001018005.1 (0)	n/a	n/a
590	Homo sapiens mitochondrion, complete genome	site-specific recombinase	NC_012920.1 (0)	YP_003425713.1 (9.6)	n/a
601	Homo sapiens tropomyosin 1 (alpha) (TPM1), transcript variant 1, mRNA	Retinol-binding protein 3	NM_001018005.1 (1.00E-98)	P12665.1 (92482)	n/a
623	Homo sapiens adenylate kinase 4 (AK4), nuclear gene encoding mitochondrial protein	n/a	NM_013410.3 (0)	n/a	n/a
665	Homo sapiens ATPase, Ca++ transporting, plasma membrane 1 (ATP2B1),	putative Fe-S oxidoreductase [Mesotoga prima MesG1.Ag.4.2]	NM_001682.2 (0)	YP_006345749.1 (4.5)	n/a
686	n/a	n/a	n/a	n/a	n/a
696	Homo sapiens PDZ and LIM domain 5 (PDLIM5),	n/a	NM_001011515.1 (0)	n/a	n/a

Clone #	Identity		Accession # e-value	Accession # e-value	Cellular location
	BLASTn	BLASTp			
713	Homo sapiens CD36 molecule (CD36) transcript variant 3, mRNA	IMV membrane protein [Tanapox virus]	NM_000072.3 (0)	YP_001497059.1 (0.24)	n/a
1008	Homo sapiens multiple coagulation factor deficiency 2 (MCFD2),	hypothetical protein LOC100426989	NM_001171509.2 (0)	XP_002800068.1 (1.00E-05)	n/a
1808	Homo sapiens tropomyosin 1 (alpha) (TPM1)	n/a	NM_001018005.1 (0)	n/a	n/a
1857	Homo sapiens chromosome 12 genomic contig	hypothetical protein Mahau_2676	NT_009759.16 (0)	YP_004464634.1 (3)	n/a
1880	Branched-chain alpha-ketoacid dehydrogenase kinase (BCKDK)	Branched-chain alpha-ketoacid dehydrogenase kinase	NM_001122957.1 (1.00E-104)	AAB82714.1 (2E-32)	Mitochondrial matrix
2011	Homo sapiens cullin-associated and neddylation-dissociated 1 (CAND1)	cullin-associated and neddylation-dissociated 1, isoform CRA_a	NM_018448.3 (0)	EAW97171.1 (6E-75)	Nucleus
2189	Homo sapiens chromosome 2 genomic contig	hypothetical protein HMPREF9430_00966	NT_022184.15 (0)	ZP_08028855.1 (4.5)	n/a
3640	Homo sapiens tropomyosin 1 (alpha) (TPM1), transcript variant 6	n/a	NM_001018008.1 (7.00E-114)	n/a	n/a

***** = Clones selected for further investigation in the present study

Appendix VI
Prokaryotic and eukaryotic phenotypes

BACTERIAL STRAIN PHENOTYPE

E.coli strain DH5α

Φ 80d *lacZ*Δ*M15* recA1, *end*A1, *Gry* A96 *thi*-1, *hsd*R17 *sup*E44, *rel*A1, *deo*R Δ (*lac*ZYA *argF*) u169

YEAST STRAIN PHNOTYPES

Yeast strain AH109

*MAT*a, *trp*-901, *leu*2-3, *ura*3-5, *his*3-200, *gal*4Δ, *gal*80Δ, LYS::*GAL1*$_{uas}$ - *GAL1*$_{TATA}$ - *HIS3*, *GAL2*$_{UAS}$ - *GAL2*$_{TATA}$ - *ADE2*, *URA*::*MEL1*$_{UAS}$ - *MEL1*$_{TATA}$ - *lacZ* (James et al. 1999)

Yeast strain Y187

MATα, *ura*3-52, *his*3-200, *ade*2-101, *trp*1-901, *leu*2-3, 112, *gal*4Δ, *mef*, *gal*80Δ, *URA*3::*GAL1*$_{UAS}$ - *GAL1*$_{TATA}$ - *lacZ* (Harper et al. 1993)

Appendix VII
List of suppliers

3-Amino-1, 2, 4-triazole	Sigma
Agarose	Whitehead scientific
Ampicillin	Roche
Autoradiography film	Thermo Scientific
β-mercapto-ethanol	Sigma
Bacto Agar	Merck
Bacto trypone	Fluka
Bradford reagent	Thermo Scientific
Bromophenol blue	Promega
$CaCl_2$	Merck
Calf intestinal alkaline phosphatase	Promega
dATP	Promega
dCTP	Promega
dGTP	Promega
Dimethylformamide	Merck
Di-Sodium tetraborate decahydrate	Merck
DMEM	Whitehead scientific
dTTP	Promega
*Eco*RI	Promega
EDTA	Boerhinger Mannheim
Ethanol	Sigma
Ethidium bromide	Roche
Foetal bovine serum	The Scientific Group
Glass beads	Amersham pharmacia
Glucose	Kimix
Glycine	Sigma
HaeIII	Promega
H9C2	American Type Culture Collection

Haemagglutinin antibody	Santa Cruz Biotechnologies
HCl	Merck
Herring sperm DNA	Promega
Horse serum	Sigma
Hybond N^+ nylon membrane	BD Biosciences
Kanamycin	Roche
Leammli sample buffer	Bio-Rad
LiAc	Sigma
Matchmaker two-hybrid system 3	BD Biosciences
$MgCl_2$	Bioline
Molecular size marker (100 bp)	Lasec
NaCl	Sigma
NdeI	Promega
Oligonucleotide Primers	Department of Molecular and Cell Biology, University of Cape Town (UCT) Cape Town, RSA
pACT2	BD Biosciences
PBS	Sigma
PEG4000	Merck
Penicillin/Streptomycin	The Scientific Group
Peptone	Difco
pGBKT7	BD Biosciences
PIPES	Merck
PMSF	Roche
Protein G agarose	Whitehead scientific
Protein ladder	Thermo Scientific
QDO	BD Biosciences
RsaI	Promega
SD^{-Ade}	BD Biosciences
SD^{-Leu}	BD Biosciences
$SD^{-Leu-Trp}$	BD Biosciences
SD^{-Met}	BD Biosciences

SDS	Merck
SD^{-Ura}	BD Biosciences
SD^{-Trp}	BD Biosciences
T4 DNA Ligase	Promega
Taq polymerase	Bioline
TDO	BD Biosciences
Tris	Merck
Tris-HCl	Merck
Triton X-100	Sigma
Trypsin	Whitehead scientific
Tween-20	Merck
Wizard® SV Gel and PCR Clean-up System	Promega
X-α-Galactosidase	Southern Cross
Yeast extract	Difco
Yeast nitrogem base (without amino acids)	BD Biosciences
Zyppy™ Plasmid Miniprep Kit	Zymo Research